THE UNIVERSITY
of EDINBURGH

Experimental & Computational Investigations into the (Bio)Synthesis of the Angiopterlactones

Marie Isabel Thomson

Degree of Doctor of Philosophy

School of Chemistry

The University of Edinburgh

2018

Declaration

I declare that:

(a) the thesis has been composed by the candidate, and

(b) either that the work is the candidate's own, or, if the candidate has been a member of a research group, that the candidate has made a substantial contribution to the work, such contribution being clearly indicated, and

(c) the work has not been submitted for any other degree or professional qualification except as specified.

Edinburgh, 14.12.2018

Marie Isabel Thomson

Publication

Some of the work contained in this thesis has been previously published:

Thomson, M. I.; Nichol, G. S.; Lawrence, A. L. Total Synthesis of (−)-Angiopterlactone B. *Org. Lett.* **2017**, *19* (9), 2199–2201.[1]

This work is discussed in Chapter 1.

Acknowledgements

Firstly I would like to thank my supervisor Dr Andrew Lawrence for welcoming me into his research group, as well as for his guidance and unwavering support throughout my PhD. I would also like to thank my second supervisor Dr Fernanda Duarte for providing me with the opportunity to work in the field of Computational Chemistry in my final year and for all of her assistance and advice. I am also grateful to the past and present members of both groups for their companionship and for being a pleasure to work with.

Next I would like to thank my family and friends for their constant support, steadfast patience and encouragement. Without their assistance, positivity and exceptional company, my time in Edinburgh would not have been nearly as fun!

Finally I would like to thank the technical staff at the University of Edinburgh, in particular Dr Gary Nichol for his work on X-ray crystallography.

Abbreviations

ν	absorption maxima (IR)
Ac	acetyl
app.	apparent
aq.	aqueous
a.u.	atomic units
ax	axial
BINAP	2,2′-bis(diphenylphosphino)-1,1′-binaphthalene
br	broad
calcd	calculated
CSA	camphorsulfonic acid
cm	centimetre
δ	chemical shift
CD	circular dichroism
c / conc	concentration
COSY	correlated spectroscopy
J	coupling constant
COD	cyclooctadiene
Glc	D-glucopyranose
dm	decimetre/s
° C	degree/s Celsius
SMD	density based solvent model
DFT	Density Functional Theory

DSO	diamagnetic spin-orbit
d.r.	diastereomeric ratio
DEAD	diethyl azodicarboxylate
DMAP	4-(dimethylamino)pyridine
DMSO	dimethylsulfoxide
d	doublet
ESI	electrospray ionisation
ent	enantiomer
e.r.	enantiomeric ratio
E	energy
H	enthalpy
eq	equatorial
eq	equivalents
FC	Fermi contact
GIAO	gauge-including atomic orbitals
G	Gibbs free energy
g	gram/s
H	Hamiltonion operator
HF	Hartree-Fock
Hz	Hertz
HMBC	heteronuclear multiple-bond coherence
HSQC	heteronuclear single quantum coherence
HMDS	hexamethyldisilazane
HPLC	high performance liquid chromatography
HRMS	high resolution mass spectrometry

h	hour/s
HIV	human immunodeficiency virus
IR	infrared
INT	intermediate
IRC	Intrinsic Reaction Coordinate
K	Kelvin
lit.	literature
L	litre/s
MS	mass spectrometry
m/z	mass to charge ratio
MAE	mean absolute error
MHz	megahertz
m.p.	melting point
*m*CPBA	*meta*-chloroperoxybenzoic acid
MTPA	α-methoxy-α-trifluoromethylphenylacetyl
Me	methyl
m	meter/s
M	Michael addition
μ	micro
min	minute/s
M	molarity
M^+	molecular ion
mol	mole/s
m	multiplet
NBS	*N*-bromosuccinimide

NMR	nuclear magnetic resonance
NOESY	nuclear Overhauser effect spectroscopy
1D	one dimensional
oM	oxa-Michael addition
ppm	parts per million
p	*para*
PMB	*para*-methoxybenzyl
PTSA	*para*-toluenesulfonic acid
PSO	paramagnetic spin-orbit
Ph	phenyl
PCM	polarisable continuum model
PES	potential energy surface
q	quartet
rac	racemic
R_f	retention factor
t_R	retention time
RC	ring contraction
rt	room temperature
SAD	Sharpless asymmetric dihydroxylation
σ	shielding tensor
SZ	single zeta
s	singlet
SD	spin-dipole
t	*tert* (tertiary)
TBAF	tetrabutylammonium fluoride

THF	tetrahydrofuran
CCDC	The Cambridge Crystallographic Data Centre
TLC	thin layer chromatography
TsDPEN	toluenesulfonyl-diphenylethylenediamine
TS	transition state
TST	transition state theory
t	triplet
2D	two dimensional
UV	ultraviolet
Ψ	wavefunction
λ	wavelength

Lay Summary

Plants have evolved over millions of years and have therefore become masters at making the molecules they require to survive. Many of these molecules (known as natural products) are valuable to us humans, as they can be used for various applications, such as in our agrochemicals and medicines. As plants often produce only small quantities of natural products, it is difficult to obtain enough material for our every-day use. It is therefore important to be able to access natural products by making them in the laboratory.

The methods used in the laboratory to make these molecules are often wasteful and come with a high economic and environmental cost. Our research group therefore tries to mimic the methods used by plants to inspire the chemical approach taken in the laboratory to make these important materials. This allows us to develop new strategies to make the process more cost-effective and efficient.

The first part of this thesis describes our efforts to synthesise two related natural products, called angiopterlactone A and angiopterlactone B. They were discovered in a fern species found in Asia, which has been used in ancient Chinese medicine to treat various ailments such as snake bites and rheumatic pains. Firstly, we analysed how the fern is likely to make these compounds. We then used this analysis to develop a short and efficient strategy with which we could access angiopterlactone B from a cheap and readily available starting material.

We also tried to make the related natural product angiopterlactone A, but after several attempts we had no success. As work in the laboratory is time intensive and expensive, it is possible to instead apply computational studies to predict structures of materials and reaction outcomes. The second part of this thesis describes the use of computational studies to understand why we did not manage to make angiopterlactone A. The results of these studies were then used to suggest new ways in which we could try and make this natural product in the laboratory.

Abstract

This thesis details our experimental and computational investigations into the (bio)synthesis of two related and structurally complex natural products: angiopterlactone A and angiopterlactone B.

Chapter 1 introduces these natural products and outlines our biosynthetic speculations. It further describes our successful total synthesis of angiopterlactone B in four steps, starting from commercially available 2-acetylfuran. Particularly noteworthy is the final dimerisation, in which three new bonds, two new rings and three new stereogenic centres are formed in a single step. The structure and absolute configuration of our synthetic material was confirmed by X-ray crystallography and led us to revise the structure of the natural material.

Chapter 2 outlines our computational nuclear magnetic resonance (NMR) studies of angiopterlactone A. These were utilised to investigate the relative configuration of angiopterlactone A, which we suspected was assigned incorrectly by the isolation chemists. A number of different methods were applied to predict the chemical shift and coupling constant data for some of our in-house synthesised compounds, as well as for angiopterlactone A. Utilising a combination of biosynthetic speculations, our synthetic experience, as well as our computational studies, we propose a revised structure for angiopterlactone A.

Chapter 3 details our computational mechanistic investigations into the (bio)synthesis of angiopterlactone B, as well as its diastereoisomer *dia*-angiopterlactone B. These studies led us to propose that the key dimerisation step proceeds *via* a domino oxa-Michael/Michael/ring contraction sequence. Various homo- and cross-couplings of lactones were investigated to shed light on the predisposed reactivity and selectivity at play in the biogenesis of these natural products. We discovered that angiopterlactone A is unlikely to be accessible *via* this (bio)synthetic route.

Chapter 4 summarises the work presented and provides further speculations on the biosynthetic origins of angiopterlactones A and B.

Table of Contents

Chapter 1: Total Synthesis of (−)-Angiopterlactone B

1.1 Introduction

1.1.1 Angiopterlactones A and B: Isolation and Structural Elucidation

Our natural product targets (−)-angiopterlactone A (**1**) and (+)-angiopterlactone B (**2**) (Figure 1) are two compact and complex bis-lactone metabolites.[2] Each contain an array of oxygen functionalities, as well as multiple contiguous stereogenic centres. The structural complexity of these metabolites, in combination with the biological activities reported for the extracts of *Angiopteris* plants,[3] make these compounds of significant interest to synthetic chemists. Both angiopterlactones (**1**, **2**) were isolated by Zou and co-workers in 2009 from the rhizomes of *Angiopteris caudatiformis*, a fern species native to Asia.[2] The rhizome of this fern is used in China to treat a variety of ailments, including but not limited to enteritis and tuberculosis.[2] It is interesting to note that from ten kilograms of *Angiopteris caudatiformis* 230 mg of (−)-angiopterlactone A (**1**) were isolated, whereas only 20 mg of (+)-angiopterlactone B (**2**) were extracted.[2]

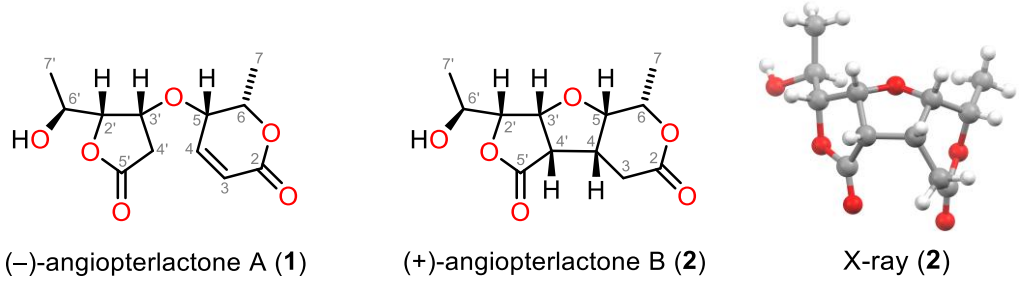

Figure 1: Structures of (−)-angiopterlactone A (**1**) and (+)-angiopterlactone B (**2**) (proposed by Zou and co-workers)[2]

The atom connectivity within the angiopterlactones (**1**, **2**) was established by Zou and co-workers, utilising 1D and 2D NMR spectroscopy.[2] The relative configuration of (−)-angiopterlactone A (**1**) was determined through NOESY experiments. A NOESY correlation between H3' and H5 led the authors to assign a *cis* relationship between these protons. However, given the rotatable nature of the ether linkage, this assignment could be flawed. They further utilised NOESY correlations to propose *cis* relationships between H2' and H3', as well as between H5 and H6. The absolute configuration of (−)-angiopterlactone A (**1**) was then determined by establishing the absolute stereochemistry of positions C6, C6' and C3'. Positions C6 and C3' were assigned as *S* and *R* respectively by employing the CD excitation

chirality method. The modified Mosher's method was utilised to determine the stereochemistry of position C6' to be *S*.[2]

The relative configuration of (+)-angiopterlactone B (**2**) was initially based on comparison to the stereochemistry observed in (−)-angiopterlactone A (**1**) and was then confirmed by X-ray crystallographic studies (Figure 1). The absolute configuration of (+)-angiopterlactone B (**2**) was then established through use of the CD excitation chirality method for positions C4 and C3' (both *R*) and modified Mosher's method for position C6' (*S*).[2] For a more detailed discussion regarding the assignment of stereochemistry, see Section 1.2.3.

1.1.2 Biosynthetic Speculation

Compounds co-isolated alongside natural products can often provide useful information and shed light upon their potential biosynthetic origins. Although the absolute configuration for each of the angiopterlactones (**1**, **2**) was clearly presented and discussed in the isolation paper, no stereochemistry (neither relative nor absolute) was provided for their co-isolated compounds (Figure 2).[2]

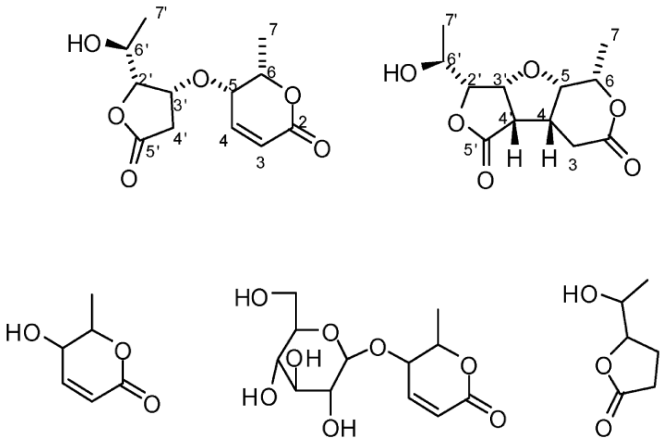

Figure 2: Representation of the angiopterlactones (**1**, **2**) and co-isolated compounds (as shown in the isolation paper)[2]

This makes it challenging to draw any firm conclusions as to plausible biosynthetic origins of the angiopterlactones (**1**, **2**), particularly as various stereoisomers of these three compounds have previously been reported in the literature (*e.g.*, compound **3** and its three stereoisomers have all been reported).[4,5,6,7,8] Despite the ambiguity surrounding the precise stereochemistry

of the co-isolated compounds, their general structures still provide useful clues regarding possible biosynthetic pathways to the angiopterlactones (**1**, **2**).

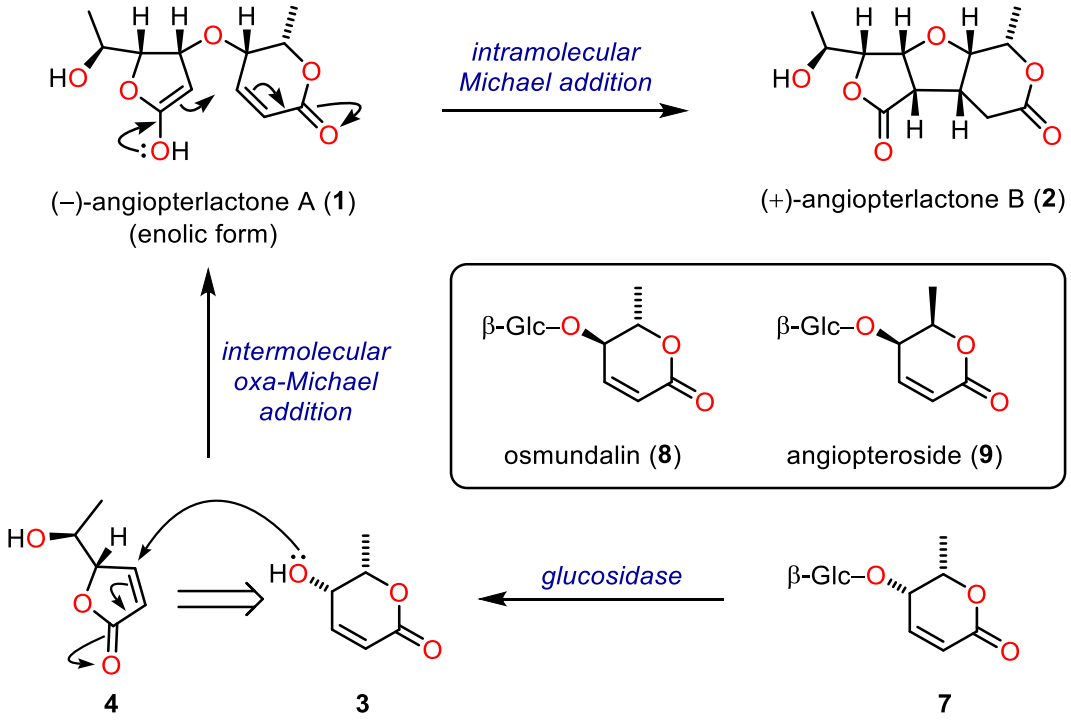

Scheme 1: Our proposed biosynthesis for angiopterlactones A (**1**) and B (**2**)

The isolation chemists speculated that (+)-angiopterlactone B (**2**) may be derived from (−)-angiopterlactone A (**1**) *via* an intramolecular Michael addition (Scheme 1).[2] With no further speculation provided, we proposed that (−)-angiopterlactone A (**1**) may be formed *via* an intermolecular oxa-Michael addition between mono-lactones **3** and **4**. We proposed this for two main reasons, the first one being that lactones **3** and **4** are isomers of one another. There is literature precedent for similar δ-lactones to undergo a ring contraction to the corresponding γ-lactone (*i.e.*, δ-lactone **5** to γ-lactone **6**: Scheme 2),[6,9] thus making δ-lactone **3** a possible biosynthetic precursor to γ-lactone **4**. Secondly, a closer inspection of δ-lactone **3**, revealed that it could conceivably be the aglycone of compound **7**, which bears resemblance to the known natural products osmundalin (**8**) and angiopteroside (**9**).[3,10] Our biosynthetic proposal raises many significant questions regarding control over chemo-, regio- and stereoselectivity and the potential need for enzyme involvement. However, there is promising literature precedent for the chemical feasibility of certain aspects of our biosynthetic speculation.

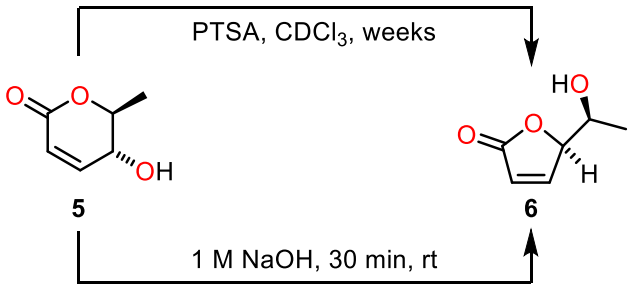

Scheme 2: Previously reported ring contractions of δ-lactone **5** to the corresponding γ-lactone **6**[6]

1.1.3 Domino oxa-Michael/Michael Reaction Sequences

In our proposed biosynthesis of the angiopterlactones (**1**, **2**), (+)-angiopterlactone B (**2**) is formed *via* a domino oxa-Michael/Michael reaction sequence. It is important to note that oxa-Michael additions (integral to our proposed domino sequence) can have significant disadvantages. These include: reversibility, poor nucleophilicity of the alcohols and a lack of stereoselectivity.[11,12] In order to increase the reactivity of the system, two possible methods of activation have been reported: employing bases to enhance the nucleophilicity of the alcohol; and applying Lewis or Brønsted acids for activation of the conjugate acceptor.[11] The issue of reversibility (prevalent particularly in intermolecular oxa-Michael additions) can be effectively negated by embedding these oxa-Michael additions into domino processes.[12] Making use of complex domino reaction sequences in target-oriented synthesis can result in a multitude of advantages. Not only is it possible to obtain significant molecular complexity in a single transformation, but domino reactions also typically provide good stereocontrol and can result in better overall yields compared to stepwise approaches.[13]

Similar domino processes containing consecutive Michael additions have previously been reported in the literature.[14,15,16,17,18,19] For example in 2002, Taylor and co-workers reported the use of stoichiometric amounts of lithium hydroxide to synthesise highly functionalised tetrahydrofuran derivatives from hydroxyenones (Scheme 3).[14] A few months later, Carreño and Ribagorda reported the use of stoichiometric amounts of sodium hydride to form pentacyclic derivatives in a single step from *p*-quinols.[15]

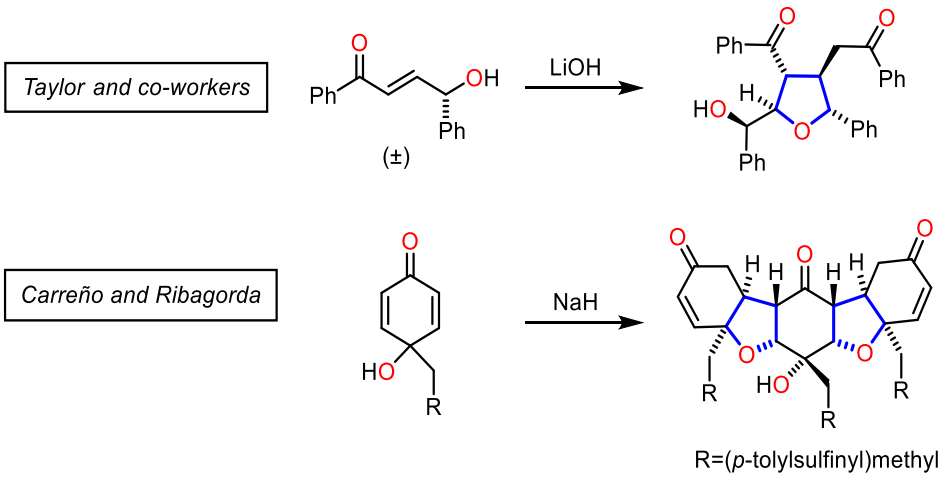

Scheme 3: Example domino oxa-Michael/Michael processes from the literature[14,15]

A pertinent example of a domino oxa-Michael/Michael process is found in the total synthesis of (±)-incarviditone (**10**), which was accomplished by a former PhD student in the Lawrence group (Dr Patrick Brown).[17] It provided a useful study for our angiopterlactone system as they share the common feature of a domino oxa-Michael/Michael tetrahydrofuran ring-forming reaction (Scheme 4). This reaction was carried out at 70 °C in dichloroethane in the presence of 0.1 equivalents of potassium carbonate. The domino sequence was initiated by the homochiral oxa-Michael addition of (±)-rengyolone (**11**). The reversibility of the oxa-Michael addition in the key dimerisation step was combatted by trapping the product in a subsequent Michael addition.[17] This successful domino oxa-Michael/Michael process gave us sufficient encouragement to utilise this proposed domino sequence toward the biomimetic synthesis of angiopterlactones A and B (**1**, **2**).

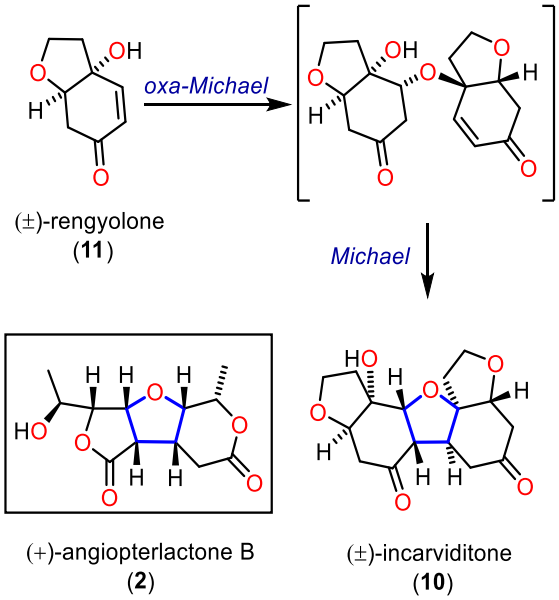

Scheme 4: Synthesis of (±)-incarviditone (**10**) from (±)-rengyolone (**11**)[17]

1.1.4 Previous Synthetic Approach

A previous synthetic approach to the angiopterlactones (**1**, **2**) was attempted by Ellen Rykers as part of an undergraduate project in the Lawrence Group at the Australian National University in Canberra.[20] At the time, γ-lactone **4** was deemed to be synthetically easier to target than δ-lactone **3** and it was proposed that angiopterlactones A and B (**1**, **2**) may be formed *via* isomerisation/dimerisation of γ-lactone **4**.

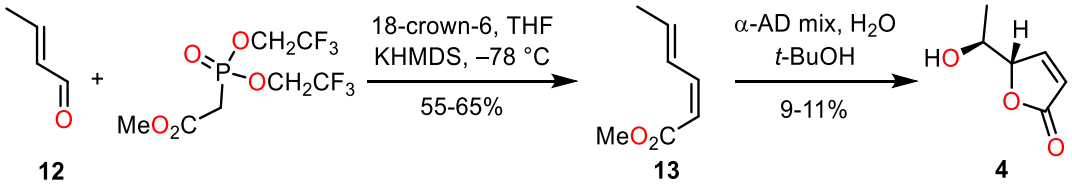

Scheme 5: Synthesis of γ-lactone **4** (*unpublished work; E. Rykers*)[20]

The enantioselective synthesis of γ-lactone **4** was achieved in two steps (Scheme 5). The first step was a Still–Gennari (modified Horner–Wadsworth–Emmons) reaction of crotonaldehyde **12**, to yield (*Z*,*E*)-dienoate **13** in 60% isolated yield. Dienoate **13** was then regio- and enantioselectively dihydroxylated using the Sharpless asymmetric dihydroxylation (SAD) reaction with subsequent spontaneous cyclisation resulting in lactone **4**. However, the fittingly named "SAD" reaction resulted in very poor overall yields and the isolation of pure compound proved to be particularly challenging. Despite these difficulties, small quantities of pure γ-lactone **4** were isolated, which were utilised to examine an array of isomerisation and dimerisation conditions. These included varying the solvent, temperature and additive (both acids and bases). None of the conditions tested resulted in successful isomerisation or dimerisation and instead the only observed outcomes were either no reaction, epimerisation of lactone **4** or dehydration of lactone **4** (see examples in Scheme 6).

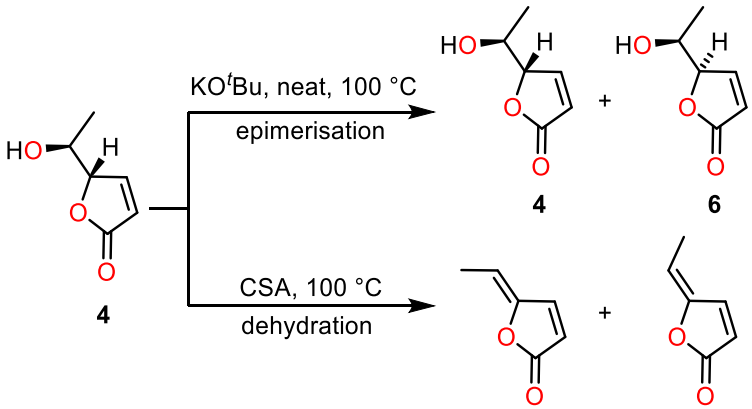

Scheme 6: Failed dimerisation attempts of lactone **4** (*unpublished work; E. Rykers*)[20]

1.1.5 Planned Synthetic Approach

The lack of success in isomerising or dimerising γ-lactone **4** indicated that accessing δ-lactone **3** was essential for further investigations into the biomimetic synthesis of (−)-angiopterlactone A (**1**) and (+)-angiopterlactone B (**2**). An extensive literature search for pre-existing syntheses of δ-lactone **3**, revealed that a variety of such procedures exist. Of the available reported syntheses, there were two of particular interest, due to their step economy (Scheme 7). The first of the two options was reported by Zhang and co-workers in 2007.[8] The authors utilise a chiral pool starting material in order to gain access to lactone **3** in four steps. The second option was presented by Guo, Tang and co-workers.[21] They achieved an enantioselective synthesis of lactone **3** in a mere three steps and so this synthesis formed the basis of our synthetic plan. The synthesis reported by Guo, Tang and co-workers began with the commercially available and inexpensive 2-acetylfuran (**14**). Upon completing an enantioselective Noyori reduction, the resulting (*S*)-alcohol **15** was subjected to an Achmatowicz reaction to form lactol **16** as an inconsequential mixture of diastereoisomers. A diastereoconvergent isomerisation then gave access to the required (*S*,*S*)-lactone **3**.

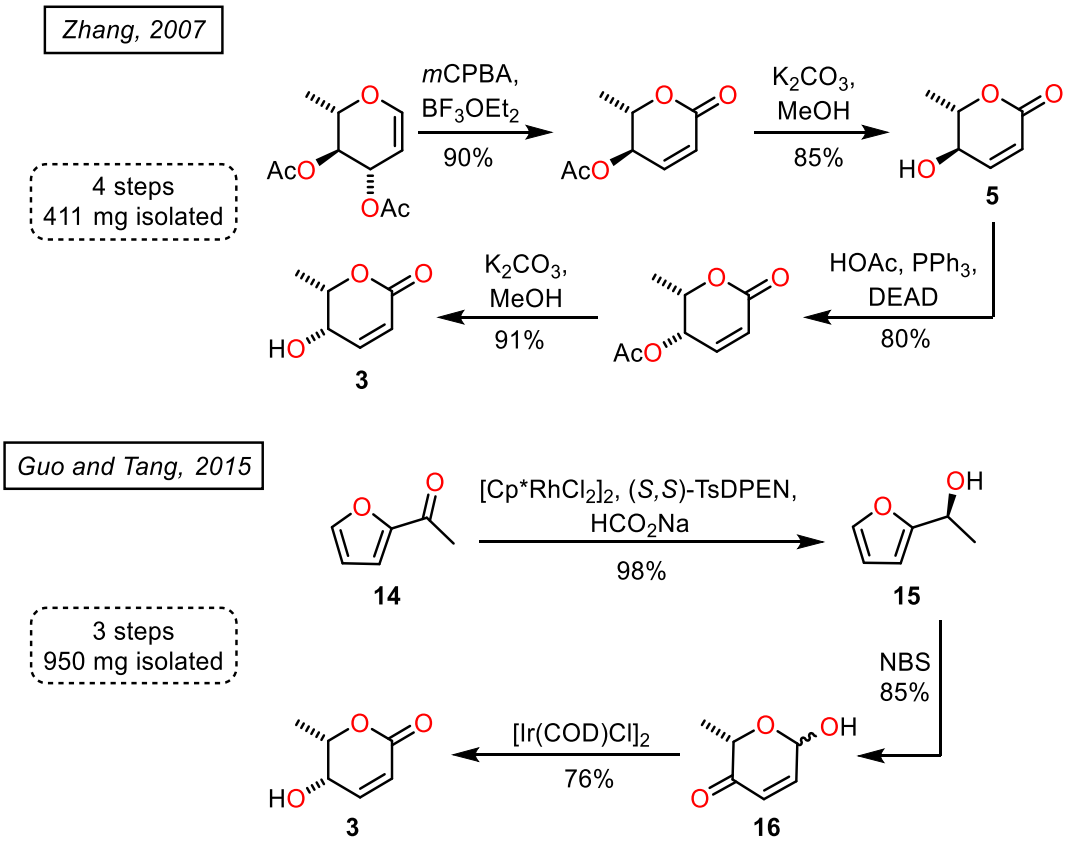

Scheme 7: Two literature syntheses of lactone **3**[8,21]

1.2 Results and Discussion

The synthesis of (−)-angiopterlactone A (**1**) and (+)-angiopterlactone B (**2**) was envisioned to proceed by isomerising and dimerising δ-lactone **3**. Following a similar protocol to that reported by Guo, Tang and co-workers,[21] our initial endeavours were focused towards synthesising δ-lactone **3** *via* a three step process from 2-acetylfuran (**14**) (Scheme 8).

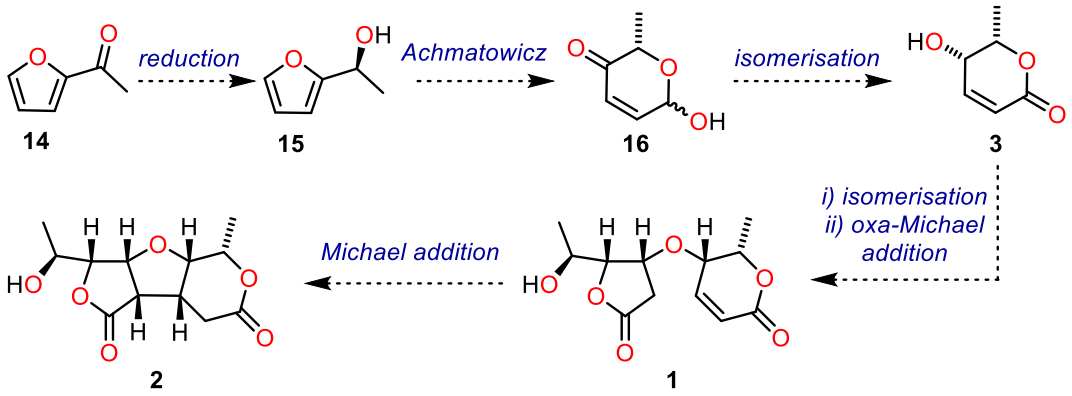

Scheme 8: Our planned synthetic route towards the angiopterlactones (**1**, **2**)

1.2.1 Synthesis of Lactone **3**

*Synthesis of (S)-Alcohol **15***

The first step in the synthesis towards lactone **3** is the enantioselective reduction of a ketone to a secondary alcohol. Our natural product targets require access to enantiopure material, as Zou and co-workers report the isolation of angiopterlactone A (**1**) and angiopterlactone B (**2**) in enantio-enriched form.[2] In the year 1980, Noyori and co-workers reported the use of cationic Rh-BINAP complexes in asymmetric hydrogenations of α-(acylamino) acrylic acid derivates to gain access to the analogous amino acid derivatives in high enantiomeric excess.[22] Since then, extensive research has been completed in the field, leading Noyori and co-workers to the discovery of oligomeric halogen-containing Ru(II)-BINAP complexes.[22] These complexes proved to be efficient catalysts for the asymmetric hydrogenation of functionalised ketones. The so-called "Noyori asymmetric hydrogenation" refers to the reduction of ketones and olefins, utilising hydrogen gas and Ru(II)-BINAP complexes. A baffling number of applications for the Noyori asymmetric hydrogenation have been reported in the literature. An example within natural product synthesis includes the stereocontrolled and convergent synthesis of the CD spiroketal unit of spongistatin 1 (**17**) (Scheme 9).[23] This natural product

is a marine macrolide that displays exceptional anti-tumour activities against a variety of human cancer cell lines.[22,24] On route to the spiroketal unit **17**, Holson and Roush utilised the (*R*)-enantiomer of the BINAP ligand to access (*R*)-alcohol **18** in good yield and high enantiomeric ratio (e.r.) (Scheme 9).[23]

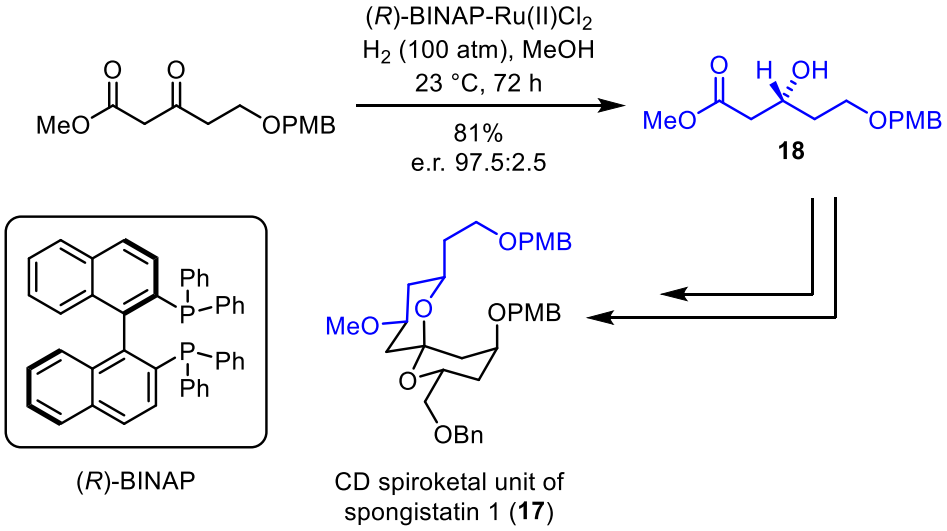

Scheme 9: Noyori asymmetric hydrogenation in the synthesis towards the CD spiroketal unit of spongistatin 1 (**17**)[23]

Since the development of Ru(II)-BINAP complexes, further research in the field led to the discovery of a highly enantioselective reduction with a new class of chiral ruthenium catalyst. These catalysts employ toluenesulfonyl-diphenylethylenediamine (TsDPEN) as a ligand and have since been applied in a wide-range of reactions, particularly for prochiral ketones and imines.[25,26] Xiao and co-workers reported asymmetric transfer hydrogenations of ketones using formate in water and a rhodium catalyst with a TsDPEN ligand.[26] Such reactions are particularly attractive due to the non-toxic and non-flammable properties of water. Carreira and co-workers report a procedure for the enantioselective reduction of 2-acetylfuran (**14**) (our proposed starting material) to alcohol ***ent*-15** utilising such a Rh-TsDPEN complex (**19**).[27] Despite requiring access to alcohol **15**, we utilised Carreira's method to initially target alcohol ***ent*-15**, simply because we had immediate access to the (*R*,*R*)-TsDPEN ligand.

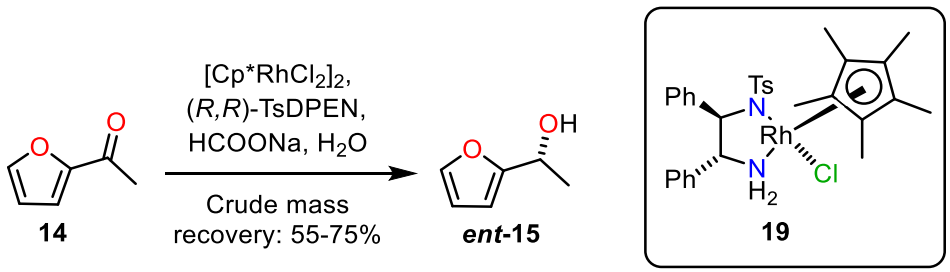

Scheme 10: Enantioselective reduction of **14** to alcohol ***ent*-15**

The procedure outlined by Carreira *et al.* involves the *in situ* formation of rhodium catalyst **19**. Subsequent addition of sodium formate and 2-acetylfuran (**14**), resulted in the formation of alcohol ***ent*-15** in 99% yield. Upon implementation of this literature procedure, we successfully accessed alcohol ***ent*-15** (Scheme 10), however we discovered several drawbacks to the reaction. Firstly, we could not reproduce the high yield reported by Carreira and co-workers.[27] Instead only a moderate crude mass recovery was achieved, ranging between 55-75%. Furthermore, full conversion of starting material to product was never observed, despite reaction times exceeding the 23 hours suggested by the literature. As we could not reliably reproduce the literature results, we investigated alternative conditions for the enantioselective reduction of 2-acetylfuran (**14**).

Alternative conditions for the enantioselective reduction of 2-acetylfuran (**14**) were developed by Paterson and Haslett.[28] This involved the use of (*S*,*S*)-Noyori catalyst **20**, formic acid and triethylamine, to afford alcohol **15** in 99% yield and in an e.r. of 99:1.[28] We synthesised (*S*,*S*)-Noyori catalyst **20** following a literature procedure reported by Noyori and co-workers, which afforded us with more than 700 mg of the catalyst in >95% yield (Scheme 11).[29] Reduction of 2-acetylfuran (**14**) to alcohol **15**, utilising freshly prepared (*S*,*S*)-Noyori catalyst **20**, was successfully accomplished with a crude mass recovery >95%. The ^{1}H NMR spectrum showed very clean formation of product. During purification by column chromatography, a loss of approximately 50% of the mass was consistently observed. It was therefore decided to use the crude material in the next step of the synthesis without purification. The e.r. was determined by chiral HPLC by comparison to authentic samples of racemic alcohol **15**. After repeating the experiment several times on various scales, it was eventually completed on a multi-gram scale, affording sufficient material with which to continue the synthesis towards δ-lactone **3**.

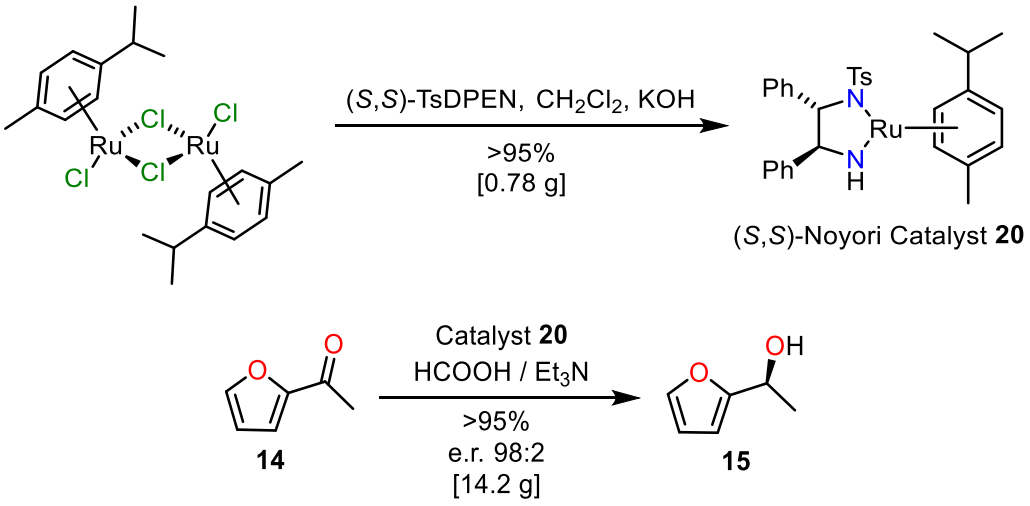

Scheme 11: Synthesis of (*S*,*S*)-Noyori catalyst **20** and the enantioselective reduction of 2-acetylfuran (**14**) to alcohol **15**

*Synthesis of Lactol **16***

With alcohol **15** in hand, we set out to investigate the subsequent conversion to lactol **16** (Scheme 8, Page 22). The conversion of alcohol **15** to lactol **16** can be achieved utilising the Achmatowicz rearrangement. The Achmatowicz rearrangement is a reaction in which furfuryl alcohols undergo an oxidative ring enlargement.[30] There are numerous conditions with which furfuryl alcohols can undergo an Achmatowicz rearrangement. One of the most common sets of conditions, which has shown great success in the total synthesis of complex natural products, utilises *N*-bromosuccinimide (NBS) in aqueous tetrahydrofuran (THF).[30] An example of an NBS mediated Achmatowicz rearrangement can be found in the total synthesis of castasterone (**21**), a plant-growth-regulating steroid (Scheme 12).[31] Upon subjecting furfuryl alcohol **22** to NBS in THF and H_2O, Honda and co-workers isolated lactol **23** in 92% yield.

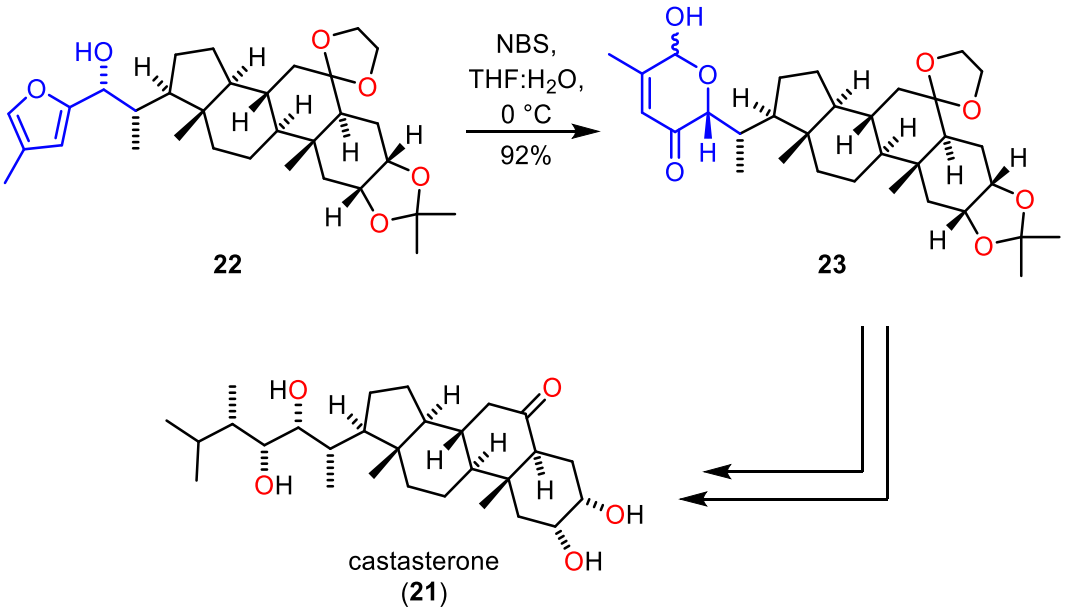

Scheme 12: Achmatowicz rearrangement step in the total synthesis of castasterone (**21**)[31]

Similar conditions were utilised by Guo, Tang and co-workers, whose general synthetic strategy we were following to gain access to lactone **3** from 2-acetylfuran (**14**) (Scheme 7, Page 21). It has been suggested in the literature that the Achmatowicz rearrangement proceeds *via* bromination and oxidation of the furfuryl alcohol, followed by ring opening and consequent ring enlargement (Scheme 13).[30,32] Implementation of this NBS-mediated rearrangement led us to the successful conversion of alcohol **15** to an inconsequential diastereomeric mixture (2:1) of lactol **16** (Scheme 13). Presumably this 2:1 ratio is in favour of the *cis* isomer, as Guo, Tang and co-workers[21] reported a 3:1 *cis*:*trans* ratio of lactol **16**. However, as the authors did not provide NMR data it is hard to determine for certain whether our attained 2:1 ratio favours the *cis*- or the *trans*-diastereoisomer. Our synthesis of lactol **16** was successfully scaled-up, with the largest scale reaction affording over four grams of material.

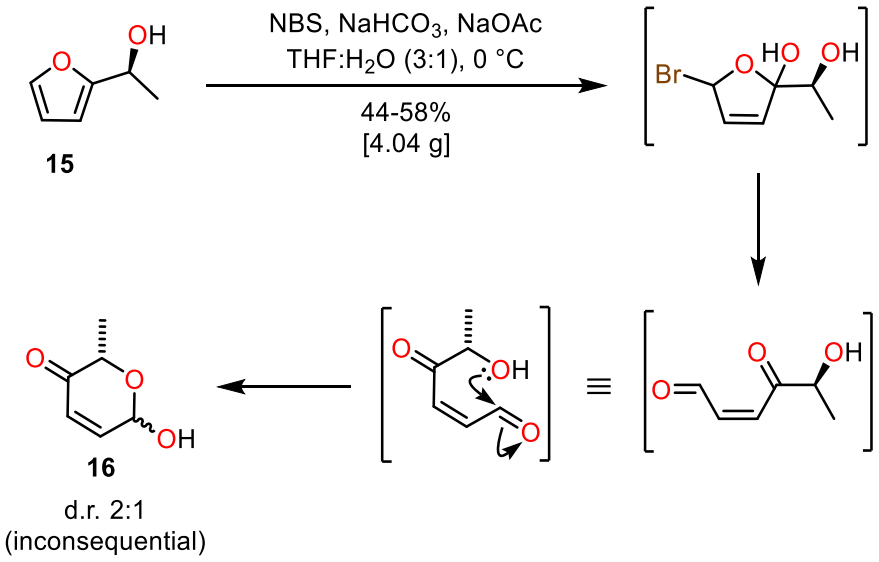

Scheme 13: Our Achmatowicz rearrangement of alcohol **15** to lactol **16**

*Synthesis of lactone **3** / Dynamic Kinetic Isomerisation*

With several grams of lactol **16** in hand, our attention turned towards the diastereoconvergent isomerisation of lactol **16** to (*S*,*S*)-lactone **3**. Guo, Tang and co-workers recently developed an iridium-catalysed dynamic kinetic isomerisation reaction which allows such a transformation.[21] This is a rare example of a stereoconvergent internal transfer hydrogenation and the authors proposed a mechanism for this reaction (Scheme 14). The dehydrogenation of **A** and **B** is presumed to afford the metal complexes **C** and **D** respectively. Hydrogenation is then thought to result in products **E** and **F**. In the absence of a Brønsted acid catalyst, Guo, Tang and co-workers observed a ratio of 3:1 of **E**:**F**. They propose this to be a result of the rate of equilibration between the hemiacetals being slower than the rate of the internal transfer hydrogenation. Upon addition of an acid additive, the rate of interconversion between **A** and **B** became significantly faster than the internal transfer hydrogenation, making the stereoselective dynamic kinetic isomerisation possible.[21]

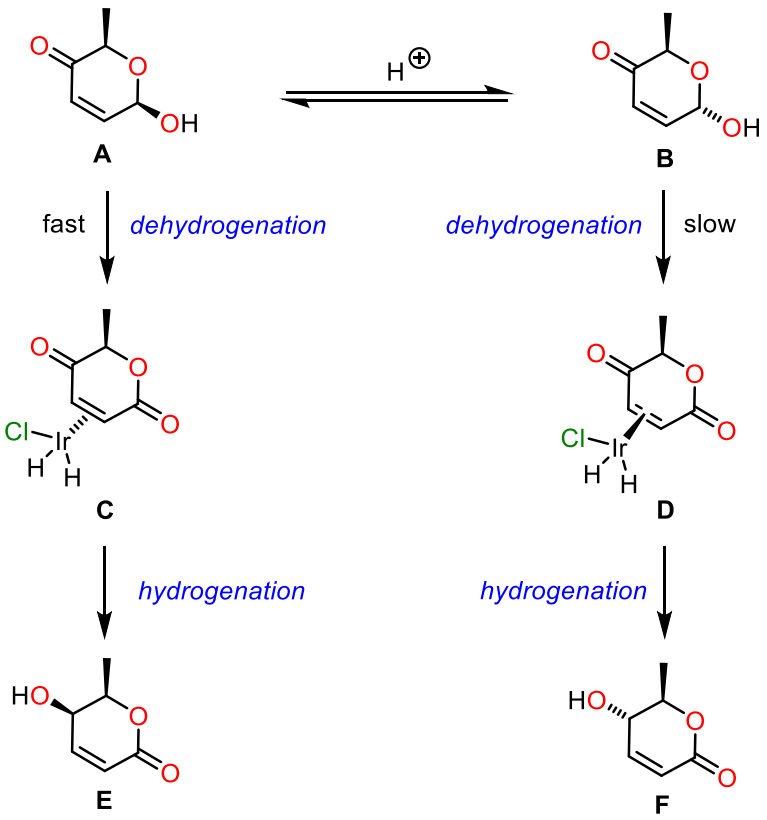

Scheme 14: Guo, Tang and co-workers' proposed mechanism for the iridium-catalysed isomerisation[21]

Guo, Tang and co-workers completed optimisation studies and tested the scope for the transformation of various lactol species to their corresponding lactones. This led them to optimised conditions which consisted of utilising an Ir(COD)Cl dimer and 2,6-dichlorobenzoic acid in chloroform.[21] We subjected our lactol **16** to these conditions, to successfully gain access to (*S*,*S*)-lactone **3** with a high e.r. of 98:2 (Scheme 15). Upon scale-up experiments the reaction was carried out on gram-scale, affording 2.7 g of lactone **3**. With several grams of the monomeric lactone **3** in hand, efforts turned toward screening dimerisation conditions to target the angiopterlactones (**1**, **2**).

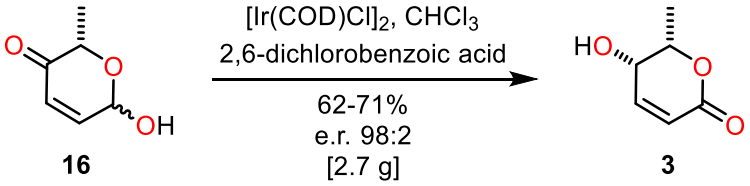

Scheme 15: Iridium-catalysed isomerisation of lactol **16** to lactone **3**

1.2.2 Dimerisation Studies

It was our aim to find suitable conditions for the dimerisation of lactone **3** and then optimise them in order to selectively access either (−)-angiopterlactone A (**1**) or (+)-angiopterlactone B (**2**).

Initially, we set out to utilise analogous dimerisation conditions to those which had previously been applied within the Lawrence group, due to the similarity in the domino oxa-Michael/Michael THF ring forming reaction (Scheme 4, Page 19).[17] These involved dissolving the starting material in dichloroethane, adding potassium carbonate and leaving the reaction mixture to stir overnight at 70 °C. The results from this first dimerisation attempt were very promising, as they successfully yielded 35% of the natural product (−)-angiopterlactone B (**2**) (Scheme 16). By inspection of the crude ^{1}H NMR data, we could also determine the presence of unreacted starting material **3**, γ-lactone **4** and γ-lactone **6**. The formation of γ-lactone **4** is presumably a result of our planned ring contraction from the starting material. The γ-lactone **6** is likely a consequence of base-mediated epimerisation of γ-lactone **4**.

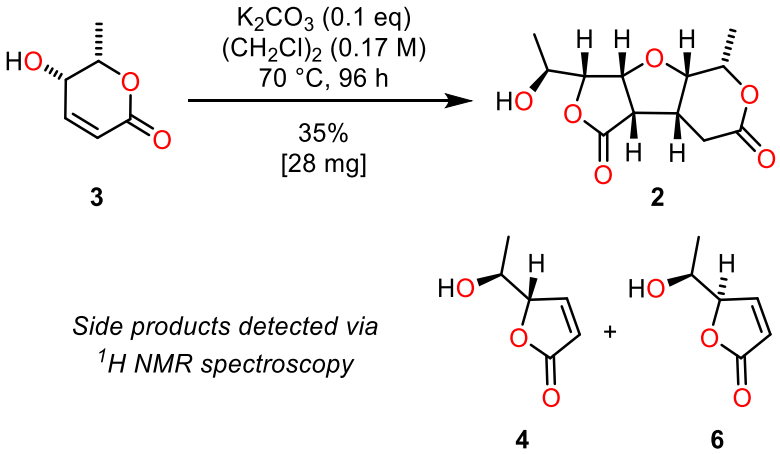

Scheme 16: Our initial dimerisation attempt of lactone **3** to yield angiopterlactone B (**2**) and side-products **4** and **6**

With our initial dimerisation attempt giving us an immediate hit, we wanted to investigate how modifying the reaction conditions might affect the outcome. We began by running the reaction at various temperatures. It was observed that at 40 °C no reaction occurred within three hours, whereas at 70 °C formation of dimer **2** could be observed within 30 minutes of starting the reaction. For temperatures exceeding 70 °C, the solvent dichloroethane (boiling point of 83 °C)[33] was removed before heating. At 110 °C, conversion of some starting material to product **2** was observed, however with significant amounts of decomposition. At 160 °C, an even higher rate of decomposition was noted. With these results in mind, all following dimerisation attempts of lactone **3** were performed at 70 °C.

Optimisation studies

Our initial conditions of potassium carbonate, dichloroethane and stirring at 70 °C overnight, formed the basis of our investigations. Dimerisation conditions were screened by completing small scale reactions, utilising internal standards and ^{1}H NMR spectroscopy to gain quantitative data. The results of these reactions are summarised in Tables 1-6.[1]

Varying the additive

The investigation began by probing whether or not an additive was necessary for the dimerisation reaction to occur. Upon heating lactone **3** in dichloroethane overnight, no consumption of starting material could be detected by ^{1}H NMR spectroscopy and thus it was concluded that an additive was indeed required. The next step was to investigate replacing potassium carbonate with alternative reagents (Table 1).

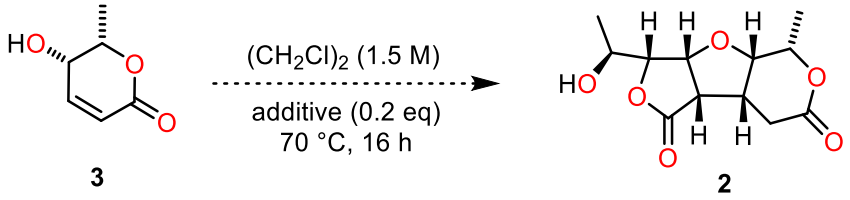

3 **2**

entry	**additive (0.2 eq)**	**δ-lactone 3 (%)**	**γ-lactone 4 (%)**	**γ-lactone 6 (%)**	**dimer 2 (%)**
1	Li_2CO_3	88	<1	<1	0
2	Na_2CO_3	84	<1	0	0
3	$NaHCO_3$	79	<1	0	0
4	K_2CO_3	9	2	2	25
5	Rb_2CO_3	6	<1	<1	19
6	Cs_2CO_3	11	1	<1	18
7	$(NH_4)_2CO_3$	29	3	1	0
8	$MgCO_3$	86	<1	<1	0
9	$CaCO_3$	87	<1	0	0
10	KOH	42	4	3	10
11	Pyrrolidine	47	20	7	0
12	PTSA	0	57	3	0

Table 1: Additive screen – Reproduced from *Org. Lett.* 2017, *19* (9), 2199–2201[1]

It is interesting to note that all trialled additives resulted in the formation of some γ-lactone **4** and epimerised γ-lactone **6** (Scheme 16). The only reactions which resulted in successful dimerisation to angiopterlactone B (**2**) were entries 4, 5, 6 and 10. Entry 4 (potassium carbonate) provided the best yield and thus we continued our investigations utilising this additive. It is also interesting to note that our reaction conditions utilising PTSA at 70 °C, allow the formation of the ring-contracted γ-lactone **4** in 57% yield, with full consumption of the starting material and only minor quantities of the epimerised γ-lactone **6** present. The

previously reported methods in the literature for such ring contractions are less efficient and practical, requiring several months to obtain full consumption of the starting material.[6,9]

Varying the potassium carbonate equivalents

With potassium carbonate shown to be the highest yielding additive, the next step was to investigate the optimal stoichiometry. We trialled 0.2, 0.5 and 1.0 equivalents and found that the largest yield was provided by 0.2 equivalents (Table 2). The scale of these reactions was too small to accurately weigh out 0.1 equivalents of potassium carbonate. A larger scale reaction (400 mg of starting material **3**) allowed the use of 0.1 equivalents of potassium carbonate and resulted in 28% isolated yield of dimer **2** (entry 1, Table 2). Further screening of conditions was completed on the same scale as previous attempts and therefore 0.2 equivalents of potassium carbonate were utilised to enable accurate measurements.

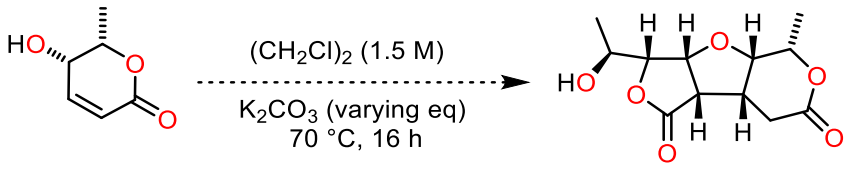

3 **2**

entry	**K_2CO_3 equivalents**	**δ-lactone 3 (%)**	**γ-lactone 4 (%)**	**γ-lactone 6 (%)**	**dimer 2 (%)**
*1**	0.1	-	-	-	28
2	0.2	9	2	2	25
3	0.5	5	<1	<1	19
4	1.0	3	0	0	16

*larger scale reaction (400 mg of starting material **3**); 1.1 M, 70 °C, 40 h; yield refers to isolated yield

Table 2: Potassium carbonate equivalents screen
Reproduced in part from *Org. Lett.* 2017, *19* (9), 2199–2201[1]

Varying the solvent

After varying the potassium carbonate equivalents, our investigation turned towards the solvent. Upon trialling alternative solvents (Table 3), it was found that dimer **2** formed in all of them (entries 1-7). Unfortunately chloroform and dichloromethane could not be heated to sufficient temperatures for a reaction to occur within an acceptable time frame.

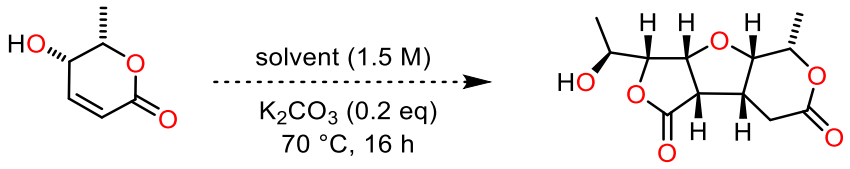

entry	**solvent***	**δ-lactone 3 (%)**	**γ-lactone 4 (%)**	**γ-lactone 6 (%)**	**dimer 2 (%)**
1	dichloroethane	9	2	2	25
2	water	23	3	1	8
3	toluene**	10	<1	<1	5
4	acetonitrile	47	5	5	11
5	carbon tetrachloride	38	2	2	11
6	cyclohexane	27	2	2	9
7	2-methyl THF	21	1	1	12

*Chloroform and dichloromethane were trialled, but these could not be heated to sufficient temperatures for the dimerisation to take place in an acceptable time frame.
**Poor crude mass recovery of <40%.

Table 3: Solvent screen – Reproduced from *Org. Lett.* 2017, *19* (9), 2199–2201[1]

Throughout the screening of conditions, the related natural product (−)-angiopterlactone A (**1**) (proposed intermediate to angiopterlactone B (**2**)) was not observed. Zou and co-workers, who isolated both angiopterlactones (**1**, **2**), reported the NMR data for (−)-angiopterlactone A (**1**) in deuterated dimethylsulfoxide (*d6*-DMSO).[2] It was therefore reasoned that running and monitoring the reaction directly in this solvent, could facilitate detection of (−)-angiopterlactone A (**1**) and/or other intermediates and side-products. Further to the results listed in Table 3, the reaction was completed in *d6*-DMSO, with initial attempts revealing a successful dimerisation process. The ^{1}H NMR spectrum of the crude dimerisation product did not reveal the presence of (−)-angiopterlactone A (**1**). Unfortunately the heterogeneous nature of the reaction mixture complicated the running of the dimerisation directly in an NMR tube in the spectrometer. Further screening of dimerisation conditions was completed utilising dichloroethane, as product extraction from DMSO in larger scale reactions led to major loss of material.

Varying the concentration

Following our investigations into various solvents, we wanted to test whether a solvent was necessary for the reaction to occur. To this end, we heated neat lactone **3** with potassium carbonate which resulted in no reaction, therefore suggesting that the starting material and potassium carbonate (partially soluble in dichloroethane) must first be homogenised. Thus we tested dissolving the starting material first and adding potassium carbonate, before removal of

the solvent from the reaction mixture and consequently heating to 70 °C. Although this led to some dimerisation, it was found that the lack of solvent hindered consumption of starting material. Thus we investigated the effect of concentration on the dimerisation reaction. The reaction was completed utilising dichloroethane, with concentrations ranging from 0.5 M to 6.8 M (Table 4). The best results were obtained at concentrations of around 1.5-3.1 M.

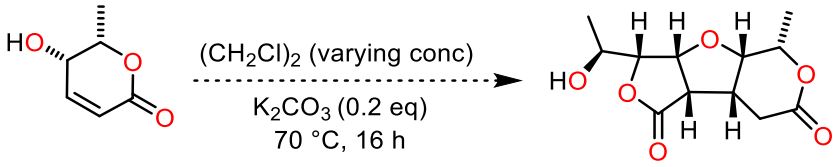

3 **2**

entry	[3] (M)	δ-lactone 3 (%)	γ-lactone 4 (%)	γ-lactone 6 (%)	dimer 2 (%)
1	0.5	66	2	<1	5
2	0.8	14	2	2	15
3	1.5	9	2	2	25
4	3.1	13	3	3	28
5	6.8	49	3	2	16

Table 4: Concentration screen – Reproduced from *Org. Lett.* 2017, *19* (9), 2199–2201[1]

Varying the reaction time

The final investigation we conducted on δ-lactone **3** was how reaction time affects the outcome. We noted that formation of dimer **2** reached a plateau after eight hours, with longer reaction times (e.g. 42 hours, entry 7, Table 5) leading to nearly full consumption of the starting material, without increasing the yield of dimer **2**.

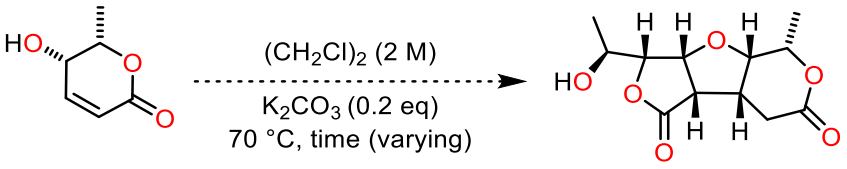

3 **2**

entry	time (h)	δ-lactone 3 (%)	γ-lactone 4 (%)	γ-lactone 6 (%)	dimer 2 (%)
1	1	66	3	2	5
2	2	56	4	2	12
3	3	55	4	3	15
4	4	44	4	3	18
5	5	37	5	4	20
6	8	15	3	2	26
7	42	2	0	0	26

Table 5: Variation of reaction time – Reproduced from *Org. Lett.* 2017, *19* (9), 2199–2201[1]

Further tests

Our investigations into various additives revealed that we could access γ-lactone **4** from δ-lactone **3** by utilising PTSA. Scaling-up this reaction led to the isolation of 75 mg of γ-lactone **4**. This material was then used to test the dimerisation conditions on this lactone, as well as on mixtures of the γ- and δ-lactones (**3**, **4**) (Table 6).

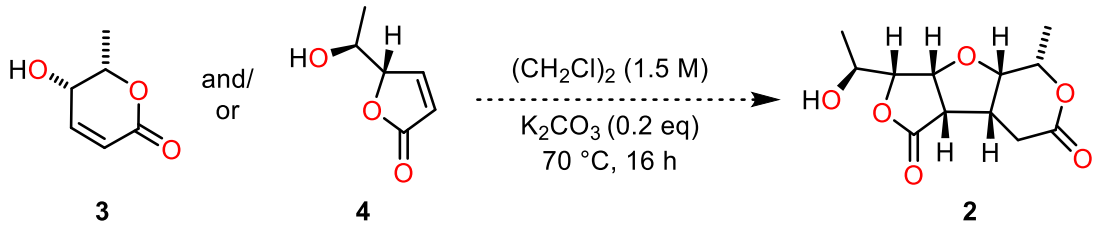

entry	starting material	δ-lactone 3 (%)	γ-lactone 4 (%)	γ-lactone 6 (%)	dimer 2 (%)
*1**	**4**	0	6	6	0
*2**	**3** (0.5 eq) & **4** (0.5 eq)	22	8	7	4
*3**,***	**3** (1 eq) & **4** (0.1 eq)	8	1	1	16
4	**3**	9	2	2	25

* Note: γ-lactone **4** was slightly wet
** Note: 1.8 M instead of 1.5 M

Table 6: Dimerisation reactions utilising γ-lactone **4**

Upon subjecting γ-lactone **4** to the dimerisation conditions previously utilised (entry 1), epimerisation to γ-lactone **6** was observed. There was no formation of dimer **2** or δ-lactone **3**. This suggests that that the ring contraction from δ-lactone **3** to γ-lactone **4** is indeed irreversible (as previously observed by Ellen Rykers; further investigations are discussed in Chapter 3)[20]. Furthermore, we noted that the ^{1}H NMR spectrum showed some evidence of decomposition, suggesting that γ-lactone **4** may not be stable to the dimerisation conditions. This could explain our previous observations that upon longer reaction times, we do not increase the yield of dimer **2**, but simultaneously consume almost all of the starting material (**3**) (Table 5).

An equal mixture of δ-lactone **3** and γ-lactone **4** (entry 2) resulted in a lower yield of dimer **2**, than when only δ-lactone **3** was utilised (4% *vs* 25%). Thus we completed a further test in which we added 10mol% of γ-lactone **4** to δ-lactone **3** (entry 3), which increased the yield of dimer **2** to 16%. This points towards the γ-lactone **4** not being directly involved in the dimerisation or perhaps even hindering the production of dimer **2**.

With the finalised reaction conditions in hand (K_2CO_3, dichloroethane, 70 °C), we turned our attention to testing the reproducibility and robustness of the dimerisation. The reaction was progressively scaled up from 20 mg to 3.5 g, with the final large scale reaction allowing for

the isolation of 864 mg of the natural product angiopterlactone B (**2**) in a single step (Scheme 17). We then subjected the purified angiopterlactone B (**2**) to the dimerisation conditions, in order to ascertain whether it is stable to these conditions. After several hours, angiopterlactone B (**2**) remained unreacted.

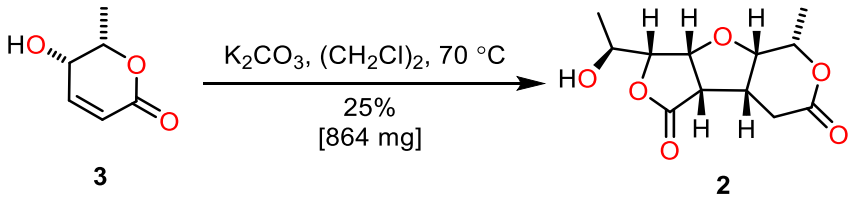

Scheme 17: Final large scale dimerisation reaction of lactone **3** to angiopterlactone B (**2**)

Intriguing observations

Examination of the ^{1}H NMR spectrum of the crude dimerisation product of enantio-enriched lactone **3** reveals a remarkably selective reaction (Figure 3). The four major species present include recovered starting material (**3**), angiopterlactone B (**2**) and the two γ-lactones **4** and **6**. Given the presence of the three lactones **3**, **4** and **6** there are nine possible permutations to combine two of the three lactones and each pairing could result in eight diastereoisomers. Thus there are 72 possible dimeric structures (9 x 8 = 72), which could form *via* a domino oxa-Michael / Michael reaction. It is therefore surprising that we observe the formation of a single dimeric structure, namely that of angiopterlactone B (**2**). The selectivity of this dimerisation reaction is further explored in Chapter 3.

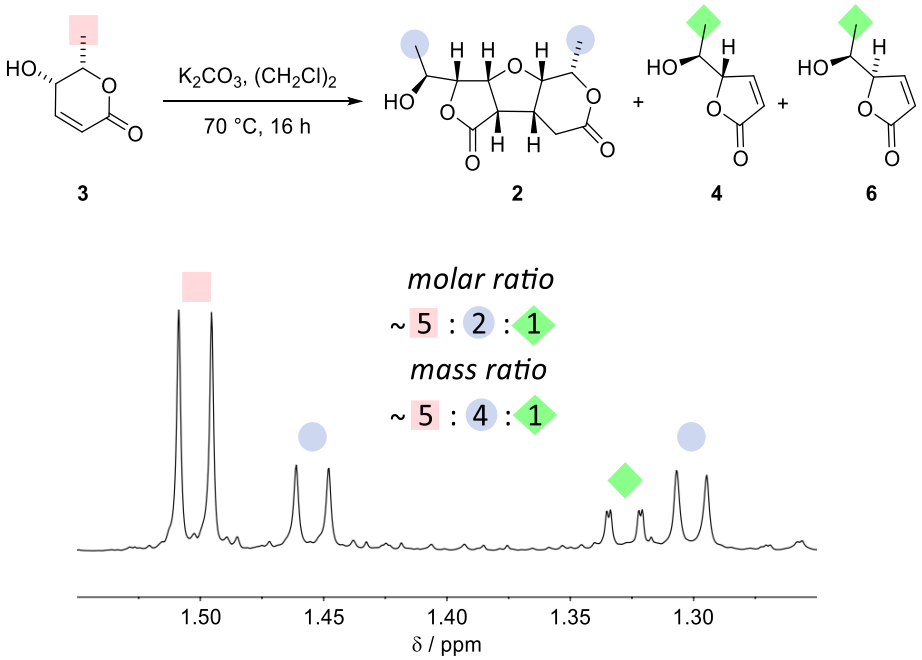

Figure 3: Methyl region of the ^{1}H NMR spectrum of the crude dimerisation product (500 MHz, $CDCl_3$) Reproduced in part from *Org. Lett.* 2017, *19* (9), 2199–2201[1]

1.2.3 Structural Revision of (+)-Angiopterlactone B

With angiopterlactone B (**2**) in hand, we investigated the structure proposed by the isolation chemists. Zou and co-workers reported an optical rotation of +22 (*c* 0.04, EtOAc),[2] whereas that measured for our synthetic material was −25 (*c* 0.04, EtOAc).[1] The absolute configuration of our synthetic material, (−)-angiopterlactone B (**2**), can be inferred from that of the preceding intermediates (**3** and **15**). It was further confirmed by the Flack parameter of 0.02(3) (explained in detail below), obtained during our X-ray crystallographic studies.[1,34] We can therefore unequivocally assign the absolute configuration of our synthetic material, (−)-angiopterlactone B (**2**). This led us to propose that the absolute configuration of the natural material, (+)-angiopterlactone B (**2**) needs to be revised (Figure 4).

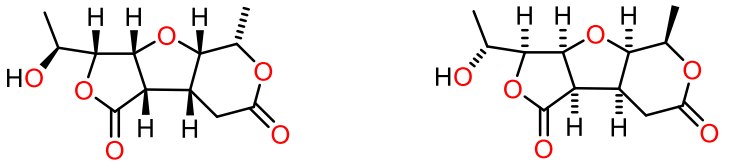

(+)-angiopterlactone B (**2**)
originally proposed structure
(Zou & co-workers, 2009)

(+)-angiopterlactone B (**2**)
revised structure

Figure 4: Originally proposed[2] structure of (+)-angiopterlactone B (**2**) and our revised structure[1]

By considering our previously proposed biosynthesis (Scheme 1, Page 17), the revision of the absolute configuration reveals the known natural product angiopteroside (**9**) as a likely biosynthetic precursor (Scheme 18). Angiopteroside (**9**) is a glycoside natural product that has been isolated from several *Angiopteris* plants and was found to display promising activity for the inhibition of HIV-1 Reverse Transcriptase.[35,10,3]

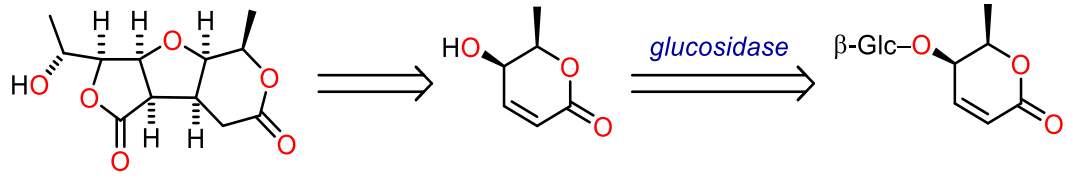

(+)-angiopterlactone B (**2**)
revised structure

***ent*-3**

angiopteroside (**9**)

Scheme 18: Angiopteroside (**9**) as a likely biosynthetic precursor to (+)-angiopterlactone B (**2**)

Two months after the publication of our total synthesis of (−)-angiopterlactone B (**2**) in *Organic Letters*,[1] Bhattacharya and co-workers published a related total synthesis in the same journal.[36] Their synthesis features the same intermediate δ-lactone **3**, which upon subjecting to TBAF in anhydrous THF, resulted in a 62% yield of (−)-angiopterlactone B (**2**). Their seven

step synthesis towards δ-lactone **3** relies on the chiral pool starting material **24** and differs largely from our three step synthesis (Scheme 19).

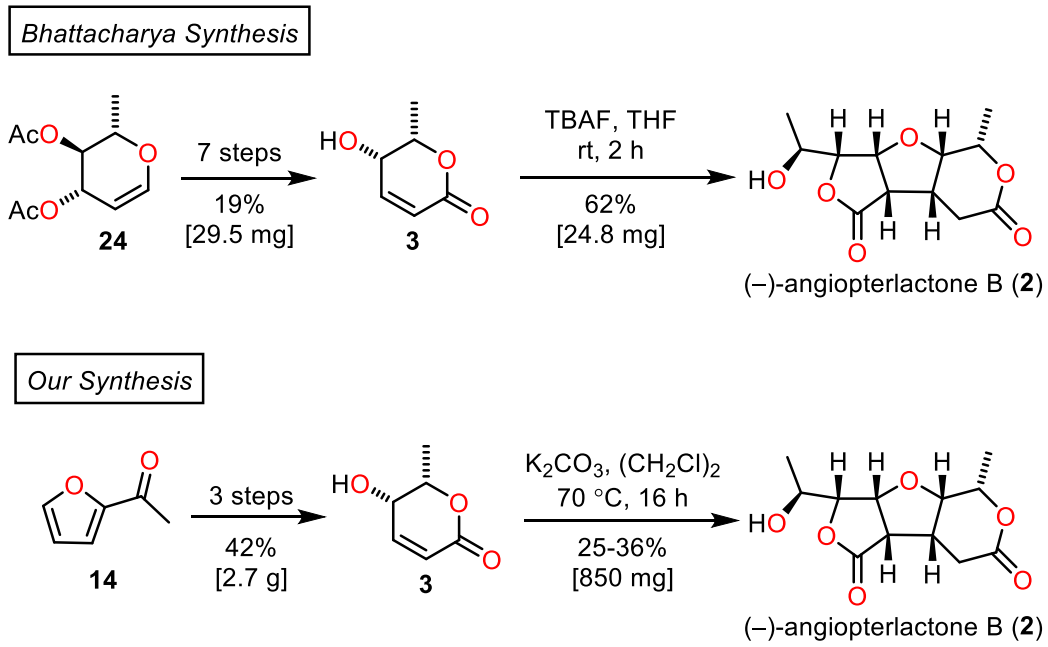

Scheme 19: Comparison of Bhattacharya synthesis[36] and our synthesis[1] of (−)-angiopterlactone B (**2**)

Similarly to ourselves, Bhattacharya and co-workers concluded that the isolation chemists' proposed structure for (+)-angiopterlactone B (**2**), did not coincide with their reported data. However, rather than re-assigning the absolute configuration of the natural material, Bhattacharya and co-workers state that their data unequivocally proves that the isolation chemists made a typographical error when reporting the sign of the optical rotation.[36] Bhattacharya *et al.* therefore suggest that the natural material is (−)-angiopterlactone B (**2**). This made us curious and thus we wanted to investigate this claim further. The methods utilised by the isolation chemists (Zou *et al.*)[2], ourselves[1] and Bhattacharya and co-workers[36] to assign the relative and absolute configuration of (+)/(−)-angiopterlactone B (**2**) are summarised in Table 7.

	Zou[2]	**Lawrence**[1]	**Bhattacharya**[36]	
$[\alpha]_D^{20}$ *(c 0.04, EtOAc)*	+22	−25	−24	+33
Cotton effect	negative		negative	positive
Relative stereochemistry determined by	X-ray	X-ray	X-ray	X-ray
Absolute stereochemistry determined by	CD: C4 & C3' Mosher: C6'	X-ray [0.02(3)]	X-ray [0.6(9)]*	X-ray [1.4(10)]*

Values within square brackets are the Flack parameter, with its standard uncertainty

*Note that Bhattacharya and co-workers did not report Flack parameters. These were extracted by our in-house crystallographer Gary Nichols using the files available on the CCDC database (1525957/1525958)

Table 7: Summary of the data recorded in each of the publications pertaining to the assignment of the relative and absolute configuration of (+)/(−)-angiopterlactone B (**2**)[1,2,36]

The basis of Bhattacharya and co-workers' claim that the natural material must be (−)-angiopterlactone B (**2**) is their observations from the CD excitation chirality method for their synthetic (+)- and (−)-angiopterlactone B (**2**). The latter resulted in a negative Cotton effect, which coincides with what the isolation chemists reported for the natural material. However, as the isolation chemists only reported the sign of the Cotton effect and did not provide the CD spectrum, it is possible that they made a typographical error when reporting the sign of the Cotton effect rather than the sign for the optical rotation. Therefore, Bhattacharya and co-workers cannot claim to have unequivocally assigned the natural material as (−)-angiopterlactone B (**2**). In order to gain further insights, we investigated how the relative and absolute configuration of angiopterlactone B (**2**) was determined in each of the publications.

Upon closer inspection of the available data, it can be said that all three publications agree upon the atom connectivity and relative stereochemistry within the molecule. However they differ in the assignment of the absolute configuration. We assigned the absolute stereochemistry based on the absolute configuration of our preceding synthetic intermediates, as well as our X-ray crystal structure. This crystal structure resulted in a Flack parameter (x) and standard uncertainty (u) of $x(u)$ = 0.02(3). Flack and Bernardinelli have previously reported that for the absolute configuration of a compound to be reliably determined by X-ray

crystallography, it must first be established that the standard uncertainty is reasonably small.[37] They state that u should be < 0.04 and x should be close to zero and within a region of three standard uncertainties (*i.e.*, $|x|/u < 3$).[37] Furthermore, Flack parameters > 0.5 typically indicate that the model of the crystal structure needs to be inverted.[34] The x and u values obtained from our X-ray crystal structure ($x = 0.02$, $u = 0.03$)) satisfy all of the aforementioned requirements, thus confirming the absolute configuration of our synthetic (−)-angiopterlactone B (**2**).

Bhattacharya and co-workers claim to have utilised X-ray crystallography to assign the absolute configuration. However, they did not provide the Flack parameter and standard uncertainty for their crystal structures and thus our in-house crystallographer Gary Nichol extracted them utilising the files available on the CCDC database. For (−)-angiopterlactone B (**2**) the Flack parameter is 0.6(9) and for (+)-angiopterlactone B (**2**) it is 1.4(10). Neither of these satisfy the above-mentioned requirements and thus Bhattacharya and co-workers cannot ascertain the absolute stereochemistry based on their crystal structure. Nevertheless, they could have deduced the absolute configuration from that of their preceding intermediates and by comparing their optical rotation to that of our synthetic (−)-angiopterlactone B (**2**).

The isolation chemists based their assignment of the absolute configuration on the CD excitation chirality method and the modified Mosher method. The modified Mosher method can be utilised to assign the configuration of secondary alcohol centres and a detailed description of how to complete a Mosher analysis was reported by Hoye, Jeffrey and Shao in 2007.[38] Upon reacting an alcohol separately with each of the enantiomers of α-methoxy-α-trifluoromethylphenylacetyl chloride (MTPA-Cl), diastereomeric esters are produced (Scheme 20).[38] Analysis of the differences in the ^{1}H NMR chemical shifts of the (*S*)- and (*R*)-Mosher esters ($\Delta\delta_H$ (*S*-*R*)) can then allow the assignment of the absolute configuration of the carbinol centre.[38] The isolation chemists utilised this method to determine the absolute stereochemistry of position C6' (Figure 5). Based on their analysis of $\Delta\delta_H$ (*S*-*R*), they conclude that H7' has a negative value (−0.09) and H2' and H4' have positive values (+0.01 and +0.02 respectively) and thus position C6' must be *S*.[2]

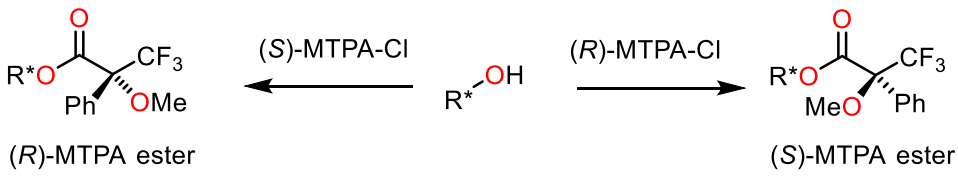

Scheme 20: Modified Mosher method; Reacting a secondary carbinol with the (S)-/(R)-MTPA-Cl to produce two diastereomeric MTPA esters[38]

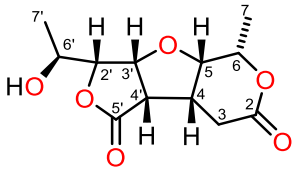

(–)-angiopterlactone B (**2**)

Figure 5: Numbering within (−)-angiopterlactone B (**2**)

The isolation chemists report the procedure to prepare the (*S*)- and (*R*)-Mosher ester of their (+)-angiopterlactone B (**2**) and also attached the relevant spectra in their supporting information, allowing us to review their analysis. Upon closer inspection of their procedure for the preparation of the MTPA esters of (+)-angiopterlactone B (**2**), we noted that the authors state that reacting (*S*)-MTPA chloride with the natural product, resulted in the (*S*)-MTPA ester. This cannot be the case as the (*R*)-MTPA chloride is required to synthesise the (*S*)-MTPA ester (Scheme 20). Without further information, we cannot determine whether the typographical error results from the stereochemical assignment of the MTPA chloride, or the MTPA ester. The following analysis assumes that the MTPA ester was correctly identified as *S*. A further ambiguity arose upon inspection of the data provided. The isolation chemists reported the chemical shifts of the Mosher esters in DMSO (this could be a typographical error), but attached spectra in $CDCl_3$. By calculating the $\Delta\delta_H$ (*S*-*R*) values based on their reported tabulated shifts and their assignments of these signals, we agreed that H7' has a negative value and H2' and H4' have positive values (see Table 8). However, the isolation chemists do not mention/provide any 2D NMR spectra for the assignment of these signals. Upon examination of the provided data (including coupling constants), we propose that the peak assignment shown in Table 8 could be ambiguous, particularly positions H2', H3' and H5.

^{1}H environment	***S* / ppm**	***R* / ppm**	**$\Delta\delta_H$ (*S*-*R*)**	**$\Delta\delta_H$ (*S*-*R*) x MHz**
6′	5.45	5.48	−0.03	−18
3′	4.56	-	-	-
5	4.43	4.46	−0.03	−18
6	4.30	4.30	0.00	0
2′	4.20	4.19	+0.01	+6
3_A	3.35	3.34	+0.01	+6
4′	3.35	3.33	+0.02	+12
4	3.31	3.29	+0.02	+12
3_B	2.51	2.50	+0.01	+6
7	1.50	1.51	−0.01	−6
7′	1.40	1.49	−0.09	−54

Table 8: $\Delta\delta_H$ (*S*-*R*) analysis based on the isolation chemists' reported peaks and assignments[2,38]

Upon completing the Mosher analysis based on the isolation chemists reported chemical shifts, we utilised the integrated spectra ($CDCl_3$) that they attached in their supporting information to select peaks in distinct environments. We could then manually calculate the coupling constants for each of the proton environments. Unfortunately peaks in the area of 3-4 ppm were overlapping and therefore we did not include these in our analysis. The assignment of the peaks was based on our assignments of (−)-angiopterlactone B (**2**) in $CDCl_3$ (see Experimental, Section 1.4.2.6). The $\Delta\delta_H$ (*S*-*R*) values indicate that H7' has a negative value, H2' also has a negative value and H3' is 0 (Table 9). These values, as well as the aforementioned uncertainties, suggest that the modified Mosher method cannot be utilised to unambiguously assign C6' as either *R* or *S*.

^{1}H environment	***S* / ppm**	***R* / ppm**	**$\Delta\delta_H$ (*S*-*R*)**	**$\Delta\delta_H$ (*S*-*R*) * MHz**
6′	5.45	5.48	−0.03	−18
3′	4.57	4.57	0.00	0
2′	4.43	4.46	−0.03	−18
6	4.31	4.30	+0.01	+6
5	4.20	4.19	+0.01	+6
3_B	2.51	2.52	−0.01	−6
7	1.50	1.51	−0.01	−6
7′	1.40	1.49	−0.09	−54

Table 9: $\Delta\delta_H$ (*S*-*R*) analysis based on our extracted values from the spectra and our assignment[38]

As a result of the ambiguities present within the isolation chemists' modified Mosher method, we investigated the assignments they made utilising the CD excitation chirality method. The isolation chemists state that "the δ-lactone ring adopted a boat conformation, which was in agreement with the negative Cotton effect (Δε −0.6) at 221 nm, suggesting the 4*R* and 3'*R* absolute configurations."[2] The first ambiguity present in this statement, is that the C3' position is not within the δ-lactone ring, but instead in the γ-lactone ring. In order to investigate if their statement holds true for the C4 position, we studied the reference provided by the isolation chemists as well as some of the associated references.

It has been previously discussed that based on X-ray crystallographic studies, the lactone group (*i.e.*, –C-CO-O-C-) within a ring must be planar.[39,40] Due to this constraint, lactone rings must be either in a boat or a half-chair conformation. Following these studies, Wolf made some empirical observations based on saturated δ-lactones.[41] He suggested that the sign of the Cotton effect is affected by the conformation adopted by the lactone ring and consequently the location of the β-carbon in relation to the lactone plane (Structures III-VI, Figure 6). In 1968, Beecham made some similar observations for γ-lactones (Structures I-II, Figure 6).[42]

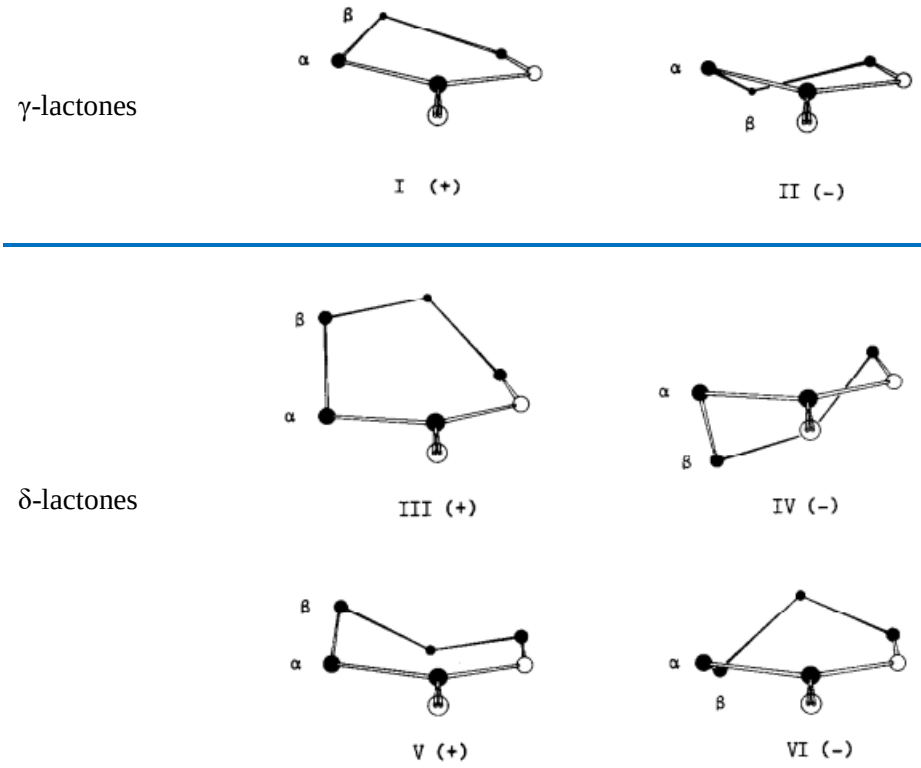

Figure 6: Beecham's representation of the possible conformations and associated Cotton effect signs for his γ-lactones I and II, and Wolf's δ-lactones III-VI[42]

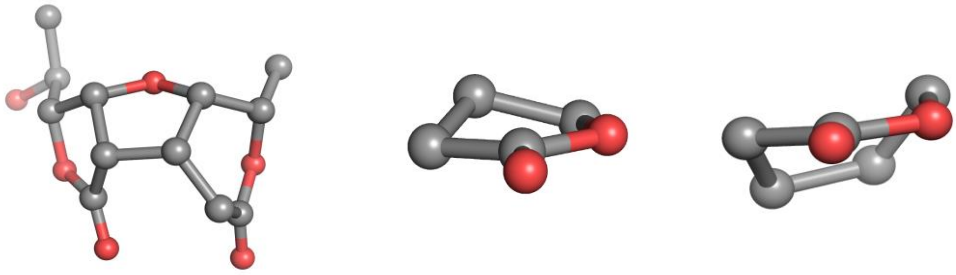

X-ray (–)-angiopterlactone B (**2**)	γ-lactone of **2**	δ-lactone of **2**
Figure 6 equivalent arrangement:	I	IV

Figure 7: X-ray crystal structure of (–)-angiopterlactone B (**2**) and the arrangement of the γ- and δ-lactones within it

Based on these empirical observations, we utilised the X-ray crystal structure of our synthetic material (−)-angiopterlactone B (**2**) in order to investigate how the sign of the Cotton effect may be affected by both the γ- and δ-lactone within the molecule (Figure 7). In the solid state, the δ-lactone is arranged in the boat conformation IV and should therefore result in a negative Cotton effect (Figure 6). The γ-lactone on the other hand is arranged as in structure I, with the

β-carbon above the plane of the lactone group. Thus the γ-lactone should contribute to a positive Cotton effect. Therefore within (−)-angiopterlactone B (**2**) there are two lactone units each contributing to opposite signs of the Cotton effect. In summary, it can be said that it is unlikely that the isolation chemists can utilise the CD excitation chirality method to unambiguously assign the stereochemistry of position C4 in their natural sample of angiopterlactone B (**2**).

1.2.4 Further Investigations into (−)-Angiopterlactone B

Following our investigations into the structure of the natural material angiopterlactone B (**2**), our attention turned towards determining the enantiopurity of our synthetic material. In order to determine the enantiomeric ratio of our synthetic (−)-angiopterlactone B (**2**), we attempted to obtain chiral HPLC data. Unfortunately, (−)-angiopterlactone B (**2**) could not be detected by the UV detector on our HPLC machine.

In some cases where compounds cannot be identified by UV detectors, they can be derivatised to install a suitable chromophore. As (−)-angiopterlactone B (**2**) contains an alcohol group, we decided to derivatise this compound by utilising benzoyl chloride.[43] Upon reacting (−)-angiopterlactone B (**2**) with benzoyl chloride, adduct **25** was successfully attained in 69% yield (Scheme 21).

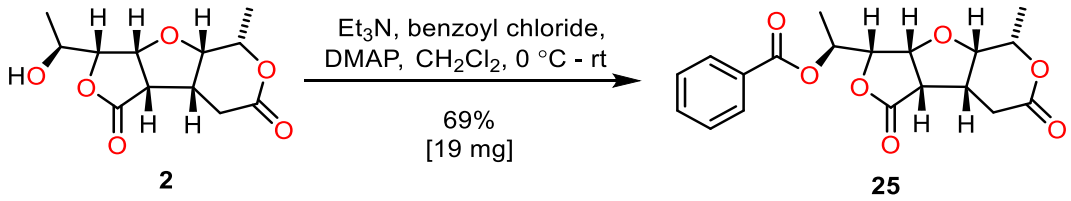

Scheme 21: Synthesis of adduct **25** from (−)-angiopterlactone B (**2**)

In order to interpret the chiral HPLC results and obtain an enantiomeric ratio, access to the other enantiomer or the racemic (rac) compound **25** was necessary. Due to the ongoing interest in selective dimerisation reactions of racemic molecules in the Lawrence group, we targeted the racemic adduct **25**. This was not a trivial endeavour, as we required access to the racemic dimer **2**, which meant that the dimerisation reaction had to be completed utilising racemic lactone **3**. As we now had a mixture of (+)- and (–)-lactone **3**, there was the potential for us to form not only homochiral dimers, but also heterochiral dimers. Therefore, unless there is an inherent selectivity towards such homochiral dimers, this venture to synthesise adduct ***rac*-25** could prove challenging.

We began the synthesis towards racemic angiopterlactone B (**2**) by completing an Achmatowicz reaction on commercially available furfuryl alcohol ***rac*-15** (Scheme 22). Following this, diastereoconvergent isomerisation successfully yielded lactone ***rac*-3**. Subjecting lactone ***rac*-3** to the dimerisation conditions we previously employed for the enantiopure material, led to the formation of racemic angiopterlactone B (**2**), but with a significantly lower yield than that observed for the enantio-enriched dimer. Racemic angiopterlactone B (**2**) was then derivatised with benzoyl chloride to give adduct ***rac*-25** in 70% yield. With racemic adduct **25** and enantio-enriched adduct **25** in hand, chiral HPLC experiments were completed. Various columns and conditions were tested, however due to poor peak separation and low intensities, none resulted in a suitable HPLC trace for the determination of the enantiomeric ratio.

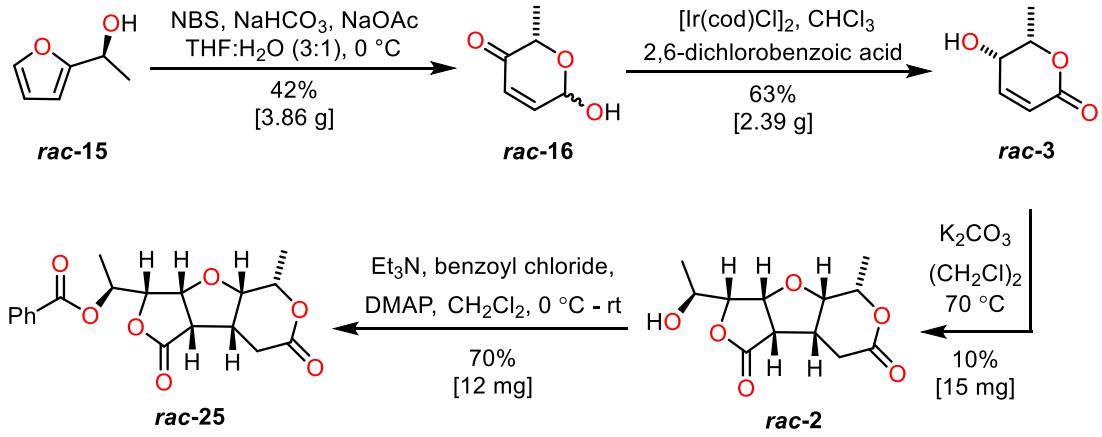

Scheme 22: Synthesis of adduct ***rac*-25** from alcohol ***rac*-15**

Despite the lack of success in determining the enantiomeric ratio of dimer **2** using HPLC, we were successful in synthesising more than two grams of racemic lactone **3**. Provided that the dimerisation reaction proceeds in the same manner as the enantio-enriched lactone **3**, the racemic material could be utilised to conduct further screening of conditions and thus preserve our enantio-enriched lactone **3**. Our synthesis towards adduct ***rac*-25** demonstrated that we successfully formed racemic angiopterlactone B (**2**). Upon closer inspection of the ^{1}H NMR spectrum of the crude dimerisation product *rac*-**2**, we noted that the spectrum looked very similar to that of the crude dimerisation product obtained using enantiopure δ-lactone **3** (Figure 8). However, it appears that the reaction proceeds less cleanly, explaining the lower yield we observed for this reaction than the one obtained with the enantio-enriched material (10% and 25-35% respectively). Upon purification by column chromatography, we were unsuccessful in characterising these impurities, but they are presumably the result of heterochiral dimerisations.

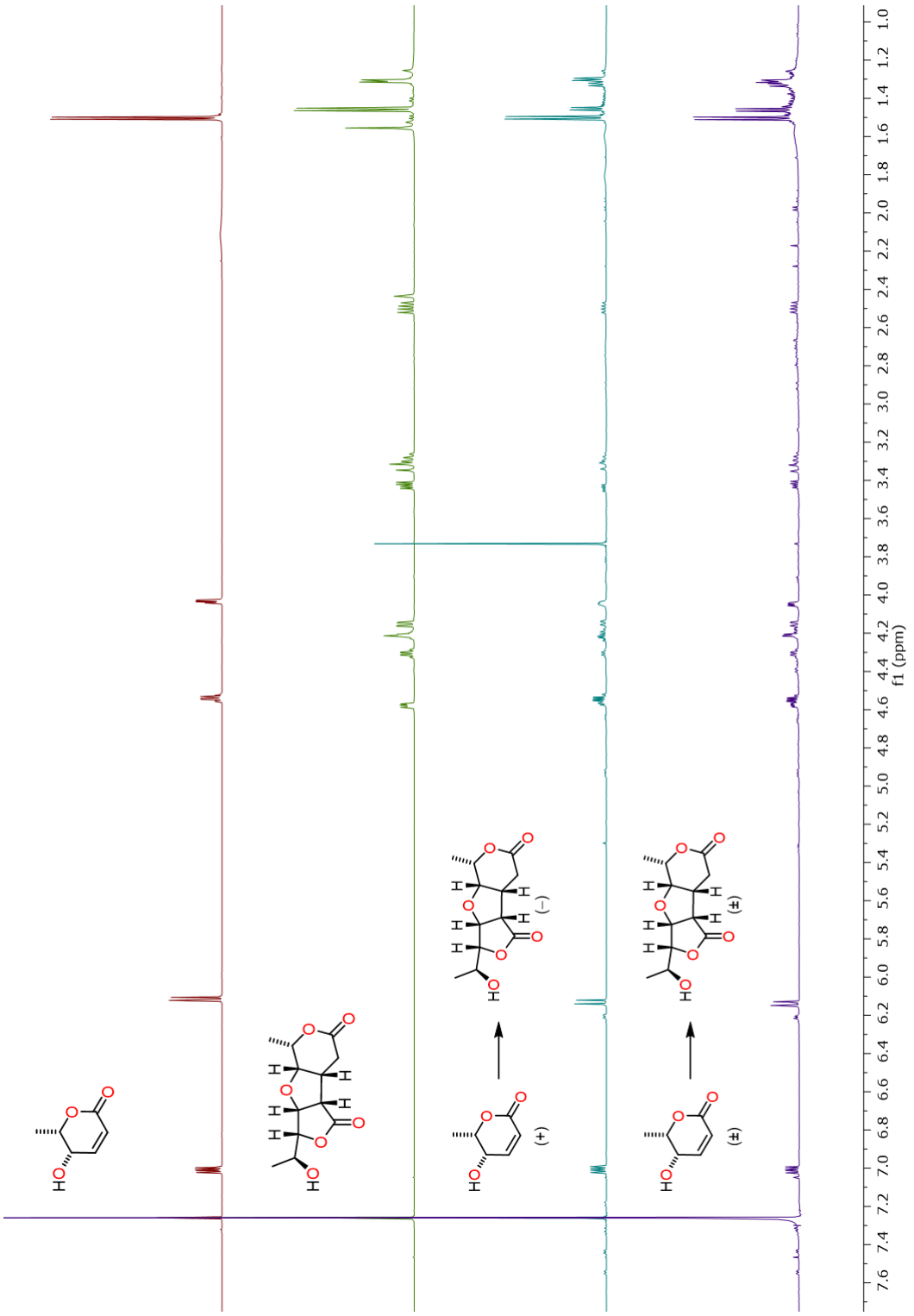

Figure 8: ^{1}H NMR spectra. From top to bottom: δ-lactone **3**, (−)-angiopterlactone B (**2**), crude of dimerisation reaction, crude of racemic dimerisation reaction

As we were unable to isolate or identify any further dimers, we hoped that completing the reaction in *d6*-DMSO (solvent in which the isolation chemists recorded the spectra for (–)-angiopterlactone A (**1**)) would allow for better identification of possible intermediates / side-products. Utilising lactone ***rac*-3**, several small scale reactions in *d6*-DMSO were attempted. However, we were unable to identify any further dimers in the ^{1}H NMR spectrum of the crude dimerisation product, although this could be a result of overlapping peaks.

The inherent selectivity observed in the dimerisation reactions for both the enantio-enriched and racemic starting material **3**, left us with several unanswered questions. Why is this reaction so selective and why hadn't we observed the related natural product (−)-angiopterlactone A (**1**)? These questions formed the basis of our interest in investigating the proposed structure of (−)-angiopterlactone A (**1**), as well as probing the underlying reaction mechanism in the formation of (−)-angiopterlactone B (**2**). If we can conclude how the dimerisation proceeds, we may be able to explain the regio- and stereo-selectivity. These examinations involved utilising computational methods in which NMR prediction studies and mechanistic investigations were completed (outlined in Chapters 2 and 3 respectively). It was hoped that these more detailed studies would shed light on the predisposed reactivity and selectivity at play in the biogenesis of these natural products.

1.3 Conclusions

The enantioselective synthesis of δ-lactone **3** was successfully accomplished in three steps and various dimerisation conditions towards angiopterlactone A (**1**) and angiopterlactone B (**2**) were tested. This led to the discovery that treatment of lactone **3** with potassium carbonate in dichloroethane at 70 °C resulted in the successful synthesis of (−)-angiopterlactone B (**2**) (Scheme 23). The four step synthesis of (−)-angiopterlactone B (**2**) is scalable, enantioselective and protecting group free. With (−)-angiopterlactone B (**2**) in hand, we proposed a structural revision of the natural material and in doing so revealed the known natural product angiopteroside (**9**) as a likely biosynthetic precursor.

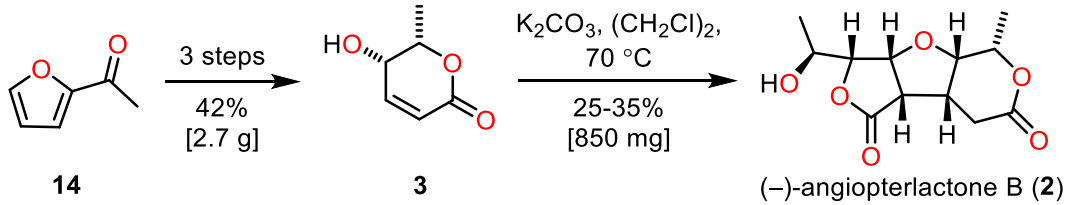

Scheme 23: Synthesis of (−)-angiopterlactone B (**2**) from 2-acetylfuran (**14**)

During our screening of various additives, we discovered that we could achieve a selective and efficient ring contraction of lactone **3** by using PTSA and heating overnight (Scheme 24). Furthermore, throughout our dimerisation studies we noted that we never observed the related natural product (−)-angiopterlactone A (**1**).

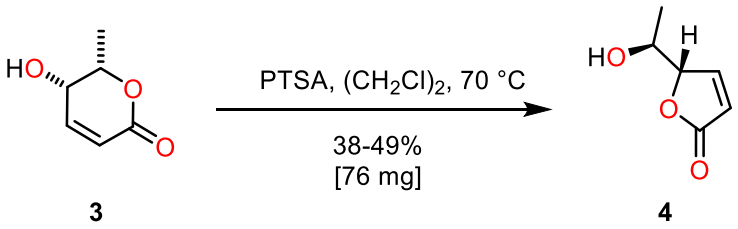

Scheme 24: Our ring contraction of δ-lactone **3** to γ-lactone **4**

1.4 Experimental

Reproduced in part from *Org. Lett.* **2017**, *19* (9), 2199–2201.[1]

1.4.1 General Experimental Conditions

Experimental Procedures, Glassware and Reagents

Unless otherwise stated, reactions were performed under anhydrous conditions, under a positive pressure of dry nitrogen and glassware was dried using a heat gun. All reagents and solvents were purchased from commercially available sources and utilised without further purification, unless stated otherwise. Experimental details are provided for the largest scale procedure completed. Where yields are reported as a range, this represents the isolated yields obtained from several reactions.

Chromatography

Reactions were monitored by thin-layer chromatography (TLC), using silica gel plates (Merck Kieselgel 60 F254). Visualisation was effected by quenching of UV fluorescence (λ_{254nm}) and by staining with a standard solution of *p*-anisaldehyde, followed by heating. Merck silica gel 60 (230-400 mesh) was utilised for flash chromatography. Analytical chiral HPLC was conducted using an Agilent 1100 series system using a G1313 autosampler, a multiwavelength detector and a binary pump.

Optical Rotation

Optical rotations were measured using a Perkin-Elmer 341 polarimeter or an Optical Activity POLAAR 20 polarimeter, at 589 nm (sodium D line) with a cell path length of 1 dm and concentrations (*c*) reported in g/100 mL. Specific rotations are denoted as $[\alpha]_D^{20}$.

Nuclear Magnetic Resonance (NMR)

^{1}H NMR spectra were recorded at 500 MHz or 600 MHz, using a Bruker Ascend 500 or Bruker UltraShield 600 spectrometer. Spectra were referenced using residual solvent peaks ($CDCl_3$ = 7.26 ppm and CD_3OD = 3.31 ppm). Coupling constants (*J*) are quoted to the nearest 0.1 Hz. Assignment of proton signals was assisted by ^{1}H-^{1}H COSY, HSQC, HMBC and NOESY experiments. ^{13}C NMR spectra were recorded at 126 MHz or 151 MHz, using a Bruker Ascend

500 or Bruker UltraShield 600 spectrometer. ^{13}C NMR spectra were referenced using solvent peaks ($CDCl_3$ = 77.16 ppm and CD_3OD = 49.00 ppm). ^{13}C NMR peaks are generally reported to one decimal place. Assignment of carbon signals was assisted by HSQC and HMBC experiments.

Infrared Spectra (IR)

Infrared spectra were recorded using a Shimadzu IR Affinity-1 Fourier transform IR spectrophotometer as neat samples, using Pike MIRacle ATR accessory. Absorption maxima (ν_{max}) are quoted in wavenumbers (cm^{-1}).

Mass Spectroscopy

High resolution mass spectra were recorded on a Bruker micrOTOF instrument using Electrospray Ionisation (ESI^+).

Melting Point

Melting points were measured on a Gallenkamp Melting Point System.

1.4.2 Specific Experimental Conditions

*1.4.2.1 Experimental Procedure for (R)-Alcohol **ent-15***

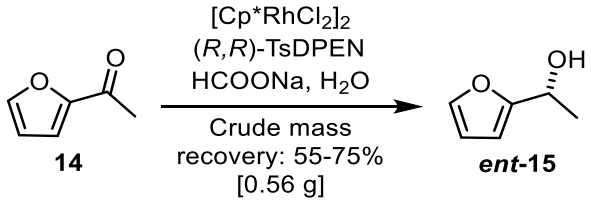

Compound ***ent*-15** was prepared utilising a modified literature procedure.[27]

A solution of $[Cp^*RhCl_2]_2$ (3.00 mg, 5.00 µmol, 0.05 mol%) and (*R*,*R*)-TsDPEN (4.00 mg, 10.9 µmol, 0.12 mol%) in H_2O (18 mL) was heated at 40 °C for 1 h and subsequently cooled to rt. HCOONa (3.10 g, 45.6 mmol) and 2-acetylfuran (**14**) (1.00 g, 9.08 mmol) were then added to this cooled catalyst solution.

The mixture was heated back up to 40 °C and left to stir for 16 h, after which the reaction was cooled to rt. The product was extracted with Et_2O (3 × 40 mL), dried over anhydrous Na_2SO_4, filtered and concentrated under reduced pressure to afford ***ent*-15** as a brown oil (crude NMR spectrum showed presence of unreacted starting material **14** [approximate starting material : product ratio was 3:1; as determined by NMR spectrum]) (crude: 0.56 g, 5.00 mmol, 55% crude mass recovery, e.r. 98:2).

HPLC (Chiral Pak IA, *i*-PrOH/hexane (1:99), 1 mL·min^{-1}, λ 210 nm) 23.224 min. See the Appendix, Section 1.2.1 for chiral HPLC traces. Data comparison was conducted with (*S*)-alcohol **15** as well as commercially available alcohol ***rac*-15**.

The remaining spectral data was in accordance with literature values[27] and matched the data collected for compound **15** in Section 1.4.2.3.

*1.4.2.2 Experimental Procedure for (S,S)-Noyori Catalyst **20***

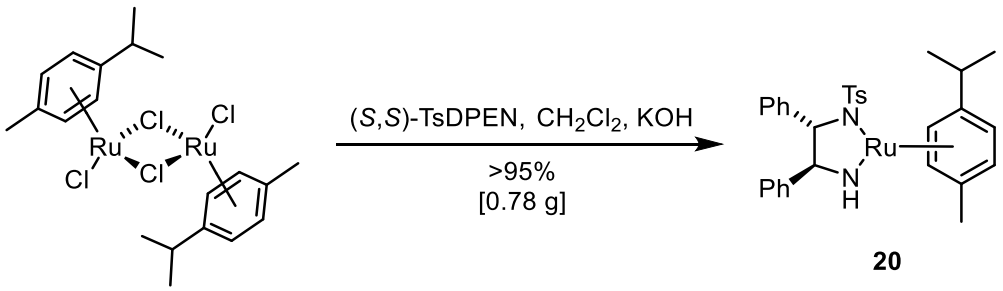

20

The (*S*,*S*)-Noyori catalyst **20** was prepared according to known procedures.[28,29,44]

(*S*,*S*)-TsDPEN (0.48 g, 1.31 mmol), $[RuCl_2(\eta^6\text{-}p\text{-cymene})]_2$ (0.40 g, 0.70 mmol) and powdered anhydrous KOH (0.54 g, 9.62 mmol) were added to anhydrous CH_2Cl_2 (25 mL). The resulting orange mixture was stirred for 5 min at rt and then H_2O (25 mL) was added in one portion.

The biphasic mixture was stirred for 10 min, diluted with H_2O (40 mL) and the layers separated. The aqueous layer was extracted with CH_2Cl_2 (2 × 40 mL). The combined organic extracts were dried over CaH_2, filtered and concentrated under reduced pressure, to afford catalyst **20** as a dark purple solid (0.78 g, 1.3 mmol, >95%). This material was used immediately, without further purification.

*1.4.2.3 Experimental Procedure for (S)-Alcohol **15***

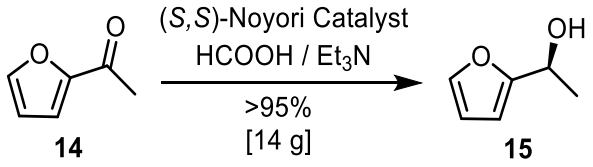

Compound **15** was prepared according to a literature procedure.[28]

The (*S*,*S*)-Noyori catalyst **20** (0.78 g, 1.30 mmol) (see Section 1.4.2.2) was added to a solution of 2-acetylfuran (**14**) (14.0 g, 0.13 mol) in HCOOH (54 mL) and Et_3N (200 mL). The resulting golden orange solution was stirred at 40 °C for 23 h.

The reaction mixture was cooled to rt, diluted with H_2O (120 mL), the layers were separated and the aqueous layer was extracted with Et_2O (5 × 200 mL). The combined organic layers were washed with saturated aq. $NaHCO_3$ (80 mL), dried over anhydrous Na_2SO_4, filtered and concentrated under reduced pressure, to afford alcohol **15** as a dark brown oil (14.0 g, 0.13 mmol, >95%, e.r. 98:2). This material was used without purification in the subsequent step (see Section 1.4.2.4). A small sample of crude material was purified by flash chromatography (silica gel, dichloromethane + 1% methanol) for analytical purposes. The obtained spectroscopic data matched literature values.[27,28]

R_f 0.43 (ethyl acetate / hexane, 1:1);

$[\alpha]_D^{20}$ synthesised **15**: −23.7 (*c* 1.27, EtOH), purchased (−)-**15**: −25.3 (*c* 1.27, EtOH);

^{1}H NMR (500 MHz, $CDCl_3$) δ 7.37 (dd, *J* = 1.9, 0.9 Hz, 1H), 6.32 (dd, *J* = 3.2, 1.8 Hz, 1H), 6.23 (app. dt, *J* = 3.3, 0.8 Hz, 1H), 4.93-4.84 (m, 1H), 1.99 (s, OH), 1.54 (d, *J* = 6.6 Hz, 3H) ppm;

^{13}C NMR (126 MHz, $CDCl_3$) δ 157.7, 142.0, 110.3, 105.2, 63.8, 21.4 ppm;

IR (thin film) 3364, 2980, 1505 cm^{-1};

HPLC (Chiral Pak IA, IPA/hexane (1:99), 1 mL·min^{-1}, λ 230 nm) t_{Rmajor} = 20.280 min, t_{Rminor} = 21.596 min. See the Appendix, Section 1.2.1 for chiral HPLC traces.

*1.4.2.4 Experimental Procedure for Lactol **16***

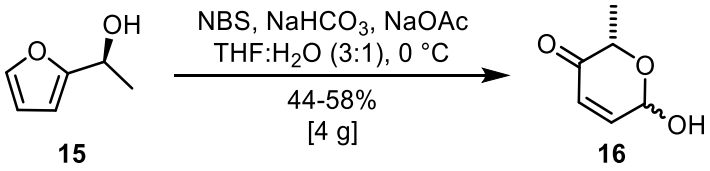

15 **16**

Compound **16** was prepared utilising a modified literature procedure.[21,27,45]

N-bromosuccinimide (NBS) was recrystallised from H_2O.[46] To a stirred solution of the crude (*S*)-1-(2-furyl)ethanol **15** (8.00 g, 71.4 mmol) in THF (88 mL) and H_2O (30 mL) at 0 °C, $NaHCO_3$ (12.0 g, 140 mmol), NaOAc (5.90 g, 71.9 mmol) and NBS (13.0 g, 73.0 mmol) were sequentially added. After 15 min, the reaction was quenched at 0 °C with saturated aq. $NaHCO_3$ (900 mL) and diluted with Et_2O (800 mL).

The layers were separated and the aqueous layer was extracted with Et_2O (3 × 800 mL) and the combined organic layers were dried over anhydrous Na_2SO_4 and concentrated under reduced pressure. The crude material was purified using flash chromatography (silica gel, petroleum spirit 40-60 / ethyl acetate, 2:1 → 1:1), to afford lactol **16** as a pale yellow solid (4.00 g, 31.3 mmol, 44%, d.r. 2:1). The obtained spectroscopic data matched literature values.[27]

R_f 0.40 (petroleum spirit 40-60 / ethyl acetate, 1:1);

^{1}H NMR (500 MHz, $CDCl_3$) δ 6.93 (dd, *J* = 10.2, 1.5 Hz, 1H‡), 6.89 (dd, *J* = 10.2, 3.4 Hz, 1H†), 6.15 (dd, *J* = 10.3, 1.6 Hz, 1H‡), 6.10 (dd, *J* = 10.2, 0.7 Hz, 1H†), 5.67 (app. dq, *J* = 7.4, 1.5 Hz, 1H‡), 5.63 (ddd, *J* = 5.0, 3.4, 0.7 Hz, 1H†), 4.71 (q, *J* = 6.8 Hz, 1H†), 4.23 (qd, *J* = 6.7, 1.3 Hz, 1H‡), 3.22 (dd, *J* = 7.4, 1.5 Hz, OH‡), 3.00 (dd, *J* = 5.1, 1.3 Hz, OH†), 1.46 (d, *J* = 6.7 Hz, 3H‡), 1.39 (d, *J* = 6.8 Hz, 3H†) ppm;

^{13}C NMR (126 MHz, $CDCl_3$) δ 196.8†, 196.4‡, 147.9‡, 144.3†, 128.7‡, 127.5†, 91.1‡, 87.9†, 75.4‡, 70.6†, 16.5‡, 15.5† ppm;

IR (thin film) 3343, 3049, 2995, 1682 cm^{-1}.

† Major diastereoisomer

‡ Minor diastereoisomer

*1.4.2.5 Experimental Procedure for (S,S)-Lactone **3***

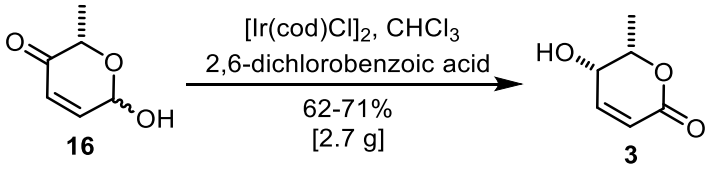

Compound **3** was prepared utilising a modified literature procedure.[21]

Lactol **16** (3.80 g, 29.7 mmol), $[Ir(COD)Cl]_2$ (0.50 g, 0.74 mmol), 2,6-dichlorobenzoic acid (2.80 g, 14.7 mmol) and anhydrous $CHCl_3$ (290 mL) were added to a flask. The reaction mixture was stirred at rt for 16 h and was then concentrated under reduced pressure and purified by flash chromatography (silica gel, petroleum spirit 40-60 / ethyl acetate, 1:2) to afford lactone **3** as a light brown oil which slowly solidified (2.70 g, 21.1 mmol, 70%, e.r. 98:2). The obtained spectroscopic data matched literature values.[47,48]

R_f 0.27 (petroleum spirit 40-60 / ethyl acetate, 1:2);

$[\boldsymbol{\alpha}]_{\boldsymbol{D}}^{\mathbf{20}}$ +148 (*c* 0.51, H_2O), lit. +143 (*c* 0.53, H_2O)[48];

^{1}H NMR (600 MHz, $CDCl_3$) δ 7.01 (dd, *J* = 9.7, 5.7 Hz, 1H), 6.11 (d, *J* = 9.7 Hz, 1H), 4.54 (qd, *J* = 6.7, 2.7 Hz, 1H), 4.03 (dd, *J* = 5.7, 2.7 Hz, 1H), 2.11 (br s, OH), 1.50 (d, *J* = 6.7 Hz, 3H) ppm;

^{13}C NMR (151 MHz, $CDCl_3$) δ 163.9, 144.6, 123.0, 77.2, 63.2, 15.9 ppm;

IR (thin film) 3445, 3056, 2991, 2947, 1690 cm^{-1};

M.p. 47-49 °C (lit. 48-53 °C)[47];

HPLC (ADH, IPA/hexane (20:80), 0.7 mL·min^{-1}, λ 254 nm) t_{Rminor} = 8.637 min, t_{Rmajor} = 10.986 min. See the Appendix, Section 1.2.2 for chiral HPLC traces.

*1.4.2.6 Experimental Procedure for (−)-Angiopterlactone B (**2**)* [17]

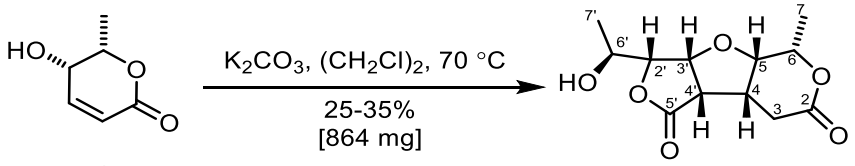

K_2CO_3 (378 mg, 2.73 mmol) was added to a solution of lactone **3** (3.50 g, 27.3 mmol) in anhydrous $(CH_2Cl)_2$ (22 mL). The reaction mixture was heated to 70 °C and was stirred for 16 h. It was evident that some solvent was lost during this process. The amorphous mixture was triturated with $CHCl_3$ to extract the product before being concentrated under reduced pressure. The crude material (3.34 g, see the Appendix, Section 1.1.7 for crude NMR spectra) was purified by flash chromatography (silica gel, dichloromethane + 8% methanol) to afford (−)-angiopterlactone B (**2**) as a white crystalline solid (864 mg, 3.38 mmol, 25%). The obtained spectroscopic data (excluding the optical rotation) matched literature values.[2]

R_f 0.20 (dichloromethane + 6% methanol);

$[\boldsymbol{\alpha}]_{\boldsymbol{D}}^{\mathbf{20}}$ −25 (*c* 0.04, EtOAc), lit. +22 (*c* 0.04, EtOAc)[2];

^{1}H NMR (500 MHz, $CDCl_3$) δ 4.58 (dd, *J* = 5.6, 3.6 Hz, $H_{3'}$), 4.31 (qd, *J* = 6.6, 1.7 Hz, H_6), 4.24 – 4.18 (m, $H_{2'+6'}$), 4.15 (dd, *J* = 8.7, 1.7 Hz, H_5), 3.43 (dd, *J* = 10.6, 5.5 Hz, $H_{4'}$), 3.33 (dd, *J* = 16.2, 1.7 Hz, H_{3A}), 3.28 (ddd, *J* = 10.0, 8.8, 1.3 Hz, H_4), 2.50 (dd, *J* = 16.4, 8.9 Hz, H_{3B}), 2.44 (br s, OH), 1.46 (d, *J* = 6.6 Hz, H_7), 1.31 (d, *J* = 5.7 Hz, $H_{7'}$) ppm;

^{13}C NMR (126 MHz, $CDCl_3$) δ 172.9 ($C_{5'}$), 169.9 (C_2), 85.0 ($C_{2'}$), 79.1 ($C_{3'}$), 79.0 (C_5), 73.4 (C_6), 66.6 ($C_{6'}$), 49.1 ($C_{4'}$), 36.8 (C_4), 28.1 (C_3), 17.7 ($C_{7'}$), 16.8 (C_7) ppm;

^{1}H NMR (500 MHz, CD_3OD) δ 4.57 (dd, *J* = 5.4, 3.8 Hz, $H_{3'}$), 4.44 (qd, *J* = 6.6, 1.7 Hz, H_6), 4.22 (dd, *J* = 8.7, 3.8 Hz, $H_{2'}$), 4.18 (dd, *J* = 8.7, 1.7 Hz, H_5), 4.05 (dq, *J* = 8.7, 6.4 Hz, $H_{6'}$), 3.53 (dd, *J* = 10.6, 5.3 Hz, $H_{4'}$), 3.37 – 3.32 (m, H_4), 3.13 (dd, *J* = 16.4, 1.0 Hz, H_{3A}), 2.67 (dd, *J* = 16.4, 9.0 Hz, H_{3B}), 1.40 (d, *J* = 6.6 Hz, H_7), 1.27 (d, *J* = 6.4 Hz, $H_{7'}$) ppm;

^{13}C NMR (126 MHz, CD_3OD) δ 176.3 ($C_{5'}$), 174.1 (C_2), 86.6 ($C_{2'}$), 80.3 ($C_{3'}$), 79.8 (C_5), 75.2 (C_6), 67.4 ($C_{6'}$), 50.2 ($C_{4'}$), 37.8 (C_4), 28.8(C_3), 18.5 ($C_{7'}$), 16.8 (C_7) ppm;

HRMS (ESI^+) $C_{12}H_{16}O_6$: 279.0798 $[M+Na]^+$ (calcd 279.0839);

IR (thin film) 3543, 2940, 1752, 1722, 1709 cm^{-1};

M.p. 166-168 °C recrystallised from $CHCl_3$ (lit. 200-202 °C)[2].

^{1}H	Natural angiopterlactone B[2] ^{1}H NMR spectra $CDCl_3$, 600 MHz δ / ppm (*J*, Hz)	Synthetic angiopterlactone B ^{1}H NMR spectra $CDCl_3$, 500 MHz δ / ppm (*J*, Hz)
3A	3.33 (d, 16.2)	3.33 (dd, 16.2, 1.7)
3B	2.50 (dd, 16.2, 9.0)	2.50 (dd, 16.4, 8.9)
4	3.28 (ddd, 9.0, 8.4, 10.2*)	3.28 (app. ddd, 10.0, 8.8, 1.3)
5	4.15 (br d, 8.4)	4.15 (dd, 8.7, 1.7)
6	4.31 (br q, 6.6)	4.31 (qd, 6.6, 1.7)
7	1.46 (d, 6.6)	1.46 (d, 6.6)
2’	4.21 (m, overlap)	4.24 – 4.18 (m, overlap)
3’	4.58 (dd, 5.4, 3.0)	4.58 (dd, 5.6, 3.6)
4’	3.43 (dd, 10.2, 5.4)	3.43 (dd, 10.6, 5.5)
6’	4.21 (m, overlap)	4.24 – 4.18 (m, overlap)
7’	1.31 (d, 6.0)	1.31 (d, 5.7)
OH	2.45 (s)	2.44 (br s)

Table 10: Comparison of reported ^{1}H NMR data for natural angiopterlactone B (**2**)[2] and ^{1}H NMR data for our synthetic material. *Peak shape similar to that observed in the ^{1}H NMR spectrum of synthetic **2**, therefore 10.2 Hz coupling constant assumed to be a typographical error.

^{13}C	Literature ^{13}C NMR spectra $CDCl_3$, 150 MHz δ / ppm	Experimental ^{13}C NMR spectra $CDCl_3$, 126 MHz δ / ppm
2	169.8	169.9
3	27.9	28.1
4	36.6	36.8
5	78.8	79.0
6	73.3	73.4
7	16.6	16.8
2’	84.9	85.0
3’	78.9	79.1
4’	48.9	49.1
5’	172.9	172.9
6’	66.4	66.6
7’	17.2 (17.5)*	17.7

Table 11: Comparison of reported ^{13}C NMR data for natural angiopterlactone B (**2**)[2] and ^{13}C NMR data for our synthetic material. *The value in brackets was taken directly from the provided NMR spectrum in the SI of the isolation paper.[2]

1.4.2.7 General Procedure for the Dimerisation Screening Process

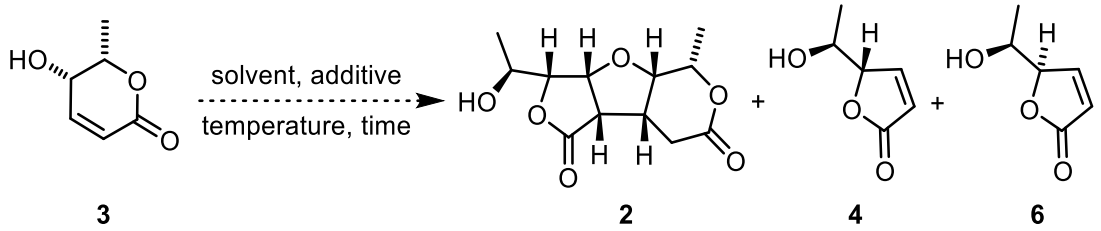

3 **2** **4** **6**

Lactone **3** and additive were weighed out into a sample vial. The solvent was added and the vial was sealed and placed into an oil bath at the designated temperature, for the designated amount of time.

The mixture was then triturated with $CHCl_3$ and concentrated under reduced pressure. The yield for each component (**3**, **4**, **6** and **2**) was calculated using ^{1}H NMR spectroscopy, utilising dimethyl sulfone in $(CD_3)_2SO$ or durene in $CDCl_3$ as internal standards.

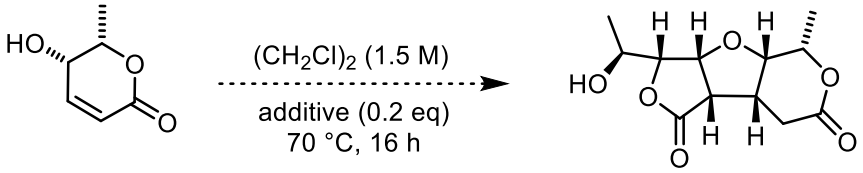

3 **2**

entry	**additive (0.2 eq)**	**δ-lactone 3 (%)**	**γ-lactone 4 (%)**	**γ-lactone 6 (%)**	**dimer 2 (%)**
1	Li_2CO_3	88	<1	<1	0
2	Na_2CO_3	84	<1	0	0
3	$NaHCO_3$	79	<1	0	0
4	K_2CO_3	9	2	2	25
5	Rb_2CO_3	6	<1	<1	19
6	Cs_2CO_3	11	1	<1	18
7	$(NH_4)_2CO_3$	29	3	1	0
8	$MgCO_3$	86	<1	<1	0
9	$CaCO_3$	87	<1	0	0
10	KOH	42	4	3	10
11	Pyrrolidine	47	20	7	0
12	PTSA	0	57	3	0

Table 12: Additive screen

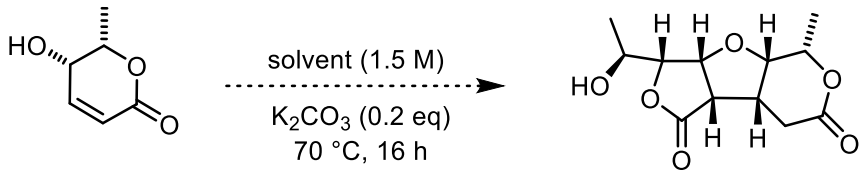

3 **2**

entry	**solvent***	**δ-lactone 3 (%)**	**γ-lactone 4 (%)**	**γ-lactone 6 (%)**	**dimer 2 (%)**
1	dichloroethane	9	2	2	25
2	water	23	3	1	8
3	toluene**	10	<1	<1	5
4	acetonitrile	47	5	5	11
5	carbon tetrachloride	38	2	2	11
6	cyclohexane	27	2	2	9
7	2-methyl THF	21	1	1	12

*Chloroform and dichloromethane were trialled, but these could not be heated to sufficient temperatures for the dimerisation to take place in an acceptable time frame.
**Poor crude mass recovery of <40%.

Table 13: Solvent screen

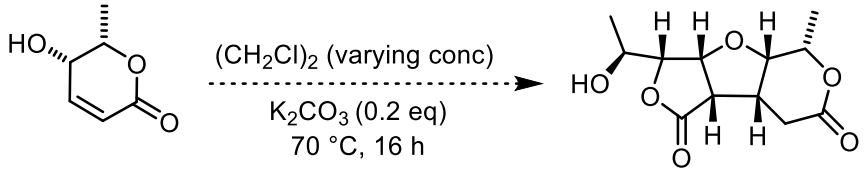

3 **2**

entry	**[3] (M)**	**δ-lactone 3 (%)**	**γ-lactone 4 (%)**	**γ-lactone 6 (%)**	**dimer 2 (%)**
1	0.5	66	2	<1	5
2	0.8	14	2	2	15
3	1.5	9	2	2	25
4	3.1	13	3	3	28
5	6.8	49	3	2	16

Table 14: Concentration screen

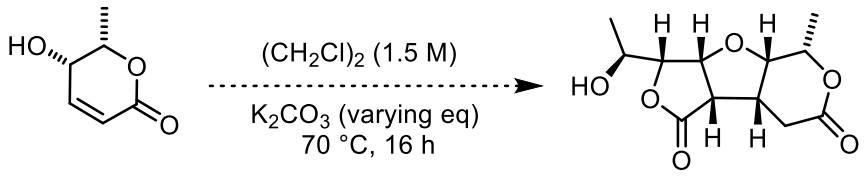

3 **2**

entry	K_2CO_3 equivalents	δ-lactone 3 (%)	γ-lactone 4 (%)	γ-lactone 6 (%)	dimer 2 (%)
*1**	0.1	-	-	-	28
2	0.2	9	2	2	25
3	0.5	5	<1	<1	19
4	1.0	3	0	0	16

*larger scale reaction (400 mg of starting material **3**); 1.1 M, 70 °C, 40 h; yield refers to isolated yield

Table 15: Potassium carbonate equivalents screen

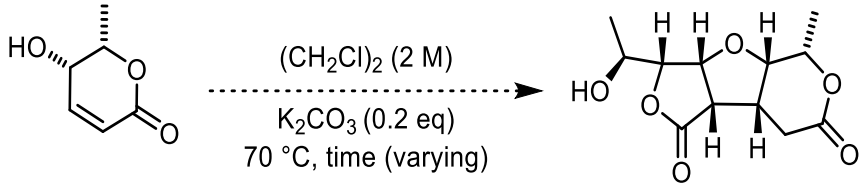

3 **2**

entry	time (h)	δ-lactone 3 (%)	γ-lactone 4 (%)	γ-lactone 6 (%)	dimer 2 (%)
1	1	66	3	2	5
2	2	56	4	2	12
3	3	55	4	3	15
4	4	44	4	3	18
5	5	37	5	4	20
6	8	15	3	2	26
7	42	2	0	0	26

Table 16: Variation of reaction time

*1.4.2.8 Experimental Procedure for (S,S)-Lactone **4***

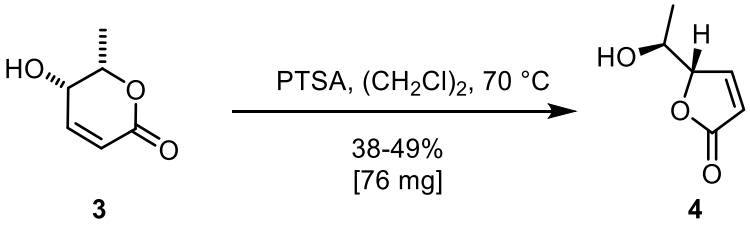

3 **4**

Lactone **3** (200 mg, 1.56 mmol) was dissolved in anhydrous $(CH_2Cl)_2$ (1 mL). PTSA (54 mg, 0.31 mmol) was added and the reaction mixture was stirred at 70 °C for 16 h. The reaction mixture was left to cool to rt and was then concentrated under reduced pressure and purified by flash chromatography (silica gel, petroleum spirit 40-60 / ethyl acetate, 1:2) to afford lactone **4** as a white crystalline solid (76 mg, 0.60 mmol, 38%). The obtained spectroscopic data matched literature values.[49,50]

R_f 0.24 (petroleum spirit 40-60 / ethyl acetate, 1:2);

^{1}H NMR (500 MHz, $CDCl_3$) δ 7.44 (dd, *J* = 5.8, 1.6 Hz, 1H), 6.19 (dd, *J* = 5.8, 2.1 Hz, 1H), 4.93 (app. dt, *J* = 5.4, 1.8 Hz, 1H), 3.93 (app. p, *J* = 6.2 Hz, 1H), 2.34 (br s, OH), 1.32 (d, *J* = 6.5 Hz, 3H) ppm;

^{13}C NMR (126 MHz, $CDCl_3$) δ 172.7, 153.3, 123.0, 87.1, 68.3, 18.8 ppm;

^{1}H NMR (600 MHz, CD_3OD) δ 7.68 (dd, *J* = 5.8, 1.5 Hz, 1H), 6.23 (dd, *J* = 5.8, 2.1 Hz, 1H), 5.06 (ddd, *J* = 4.4, 2.1, 1.6 Hz, 1H), 4.00 (qd, *J* = 6.5, 4.3 Hz, 1H), 1.29 (d, *J* = 6.5 Hz, 3H) ppm;

^{13}C NMR (151 MHz, CD_3OD) δ 175.6, 156.7, 122.9, 88.9, 68.1, 19.1 ppm;

IR (thin film) 3400, 3074, 2947, 1716, 1690 cm^{-1};

M.p. 59-61 °C (no literature value available).

*1.4.2.9 Experimental Procedure for Adduct **25***

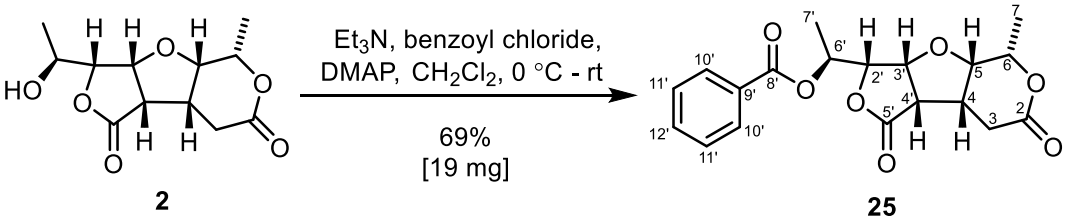

Compound **25** was prepared utilising a modified literature procedure.[43]

(−)-Angiopterlactone B (**2**) (20 mg, 78 µmol) was dissolved in CH_2Cl_2 (2 mL) and the solution was cooled to 0 °C. Et_3N (110 µL, 780 µmol), benzoyl chloride (27 µL, 230 µmol) and DMAP (few crystals) were added in sequence and the solution was consequently warmed to rt and left to stir for 0.5 h. The reaction mixture was then concentrated under reduced pressure and the crude material was purified by flash chromatography (silica gel, dichloromethane + 4% methanol) to afford adduct **25** as a white crystalline solid (19 mg, 53 µmol, 67%).

^{1}H NMR (500 MHz, $CDCl_3$) δ 8.06-8.00 (m, $H_{10'}$), 7.58-7.52 (m, $H_{12'}$), 7.45-7.39 (m, $H_{11'}$), 5.46 (dq, *J* = 8.6, 6.4 Hz, $H_{6'}$), 4.63 (dd, *J* = 5.1, 3.7 Hz, $H_{3'}$), 4.57 (dd, *J* = 8.6, 3.7 Hz, $H_{2'}$), 4.29 (qd, *J* = 6.6, 1.9 Hz, H_6), 4.19 (dd, *J* = 8.9, 1.9 Hz, H_5), 3.41 (dd, *J* = 10.4, 5.1 Hz, $H_{4'}$), 3.36-3.26 (m, H_{3A+4}), 2.50 (dd, *J* = 16.7, 8.8 Hz, H_{3B}), 1.50 (d, *J* = 6.3 Hz, $H_{7'}$), 1.45 (d, *J* = 6.6 Hz, H_7) ppm;

^{13}C NMR (126 MHz, $CDCl_3$) δ 173.0 ($C_{5'}$), 169.8 (C_2), 165.7 ($C_{8'}$), 133.2 ($C_{12'}$), 130.3 ($C_{9'}$), 129.9 ($C_{10'}$), 128.4 ($C_{11'}$), 81.6 ($C_{2'}$), 79.0 ($C_{3'}$), 78.8 (C_5), 73.5 (C_6), 70.1 ($C_{6'}$), 48.7 ($C_{4'}$), 36.8 (C_4), 28.0 (C_3), 16.6 (C_7), 16.2 ($C_{7'}$) ppm;

HRMS (ESI^+) $C_{12}H_{16}O_6$: 383.1117 $[M+Na]^+$ (calcd 360.1101);

IR (thin film) 3001, 2909, 1778, 1736, 1715 cm^{-1};

M.p. 179-181 °C (no literature value available).

*1.4.2.10 Experimental Procedure for Lactol **rac-16***

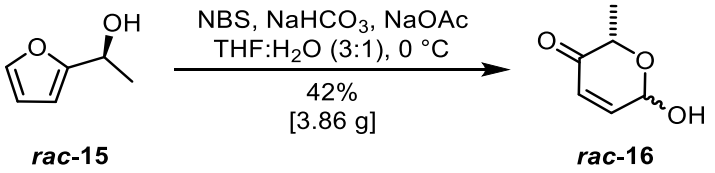

***rac*-15** ***rac*-16**

Compound ***rac*-16** was prepared utilising a modified literature procedure.[21,27,45]

N-bromosuccinimide (NBS) was recrystallised from H_2O.[46] To a stirred solution of purchased 1-(2-furyl)ethanol ***rac*-15** (8.00 g, 71.4 mmol) in THF (88 mL) and H_2O (30 mL) at 0 °C, $NaHCO_3$ (12.0 g, 140 mmol), NaOAc (5.85 g, 71.3 mmol) and NBS (12.7 g, 71.4 mmol) were sequentially added. After 20 min, the reaction was quenched at 0 °C with saturated aq. $NaHCO_3$ (900 mL) and diluted with Et_2O (800 mL).

The layers were separated and the aqueous layer was extracted with Et_2O (3 × 800 mL) and the combined organic layers were dried over anhydrous Na_2SO_4 and concentrated under reduced pressure. The crude material was purified using flash chromatography (silica gel, petroleum spirit 40-60 / ethyl acetate, 2:1), to afford lactol ***rac*-16** as a pale yellow solid (3.86 g, 30.1 mmol, 42%, d.r. 2:1). The NMR data matched the data collected for compound **16** in Section 1.4.2.4.

*1.4.2.11 Experimental Procedure for Lactone **rac-3***

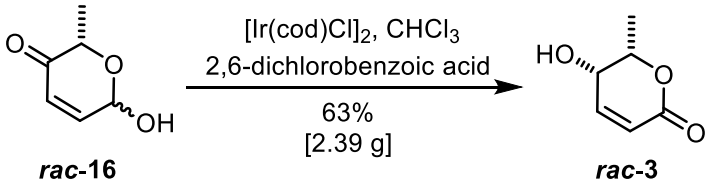

Compound ***rac*-3** was prepared utilising a modified literature procedure.[21]

Lactol ***rac*-16** (3.82 g, 29.8 mmol), $[Ir(COD)Cl]_2$ (0.50 g, 0.74 mmol), 2,6-dichlorobenzoic acid (2.84 g, 14.9 mmol) and anhydrous $CHCl_3$ (290 mL) were added to a flask. The reaction mixture was stirred at rt for 16 h and was then concentrated under reduced pressure and purified by flash chromatography (silica gel, petroleum spirit 40-60 / ethyl acetate, 1:2) to afford lactone ***rac*-3** as a light brown oil which slowly solidified (2.39 g, 18.7 mmol, 63%). The NMR data matched the data collected for compound **3** in Section 1.4.2.5.

*1.4.2.12 Experimental Procedure for Angiopterlactone B (**rac-2**)* [17]

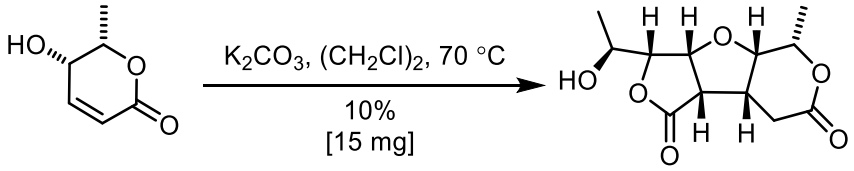

***rac*-3** **rac-2**

K_2CO_3 (16 mg, 0.12 mmol) was added to a solution of lactone ***rac*-3** (154 mg, 1.20 mmol) in anhydrous $(CH_2Cl)_2$ (1 mL). The reaction mixture was heated to 70 °C and was stirred for 16 h. It was evident that some solvent was lost during this process. The amorphous mixture was triturated with $CHCl_3$ to extract the product before being concentrated under reduced pressure. The crude material was purified by flash chromatography (silica gel, dichloromethane + 5% methanol) to afford racemic angiopterlactone B (**2**) as a white crystalline solid (14.8 mg, 0.06 mmol, 10%). The NMR data matched the data collected for compound **2** in Section 1.4.2.6.

*1.4.2.13 Experimental Procedure for Adduct **rac-25***

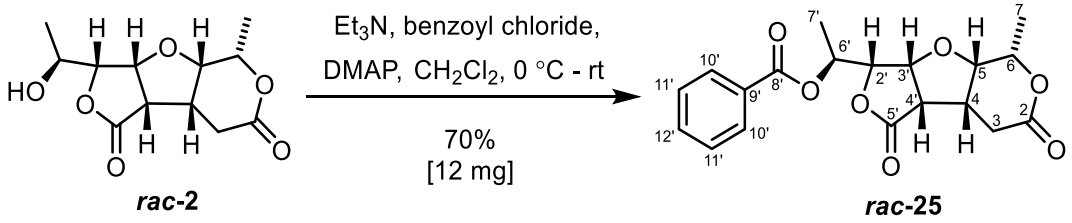

Compound ***rac*-25** was prepared utilising a modified literature procedure.[43]

Racemic angiopterlactone B (**2**) (12.5 mg, 48.8 µmol) was dissolved in CH_2Cl_2 (1 mL) and the solution was cooled to 0 °C. Et_3N (68.0 µL, 488 µmol), benzoyl chloride (17.0 µL, 146 µmol) and DMAP (few crystals) were added in sequence and the solution was consequently warmed to rt and left to stir for 0.5 h. The reaction mixture was then concentrated under reduced pressure and the crude material was purified by flash chromatography (silica gel, dichloromethane + 4% methanol) to afford adduct ***rac*-25** as a white crystalline solid (12 mg, 34 µmol, 70%). The NMR data matched the data collected for compound **25** in Section 1.4.2.9.

Chapter 2: Computational NMR Prediction Studies

Chapter 1 provided a detailed description of the successful total synthesis of (–)-angiopterlactone B (**2**). Next we set out to understand why we had not observed the related natural product angiopterlactone A (**1**) (Figure 9). This compound was co-isolated with angiopterlactone B (**2**) in substantial amounts and was presumed to be its biosynthetic precursor.[2]

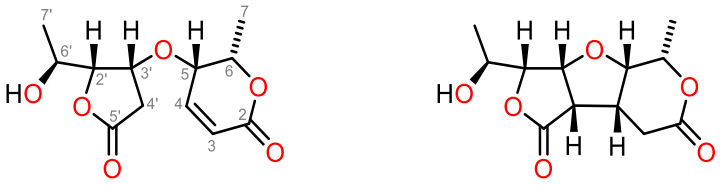

angiopterlactone A (**1**)
230 mg isolated

angiopterlactone B (**2**)
20 mg isolated

Figure 9: Isolation chemists' representation of the angiopterlactones (**1**, **2**)[2]

2.1 Introduction

2.1.1 Project Aims and Objectives

Based on biosynthetic speculations, angiopterlactone A (**1**) should presumably have been observed as an intermediate to angiopterlactone B (**2**) (Scheme 25). After analysing the 1D and 2D NMR spectra provided in the appendix of the isolation paper[2], we believe the general atom connectivity within the structure to be correct. However the question arose as to whether the isolation chemists can unequivocally assign the relative/absolute configuration within the molecule. The relative stereochemistry between H3'-H5 was assigned as *cis* based on their NOESY correlation. Considering these protons are located next to freely rotatable bonds, a NOESY correlation is not sufficient evidence that the relative assignment of these protons should be *cis*. Furthermore, the absolute configuration of position C6' was assigned utilising the modified Mosher's method. As we previously discovered some typographical errors and discrepancies in their Mosher method (see Chapter 1, Section 1.2.3), we are not certain that position C6' can be unequivocally assigned as *S*. Thus, we speculated that (–)-angiopterlactone A (**1**), may actually be a diastereoisomer of the reported structure. To this end, a series of computational NMR prediction studies were completed to investigate the relative configuration of (–)-angiopterlactone A (**1**).

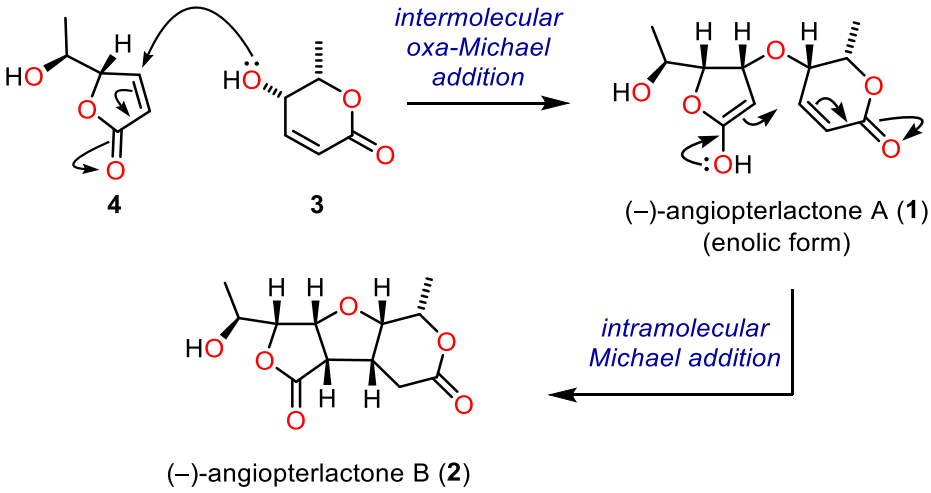

Scheme 25: Summary of our biosynthetic speculations from Chapter 1

2.1.2 General Background Theory

Quantum Mechanics and the Schrödinger Equation

At the heart of quantum chemistry lies the Schrödinger equation, for which the time-independent equation is given in shorthand form by:

$$\boldsymbol{H}\psi = E\psi \qquad \textbf{Eq. 1}$$

where the action of the Hamiltonian operator ($\boldsymbol{H}$) on a system described by the wavefunction (ψ), returns the total energy (E) of the system.[51] This equation can only be solved exactly for single electron systems and thus for larger molecules, approximations must be introduced. One key step in this direction is the *Born-Oppenheimer* (BO) approximation, which separates nuclear and electronic motion as a result of their large differences in mass.[51,52] This allows the electronic part to be solved utilising nuclear positions as parameters, resulting in a potential energy surface (PES) for which minima and saddle-points (transition states) may be located.[51,53,54]

One of the main approaches to solving the Schrödinger equation within the BO approximation is the density functional theory (DFT). The foundation of this approach was introduced by Hohenberg and Kohn in 1964, who proved that the ground state energy of a system can be obtained from its electron density.[55] However, difficulties were encountered when describing all energy components as a functional of electron density.[56] In 1965, Kohn and Sham developed a practical solution to this problem.[57] The basis of their approach involved splitting the kinetic energy functional into two parts: one which can be calculated exactly (electrons are

considered as non-interacting) and another which required approximations to be made to account for electron-electron interactions.[58] The Hamiltonian operator can be divided into four terms:

$$\boldsymbol{H = H_K + H_V + H_J + H_{XC}} \qquad \textbf{Eq. 2}$$

where *K* represents the kinetic component, *V* the electron nuclear interaction, *J* the Coloumb component and *XC* the exchange-correlation term (to account for electron-electron interactions). A number of approaches have been developed for the approximation of this exchange-correlation term and a hierarchy of these methods and example functionals are presented in Figure 10.

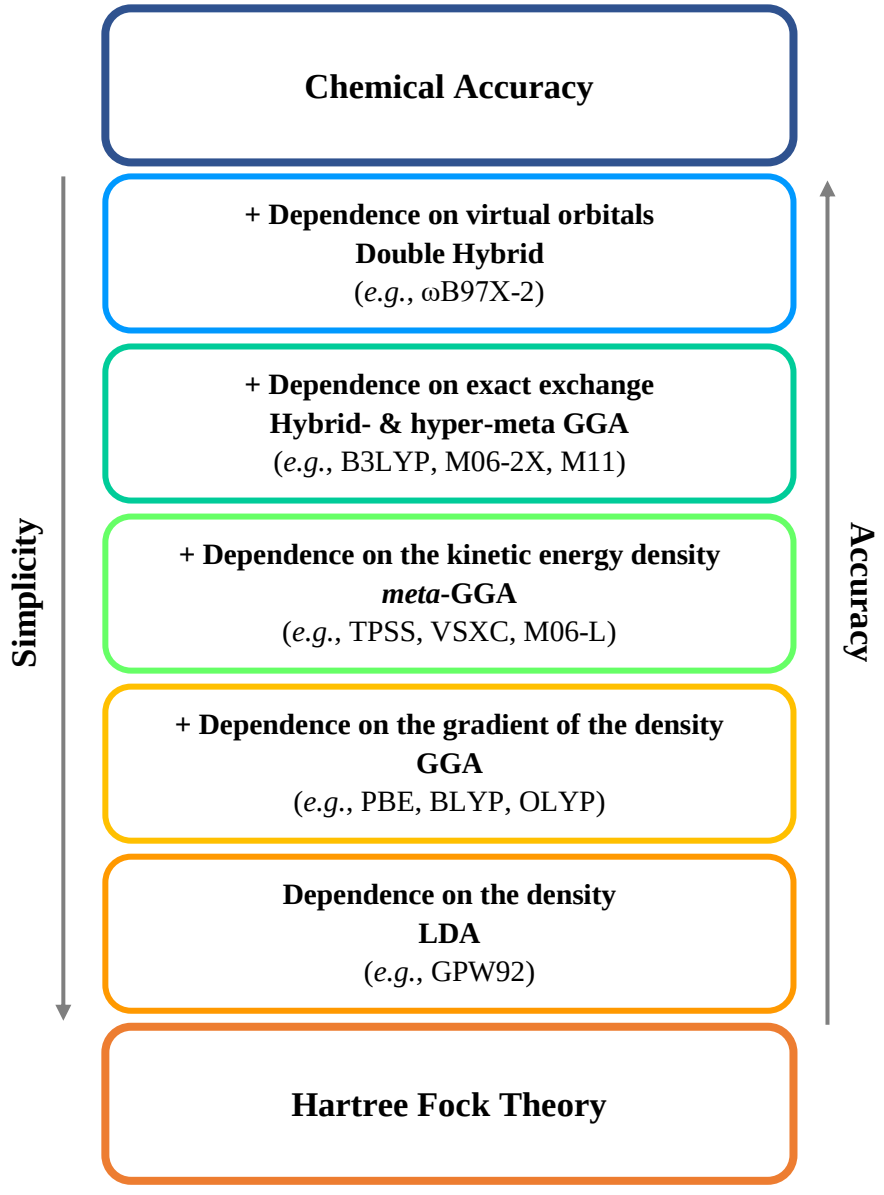

Figure 10: Hierarchy of exchange-correlation functionals; representative examples are provided in parentheses (adapted from *Chem. Soc. Rev.* **2016**, *45*, 6093-6107)[59]

Basis Sets

Basis sets are a combination of functions (basis functions) that describe molecular orbitals. In theory, any type of function (*e.g.*, Slater or Gaussian) may be utilised, as long as i) it describes the physics of the system and ii) it is easy to calculate.[56] Slater functions (based on hydrogen atomic orbitals), fulfil the first requirement, however their evaluation is computationally demanding.[53] To overcome this problem, Gaussian functions were introduced, as they can be more readily solved.[53] However, Gaussian functions provide less accurate descriptions of the system and thus a combination of Gaussian functions is typically used.[56] A minimum description of the occupied orbitals is provided by Single Zeta (SZ) basis sets, which utilise a single function for every occupied orbital. Double Zeta (DZ) basis sets double the number of functions utilised for each occupied orbital and these can be further increased to Triple (Quadruple, etc.) Zeta basis sets.[56] Pople developed split valence basis sets in which core and valence electrons are treated separately. For example the 3-21G basis set utilises 3 functions to describe the core atomic orbitals, 2 for the first valence orbital and 1 for the second valence orbital.

A further improvement in the description of a system can be achieved by the addition of diffuse (with small exponents) and polarisation (with increased angular momentum) functions. Diffuse functions improve the description of electron densities (which may be far from the nucleus), while polarisation functions can improve the modelling of bonding and electron distribution.[53,56]

Transition State Theory

Transition state theory (TST) allows the connection between computed and experimental observables. Within the *BO* approximation, a chemical reaction can be described as the movement of nuclei from one minimum to the next, *via* a transition state (TS) (Figure 11).[56] The TS is the configuration of the molecule which divides the reactant from the product and is represented by saddle points on the PES.

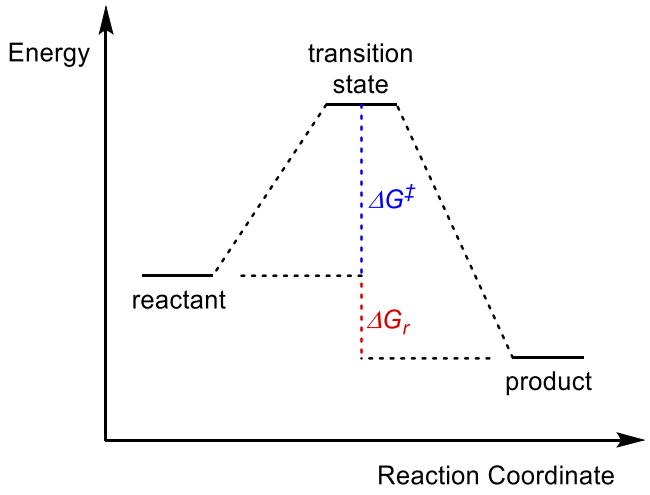

Figure 11: Graphical representation of a generic reaction pathway

The free energy of activation ($\Delta G^{\ddagger}$) and the free energy of the reaction (ΔG_r) can be obtained from energy profiles (Figure 11). The free energy of activation is the energy difference between a transition state of a reaction and its corresponding reactants and can be utilised to estimate the rate constant (k) for a chemical reaction. The rate constant can be described by the Eyring equation (Eq. 3), where h is Planck's constant, k_B is Boltzmann's constant, R is the ideal gas constant and T is the temperature.[56]

$$k = \frac{k_B T}{h} e^{\frac{-\Delta G^{\ddagger}}{RT}} \qquad \textbf{Eq. 3}$$

Solvent Considerations

Another important aspect to consider when describing the environment of a system, is the inclusion of a solvent. Computations are often completed in the gas-phase, in which the surroundings of a molecule are treated as a vacuum.[60] However, interactions between the solute and the solvent (*e.g.*, *via* hydrogen bonding) can affect the compound's geometry and thus treating a molecule in the gas-phase can incur inaccuracies and errors. Such errors can be minimised by utilising solvent models, which are generally divided into explicit and implicit methods.

The explicit solvation model involves the inclusion of individual solvent molecules around the compound of interest and therefore requires extensive sampling of the conformational space.[56,60] This is computationally demanding and makes the use of implicit solvent models an attractive alternative. These model the solvent according to its dielectric constant and therefore lack an explicit description of non-covalent interactions. Examples of implicit solvent models

include the polarisable continuum model (PCM) and the density based solvation model (SMD).[60]

2.1.3 Computational Nuclear Magnetic Resonance Spectroscopy (NMR)

NMR Spectroscopy for Structural Elucidation

NMR spectroscopy is a powerful and versatile tool, which provides chemists with the ability to complete structural elucidations.[61] Despite the developments in the field of NMR spectroscopy and the wide array of techniques available (ranging from 1D spectra to powerful 2D techniques), incomplete or incorrect structural assignments of natural products still occur.[62]

The assignment of stereochemistry can be complex, particularly if multiple diastereoisomers are possible. Such cases can necessitate the synthesis of multiple diastereoisomers and interpretation of the NMR data to make a conclusive structural assignment. This is a time-consuming and challenging process and thus the ability to accurately simulate and predict NMR spectra could provide the experimental chemist with invaluable insights. Such computational techniques have become increasingly popular and thus efforts have gone into the development of reliable methods to allow steadfast computations of NMR properties, such as chemical shifts (δ) and coupling constants (*J*).

Chemical Shifts

The computational prediction of NMR chemical shift values relies on the ability to describe the electron density around a nucleus, as well as how this electron density responds to a magnetic field.[61] The NMR shielding tensor (σ) is obtained from the second derivative of the total energy (*E*) with respect to the magnetic field (*B*) and the nuclear magnetic moment (μ) (Eq. 4).[61,63]

$$\sigma = \left.\frac{\partial^2 E}{\partial B \partial \mu}\right|_0 \qquad \textbf{Eq. 4}$$

When applying a magnetic field vector to electronic structure computations, a problem termed the *gauge problem* is encountered.[61] In order to introduce a magnetic field into calculations, an arbitrary origin needs to be defined for the associated vector potential. This is impractical, as the computed shielding tensor would therefore depend upon the position of the vector. To

avoid this dependence, the most common approach is to utilise gauge-including atomic orbitals (GIAOs) in the NMR property computation.[60,61]

In order to compare the computational to the experimental results, the shielding tensor needs to be converted into a chemical shift. There are two main approaches commonly utilised for this conversion: utilising a reference compound or applying the linear scaling method. The use of a reference compound (for example tetramethylsilane, $SiMe_4$) involves the calculation of both the compound of interest and the reference compound, utilising the same computational method. The chemical shift (δ_i, in parts per million) can then be obtained by subtracting the shielding tensor of the compound of interest (σ_i), from the shielding tensor of the reference compound (σ_{ref}) (Eq. 5).[64]

$$\delta_i = \sigma_{ref} - \sigma_i \qquad \textbf{Eq. 5}$$

The second way to obtain NMR chemical shifts from shielding tensors, is to use the linear scaling method. This involves the use of several reference compounds, whose shielding tensors must be computed utilising the same computational method as for the compound of interest. The computed shielding tensors are then plotted against their corresponding experimental chemical shifts and a line of best fit is obtained. Utilising the slope and intercept from this line of best fit, the chemical shift of the compound of interest can be obtained from its shielding tensor following Eq. 6.[60] This approach has the advantage that it can remove systematic errors and it has been reported that well-performing methods have slopes deviating no more than ±0.05 from –1 and R^2 values ≥0.995.[60,65]

$$\delta = \frac{intercept - \sigma}{-slope} \qquad \textbf{Eq. 6}$$

Coupling Constants

Coupling constants (*J*-values) can prove to be useful in the assignment of the relative configuration and conformation of molecules, due to their dependence on geometry. They are typically reported in units of Hertz and their magnitude is a result of a combination of factors, such as bond distances and dihedral angles.[61] The magnitude of $^3J_{H\text{-}H}$ can be predicted utilising the Karplus equation (Eq. 7), where A, B and C are empirically derived constants dependent on the atoms and substituents in a system and ϕ is the dihedral angle between H-C-C-H.[61,66]

$$J_{H-H} = A + B\cos\phi + C\cos 2\phi \qquad \textbf{Eq. 7}$$

Reports in the literature show that both homonuclear and heteronuclear total nuclear spin-spin coupling constants can be computed utilising DFT.[67,68,69] The contributing factors are the spin-dipole (SD), the Fermi contact (FC), diamagnetic spin-orbit (DSO) and paramagnetic spin-orbit (PSO) terms:[70]

$$^{n}J = {}^{n}J_{FC} + {}^{n}J_{SD} + {}^{n}J_{PSO} + {}^{n}J_{DSO} \qquad \textbf{Eq. 8}$$

where *n* is the number of chemical bonds between the two nuclei under study. The SD and FC terms are a result of the interaction between the nuclear magnetic field and the spin of the electrons, whereas the DSO and PSO terms represent the interactions between the nuclear magnetic moments and those created by the movement of electrons. These four terms vary in their contribution to the coupling constant depending on the nuclei and the extent of their separation.[61,68]

General Workflow

Computational NMR spectroscopy studies involve a number of steps (Figure 12). As some molecular fragments are flexible, these studies typically necessitate an initial conformational search to locate the lowest energy conformers of the compound of interest. Each conformer is then subjected to geometry optimisation and characterised as a real minimum (DFT optimisation). This is followed by NMR calculations, from which electronic energies and isotropic shielding constants are extracted. Once the computed isotropic shielding constants are in hand, their relative contributions are calculated utilising the Boltzmann analysis (conformer averaging). The Boltzmann weighted isotropic values must then be converted into chemical shifts (δ). Computed chemical shifts are then compared to experimental/ literature values, in order to perform an error evaluation. More detailed descriptions of each of these steps are in the sections to follow.

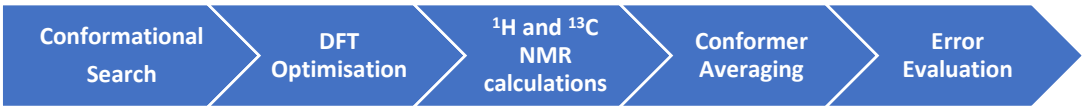

Figure 12: General workflow for a computational NMR prediction study

Conformational Sampling

Organic molecules exist in different low energy conformers, which depend on their flexibility and the experimental conditions. Flexible molecules may access several conformations at the

temperature at which the NMR experiment is run and therefore experimental NMR spectra represent a Boltzmann-weighted average of all of the conformers. As NMR property calculations are completed on static structures with specific coordinates, a similar consideration must be implemented computationally.

Conformational searches depend on the size and complexity of the molecule, as well as the presence of rotatable bonds. For small molecules with few rotatable bonds, one may opt to manually locate relevant conformers by making educated guesses as to the geometries, followed by running them through an optimisation process.[60] Alternatively, an automated conformational search employing molecular mechanics can be employed. Several programs capable of such a search exist, including but not limited to Macromodel, Spartan and TINKER.

DFT Optimisation and NMR Calculations

A number of DFT functionals for the completion of geometry optimisations and NMR property calculations have been used in the literature, including mPW91PW91, ωB97XD, M06-2X and B3LYP.[71] A common choice of basis set are Pople's split valence basis sets. Jensen developed specific basis sets for the calculation of nuclear magnetic shielding constants (termed pcSseg-*n*), however concluded that these often perform worse than standard basis sets.[72] Tantillo has created an online repository summarising linear regression parameters for various combinations of functionals and basis sets utilised for geometry optimisation and isotropic shielding constant calculation.[73]

Boltzmann Weighting

Upon extraction of the energies, a Boltzmann weighting is completed to determine the relative contribution of each conformer. The weighting of each conformer (ω_i) can be described by Eq. 9, where *E* is the energy extracted from the single point calculation, R is the gas constant and T is the temperature.[61] These Boltzmann weighted isotropic values are then converted into a chemical shift, which can be achieved utilising different approaches (see *Chemical Shifts* section above).

$$\omega_i = \frac{e^{\frac{-\Delta E_i}{RT}}}{\sum_i^N e^{\frac{-\Delta E_i}{RT}}} \qquad \textbf{Eq. 9}$$

Analysis and Error Evaluation

In order to compare different computational techniques and their ability to accurately predict NMR data, a set of parameters or statistical methods are required. Common parameters utilised in the literature include the mean absolute error (MAE), standard deviation, regression analysis (R^2) and root-mean-square-error (RMSE).[64,74,75,76] The mean absolute error can be described by Eq. 10, where N is the number of chemical shifts used in the comparison, δ_{calc} is the computed chemical shift and δ_{exp} is the experimental chemical shift.[74]

$$MAE = \frac{1}{N}\sum_{i}^{N}\left|\delta_{calc} - \delta_{exp}\right| \qquad \textbf{Eq. 10}$$

Although these parameters can prove useful in comparing computational techniques, there are situations in which more sophisticated processes are required. For example in the case of diastereoisomers, their chemical shifts can be similar to one another thus preventing the ability to confidently assign the correct structure based on these parameters. Alternatively/additionally to utilising these parameters, a number of statistical methods have been developed, whose increased complexity provide more confidence in structural assignments.

In 2009, Smith and Goodman introduced the CP3 parameter, which addressed the problem of assigning two sets of experimental data to two possible structures.[74] CP3 is based on the comparison between differences in computed chemical shifts and differences in experimental chemical shifts. In conjunction with Bayes' theorem, utilising this parameter then allows the assignment of the structure.[74] One of the biggest limitations of CP3 is the constraint of needing two sets of experimental data and two or more candidate structures.[77] This limitation led Smith and Goodman to the development of a new probability measure in 2010, which they termed DP4.[77]

The major advantage of DP4 over CP3 is that it only requires one set of experimental data, to which two or more candidate structures can be compared.[77] The DP4 analysis is based on calculated error probabilities for scaled computed chemical shifts for each hydrogen and carbon atom. It assumes that these errors follow a statistical Student's *t*-distribution. Bayes' thereom is then applied to transform the product of the individual error probabilities for each atom in the structure, into an overall probability that the structure is correct. This can be summarised by:

$$P_i = \frac{\prod_{k=1}^{N}(1 - T^{v}\left(\frac{\left|\left(\delta^{i}_{scaled,k} - \delta_{exp,k}\right) - \mu\right|}{\sigma}\right))}{\sum_{j=1}^{m}\left[\prod_{k=1}^{N}(1 - T^{v}\left(\frac{\left|\left(\delta^{j}_{scaled,k} - \delta_{exp,k}\right) - \mu\right|}{\sigma}\right))\right]} \quad \textbf{Eq. 11}$$

This equation[77] provides the probability (*P*) that candidate structure '*i'* is the correct one out of the available possibilities (*m*). The cumulative Student's t-distribution function (T^{v} with *v* degrees of freedom) is characterised by the experimental chemical shift of nucleus *k* ($\delta_{exp,k}$), the scaled calculated chemical shift (using the linear analysis technique) of nucleus *k* in candidate structure *j* ($\delta^{j}_{scaled,k}$), the mean (μ) and the standard deviation (σ). The values of *v*, μ and σ were obtained from an analysis of a set of test molecules for which the authors had experimental data, where *v* = 11.38 (^{13}C) or 14.18 (^{1}H), μ = 0 and σ = 2.306 ppm (^{13}C) or 0.185 ppm (^{1}H).[77]

DP4 was further developed and expanded upon by Sarotti and co-workers in 2015 and was termed DP4+.[78] In order to improve the accuracy of the DP4 predictions, they modified the procedure to include unscaled chemical shifts, as well as utilising higher levels of theory for the GIAO NMR calculations.[78,79]

2.1.4 Example Case Studies from the Literature

Computational NMR prediction studies have been utilised to facilitate numerous structural reassignments of natural products. Here we have chosen three representative examples, which showcase how the applications of such computational studies have developed over time.

The first example (vannusal B) utilised NMR prediction studies post-synthesis. The structure (with the exception of absolute configuration) of the marine natural product vannusal B, was originally assigned in 1999 by Pietra and co-workers using a combination of mass spectroscopy and NMR spectroscopy techniques (Figure 13).[80] In 2010, Nicolaou and co-workers successfully synthesised the originally proposed structure of vannusal B, which led to the discovery that the spectroscopic data did not match that of the natural product.[81] By completing the laborious synthesis of eight diastereoisomers, the authors successfully revised the structure of vannusal B (Figure 13).[82]

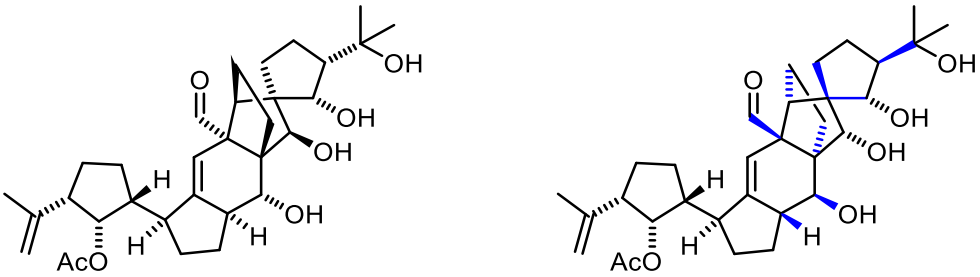

vannusal B
originally assigned structure

vannusal B
revised structure

Figure 13: Originally assigned and revised structures of vannusal B[80,82]

After the structural revision of the molecule, Bagno and co-workers published a computational study of the NMR properties for the eight synthesised diastereoisomers of vannusal B.[83] Calculated ^{13}C chemical shifts and coupling constants ($J_{H\text{-}H}$) revealed that out of the examined structures, the revised structure was the closest match to the experimental data. This demonstrates that the use of computational methods throughout the structural investigations of vannusal B, may have assisted in narrowing down the number of viable targets, on which synthetic efforts could then be focused.

In our second example, computational studies were applied prior to synthesis in order to identify the most likely structure of the natural product nobilisitine A, which was consequently synthesised in the laboratory. This compound was first isolated in 1999 by Evidente and co-workers and its structure was assigned by IR and NMR spectroscopy (Figure 14).[84] Upon the synthesis of the enantiomer of the originally proposed structure, Banwell and co-workers noted that the ^{1}H and ^{13}C spectra did not match those reported for the natural product.[85] This led Tantillo and Lodewyk into a computational NMR spectroscopy investigation in an effort to predict the true structure of nobilisitine A.[86] Upon computing ^{1}H and ^{13}C chemical shifts for eight diastereoisomers and comparing them to experimental results of the originally proposed structures, they predicted a revised relative stereochemistry (Figure 14). They then utilised the DP4 method to gain confidence in their tentative assignment of the structure, which resulted in a 99.8% calculated probability.[86] Based on these computational studies, Banwell and co-workers set out to synthesise this newly proposed structure, during which they confirmed a match to the spectroscopic data of the natural product.[87]

nobilisitine A
originally assigned structure

nobilisitine A
revised structure

Figure 14: Originally assigned and revised structure of nobilisitine A[84,87]

The final example involved the natural products dichrocephone A and dichrocephone B. Tantillo, Christmann and co-workers combined the power of biosynthetic considerations with computational NMR spectroscopy studies and total synthesis, to successfully complete the total synthesis and structural revision of dichrocephone A (Figure 15).[88] Upon synthesising the structure originally assigned as dichrocephone A, the authors realised that the ^{1}H and ^{13}C NMR spectra did not match those reported for the natural product.[88,89] Inspection of heteronuclear multiple-bond coherence spectra led the authors to the conclusion that the correct structure for dichrocephone A would likely be a diastereoisomer of the proposed structure. Utilising biosynthetic speculations, in which they suggest that dichrocephone A is the precursor to dichrocephone B, they concluded that only two diastereoisomers were conducive to their proposed pathway (these correspond to the originally assigned and the revised structures of dichrocephone A in Figure 15). This significantly narrowed down the possibilities and thus the synthetic targets. In order to support their proposal and possibly eliminate a further diastereoisomer, the authors then completed computational studies. DP4 analysis resulted in a 99.8% probability that the correct structure of dichrocephone A is the diastereoisomer depicted as the 'revised structure' in Figure 15. They successfully synthesised this diastereoisomer, which they confirmed to be the correct structure of dichrocephone A (Figure 15).

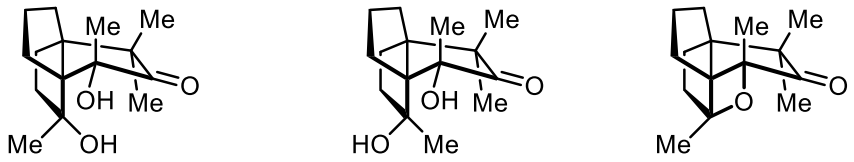

dichrocephone A
originally assigned structure

dichrocephone A
revised structure

dichrocephone B

Figure 15: Originally assigned and revised structures of dichrocephone A and the related natural product dichrocephone B[88]

2.1.5 Biosynthetic Considerations / Structures to Investigate

The case studies from the literature provided examples for the use of computational NMR chemical shift predictions to facilitate structural reassignments of natural products. We began our investigations by examining the originally proposed structure of (–)-angiopterlactone A (**1**). Assuming that the relative stereochemistry is incorrect, there were 16 possible diastereoisomers which needed to be investigated (five stereogenic centres, therefore $2^5 = 32$ potential stereoisomers; 16 pairs of enantiomers). Synthesising these 16 compounds would be a time-consuming process and thus we needed to use an approach that would allow us to narrow down the number of possible structures.

Our biosynthetic speculations proposed reacting γ-lactone **4** and δ-lactone **3** to form angiopterlactone A (**1**) (Scheme 25, Page 69).[1] Based on the assumption that this proposal is correct, we searched the literature for viable building blocks that match our biosynthesis. The δ-lactones ***ent*-3** and **5** have previously been isolated from natural sources and are presumably the aglycones of the known natural products angiopteroside (**9**) and osmundalin (**8**) (Figure 16).[35,90] Thus these compounds formed the basis of our available starting materials. We know from our synthetic experience that such δ-lactones can undergo ring-contractions to their corresponding γ-lactones, which is a process that has also previously been reported in the literature.[6] Thus δ-lactones ***ent*-3** and **5** could form γ-lactones ***ent*-4** and **6** respectively (Figure 16).

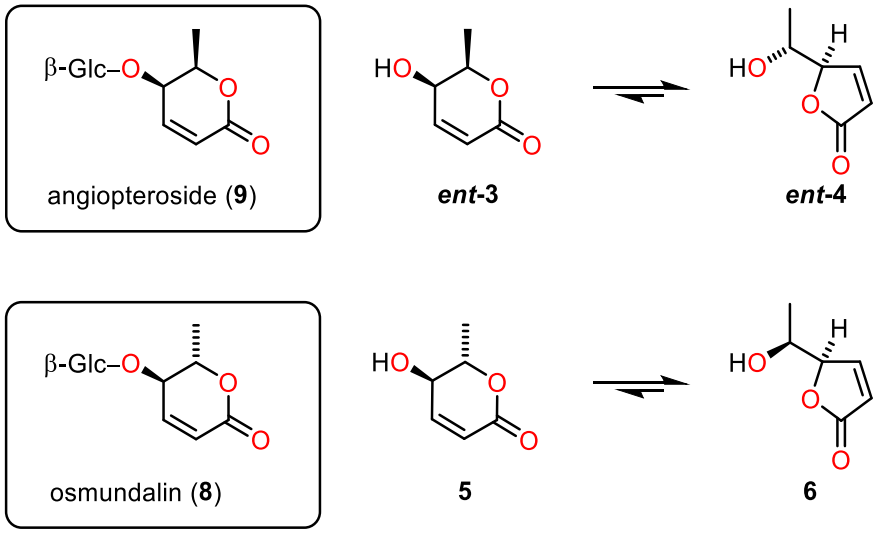

Figure 16: Possible monomeric γ- and δ-lactones ***ent*-3**, ***ent*-4**, **5** and **6**

Based on the assumption that these four lactones are the only ones available in nature for an oxa-Michael addition to occur between a γ- and a δ-lactone, we now have a limited number of

possible combinations. Four structures arise from the combination of each δ-lactone (acting as the Michael donor) with either of the γ-lactones (acting as the Michael acceptor). As the oxa-Michael addition can occur from either the *Si* or *Re* face (labelled in blue and red respectively, Figure 17), these combinations result in a total of eight possible structures of angiopterlactone A (**1**) (labelled I-VIII in Figure 17). These diastereoisomers became the basis for our computational investigations.

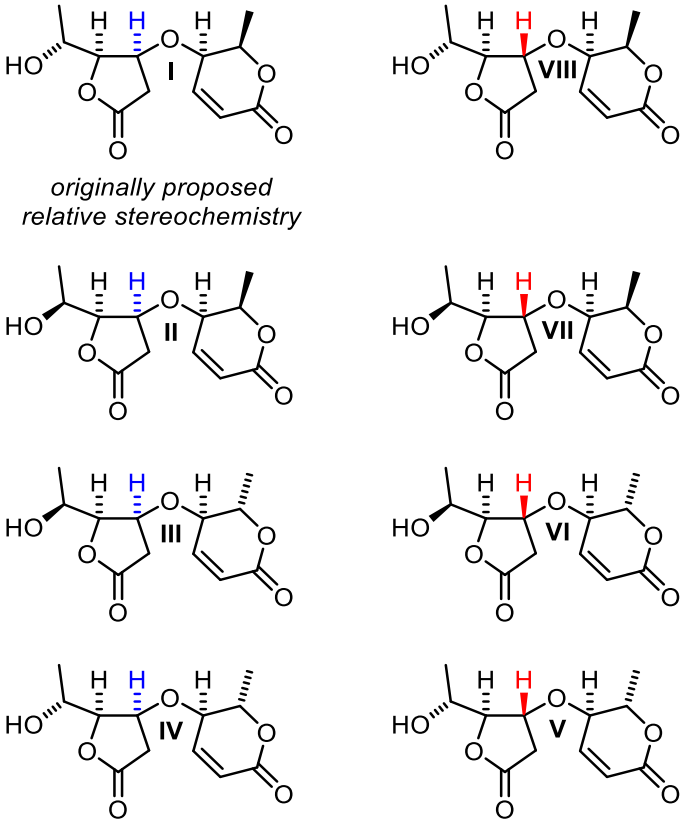

Figure 17: Our suggested eight possible structures of angiopterlactone A (**1**) (originally proposed relative stereochemistry by isolation chemists is represented in I) (*Si* face oxa-Michael addition denoted by blue, *Re* by red)

2.1.6 Literature Protocols and Method Choice

Upon reducing the number of possible structures from 16 to 8, decisions had to be made with regards to our computational methods. These included choosing the functional, basis set size and whether to include solvent in the calculation. A large variety of computational NMR prediction studies have been reported in the literature. We chose four well-reported and detailed protocols (summarised in Table 17) for preliminary testing, which varied in the

computational methods used. Methods 1-3 (M1-M3) utilise the linear regression analysis (see Section 2.1.3) to remove any systematic errors. This requires scaling factors specific to the level of theory applied for both the geometry optimisation and shielding tensor calculations, which are summarised in the Appendix, Table 36, Page 204.

Approach	Geometry Optimisation		NMR Calculation	
	Method	**Solvent (model)**	**Method**	**Solvent (model)**
Method M1[75]	M06-2X 6-31+G(d,p)	**Yes (PCM)**	B3LYP 6-11+G(2d,p)	**Yes (PCM)**
Method M2A[73]	M06-2X 6-31+G(d,p)	**No**	mPW1PW91 6-311+G(2d,p)	**Yes (SMD)**
Method M2B[73]	M06-2X 6-311+G(2d,p)	**No**	mPW1PW91 6-311+G(2d,p)	**Yes (SMD)**
Method M3[65]	B3LYP 6-31+G(d,p)	**No**	mPW1PW91 6-311+G(2d,p)	**Yes (PCM)**
Method M4[91]	mPW1PW91 6-311G(d,p)	**Yes (PCM)**	mPW1PW91 6-311G(d,p)	**Yes (PCM)**

Table 17: Summary of conditions used for each of the approaches

Hoye and co-workers[75] have combined the use of molecular mechanics and DFT to characterise small organic molecules (Table 17, approach M1). They utilised the M06-2X functional for geometry optimisation, followed by NMR calculations using the GIAO method at the B3LYP/6-311+G(2d,p) level of theory. Tantillo *et al.*[60] generated a repository[73] which provides access to empirical scaling factors for computed chemical shifts utilising various combinations of functionals. In our study we utilised the M06-2X functional for the geometry optimisation and the mPW1PW91 functional for NMR calculations (Table 17, approaches M2A and M2B). Utilising these methodologies to form the basis for our investigations, we also tested variations of these approaches to evaluate the effect of solvent and basis set size on the final results. Pierens[65] reported the use of the B3LYP functional for geometry optimisation and the mPW1PW91 functional for the calculation of shielding tensors (Table 17, approach M3). The main advantage of this method is that Pierens utilised a variety of solvents, whereas methods M1 and M2 are restricted to using chloroform, so this methodology formed the basis of our third approach. The final approach we tested (method M4, Table 17) was recently

published by Butts, Myers, Aggarwal and co-workers.[91] They utilised the mPW1PW91 functional for both the geometry optimisation and NMR calculation. Their investigations were aimed towards utilising NMR prediction studies to aid in the identification of the true structures of the natural products baulamycins A and B. This approach is not dissimilar to our endeavours and thus we utilised their studies as a comparison to the previously listed methods.

2.2 Computational Methods

All DFT calculations were performed using the Gaussian 09[92] software. Details of the level of theory utilised for each method are summarised in Table 17, Page 83. All NMR calculations were completed utilising the GIAO method. The functionals used include B3LYP, mPW91PW91, M06-2X and ωB97XD. The B3LYP[93,94] functional is Becke's hybrid 3-parameter functional. MPW1PW91[95,96] is a hybrid functional utilising mPW exchange and PW91 correlation. M06-2X[97] is a hybrid meta exchange correlation functional which has 54% HF exchange (twice the exchange from Truhlar's Minnesota-06 (M06) functional). The ωB97XD[98] functional is a range separated functional which was developed by Head-Gordon and includes empirical dispersion corrections.

Solvent was modelled using an implicit description of chloroform / dimethylsulfoxide applying either the SMD or PCM continuum model. Solvent cavities were defined by the default SMD-Coulomb[99] and UFF[100] atomic radii respectively, except for method M1 in which they were defined by UA0[92] atomic radii for the geometry optimisation and Bondi[101] for the NMR calculation.

Energies (*E*) were evaluated at 298 Kelvin (K). Vibrational entropy contributions towards Gibbs Free energy values (*G*) were calculated utilising a free-rotor approximation for low frequency modes. These calculations were completed utilising GoodVibes.[102] To switch between free-rotor approximations and harmonic approximations for vibrations, a smooth damping function centred around a frequency of 100 cm^{-1} was used.[103] Throughout the discussion, varying energy terms are utilised. *E* is the potential energy taken from the higher level of theory single point calculation (see Table 17, page 83 for the level of theory used). *H* is the enthalpy including the thermal correction from the vibrational contributions $H = E + (H_{low} - E_{low})$, where H_{low} and E_{low} are the enthalpy and potential energy extracted from the geometry optimisation. The final term utilised is *G*, which refers to the Gibbs free energy that has been corrected to consider ro-vibrational frequencies. It can be described by $G = E + (G_{low} - E_{low})$, where G_{low} is the Gibbs Free energy after geometry optimisation.

In order to complete our conformational sampling, we utilised the conformational scanning function (*scan*) installed in the TINKER[104] modelling package. This function uses a basin hopping algorithm to efficiently sample the conformational space, where each basin represents a distinct region of this space. This is followed by local minimisation to identify the lowest energy conformer within each basin. The energy window of conformational minima was set to 10 kcal/mol.

2.3 Results and Discussion

In Section 2.1.1 we proposed that the isolation chemists may have incorrectly assigned the relative configuration of the natural product (–)-angiopterlactone A (**1**). We investigated this proposal by completing computational NMR prediction studies. Methods M1-M4 (Table 17, Page 83) were employed to examine a number of variables and how they might affect our ability to distinguish between diastereoisomers. Methods M3 and M4 were then utilised to compute ^{1}H and ^{13}C chemical shifts and $J_{H\text{-}H}$ coupling constants to distinguish between the eight structures under investigation for (–)-angiopterlactone A (**1**) (compounds I-VIII, Figure 17, Page 82). We then proposed a revised structure for (–)-angiopterlactone A (**1**) and utilised the DP4 analysis to further support this revision.

Please note: *for ready ease of access, a removable, laminated sheet, containing the structures of the investigated diastereoisomers of angiopterlactones A and B (**1**, **2**), can be found at the back of this thesis. These figures have also been reproduced on the final page of this thesis.*

2.3.1 Preliminary Testing

Conformational Search

The first step of a computational NMR prediction study typically involves a conformational search in order to locate the lowest energy conformers of the compound of interest (see Section 2.1.3). For small molecules with few rotatable bonds, relevant conformers can be located manually, however this process can be time consuming and subject to human error. It could therefore be advantageous, particularly for larger systems, to employ automated conformational searches. We tested both techniques on δ-lactone **3** and γ-lactone **4** (Table 18) and utilised method M3 (Table 17, Page 83) to compute ^{1}H and ^{13}C chemical shifts in both chloroform and dimethylsulfoxide (DMSO). A commonly used technique to compare computed and experimental chemical shifts and establish the 'goodness of fit' of a data set is the mean absolute error (MAE) (Eq. 10, Page 77).[75] Thus for both the ^{1}H NMR and ^{13}C NMR data the computed chemical shifts were compared to their respective experimental values to provide MAE values (Table 18).

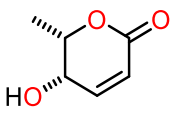
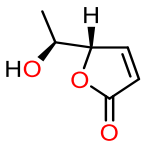

MAE / ppm		δ-lactone 3		γ-lactone 4	
Solvent	**Method**	**^{1}H MAE**	**^{13}C MAE**	**^{1}H MAE**	**^{13}C MAE**
$CHCl_3$	Manual	0.07	5.1	0.15	1.9
	Automated	0.10	1.0	0.13	1.6
DMSO	Manual	0.19	2.9	0.18	1.7
	Automated	0.07	1.0	0.19	1.5

Table 18: ^{1}H and ^{13}C MAE values (ppm) for manual *vs* automated generated conformers of δ-lactone **3** and γ-lactone **4** (method: M3, solvent: $CHCl_3$ / DMSO, energy utilised for Boltzmann analysis: *E*)

The results indicated that generally the use of the automated conformational search resulted in lower ^{1}H and ^{13}C MAE values compared to those obtained when using a manual technique (Table 18). Thus we utilised the conformational scanning function for all future calculations.

Effect of Basis Set Size on Geometry Optimisation

Next, we examined if the basis set size utilised for the geometry optimisation affects the NMR chemical shift predictions. This was analysed using methods M2A and M2B, as both approaches use identical conditions for the NMR calculation, but differ in their basis set size for the geometry optimisation (Table 17, Page 83). The ^{1}H and ^{13}C MAE values were calculated for the δ- and γ-lactones **3** and **4**, as well as their respective diastereoisomers **5** and **6** and are summarised in Table 19.

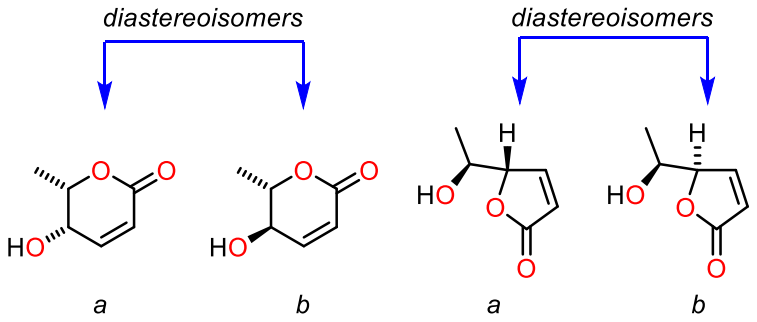

	Method	δ-lactone 3	δ-lactone 5	γ-lactone 4	γ-lactone 6
^{1}H MAE / ppm	*M2A*	0.15	0.22	0.19	0.21
	M2B	0.16	0.22	0.18	0.19
^{13}C MAE / ppm	*M2A*	1.5	3.3	1.4	1.8
	M2B	1.4	3.3	1.4	1.8

Table 19: ^{1}H and ^{13}C MAE values for δ-lactone **3**, γ-lactone **4** and their respective diastereoisomers **5** and **6**. MAE values are calculated by comparing the computed chemical shift of the compound (*a* or *b*), to the experimental shift of *a* (M2A / M2B, $CHCl_3$, *G*)

MAE values can be utilised in order to ascertain the predictive power between diastereoisomers. An example to illustrate how MAE values can be used to distinguish between diastereoisomers is made utilising data from δ-lactone **3** and its diastereoisomer **5**. The ^{13}C MAE value of 1.5 ppm for δ-lactone **3** (M2A, *a*, Table 19) is obtained by comparing the computed shift of lactone **3** (*a*) to the experimental chemical shift of lactone **3** (*a*). In theory, if the computed ^{13}C chemical shift of lactone **5** (*b*) is compared to the experimental value of δ-lactone **3** (*a*), we should observe a much larger MAE value. Utilising our example of diastereoisomer **5** (*b*) and comparing the computed ^{13}C chemical shifts to the experimental values of δ-lactone **3** (*a*), results in an MAE value of 3.3 ppm. This is much larger than the previously observed value of 1.5 ppm and therefore this method provides us with a distinguishing power between these two diastereoisomers.

The comparison of the MAE values between methods M2A and M2B for lactones **3**, **5**, **4** and **6** (Table 19), shows that the differences in MAE values are minimal. Furthermore, based on these MAE values, our ability to distinguish between diastereoisomers remains unaffected. This suggests that for the purposes of our investigations, the use of the computationally more expensive and larger basis set (*i.e.*, method M2B) is not warranted. It has previously been reported in the literature that smaller basis sets in the geometry optimisation are sufficient.[65,105]

Solvent Effects on the Geometry Optimisation

Following our conclusion that larger basis sets for the geometry optimisation did not significantly affect the MAE values or our ability to distinguish between diastereoisomers, we investigated solvent effects. This involved studying how the inclusion/exclusion of solvent in the geometry optimisation affects the subsequently calculated chemical shift values. To explore this we utilised γ-lactone **4** and δ-lactone **3** and methods M1 and M2A (Table 17, Page 83). For each method the geometry optimisation was separately run in the gas and the solvent phase. As this involved modifying the literature procedure, the slope and intercept values reported for methods M1 and M2A (Table 36, Page 204) were no longer applicable and thus isotropic shielding values could not be converted to chemical shifts using the linear scaling method. Instead we utilised the tetramethylsilane (TMS) referencing method (see Section 2.1.3) to obtain chemical shifts. This required an NMR calculation of TMS at the same level of theory as that of each of the methods M1 and M2A, as well as the modified procedures. The corresponding ^{1}H and ^{13}C chemical shift values can be found in the Appendix, Table 37, Page 205.

Method M2A was originally reported as utilising the gas phase in the geometry optimisation. Upon calculating ^{1}H and ^{13}C MAE values for γ-lactone **4** and δ-lactone **3**, we found that regardless of whether the geometry optimisation was run in the solvent or gas phase, MAE values are nearly identical (Table 20).

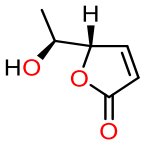

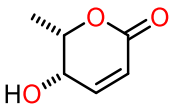

		γ-lactone 4	δ-lactone 3
^{1}H MAE / ppm	***Gas***	0.20	0.20
	Solvent	0.19	0.20
^{13}C MAE / ppm	***Gas***	6.1	5.5
	Solvent	5.9	5.4

Table 20: ^{1}H and ^{13}C MAE values for γ-lactone **4** and δ-lactone **3** (M2A, gas / $CHCl_3$, *G*)

An analogous approach was taken utilising method M1, which usually includes solvent in the geometry optimisation. The MAE values for γ-lactone **4** and δ-lactone **3**, reflect that the differences in MAE values for calculations run in the gas or solvent phase were minimal (Table 21). Thus the added computational cost of using solvent in the geometry optimisations is unlikely to outweigh the gain in accuracy of the results.

		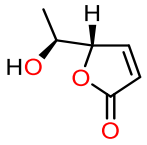 γ-lactone 4	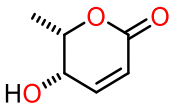 δ-lactone 3
^{1}H MAE / ppm	***Gas***	0.26	0.28
	Solvent	0.25	0.27
^{13}C MAE / ppm	***Gas***	3.0	2.9
	Solvent	2.8	2.9

Table 21: ^{1}H and ^{13}C MAE values for γ-lactone **4** and δ-lactone **3** (M1, gas / $CHCl_3$, *G*)

Drawing Comparisons Between Methods - M1 vs. M2 vs. M3

We previously investigated the effect of basis set size on the geometry optimisation and found that the smaller basis set gave us satisfactory results. Next we investigated whether including solvent in the geometry optimisation affects the results and found that for our purposes, calculations in the gas phase were sufficient. These factors were taken into consideration when choosing with which method(s) to proceed for the analysis of the angiopterlactones (**1**, **2**).

Based on our previous investigations we could eliminate method M1, as the geometry optimisation is run in the solvent phase. Furthermore we could also disregard method M2B, due to the larger basis set size used in the geometry optimisation. Next we compared the results of methods M2A and M3, both of which run the geometry optimisation in the gas phase and utilise a relatively small basis set of 6-31+G(d,p). Whereas method M2A restricts the user to computing NMR data in chloroform, method M3 has the distinct advantage that the authors completed investigations using a variety of solvents. As the isolation chemists reported the NMR data of (−)-angiopterlactone A (**1**) in DMSO, we required the ability to utilise this solvent in our computations. Therefore we needed to investigate if method M3 provides similarly accurate results to method M2A.

Previously, we computed ^{1}H and ^{13}C MAE values for the γ-lactone **4** and δ-lactone **3** utilising method M2A (Table 17, Page 83). This approach was then used to complete computations for (+)-angiopterlactone B (**2**) (Table 22). Following this, method M3 was applied to obtain ^{1}H and ^{13}C MAE values for γ-lactone **4**, δ-lactone **3** and (+)-angiopterlactone B (**2**) (Table 22).

Method	MAE / ppm	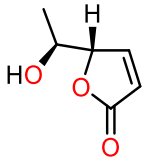 γ-lactone 4	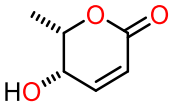 δ-lactone 3	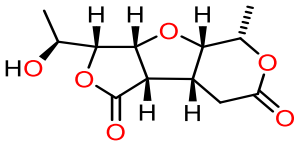 angiopterlactone 2
M2A	**^{1}H**	0.19	0.15	0.17
(CHCl$_3$)	**^{13}C**	1.4	1.5	1.0
M3	**^{1}H**	0.12	0.09	0.09
(CHCl$_3$)	**^{13}C**	1.5	1.0	1.0
M3	**^{1}H**	0.17	0.06	0.12
(DMSO)	**^{13}C**	1.3	1.0	1.3

Table 22: ^{1}H and ^{13}C MAE values for γ- and δ-lactones **4** and **3**, as well as (+)-angiopterlactone B (**2**) (M2A / M3, $CHCl_3$ / DMSO, *G*)

The data in Table 22, shows that generally method M3 provides more accurate ^{1}H and ^{13}C chemical shift predictions (reflected by the smaller MAE values). Thus we moved forward with this methodology to compute the NMR chemical shifts of these compounds in the solvent DMSO (Table 22). The results suggest that the predictions in DMSO give us similar ^{1}H and ^{13}C MAE values to those observed when utilising chloroform and thus we could now utilise this method to compute the chemical shifts of the diastereoisomers of the angiopterlactones (**1**, **2**).

Method M3 (DMSO) – Investigation into Energies

Next we investigated whether the inclusion of thermal and entropic effects (*E vs. H vs. G*) would affect our ability to distinguish between diastereoisomers. Employing method M3 (DMSO), the ^{1}H and ^{13}C chemical shifts and coupling constants ($J_{H\text{-}H}$) were computed for γ-lactone **4**, δ-lactone **3**, angiopterlactone B (**2**) and the seven relevant diastereoisomers (based on the diastereoisomers under investigation for (–)-angiopterlactone A (**1**), discussed in Section 2.1.5).

The ^{1}H, ^{13}C and $J_{H\text{-}H}$ MAE values for γ-lactones **4** and **6** were calculated by comparing their respective computed NMR data, to the experimental data of lactone **4** (Table 23). This method is used for all compounds throughout the remainder of this chapter. The results reflect that inclusion of thermal and entropic corrections barely affect the MAE values. The same trend was observed for δ-lactones **3** and **5** (Table 23). When comparing the MAE values of

diastereoisomers **4** and **6**, we noted that it was not possible to distinguish between them. For δ-lactone **3** and its diastereoisomer **5** on the other hand, the distinguishing power between the correct and the incorrect structure remains intact for all three energies.

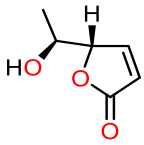

γ-lactone 4 (*a*)

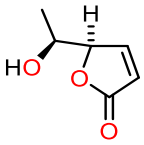

γ-lactone 6 (*b*)

	E	***H***	***G***	***E***	***H***	***G***
^{1}H MAE / ppm	0.19	0.18	0.17	0.12	0.11	0.11
^{13}C MAE / ppm	1.5	1.4	1.3	1.4	1.4	1.5
J MAE / Hz	0.7	0.7	0.7	0.6	0.6	0.7

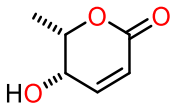

δ-lactone 3 (*a*)

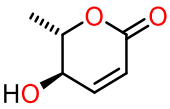

δ-lactone 5 (*b*)

	E	***H***	***G***	***E***	***H***	***G***
^{1}H MAE / ppm	0.07	0.07	0.06	0.14	0.15	0.16
^{13}C MAE / ppm	1.0	1.0	1.0	3.1	3.2	3.2
J MAE / Hz	0.4	0.4	0.4	2.0	2.2	2.2

Table 23: ^{1}H, ^{13}C and $J_{H\text{-}H}$ MAE values for lactones **4** and **3**, as well as their diastereoisomers **6** and **5**. MAE values are calculated by comparing the computed chemical shift of the compound (*a* or *b*), to the experimental shift of *a* (M3, *E* / *H* / *G*, DMSO)

To complete further investigations into the thermal/entropic/enthalpic effects on the predicted chemical shifts and coupling constant data, calculations were completed for (+)-angiopterlactone B (**2**) (compound I) and seven of its diastereoisomers (II-VIII) (Table 24). ^{1}H, ^{13}C and $J_{H\text{-}H}$ MAE values were calculated by comparing the computed NMR data of a compound (*e.g.*, compound IV), to the experimental NMR data of (–)-angiopterlactone B (**2**).

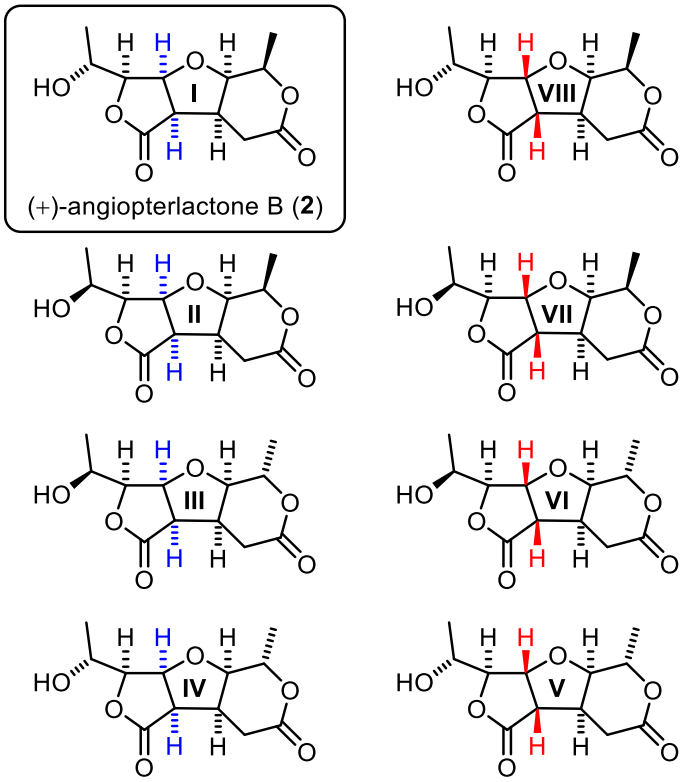

^{1}H MAE / ppm	I	II	III	IV	V	VI	VII	VIII
E	0.12	0.11	0.17	0.18	0.17	0.26	0.23	0.14
H	0.12	0.12	0.17	0.18	0.17	0.26	0.23	0.14
G	0.12	0.12	0.18	0.18	0.18	0.26	0.23	0.15
^{13}C MAE / ppm	**I**	**II**	**III**	**IV**	**V**	**VI**	**VII**	**VIII**
E	1.4	1.5	2.2	2.3	3.1	2.7	3.1	3.5
H	1.4	1.4	2.2	2.3	3.1	2.7	3.1	3.5
G	1.3	1.4	2.2	2.2	3.1	2.7	3.1	3.4
$J_{H\text{-}H}$ MAE / Hz	**I**	**II**	**III**	**IV**	**V**	**VI**	**VII**	**VIII**
E	1.0	0.9	2.4	2.6	4.1	3.5	1.8	2.3
H	1.0	0.8	2.4	2.6	4.1	3.6	1.8	2.3
G	0.9	0.8	2.4	2.5	4.1	3.6	1.8	2.3

Table 24: ^{1}H, ^{13}C and $J_{H\text{-}H}$ MAE values for (+)-angiopterlactone B (**2**) (compound I) and seven of its diastereoisomers (II-VIII) (blue: initial oxa-Michael addition from *Si* face; red: initial oxa-Michael addition from *Re* face). MAE values are calculated by comparing the computed chemical shift of the relevant compound (I-VIII) to the experimental shift of I (M3, *E* / *H* / *G*, DMSO)

The results show that differences between ^{1}H, ^{13}C and $J_{H\text{-}H}$ MAE values across the three energies are relatively small and thus inclusion/exclusion of thermal and entropic contributions does not significantly affect the data. As the MAE values for *G* of γ-lactone **4**, δ-lactone **3** and

(+)-angiopterlactone B (**2**) (compound I) were always less than or equal to those of *E* and *H*, we decided to utilise *G* for all future calculations.

2.3.2 An Alternative Approach: Method M4

During our investigations we became aware of the work of Butts, Myers, Aggarwal and co-workers who published an alternative protocol (herein described as method M4).[91] In this protocol, final geometry optimisations were carried out at the mPW1PW91/6-311G(d,p) [PCM (CH_3OH)] level of theory, followed by the NMR calculation at the mPW1PW91/6-311G(d,p) [PCM (CH_3OH)] level of theory (Table 17, Page 83).[91] The authors then used Boltzmann population analyses, as we have done previously, to weight the conformers generated for each structure. M4 differs from our previously employed methods in that instead of using the linear regression method to convert the isotropic shielding tensors into chemical shifts, they used the TMS referencing technique (see Section 2.1.3). Upon acquiring the calculated chemical shifts, systematic errors were then removed by calculating a scaled chemical shift according to the linear scaling method. This is a similar approach to that detailed by Goodman and Smith to complete their DP4 analysis (Section 2.1.3).[77] Method M4 further details the use of Boltzmann averaged scalar coupling constants ($J_{H\text{-}H}$ and $J_{H\text{-}C}$) to distinguish between diastereoisomers. Upon computing the ^{1}H-^{1}H and ^{1}H-^{13}C coupling constants, they were weighted according to the Boltzmann population. Butts, Myers, Aggarwal and co-workers then applied a 6% linear scaling correction to the total calculated nuclear spin-spin coupling constant prior to calculating the Boltzmann populations.

Butts, Myers, Aggarwal and co-workers used a variety of analytical techniques, which included the use of MAE values as well as the DP4 analysis. The authors noted that these alone were insufficient in providing structural discrimination between their proposed diastereoisomers. They then utilised the χ^2 (reduced) analysis to better distinguish between structures. The χ^2 values were calculated utilising Eq. 12, in which δ_{cal}^{i} is the calculated and Boltzmann averaged chemical shift for nucleus *i*, δ_{exp}^{i} is the experimental chemical shift and σ_{δ}^{2} is the square of the expected standard deviation. The authors based these expected standard deviations on some literature values for rigid molecules, as well as their own in-house experience. The values of these standard deviations are: 0.15 ppm for δH, 1.5 ppm for δC and 1 Hz for $J_{H\text{-}H}$ (and $J_{H\text{-}C}$).[91] Eq. 12 is also utilised when calculating χ^2 values for the coupling constants, exchanging the δ chemical shifts for the scalar coupling constants.

$$\chi^2_\delta = \sum \frac{(\delta^i_{cal} - \delta^i_{exp})^2}{\sigma^2_\delta}$$ **Eq. 12**

As a result of χ^2 values being dependant on the number of deviations utilised to calculate them, the authors calculated χ^2 (reduced) values for each diastereoisomer (Eq. 13). The number of deviations utilised to calculate the χ^2 value is represented by *n* and the number of parameters fitted is incorporated by *m*.

$$\chi^2(reduced) = \frac{\chi^2}{n - m}$$ **Eq. 13**

*The γ-lactones **4** and **6** and δ-lactones **3** and **5***

In order to apply method M4 to our own compounds we had to complete a computation of TMS utilising the authors' described level of theory, but exchanging methanol with DMSO (See Appendix, Table 37, Page 205). We then computed isotropic shielding constants and consequently Boltzmann weighted and TMS scaled ^{1}H and ^{13}C chemical shifts for γ-lactone **4** and its diastereoisomer **6**.

Butts, Myers, Aggarwal and co-workers noted in their study, that specific data points were excluded from linear scaling and further analysis. Upon contacting the authors they detailed that certain calculated NMR data was disregarded as it resulted in a poor fit to the corresponding experimental values (*e.g.*, the authors noted that ^{13}C chemical shift data for carbonyl positions frequently resulted in deviations of 5-10 ppm).

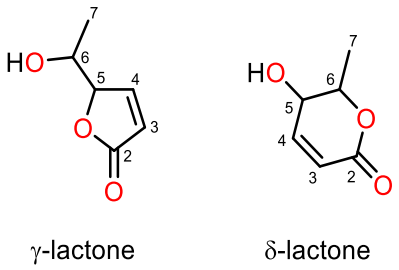

γ-lactone δ-lactone

Figure 18: Numbered γ- and δ-lactone for analytical purposes

Upon studying the difference between the predicted chemical shifts of γ-lactone **4** and the corresponding experimental values, we noted that ^{1}H chemical shifts mostly provided a good data fit. We therefore utilised all chemical shifts and scaled them using the linear regression

method. Most of the computed ^{13}C chemical shifts on the other hand (except the methyl position, C7, Figure 18), resulted in large differences when compared to their experimental values (> 4 ppm). Thus we excluded the ^{13}C chemical shifts for γ-lactones **4** and **6** from the analysis. We then turned to calculating the $J_{H\text{-}H}$ coupling constants for each of the γ-lactones **4** and **6**, which provided a good fit to the experimental data. Application of a 6% linear scaling to these coupling constants (as previously suggested in the literature)[67,91] improved the predicted $J_{H\text{-}H}$ coupling constant values. Consequently we utilised the scaled ^{1}H and $J_{H\text{-}H}$ data to calculate the MAE, standard deviation and χ^2 (reduced) values. These values reflect a minimal distinguishing power between γ-lactone **4** and its diastereoisomer **6** (Figure 19).

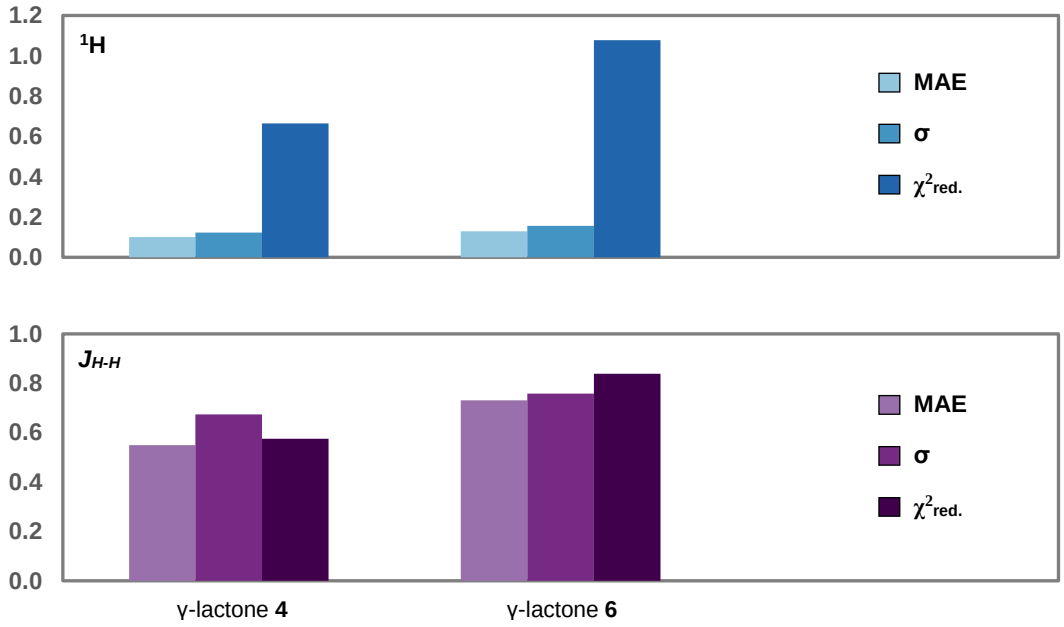

Figure 19: MAE, standard deviation and χ^2 (reduced) values for the scaled ^{1}H and $J_{H\text{-}H}$ data of γ-lactone **4** and its diastereoisomer **6** (M4, DMSO)

We completed the same calculations for δ-lactones **3** and **5**. The computed ^{1}H NMR chemical shift data provided a good fit to the experimental values, except for position C4 (Figure 18) which was thus excluded from further analysis. Once more we excluded the carbon chemical shifts from further analysis as most of the TMS scaled ^{13}C chemical shifts largely deviated from the experimental data. The $J_{H\text{-}H}$ coupling constants provided a good fit to the data, which improved when the 6% linear scaling was applied. Upon calculating the MAE, standard deviation and χ^2 (reduced) values, we noticed that the data provided us with a clear distinguishing power between the diastereoisomers (Figure 20). Particularly the χ^2 (reduced) values of the ^{1}H chemical shifts, as well as all statistical $J_{H\text{-}H}$ coupling constant values allowed for a clear distinction between the two diastereoisomers. Given these positive results we

moved forward to computing the data for (+)-angiopterlactone B (**2**) and seven of its diastereoisomers.

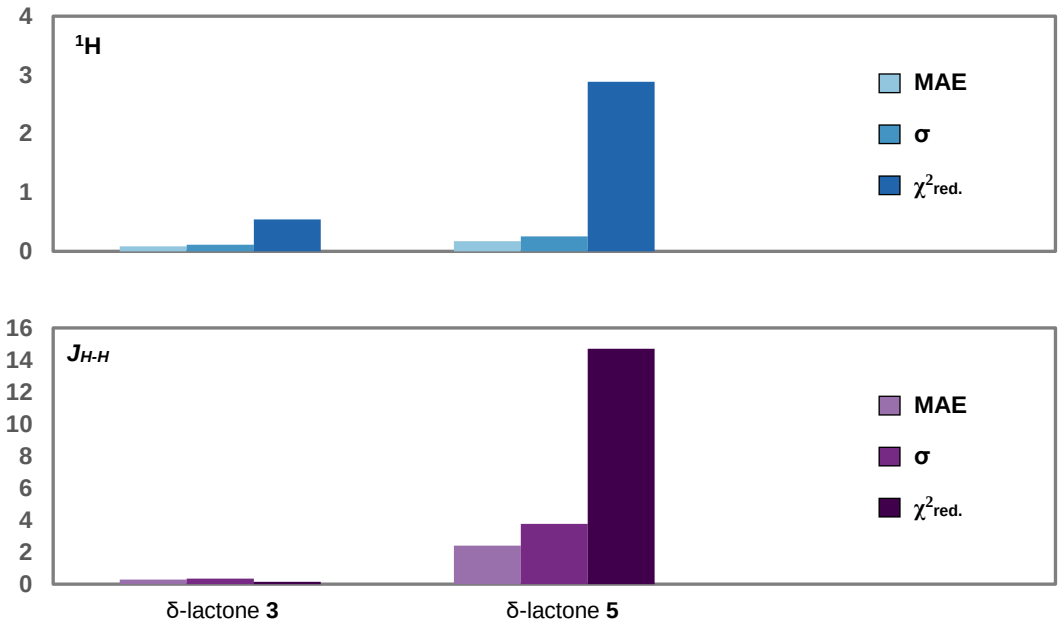

Figure 20: MAE, standard deviation and χ^2 (reduced) values for the ^{1}H and $J_{H\text{-}H}$ data of δ-lactone **3** and its diastereoisomer **5** (M4, DMSO)

*(+)-Angiopterlactone B (**2**) and seven of its diastereoisomers*

Next we investigated whether this method would allow us to distinguish between diastereoisomers in larger systems. Therefore we tested method M4 on (+)-angiopterlactone B (**2**) (compound I) and seven of its diastereoisomers (Table 24, Page 93 *or removable sheet, Figure B*). Utilising the same procedure as for lactones **3** and **4**, the chemical shift and coupling constant data for the eight compounds I-VIII were computed. Based on the computed values of (+)-angiopterlactone B (**2**) (compound I), the ^{1}H and ^{13}C chemical shifts and $J_{H\text{-}H}$ coupling constants shown in Figure 21 were excluded from the scaling and processing of the data. This was mainly due to their large deviations from the experimental value in all diastereoisomers. The CH_2 protons as well as their associated coupling constants were excluded as conformational rotations caused these positions to swap frequently and thus could not be assigned a corresponding experimental value. For a direct comparison of how the inclusion of all data points and the exclusion of poorly fitting data points affects the overall ^{1}H, ^{13}C and $J_{H\text{-}H}$ MAE values, see Table 48 and Table 49 in the Appendix.

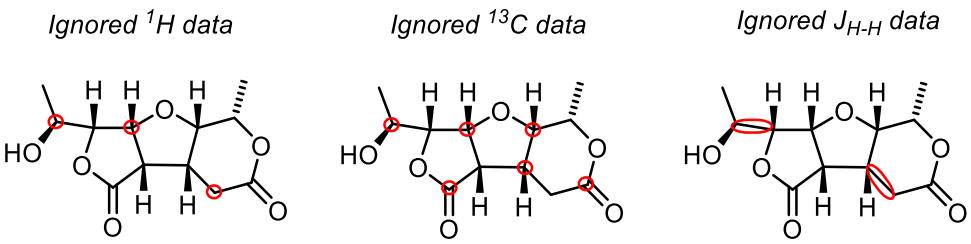

Figure 21: ^{1}H, ^{13}C and J_{H-H} data which was ignored (labelled in red) for the linear scaling and further analysis of (+)-angiopterlactone B (**2**) and seven of its diastereoisomers

The ^{1}H, ^{13}C and J_{H-H} data was used to calculate the corresponding MAE, standard deviation and χ^2 (reduced) values (Figure 22). The results indicate that based on these values, compounds III-VIII can be excluded. This leaves us with only two structures likely to correspond to (+)-angiopterlactone B (**2**), diastereoisomers I or II. As the majority of the chemical shift and J_{H-H} coupling constant data surrounding the carbinol centre were excluded, we were not able to distinguish between these two structures.

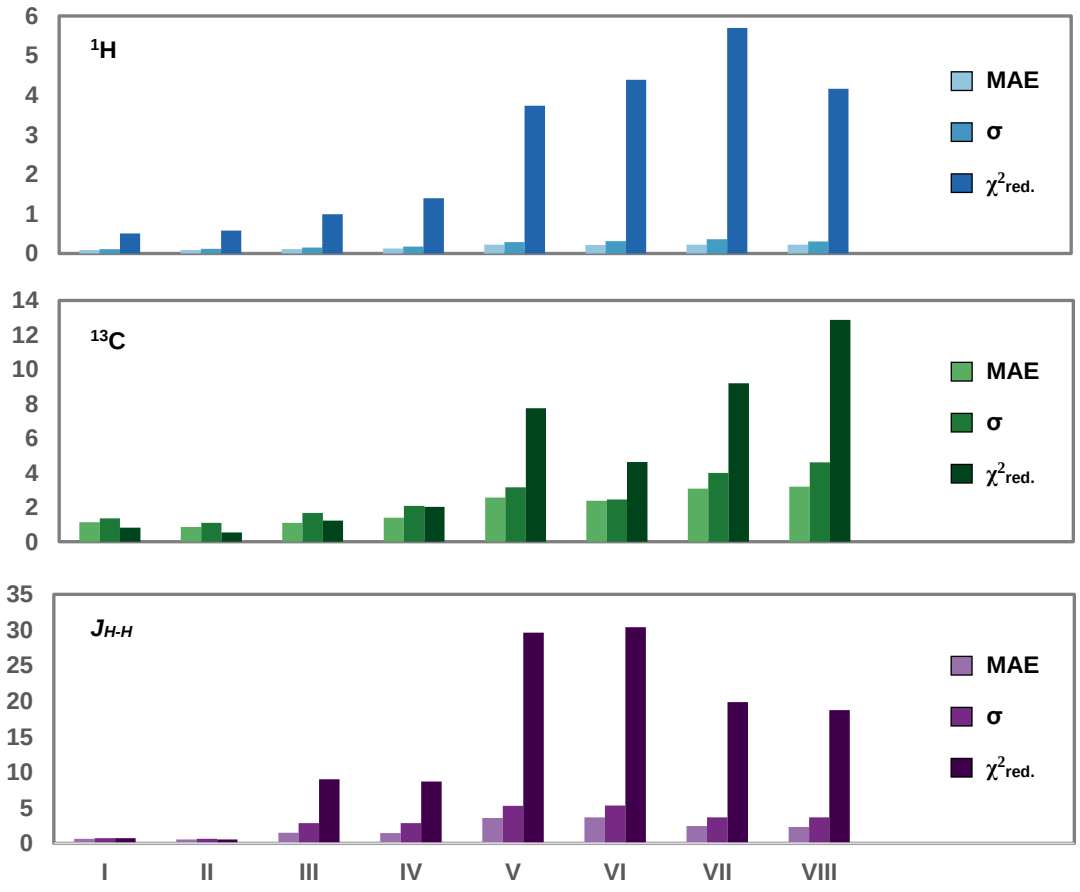

Figure 22: MAE, standard deviation and χ^2 (reduced) values for the ^{1}H and J_{H-H} data of (+)-angiopterlactone B **2** (compound I) and seven of its diastereoisomers (M4, DMSO)

We previously noted for δ-lactone **3** that excellent structural discrimination was provided by the $J_{H\text{-}H}$ values. This trend was also observed for compounds I-VIII of angiopterlactone B (**2**). As we ultimately aim to predict whether the structure initially proposed by the isolation chemists for (–)-angiopterlactone A (**1**) is correct, we were most interested in stereogenic centres C2', C3', C6', C5 and C6 (Figure 23). If we can establish the correct *cis*/*trans* relationship between protons H2'-H6', H2'-H3' and H5-H6, we should in theory be able to eliminate seven of the eight structures and therefore identify the correct diastereoisomer.

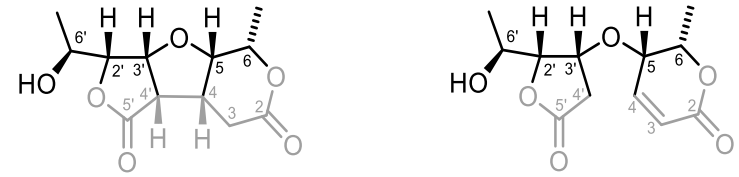

Figure 23: Stereogenic centres we are most interested in identifying (labelled in black)

As noted in Figure 21, the coupling constants between protons H2'-H6' varied largely and thus had to be eliminated, which meant we weren't able to distinguish between compounds I and II. The large variation of these coupling constants, could be due to the flexibility of the side chain. A literature search suggested that corresponding coupling constants in related γ-lactones also vary greatly.[106,107] Despite not being able to utilise the $J_{H2'\text{-}H6'}$ to distinguish between diastereoisomers I and II, utilising the $J_{H\text{-}H}$ coupling constant values of H2'-H3' and H5-H6 should in theory allow us to eliminate six of the eight structures. Thus for each of the structures I-VIII, the deviations of each of these coupling constants from the experimental values were calculated (Table 25).

entry	$J_{H\text{-}H}$ **deviation / Hz**	**I**	**II**	**III**	**IV**	**V**	**VI**	**VII**	**VIII**
1	H2'-H3'	1.4	1.3	0.3	0.0	3.7	3.7	3.7	3.7
2	H5-H6	0.3	0.2	6.6	6.5	6.9	7.0	0.4	0.5

Table 25: Deviation of computed $J_{H\text{-}H}$ values for H2'-H3' and H5-H6 from their experimental values for compounds I-VIII of angiopterlactone B (**2**)

Protons H2' and H3' have a *cis* relationship in structures I-IV, whereas structures V-VIII all have a *trans* relationship (Table 24, Page 93 *or removable sheet, Figure B*). Table 25 shows that the $J_{H\text{-}H}$ deviation of H2'-H3' from the experimental values is < 1.5 Hz for structures I-IV and > 3.5 Hz for structures V-VIII. Thus structures V-VIII can be eliminated and the H2'-H3' protons can be assigned as *cis*. Diastereoisomers I, II, VII and VIII all display a *cis* relationship between H5-H6. The deviation of the computed values from the experimental values clearly reflect that whilst these structures all have values ≤ 0.5 Hz, those with the *trans* protons (III-

VI) all have values ≥ 6.5 Hz. Therefore structures III-VI can be eliminated and H5-H6 assigned as *cis*. Thus utilising only the two $J_{H\text{-}H}$ coupling constants H2'-H3' and H5-H6, we have eliminated structures III-VIII, leaving us with diastereoisomers I and II. Utilising the two coupling constants H2'-H3' and H5-H6, we calculated the MAE, standard deviation and χ^2 (reduced) values (Figure 24). These validated that based on these two $J_{H\text{-}H}$ coupling constants, structures III-VIII could be eliminated. Given this success in narrowing down the possible structures from eight to two, we moved forward with computing the data for the structures we deemed most likely for the natural product (–)-angiopterlactone A (**1**).

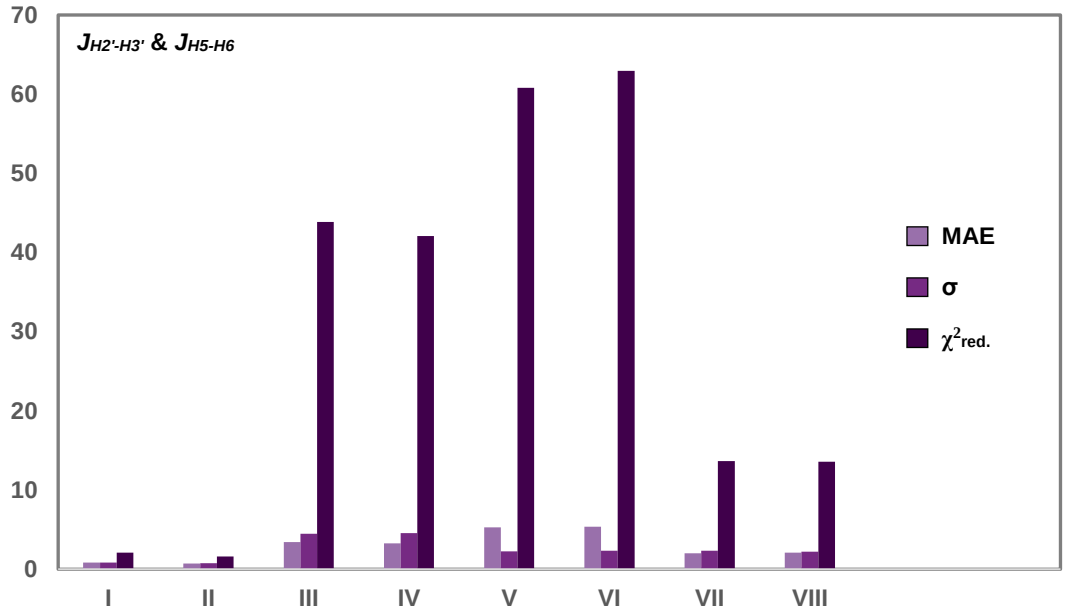

Figure 24: MAE, standard deviation and χ^2 (reduced) values for the $J_{H\text{-}H}$ data of H2'-H3' and H5-H6 of (+)-angiopterlactone B (**2**) (compound I) and seven of its diastereoisomers (M4, DMSO)

*(–)-Angiopterlactone A (**1**)*

Our investigations continued by studying the proposed structures (I-VIII) for (–)-angiopterlactone A (**1**) (see Figure 17, Page 82 *or removable sheet, Figure A*). Compound I represents the opposite enantiomer of the structure which was previously proposed by the isolation chemists.[2] Based on our results and analysis for compounds γ-lactone **4**, δ-lactone **3** and (+)-angiopterlactone B (**2**), we excluded the positions summarised in Figure 25, as well as all ^{13}C chemical shifts from further analysis. The remaining values were then utilised to scale the data as previously described and calculate the relevant MAE, standard deviation and χ^2 (reduced) values (Figure 26). Although these did not allow us to identify a single

diastereoisomer, preliminary results suggest that structures V-VIII could be excluded. We thus completed further examinations of the data.

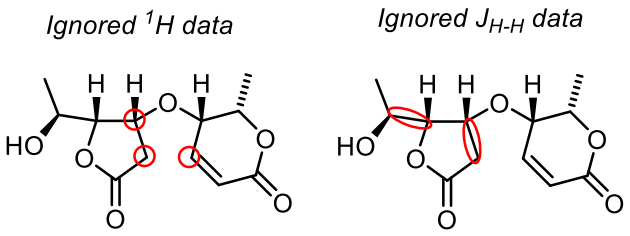

Figure 25: ^1H and J_{H-H} data which was ignored for the scaling and further analysis of the structures under investigation for (–)-angiopterlactone A (**1**)

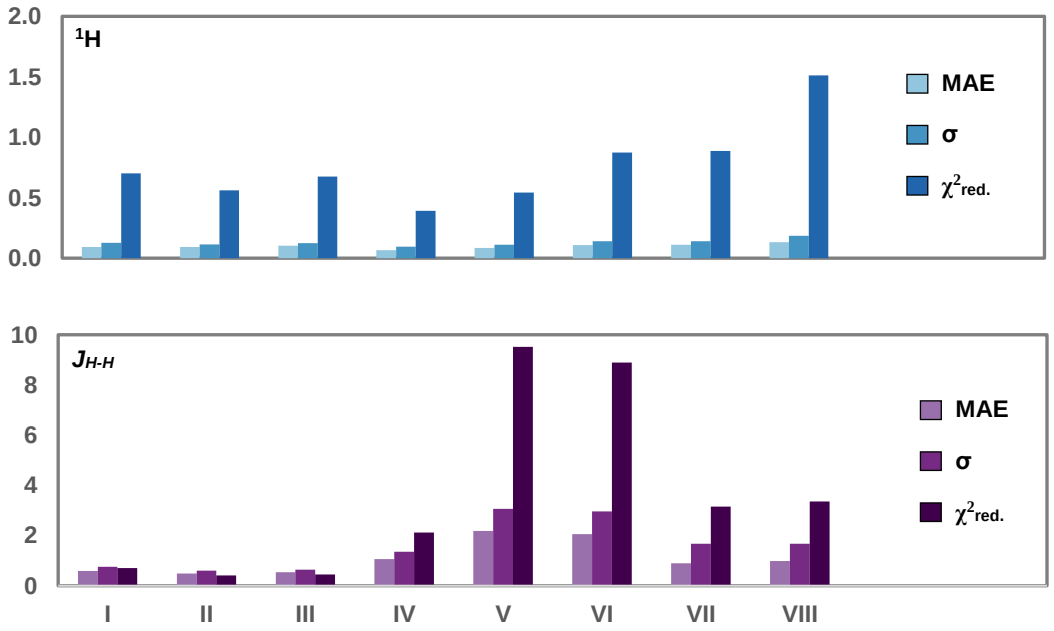

Figure 26: MAE, standard deviation and χ^2 (reduced) values for the ^1H and J_{H-H} data of the eight diastereoisomers under consideration for (–)-angiopterlactone A (**1**) (M4, DMSO)

Similarly to our analysis of (+)-angiopterlactone B (**2**) and its diastereoisomers, we analysed coupling constants H2'-H3' and H5-H6 to eliminate further structures. Thus we completed a separate analysis in which only these two coupling constants were considered for structures I-VIII (Figure 27). The computed $J_{H2'-H3'}$ values for structures V-VIII (H2'-H3' *trans)*, deviated > 3.6 Hz from the experimental values, which means we can eliminate these options and assign H2'-H3' as *cis*. With the exception of structure III, the J_{H-H} deviation values for H5-H6 reflect whether these are arranged *cis* or *trans* to each other.

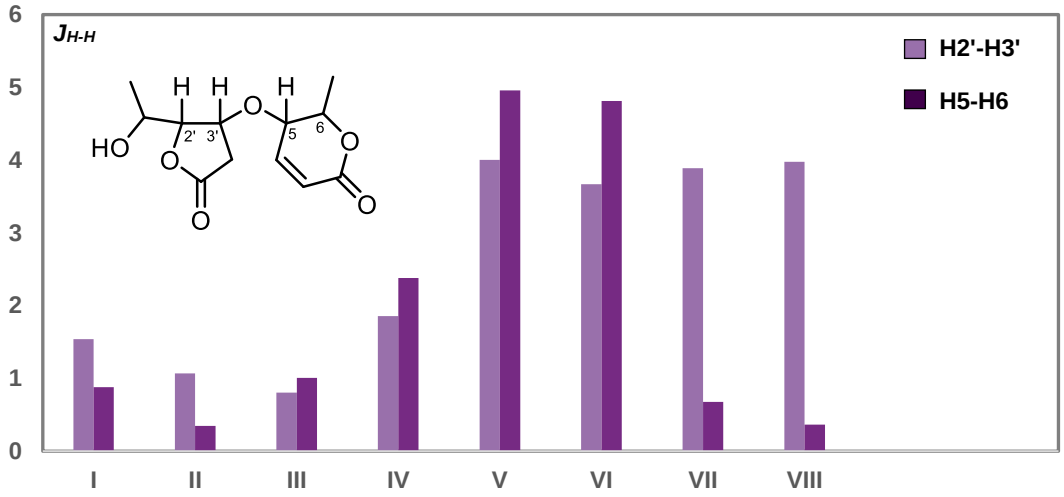

Figure 27: Deviation (in Hz) of computed J_{H-H} values for H2'-H3' and H5-H6 from their experimental values for compounds I-VIII of (–)-angiopterlactone A (**1**) (M4, DMSO)

Based on our observations that H2'-H3' are *cis*, we narrowed down the viable structures to compounds I-IV. These differ in the stereochemistry at the C6 and the C6' (hydroxyl) position. As the poor data fit of TMS scaled ^{13}C chemical shifts to the experimental values limited us to ^{1}H chemical shifts and J_{H-H} coupling constants, we proceeded by investigating these compounds with method M3, which previously provided a good data fit.

2.3.3 Final Method Choice: Method M3

Method M3 (DMSO) was utilised to compute the NMR data for γ-lactone **4**, δ-lactone **3**, the angiopterlactones (**1**, **2**) as well as all relevant diastereoisomers.

*The γ-lactones **4** and **6** and δ-lactones **3** and **5***

For γ-lactones **4** and **6**, we noted that the ^{1}H chemical shifts provided a good fit to the experimental values. This was also the case for the ^{13}C chemical shifts, with the exception of position C6 (Figure 18, Page 95) which was thus excluded from further analysis. None of the J_{H-H} coupling constants deviated largely from the experimental data and therefore all values were included in the analysis. Upon testing the 6% linear scaling on the coupling constants (which we completed for all compounds when utilising method M4), we found that for the monomeric lactone units **3** and **4**, as well as (+)-angiopterlactone B (**2**), the data fit was not significantly improved and thus a 6% linear scaling was not applied to any of the compounds. We then calculated ^{1}H, ^{13}C and J_{H-H} MAE, standard deviation and χ^2 (reduced) values for γ-

lactones **4** and **6** (Figure 28). Similarly to method M4 we found a lack in distinguishing power between these diastereoisomers.

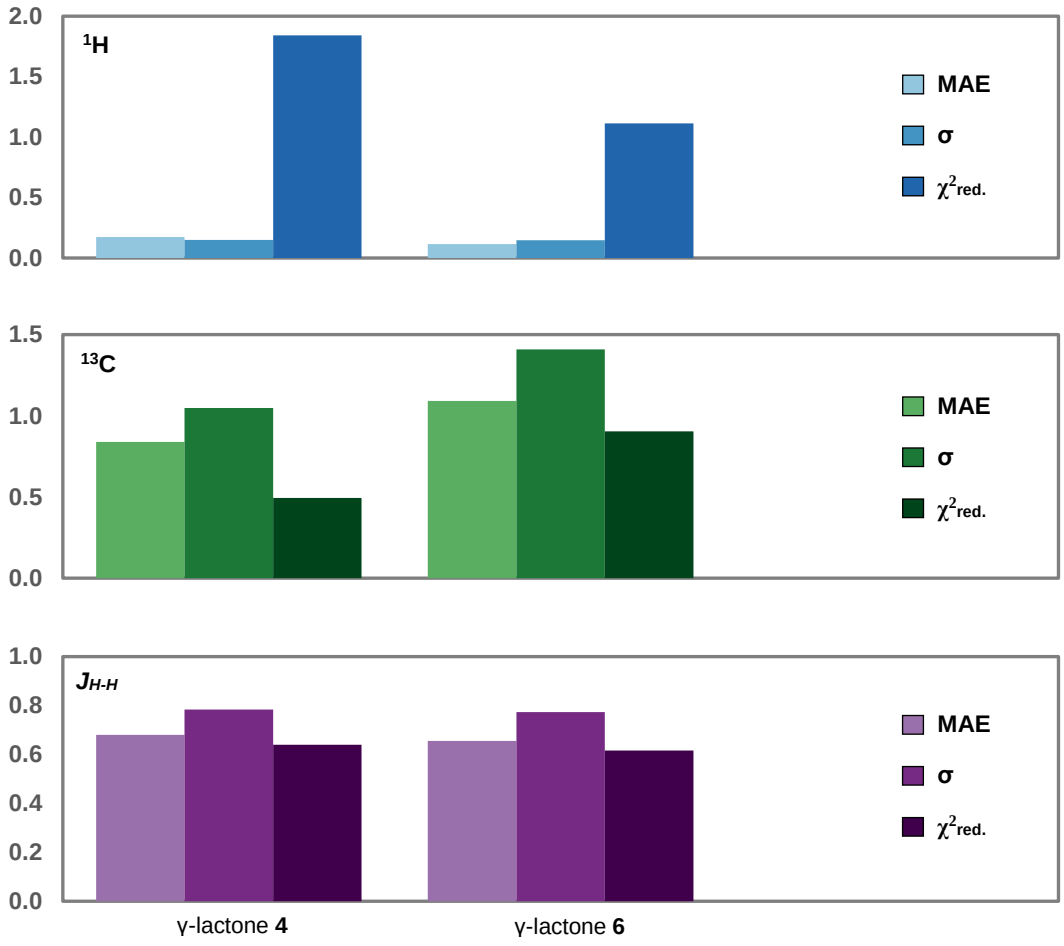

Figure 28: MAE, standard deviation and χ^2 (reduced) values for the ^{1}H and ^{13}C chemical shift data and $J_{H\text{-}H}$ coupling constant data for γ-lactone **4** and its diastereoisomer **6** (M3, DMSO)

Following our analysis of the data for γ-lactones **4** and **6**, we investigated δ-lactones **3** and **5**. All of the ^{1}H and ^{13}C chemical shifts, as well as the coupling constants provided a good data fit and thus no positions were excluded from further analysis. Analysis of the MAE, standard deviation and χ^2 (reduced) values showed that the data provided a clear distinction between the diastereoisomers (Figure 29).

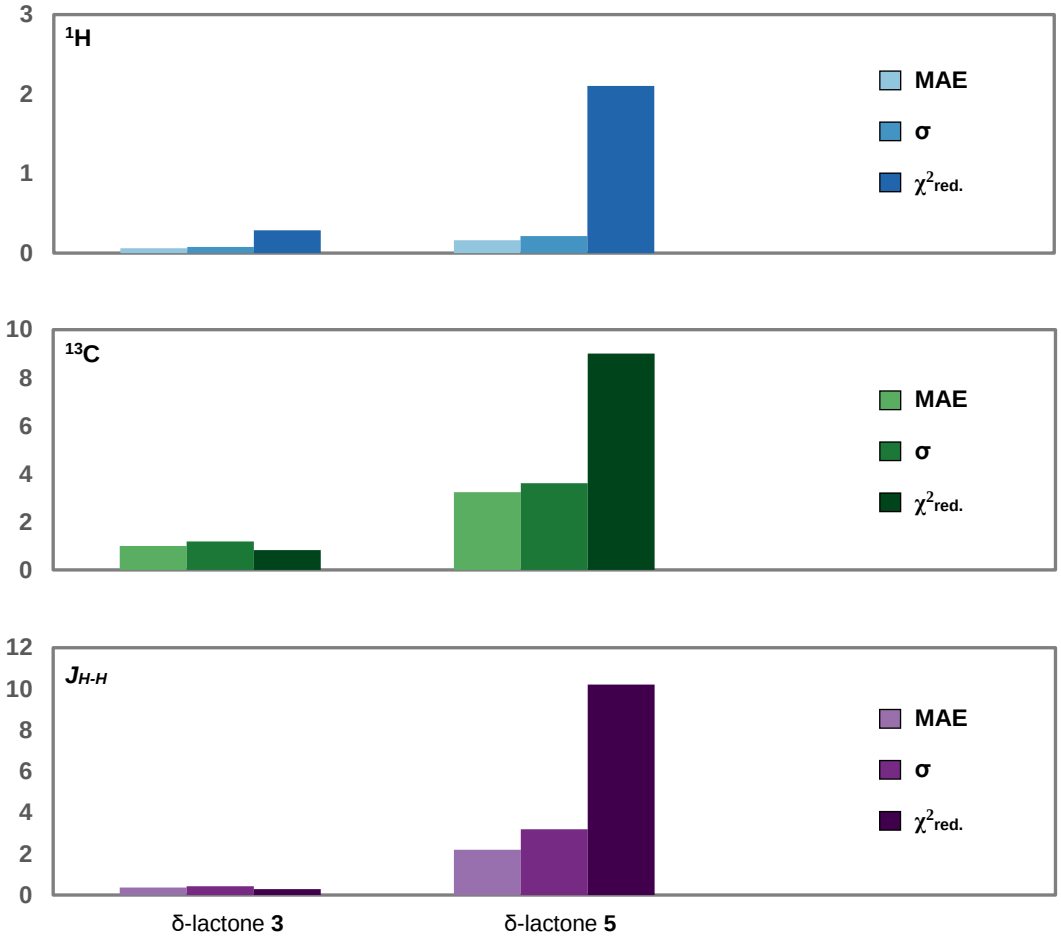

Figure 29: MAE, standard deviation and χ^2 (reduced) values for the ^{1}H and ^{13}C chemical shift data and $J_{H\text{-}H}$ coupling constant data for δ-lactone **3** and its diastereoisomer **5** (M3, DMSO)

*(+)-Angiopterlactone B (**2**) and seven of its diastereoisomers*

Following the computation of NMR properties of the γ- and δ-lactone units, we utilised method M3 (DMSO) to investigate the ^{1}H and ^{13}C chemical shifts and $J_{H\text{-}H}$ coupling constant values for (+)-angiopterlactone B (**2**) (compound I) and seven of its diastereoisomers II-VIII (see Table 24, Page 93 *or removable sheet, Figure B*). Upon computing these values, several data points were excluded. For the ^{1}H chemical shifts the CH_2 protons were removed as conformational rotations caused these positions to swap frequently and thus could not be assigned a corresponding experimental value. Their associated $J_{H\text{-}H}$ coupling constants were also excluded, as well as $J_{H2'\text{-}H6'}$, which resulted in large variations due to the nature of the rotatable bonds. Except for carbons C4 and C4' (typically an error of 4-8 ppm), the ^{13}C chemical shifts provided a good data fit, which meant that we now had more data to work with than with method M4. Upon calculating the ^{1}H, ^{13}C and $J_{H\text{-}H}$ MAE, standard deviation and χ^2 (reduced) values, we were pleased to find that the overall data allowed exclusion of structures

III-VIII, leaving only structures I or II as viable options (Figure 30). This observation is consistent with what we previously observed when utilising method M4. For a direct comparison of how the inclusion of all data points and the exclusion of poorly fitting data points affects the overall ^{1}H, ^{13}C and $J_{H\text{-}H}$ MAE values, see Table 51 and Table 52 in the Appendix.

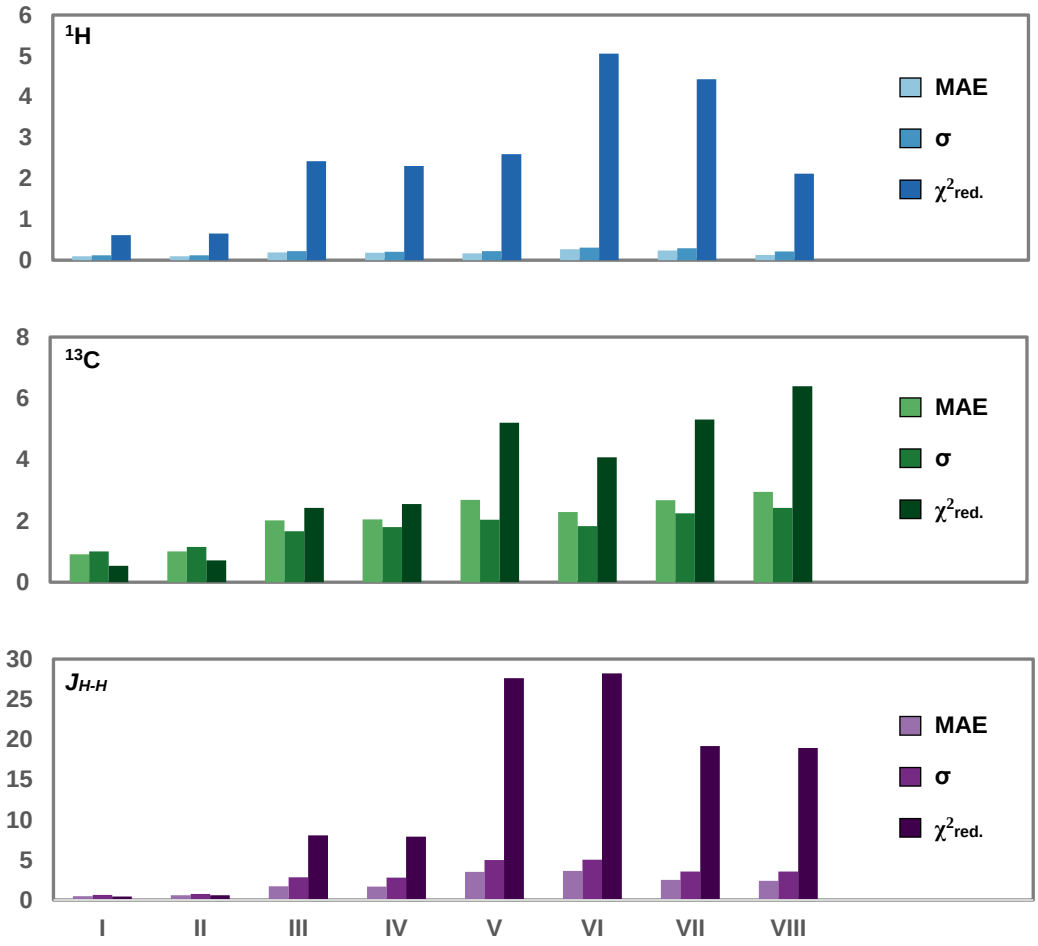

Figure 30: MAE, standard deviation and χ^2 (reduced) values for the ^{1}H and ^{13}C chemical shift data and $J_{H\text{-}H}$ coupling constant data for (+)-angiopterlactone B (**2**) and seven of its diastereoisomers (II-VIII) (M3, DMSO)

*(–)-Angiopterlactone A (**1**)*

Based on our success in narrowing down the number of structures for (+)-angiopterlactone B (**2**) from eight to two, we moved forward to compute the ^{1}H, ^{13}C chemical shifts and $J_{H\text{-}H}$ coupling constants for the proposed structures of (–)-angiopterlactone A (**1**) (see Figure 17, Page 82 *or removable sheet, Figure A*). By taking into consideration problematic positions that we encountered for the γ- and δ-lactones **4** and **3**, as well as (+)-angiopterlactone B (**2**),

we once more excluded certain positions from further data analysis. For the ^{1}H chemical shifts we excluded the CH_2 protons and for the coupling constants we excluded H2'-H6', as well as all coupling constants associated with the CH_2 group. No data was removed for the ^{13}C chemical shifts. The ^{1}H, ^{13}C and J_{H-H} MAE, standard deviation and χ^2 (reduced) values for the eight diastereoisomers of angiopterlactone A (**1**) were then calculated (Figure 31).

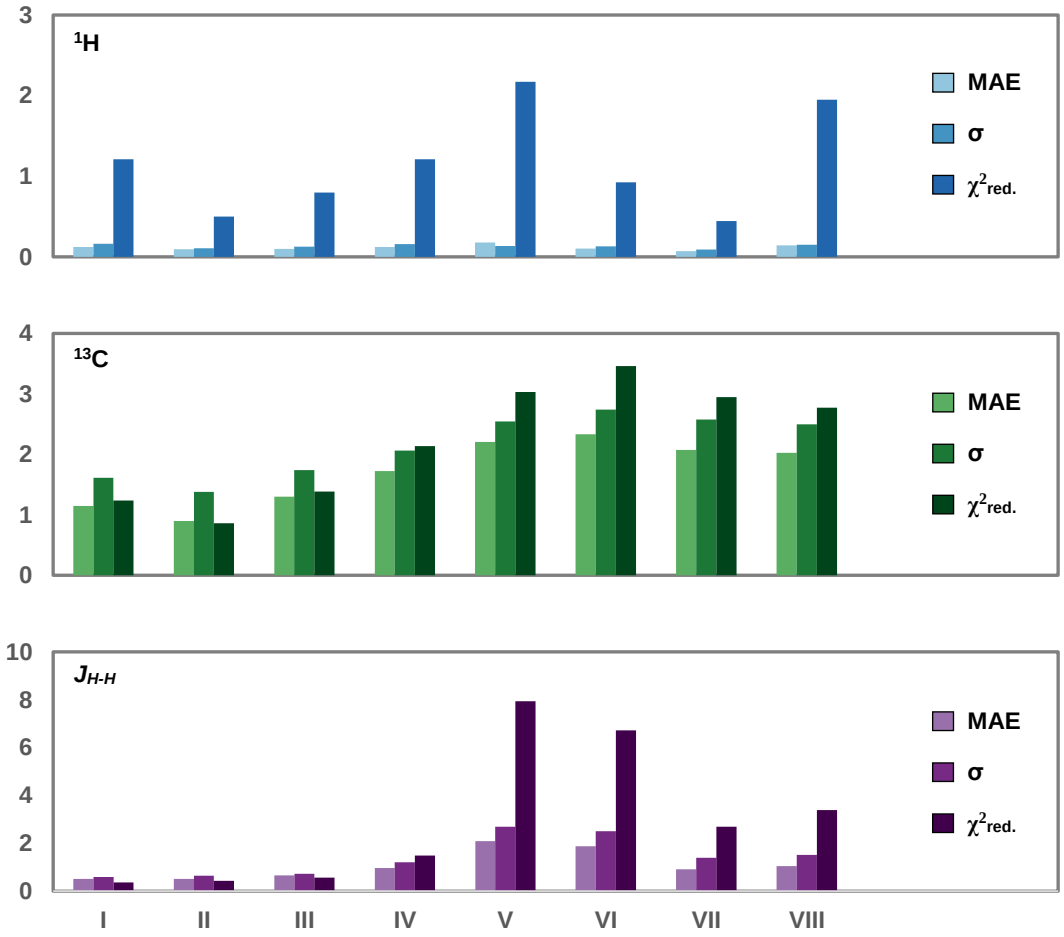

Figure 31: MAE, standard deviation and χ^2 (reduced) values for the ^{1}H and ^{13}C chemical shift data and J_{H-H} coupling constant data for eight possible structures (I-VIII) for (–)-angiopterlactone A (**1**) (M3, DMSO)

Initial results allowed us to eliminate structures V-VIII. By comparing solely the χ^2 (reduced) values (Figure 32), we could tentatively narrow down the possible structures to compounds I-III. From these structures, compound II provided the best fit to the data. However, given how close the values for compounds I-III are, we cannot confidently identify a particular diastereoisomer and thus we revisited our previous approach of completing a separate analysis of the J_{H-H} coupling constants for H5-H6 and H2'-H3'.

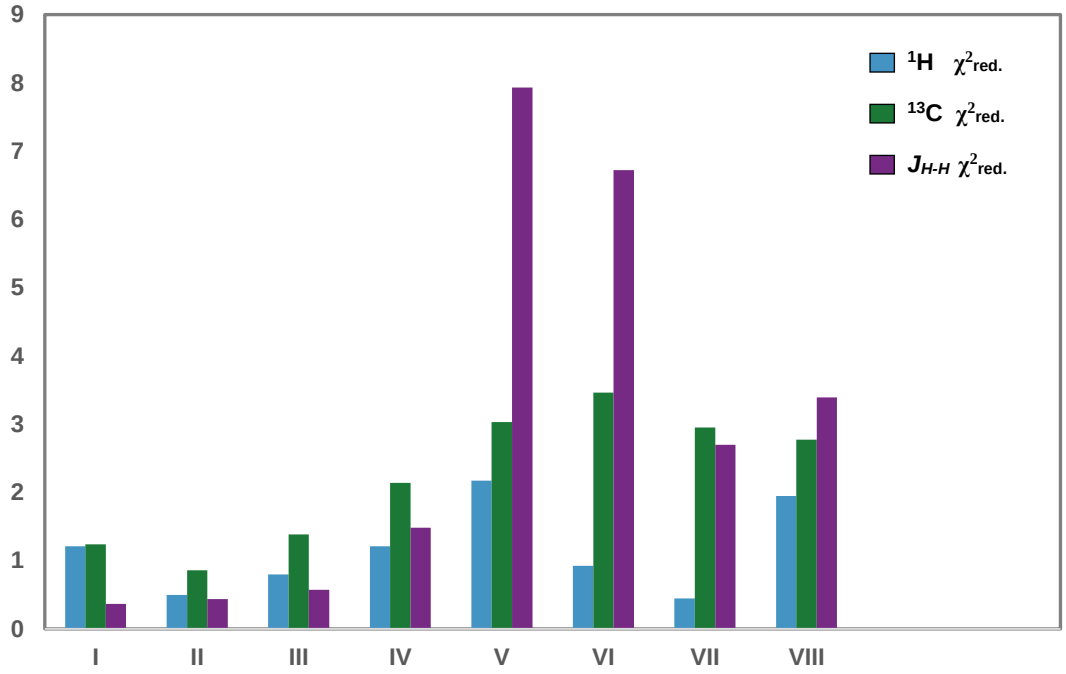

Figure 32: χ^2 (reduced) values for the ^{1}H and ^{13}C chemical shift data and $J_{H\text{-}H}$ coupling constant data for eight possible structures (I-VIII) for (–)-angiopterlactone A (**1**) (M3, DMSO)

By considering only the $J_{H\text{-}H}$ coupling constants for H5-H6 and H2'-H3' and plotting the deviation (in Hz) from the experimental values for each of the diastereoisomers I-VIII, it became clear that the only structures which provide suitable results were structures I-III (Figure 33). This supports our previous tentative exclusions of structures IV-VIII. As the deviations for the H2'-H3' coupling constants from the experimental values follow the trends of the structures (low deviations for *cis* compounds I-IV; high deviations for *trans* compounds V-VIII), H2'-H3' could be assigned as *cis*. Our proposed viable structures are therefore diastereoisomers I-III. As the $J_{H\text{-}H}$ coupling constants for H5-H6 did not allow us to confidently assign these protons as *cis* or *trans*, further investigations into the H5-H6 relationship were necessary.

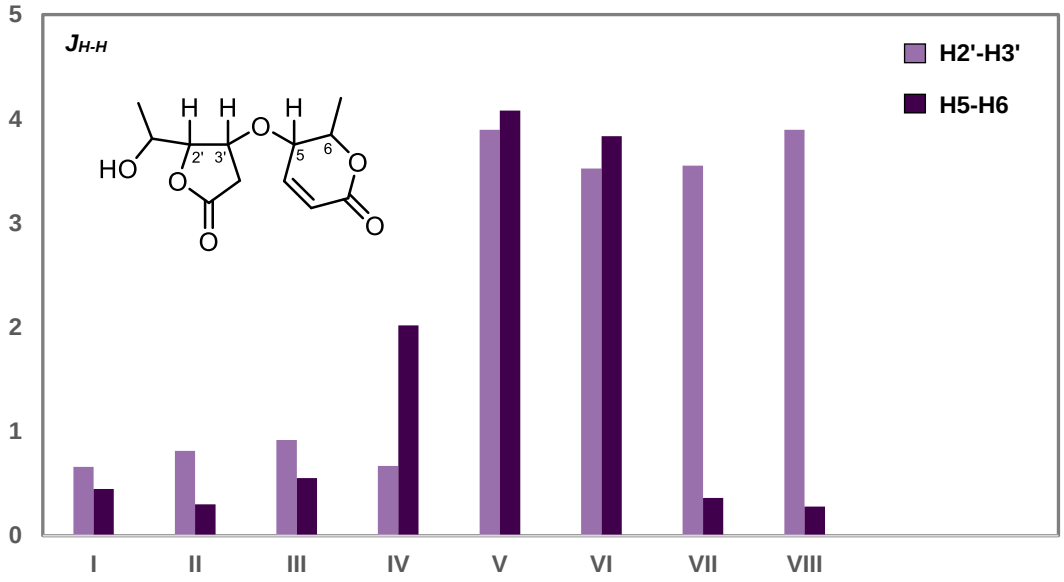

Figure 33: Deviation (in Hz) of computed $J_{H\text{-}H}$ values for H2'-H3' and H5-H6 from their experimental values for compounds I-VIII of angiopterlactone A (**1**) (M3, DMSO)

We concluded that the most viable structures were I-III. Structures I and II have the *cis* relationship between protons H5-H6 in common, whereas structure III has a *trans* relationship. If we can more confidently assign these protons as being either *cis* or *trans*, we can further narrow down the viable structures from three to two/one. Therefore we turned our attention to some of our in-house synthesised compounds (Figure 34). Relevant coupling constants are summarised in Table 26.

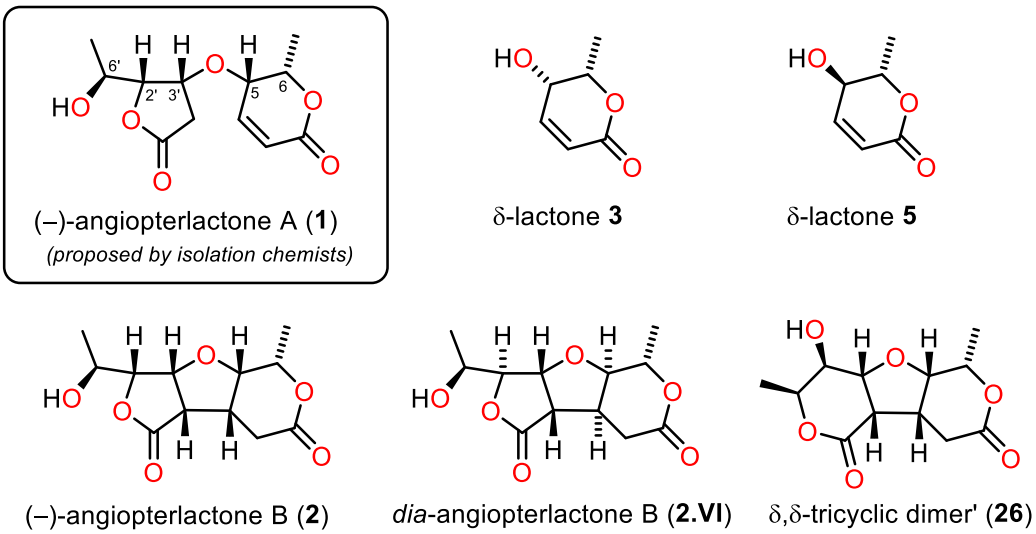

Figure 34: In-house synthesised compounds and the structure proposed by isolation chemists for (–)-angiopterlactone A (**1**)

$J_{H5\text{-}H6}$	*cis*	*trans*
Lactones 3 & 5	2.9 Hz	8.9 Hz
Angiopterlactones 2 & 2.VI	1.6 Hz	8.4 Hz
δ,δ-tricyclic dimer 26	0.9 Hz	
(–)-angiopterlactone A (1)[2]	3.0 Hz	

Table 26: The $J_{H5\text{-}H6}$ coupling constants for our in-house synthesised compounds and the literature value of (–)-angiopterlactone A (**1**)[2]

The isolation chemists reported a coupling constant of 3.0 Hz for $J_{H5\text{-}H6}$ in (–)-angiopterlactone A (**1**).[2] The coupling constant $J_{H5\text{-}H6}$ for our synthesised *cis*-δ-lactone **3** was 2.9 Hz whereas that for *trans*-δ-lactone **5** (recently synthesised by Dr Katherine Law, Lawrence group) was 8.9 Hz. Furthermore, our synthetic material (–)-angiopterlactone B (**2**) had a *cis*-relationship between H5-H6 and the $J_{H\text{-}H}$ coupling constant was 1.6 Hz. Dr Katherine Law synthesised a diastereoisomer of (–)-angiopterlactone B (**2**) in which the H5-H6 protons are *trans* (herein named *dia*-angiopterlactone B (**2.VI**)) and the corresponding $J_{5H\text{-}6H}$ was 8.4 Hz. In addition, Dr Katherine Law synthesised δ,δ-tricyclic dimer **26**, which has a *cis* relationship and a coupling constant of 0.9 Hz. These coupling constants would suggest that H5-H6 in (–)-angiopterlactone A (**1**) are arranged in a *cis*-relationship, thus eliminating structure III. Therefore the remaining viable structures are diastereoisomers I and II.

To gain further confidence in excluding structure III we tested an alternate approach. In the monomeric lactone units we previously observed excellent distinguishing power between the pair of diastereoisomers for δ-lactone **3** and **5**. Thus for the purpose of the analysis of (–)-angiopterlactone A (**1**), we split the molecule in half in order to better reflect the δ-lactone **3** (Figure 35). The MAE, standard deviation and χ^2 (reduced) values for the 'δ-ring half' of (–)-angiopterlactone A (**1**) were then calculated (Figure 36).

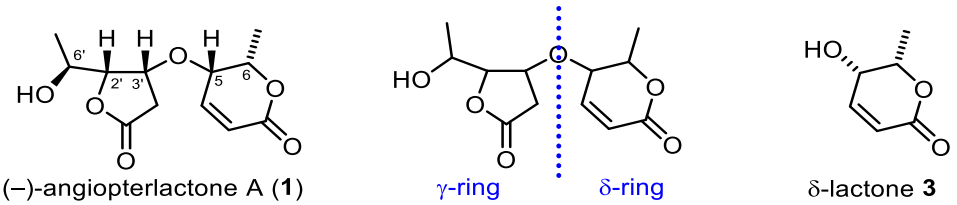

Figure 35: Splitting of angiopterlactone A (**1**) into two halves for analytical purposes

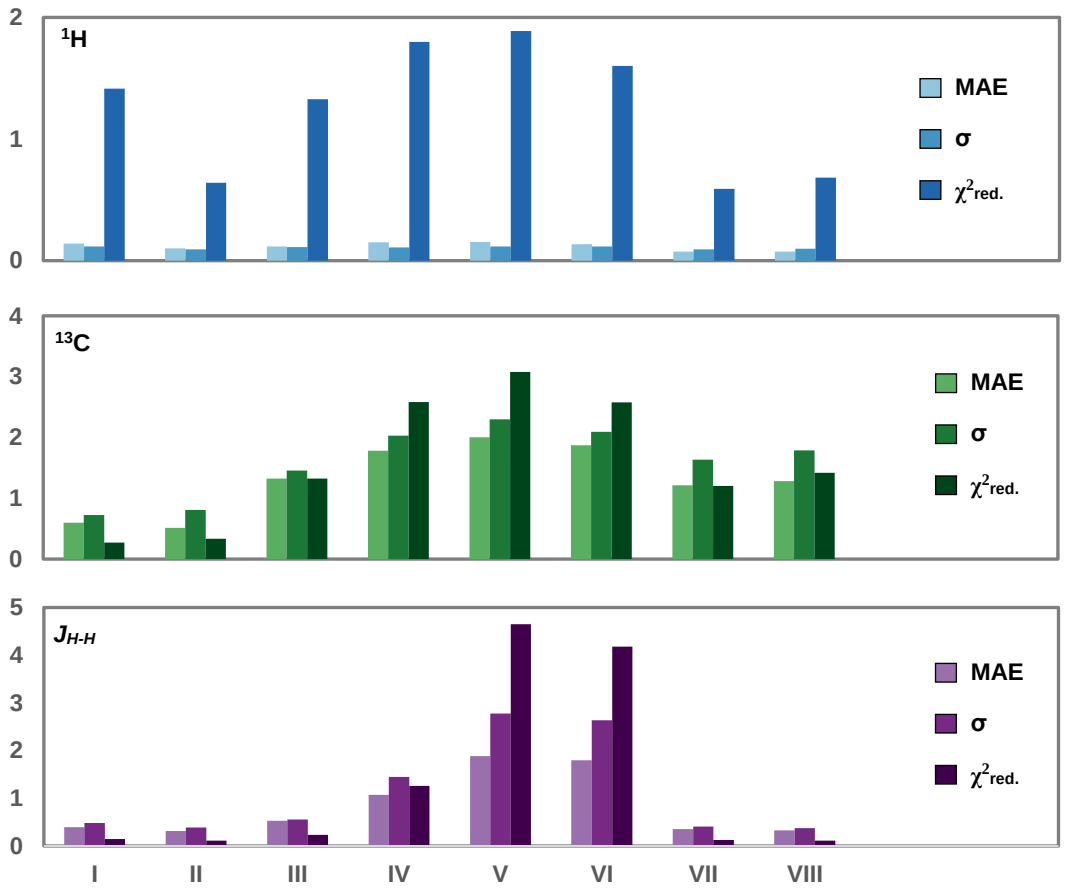

Figure 36: 'δ-ring half' MAE, standard deviation and χ^2 (reduced) values for the ^{1}H and ^{13}C chemical shift data and $J_{H\text{-}H}$ coupling constant data for eight possible structures (I-VIII) for (–)-angiopterlactone A (**1**) (M3, DMSO)

Out of the eight structures, the best data fit for all analysis techniques was provided by diastereoisomer II, suggesting that this may be the correct structure of (–)-angiopterlactone A (**1**). This would be a very interesting result as it suggests (based on the assumption that a δ-lactone is the biosynthetic precursor to the angiopterlactones (**1** and **2**)) that the dimer consists of a cross dimerisation between the δ-lactone ***ent*-3** and its diastereoisomer **5** (Scheme 26). (+)-Angiopterlactone B (**2**) on the other hand is formed *via* a homo-coupling of two units of δ-lactone ***ent*-3** (see Chapter 3 for mechanistic studies).

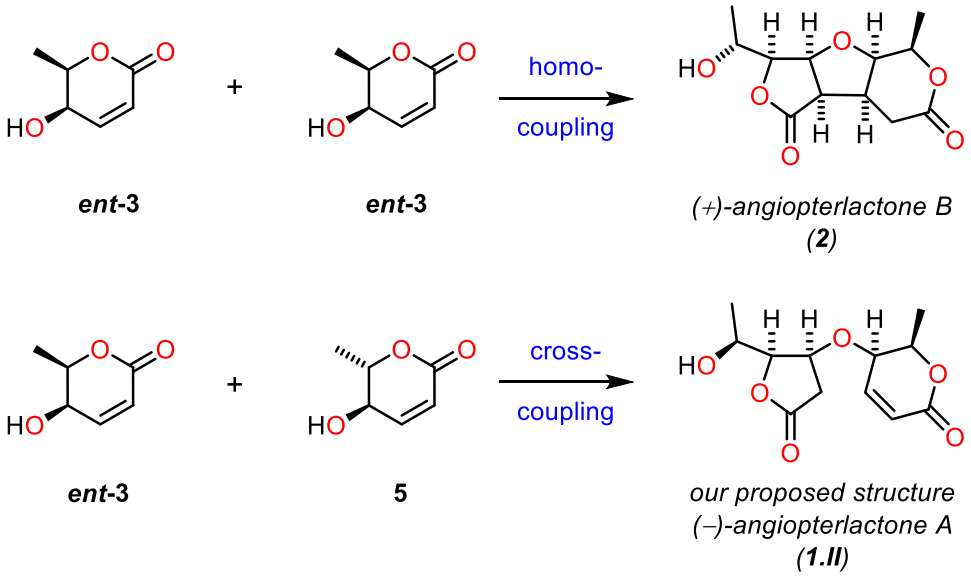

Scheme 26: Proposed coupling towards the angiopterlactones (**1**, **2**)

The DP4 Analysis

In order to gain greater confidence in our tentative conclusion that diastereoisomer II represents the correct structure for angiopterlactone A (**1**), we turned to the DP4 probability analysis developed by Smith and Goodman in 2010 (see Section 2.1.3).[77] This analysis has been suggested to be more successful than probabilities based on the mean absolute errors at assigning structures correctly with high confidence.[77]

To complete the DP4 analysis on our obtained data set (utilising method M3), it was necessary to compute TMS at the same level of theory (see Appendix, Table 37, Page 205). Utilising Eq. 11 (Page 78) and TMS scaled ^{1}H and ^{13}C chemical shifts, we completed the DP4 analysis for each of our sets of diastereoisomers for γ-lactone **4**, δ-lactone **3**, angiopterlactone B (**2**) and angiopterlactone A (**1**).

It is interesting to note that subsequent to completing the computational NMR prediction studies and the writing of this chapter, Sarotti and co-workers published a quantum-based NMR method for the assignment of absolute configuration of compounds.[108] This included a case study of (–)- and (+)-angiopterlactone B (**2**) to assign their absolute stereochemistry. Utilising their DP4+ probability (modification of DP4), the authors attained >99.9% probability for the stereoisomer with the correct relative stereochemistry. We utilised the shielding tensors provided in their supporting information which corresponded to structures I-VIII of angiopterlactone B (**2**), to calculate the DP4 probability. This involved computing TMS

at their described level of theory (mPW1PW91/6-31+G(d,p)[PCM(CH_3OH)]//B3LYP/6-31G(d)) (see Appendix, Table 37, Page 205). This resulted in an overall probability of 85% to assign the correct structure. We then utilised their provided excel spreadsheet and shielding tensors to complete the DP4+ analysis for the eight diastereoisomers corresponding to I-VIII (Table 24, Page 93 *or removable sheet, Figure B*). This yielded a 99% probability of correctly identifying structure I as the correct diastereoisomer, a significant improvement to the 85% attained applying DP4. However, during our computational NMR prediction studies and prior to their publication detailing the examination of (+)-angiopterlactone B (**2**), we had contacted the developers[78] of the DP4+ method. Before applying this analysis, we were interested in gaining a better understanding of how the DP4+ probability is calculated (their provided excel spreadsheet is a 'black box' in which shielding tensor values are added and percentages appear, without being able to follow how this occurs). Unfortunately the authors did not provide us with any details and thus we utilised only the DP4 method for our data.

Lactones 4 and 3

We began by investigating DP4 analyses of γ-lactone **4**, δ-lactone **3** as well as their respective diastereoisomers **6** and **5**. The DP4 analysis includes three variations, one in which only the proton data is utilised to calculate error probabilities, one in which only the carbon data is used and finally one in which a combination of both the proton and the carbon data is used.

Initially we utilised all available computed and experimental ^{1}H and ^{13}C chemical shifts (without excluding any positions) to complete the analyses (Type X, Entry 1, Table 27). We then separately completed a DP4 analysis utilising a similar technique to that in method M4, in which TMS referenced chemical shifts largely deviating from the experimental data were excluded prior to analysis (Type Y, Entry 2, Table 27). Finally we completed the DP4 analysis by ignoring the positions discussed in each of the above sub-sections for method M3 (Type Z, Entry 3, Table 27). It is interesting to note that whereas previously (utilising MAE, standard deviation and χ^2 (reduced) values) we could not distinguish between γ-lactone **4** and its diastereoisomer **6**, the DP4 analysis provided us with some structural discrimination.

Entry	Type	% probability	γ-lactone 4	γ-lactone 6	δ-lactone 3	δ-lactone 5
1	X	^{1}H only	70	30	97	3
		^{13}C only	60	40	100	0
		Both ^{1}H & ^{13}C	78	22	100	0
2	Y	^{1}H only	70	30	98	2
		^{13}C only	N/A	N/A	N/A	N/A
		Both ^{1}H & ^{13}C	N/A	N/A	N/A	N/A
3	Z	^{1}H only	70	30	97	3
		^{13}C only	50	50	100	0
		Both ^{1}H & ^{13}C	70	30	100	0

Table 27: DP4 analysis of γ-lactone **4** and δ-lactone **3**, as well as their respective diastereoisomers **6** and **5** (N/A = not applicable)

When utilising all of the available ^{1}H and ^{13}C chemical shifts (Entry 1, Table 27) we observed that the analysis incorporating both proton and carbon data provided the best structural discrimination. By excluding chemical shifts largely deviating from the experimental shifts (Entry 2, Table 27) we were restricted to solely ^{1}H chemical shift data. This resulted in a less accurate prediction of the correct diastereoisomer than for the best result of Entry 1. It is interesting to note that by excluding positions discussed in the above sub-sections, we observed less accurate prediction of the correct diastereoisomer for the γ-lactones **4** and **6**, however equivalent predictive power for δ-lactones **3** and **5** as compared to Entry 1 (Entry 3, Table 27). We decided to take forward method types X and Z to complete a DP4 analysis of (+)-angiopterlactone B (**2**) (structure I) and seven of its diastereoisomers (II-VIII) (Table 28).

(+)-Angiopterlactone B (Compound I) and seven diastereoisomers (II-VIII)

Entry	Type	% probability	I	II	III	IV	V	VI	VII	VIII
1	X	^{1}H only	57	41	0	0	0	0	0	1
		^{13}C only	38	37	14	6	1	3	0	0
		Both ^{1}H & ^{13}C	59	41	0	0	0	0	0	0
2	Z	^{1}H only	57	41	0	0	0	0	0	1
		^{13}C only	48	43	4	2	1	2	1	0
		Both ^{1}H & ^{13}C	61	39	0	0	0	0	0	0

Table 28: DP4 analysis of (+)-angiopterlactone B (**2**) (I) and seven of its diastereoisomers (II-VIII)

The results in Table 28 show that by following method type Z, the distinguishing power between the diastereoisomers is better for the carbon only data than for method type X. This led to the overall percentages for both the ^{1}H and ^{13}C data to be slightly larger for the correct structure (compound I). Generally the data fit and DP4 analysis of (+)-angiopterlactone B (**2**)

and seven of its diastereoisomers reflected trends previously observed and allowed us to narrow down the possible structures from eight to two. We therefore completed the DP4 analysis for the eight structures proposed for (–)-angiopterlactone A (**1**) (compounds I-VIII).

(–)-Angiopterlactone A (Compounds I-VIII)

As we did not exclude any of the chemical shifts which can be assigned for our previous analysis of angiopterlactone A (**1**) when following method M3, method type X and Z were equivalent and the results are summarised in Table 29 and Figure 37.

% probability	I	II	III	IV	V	VI	VII	VIII
^{1}H data only	3	53	15	3	4	6	14	1
^{13}C data only	19	73	7	1	0	0	0	0
^{1}H & ^{13}C data	1	96	3	0	0	0	0	0

Table 29: DP4 analysis of the eight possible structures (I-VIII) for (–)-angiopterlactone A (**1**)

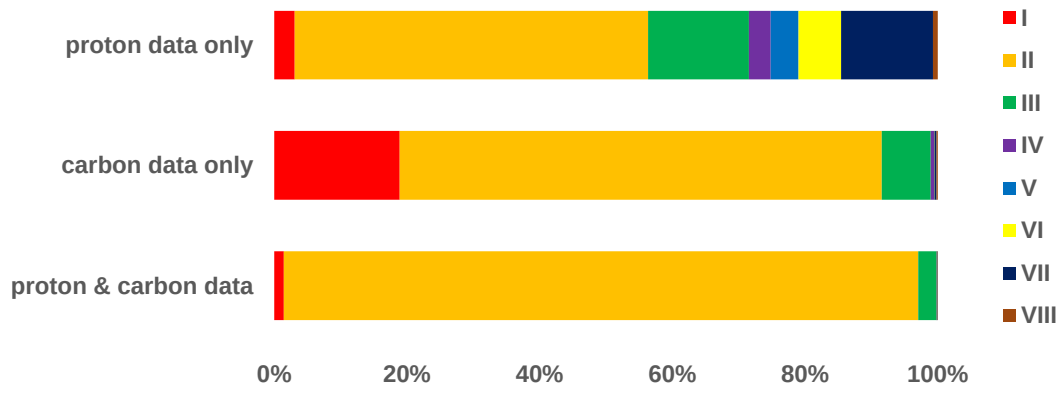

Figure 37: DP4 analysis of the eight possible structures (I-VIII) for (–)-angiopterlactone A (**1**)

As the combination of proton and carbon data has always given us the most distinguishing power between diastereoisomers, it is reassuring that our DP4 analysis of the eight diastereoisomers I-VIII result in a 96% probability that structure II is the correct one. This agrees with all of our previously made observations. Based on this large probability, synthetic investigations are underway in the laboratory in an attempt to synthesise diastereoisomer II.

2.4 Conclusions

In Section 2.1.1 we proposed that (–)-angiopterlactone A (**1**) may be a diastereoisomer of the structure initially suggested by the isolation chemists. By completing computational NMR prediction studies, utilising methods M1-M4 (Table 17, Page 83) and variations thereof, we concluded that the best method for our lactone systems was provided by method M3. Utilising method M3 and investigating various analytical techniques, we tentatively proposed a structure for (–)-angiopterlactone A (**1.II**) (Figure 38). This tentative conclusion was further confirmed upon completing Goodman and Smith's DP4 analysis, which provided us with a 96% probability that this was the correct structure. Therefore by utilising a combination of biosynthetic speculations, our synthetic experience with these compounds, as well as computational studies, we narrowed down the possible structures for (–)-angiopterlactone A (**1**) from 16 diastereoisomers, to just 1. Given the encouraging results, Dr Katherine Law (Lawrence Group) is currently completing synthetic investigations in which she is targeting our proposed structure for (–)-angiopterlactone A (**1.II**).

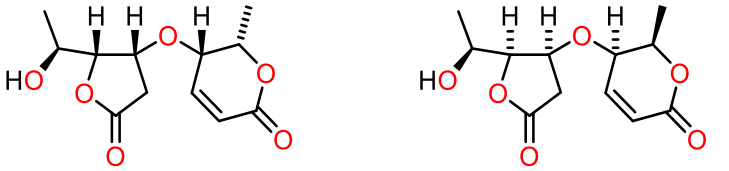

isolation chemists' proposal
*(–)-angiopterlactone A (**1**)*

our proposed structure
*(–)-angiopterlactone A (**1.II**)*

Figure 38: Structure proposed by isolation chemists for (–)-angiopterlactone A (**1**) and our proposed structure (**1.II**)

Following our investigations into the structure of (–)-angiopterlactone A (**1**), questions regarding the selectivity of the dimerisation reaction encountered in Chapter 1 still remained. Furthermore our proposed structure for (–)-angiopterlactone A (**1.II**) implicates a cross- rather than a homo-dimerisation (Scheme 26, Page 111). We therefore completed mechanistic investigations for the formation of the angiopterlactones (**1**, **2**), which will be discussed in Chapter 3.

Chapter 3: Computational Mechanistic Investigations

Chapter 1 detailed the successful total synthesis of (–)-angiopterlactone B (**2**) (Figure 39). Computational nuclear magnetic resonance (NMR) studies were outlined in Chapter 2 and led to a proposed revised structure for (–)-angiopterlactone A (**1**) (Figure 39). Next we set out to investigate the reaction mechanism for the (bio)synthesis of (–)-angiopterlactone B (**2**), as well as for our proposed structure of (–)-angiopterlactone A (**1.II**).

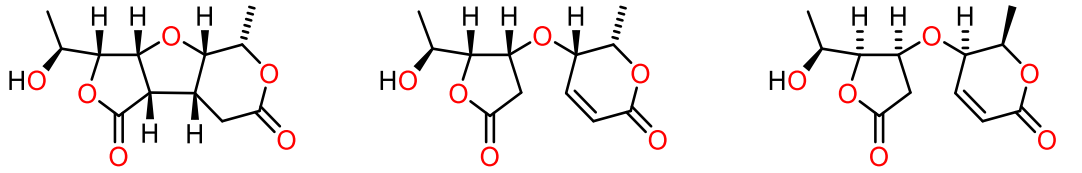

*(–)-angiopterlactone B (**2**)*

*isolation chemists' proposed (–)-angiopterlactone A (**1**)*

*our proposed structure (–)-angiopterlactone A (**1.II**)*

Figure 39: Our synthetic (–)-angiopterlactone B (**2**), the structure of (–)-angiopterlactone A proposed by the isolation chemists[2] (**1**) and our revised structure (**1.II**)

3.1 Project Background and Aims

Following our success in synthesising (–)-angiopterlactone B (**2**), a number of unanswered questions remained, the first of which was why we had not observed the related and co-isolated natural product (–)-angiopterlactone A (**1**). Upon examining the NMR spectra and methods utilised by the isolation chemists to assign the relative and absolute configuration within the angiopterlactones (**1**, **2**), we completed NMR prediction studies and suggested that (–)-angiopterlactone A (**1**) may be a diastereoisomer of the originally proposed structure. Based on our biosynthetic speculations (Chapter 1, Section 1.1.2), this structure is unlikely to be accessible from a homo-dimerisation of δ-lactone ***ent*-3** and instead requires a cross-dimerisation between δ-lactone ***ent*-3** with δ-lactone **5** (Scheme 27).

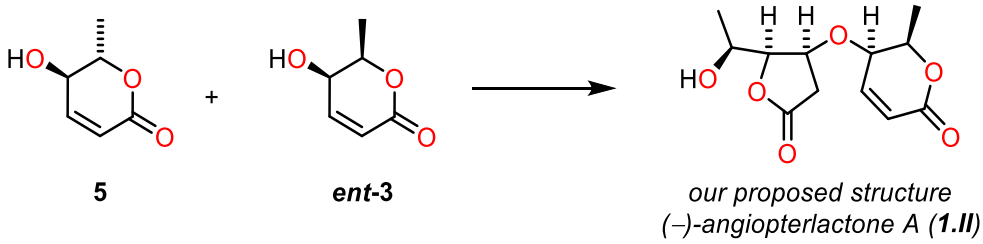

Scheme 27: Proposed starting materials necessary to synthesise the revised structure of (–)-angiopterlactone A (**1.II**)

A further question which remained unanswered following our synthetic investigations in Chapter 1, was the inherent selectivity we observed in the dimerisation reaction. The NMR spectrum of the crude dimerisation product showed a remarkably selective reaction. In an effort to shed light upon this selectivity and to investigate likely biosynthetic/synthetic pathways to our proposed structure for (–)-angiopterlactone A (**1.II**), we performed computational mechanistic studies.

These mechanistic studies are outlined in this chapter and are divided into three main sections. The first section describes our investigations into the mechanism for the (bio)synthesis of (+)-angiopterlactone B (**2**). The second one examines the mechanism for the synthesis of the related dimer, *dia*-angiopterlactone B (**2.VI**). The final section explores cross-dimerisations between δ-lactone ***ent*-3** with δ-lactone **5**, to probe whether these might provide access to angiopterlactone A (**1**).

3.2 Computational Methods

All DFT calculations were performed using the Gaussian 09[92] software, employing the ωB97XD[98] DFT functional in combination with the 6-311++g(d,p) basis set. Solvent was modelled using an implicit description of dichloroethane applying the SMD continuum model. Solvent cavities were defined by the default SMD-Coulomb radii.[99] Due to the flexibility of the systems studied, conformational sampling was completed utilising the conformational scanning function (*scan*) implemented in the TINKER[104] modelling package. This function uses a basin hopping algorithm to efficiently sample the conformational space, where each basin represents a distinct region of this space. This is followed by local minimisation to identify the lowest energy conformer within each basin. The energy window of conformational minima was set to 10 kcal/mol. Hydrogen bond interactions were confirmed by using the natural bond orbital (NBO) analysis within the Gaussian software (NBO version 3)[109]. Molecular graphics were created utilising Pymol[110].

Gibbs free energies (*G*) are reported at the reaction temperature of 343 K using a quasi-RRHO treatment. These calculations were completed utilising GoodVibes.[102] To switch between free-rotor approximations and harmonic approximations for vibrations, a smooth damping function centred around a frequency of 100 cm^{-1} was used.[103] Vibrational frequencies were utilised to confirm stationary points as transition states (TS, presence of one imaginary frequency) or minima (no imaginary frequencies). The connection of TS species with corresponding ground state species was confirmed by utilising intrinsic reaction coordinate (IRC) calculations.[111]

In each of the energy profiles, the energies of the intermediate (INT) and transition state (TS) species have been reported relative to the starting material. $RC_{1/2}$ are the first and second step of the ring contraction, *oM* is the oxa-Michael addition and *M* is the Michael addition. As the monomer is neutral and the species on the energy profile are negatively charged, a balance of charge was required. As we are investigating the reaction mechanism for the synthesis of (–)-angiopterlactone B (**2**), we utilised HCO_3^- and CO_3^{2-} to balance the charge. HCO_3^- and CO_3^{2-} were thus computed at the same level of theory as the transition state and ground state species we investigated.

3.3 Results and Discussion

3.3.1 Investigating the mechanism for the synthesis of angiopterlactone B

Our investigations began by studying the mechanism for the (bio)synthesis of angiopterlactone B (**2**). During our biosynthetic speculations (Chapter 1, Section 1.1.2), we proposed that the formation of dimer **2** could follow a domino oxa-Michael/Michael reaction utilising δ-lactone **3** and the ring-contracted γ-lactone **4** (Scheme 28). Based on these initial speculations, we set out to probe this reaction mechanism.

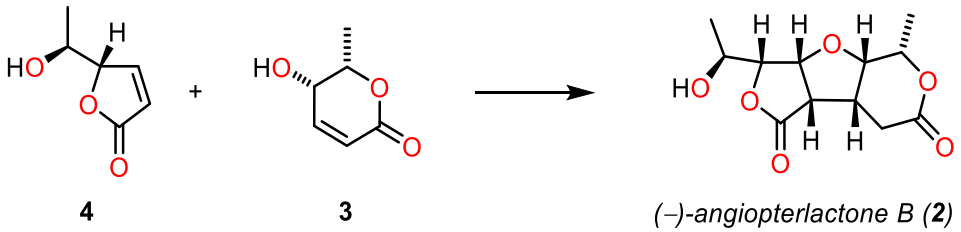

Scheme 28: Initially proposed starting materials to synthesise (–)-angiopterlactone B (**2**)

Michael Donor vs Michael Acceptor

With lactones **3** and **4** each containing a Michael donor and acceptor, there are a variety of potential oxa-Michael reactions that could occur. In order to limit these options, we first investigated which of the two lactones (**3** or **4**) would be more likely to act as the nucleophile.

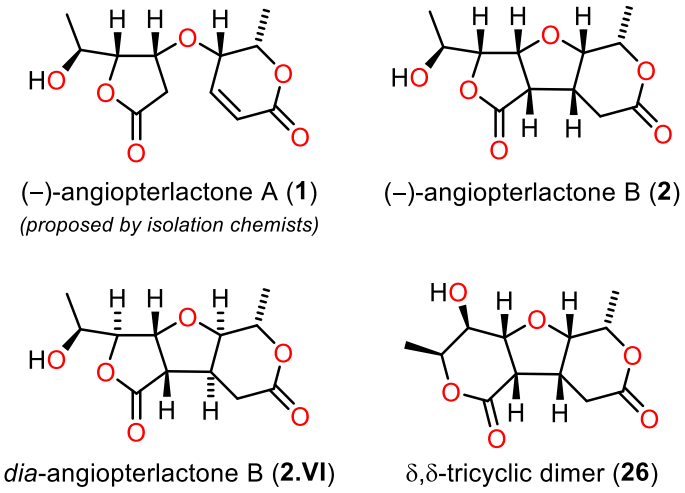

Figure 40: Isolation chemists'[2] proposed structure of (–)-angiopterlactone A (**1**) and in-house synthesised dimers (Note: *dia*-angiopterlactone B (**2.VI**) has also been synthesised by Bhattacharya and co-workers)[36]

In all our experiments and those reported by Bhattacharya and co-workers[36], no dimers resulting from γ-lactone **4** acting as the nucleophile were formed (see Figure 40 for examples). This led us to calculate pK_a values for the alcohol group in each of the lactones ***ent*-3** and ***ent*-4** (Table 30). The pK_a studies were completed by Dr Fernanda Duarte and a summary of the methodology can be found in the Appendix (Section 3.2). Note that this approach tends to over-estimates p*Ka* values and that empirical corrections have been suggested based on the nature of the chemical groups and the method used.[112] As the aim of this work was to compare the relative pK_a values for the deprotonation of the alcohol in the two species rather than obtain an absolute pK_a, we did not include a correction.

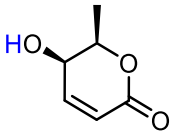

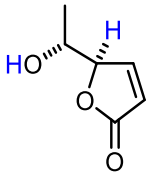

		δ-lactone *ent*-3	**γ-lactone *ent*-4**	
Solvent	**Property**	**OH → O⁻**	**OH → O⁻**	**CH → C⁻**
DCE	***ΔG* (kcal/mol)**	45.7	50.9	38.5
	pK_a	30.5	33.8	25.9
DMSO	***ΔG* (kcal/mol)**	34.1	38.9	26.3
	pK_a	23.1	26.2	18.2

Table 30: Free energy (*ΔG*) and pK_a values for lactones ***ent*-3** and ***ent*-4** in DCE and DMSO at 343 K

The results in Table 30 show that the p*Ka* for the alcohol moiety of δ-lactone ***ent*-3** is three orders of magnitude lower than that of γ-lactone ***ent*-4** in both DCE and DMSO. This suggests that at the reaction temperature, higher concentrations of the alkoxide of δ-lactone ***ent*-3** will be present than of γ-lactone ***ent*-4**. It is interesting to note that the acidity of the CH proton in γ-lactone ***ent*-4** (included for general interest and labelled in blue in Table 30) resulted in a p*Ka* value of approximately 8 orders of magnitudes less than that of the OH proton. This could provide an explanation for the experimentally observed epimerisation at this position (discussed in Chapter 1, Section 1.2.2). These pK_a studies and our previous observations led us to only investigate possible mechanistic pathways in which δ-lactone **3** acts as the nucleophile in the synthesis of (–)-angiopterlactone B (**2**).

Potential Mechanistic Pathways

Based on the assumption that δ-lactone ***ent*-3** acts as the nucleophile, a number of pathways remain which need to be considered for the synthesis of (+)-angiopterlactone B (**2**). The three mechanistic pathways we considered as the most plausible are summarised in Figure 41 and are outlined in the sections to follow. The pathways have been colour-coded for ease of reading and these colours remain throughout the chapter. Structures following the general connectivity within angiopterlactone A (**1**) will henceforth be referred to as γ,δ-dimers (see Figure 41).

Pathway 1 (**P1**, red) is initiated by ring contraction of δ-lactone ***ent*-3** to the corresponding γ-lactone ***ent*-4**. An intermolecular oxa-Michael addition could then give access to a γ,δ-dimer (**X**, Figure 41). A final intramolecular Michael addition could then provide (+)-angiopterlactone B (**2**).

Pathway 2 (**P2**, black) involves an oxa-Michael addition between two units of δ-lactone ***ent*-3** to provide a δ,δ-dimer (**Y**, Figure 41). Ring contraction could then result in a γ,δ-dimer (**X**, Figure 41). Finally an intramolecular Michael addition could provide (+)-angiopterlactone B (**2**).

Pathway 3 (**P3**, blue) commences with dimerisation of two units of δ-lactone ***ent*-3** *via* an oxa-Michael addition to provide a δ,δ-dimer (**Y**, Figure 41). This could then be followed by a Michael addition to provide a δ,δ-tricyclic dimer (**Z**, Figure 41). A ring contraction could then result in (+)-angiopterlactone B (**2**). It is important to note that this pathway does not proceed *via* a γ,δ-dimer intermediate.

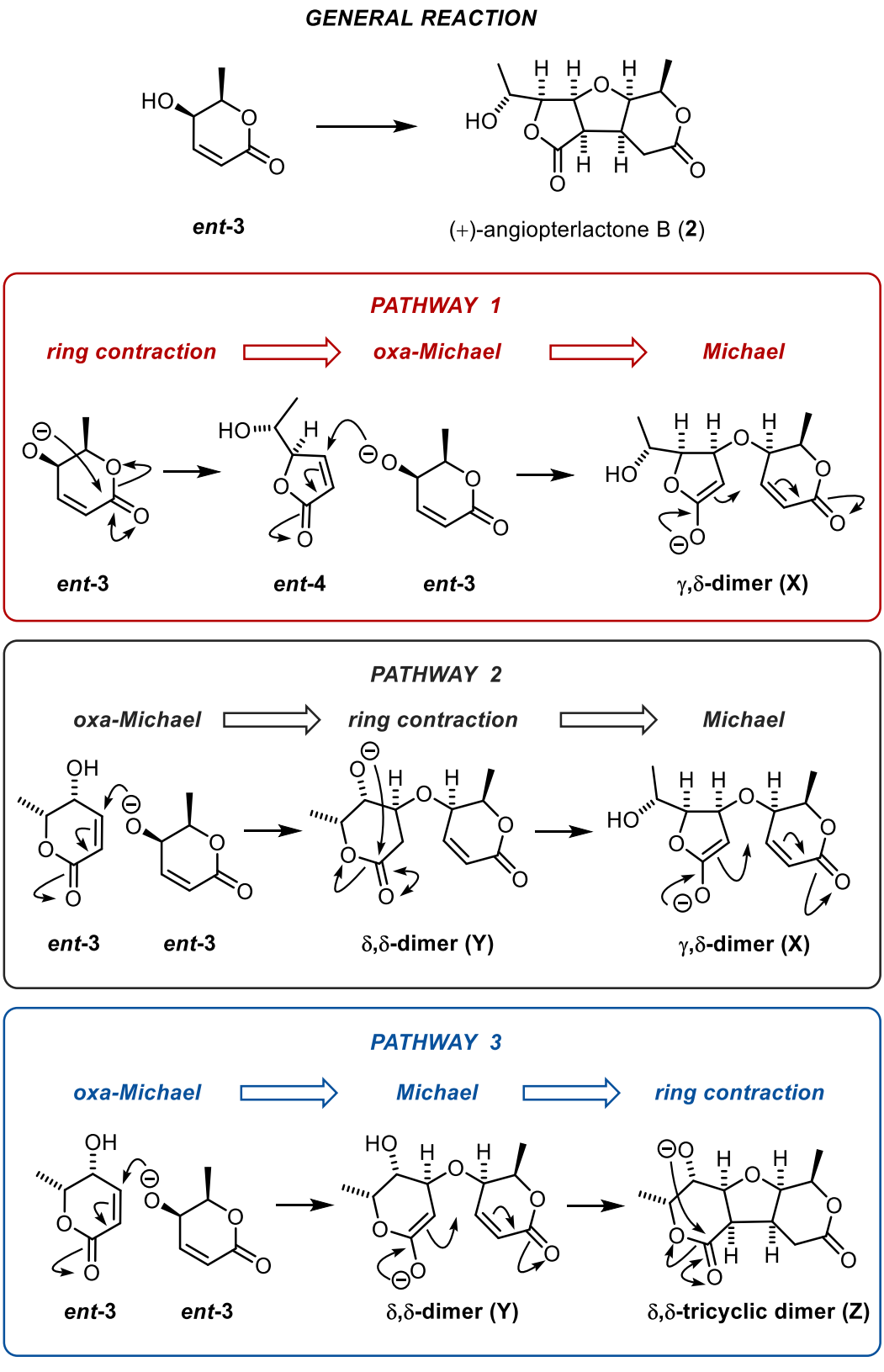

Figure 41: Three possible mechanistic pathways for the synthesis of (+)-angiopterlactone B (**2**)

Possible Outcomes from a Domino Oxa-Michael / Michael Reaction

Now that we had established the three mechanistic pathways we were investigating, there were a number of possible orientations in which the oxa-Michael and the subsequent Michael additions could occur. The example provided in Scheme 29, follows Pathway 1.

For the initial intermolecular oxa-Michael addition of δ-lactone ***ent*-3** to γ-lactone ***ent*-4** there are two possibilities: it can either occur from the *Re* face or from the *Si* face (Scheme 29). The next step is the intramolecular Michael addition, which can proceed through four different transition states (products differ in the relative orientation of the hydrogen atoms around the central THF ring being formed; see Scheme 29). Thus, the domino oxa-Michael/Michael reaction between lactones ***ent*-3** and ***ent*-4** has eight possible outcomes. In principle, these alternatives are available for each of our three proposed mechanistic pathways (Figure 41). While these different alternatives were explored, we limit our discussion herein to just two possible outcomes for the domino oxa-Michael/Michael addition. Throughout all our mechanistic studies, the *Re* pathway always results in the *cis-anti-cis* product and the *Si* pathway in the *cis-syn-cis* product (preferred pathway is substantially lower in energy) (Scheme 29). This can be readily understood, as it has previously been reported that due to steric strain and geometric requirements, five-five and five-six bicyclic systems are energetically favoured when they are *cis*-fused.[113] To demonstrate how these *cis*- and *trans*-fused rings compare, we calculated their relative energies (Table 31).

Option	***cis*-fused**	***trans*-fused**	***ΔG* (kcal/mol)**
A	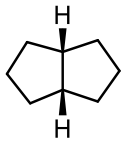	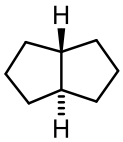	–8.0
B	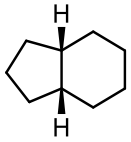	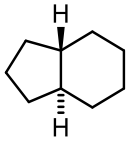	–5.1

Table 31: Investigating *cis*- and *trans*-fused ring systems. Negative values indicate that the *cis*- is favoured over the *trans*-fused ring

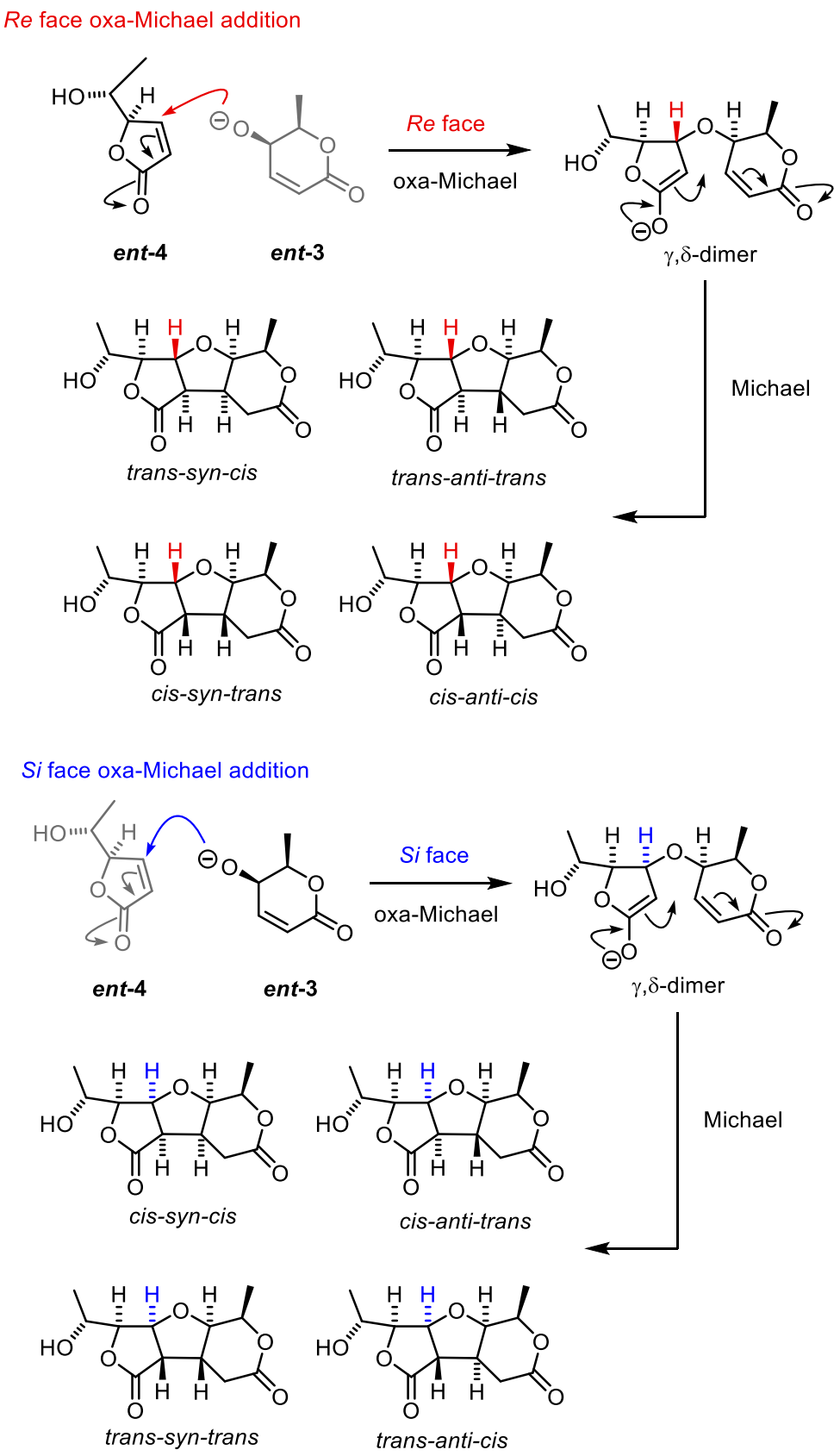

Scheme 29: Domino oxa-Michael/Michael process, resulting in eight possible products (labelling of products results from relative relationship of hydrogen atoms around the central THF ring)

Pathway 1 (P1)

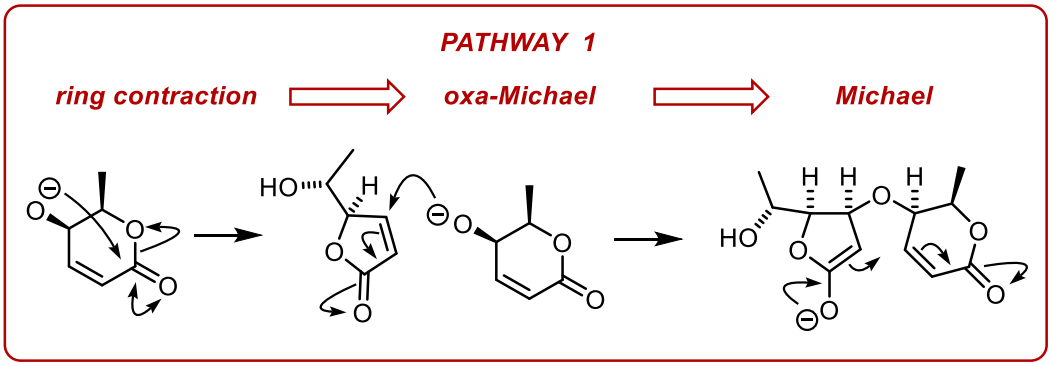

The mechanistic investigations began by considering δ-lactone ***ent*-3** and pathway 1 (**P1**) (Figure 42). The first step involves the ring contraction (RC) from δ-lactone ***ent*-3** to the corresponding γ-lactone ***ent*-4**. Our calculations revealed that this ring contraction proceeded as a two-step process, in which the first step corresponds to a 5-*exo*-trig cyclisation (RC1) and the second to a *retro*-5-*exo*-trig ring opening (RC2). Upon considering the methyl group in either the pseudo-axial or the pseudo-equatorial orientation, we found that the lowest energy conformer resulted from the methyl group being placed in the pseudo-equatorial position (as for the protonated species in Chapter 2) (see Appendix, Table 68). The activation energy required to achieve the ring contraction of δ-lactone ***ent*-3**, was 19.3 kcal/mol at the ωB97XD/6-311++g(d,p) level of theory (TS_{RC1}, Figure 42). Similar results were obtained employing the M06-2X functional and the same basis set (study initiated by Dr Fernanda Duarte and completed by myself). Thus we continued utilising the ωB97XD functional.

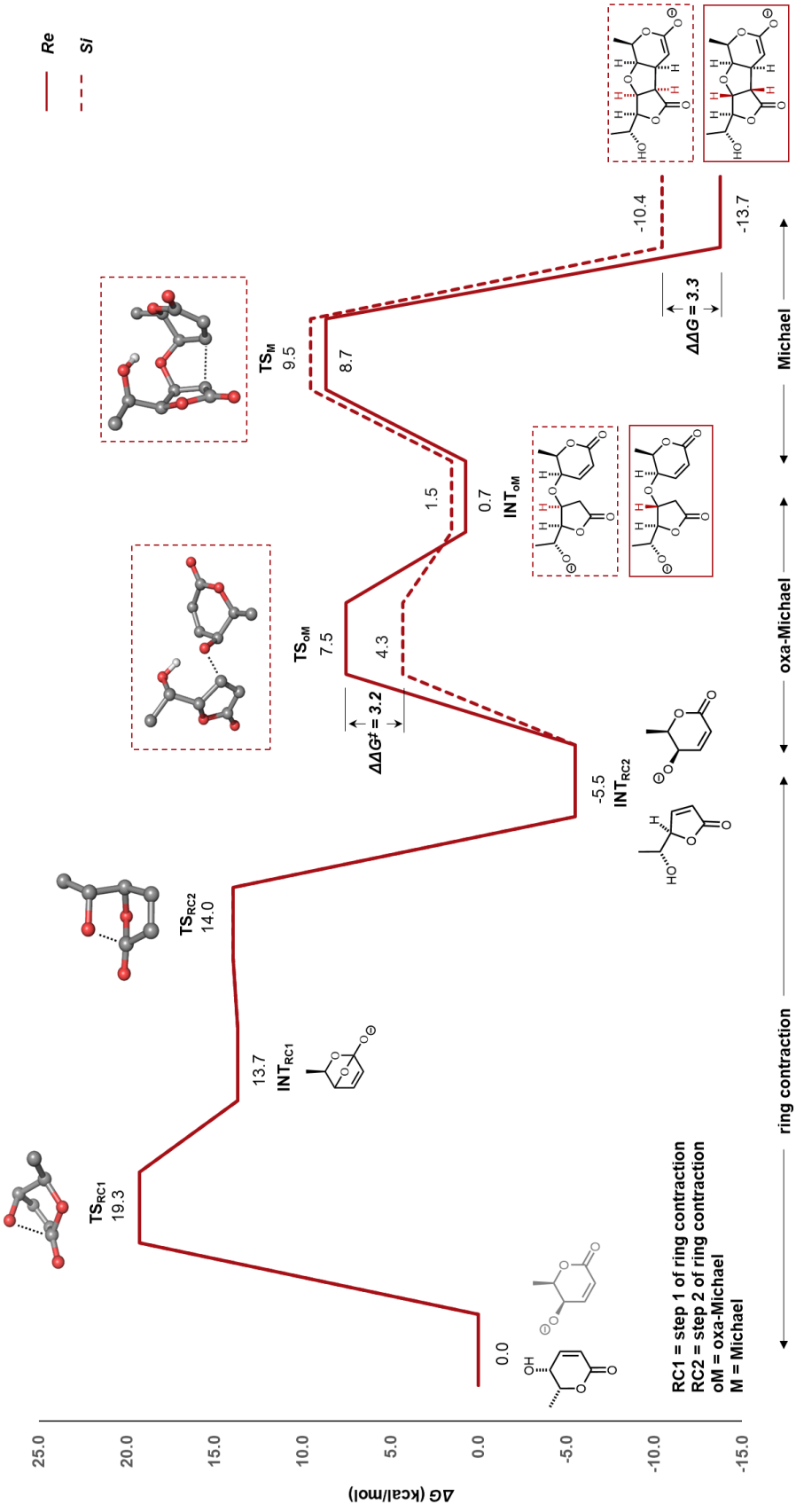

Figure 42: Pathway 1 energy profile for the homo-coupling of δ-lactone ***ent*-3**

It is interesting to note that INT_{RC2} is 5.5 kcal/mol more stable than the starting δ-lactone ***ent*-3** (at 0.0 kcal/mol). This result made us curious as to why a 5-membered lactone ring should be lower in energy than its 6-membered analogue. Upon searching the literature, we found that Stedjan and Augspurger completed a study of ring strain energy within lactones.[114] This resulted in the observation that ring strain energies for δ-lactones were typically 1-2 kcal/mol higher than those of γ-lactones. As this does not account for the large difference of 5.5 kcal/mol that we observed, we investigated the relative energies of a number of 5- and 6-membered rings, which were based on the initial δ-lactone **3** and γ-lactone **4** (Table 32). The results showed that for each of the lactones investigated (options A-D, Table 32), the γ-lactone was around 5-6 kcal/mol lower in energy than the δ-lactone equivalent. As soon as the lactone moiety is removed, however, the 6-membered ring becomes more favourable (options E-G, Table 32). Upon further examination, we noted that whereas the 6-membered rings in options E-G were in a chair conformation, the lactones in options A-D were in a boat conformation (some structures are summarised in Figure 43, indicating key bond angles). This is a result of the planarity of the lactone moiety (see Chapter 1, Section 1.2.3). Upon calculating the 6-membered ring in option G in the twist-boat conformation (Table 32), a decrease in ΔG from +2.1 to –2.8 kcal/mol was observed. This is equivalent to an energy difference between the chair and twist-boat conformation of 4.9 kcal/mol, which matches literature values (5.0 kcal/mol[115]).

Option	6-membered ring	5-membered ring	*ΔG* (kcal/mol)
A	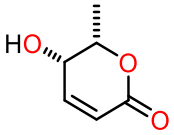	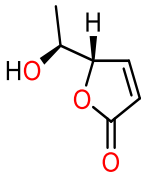	–4.9
B	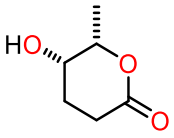	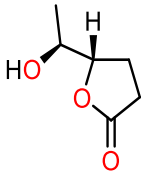	–5.1
C	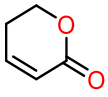	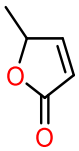	–6.0
D	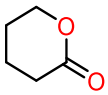	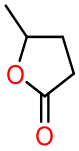	–6.0
E		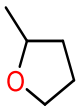	–0.7
F	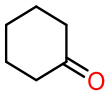	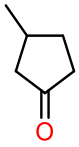	+0.9
G		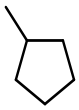	6-chair: +2.1 6-twist-boat: –2.8

Table 32: Investigating and comparing energies of 6- and 5-membered rings. Negative values indicate that the 5-membered ring is favoured over the 6-membered ring.

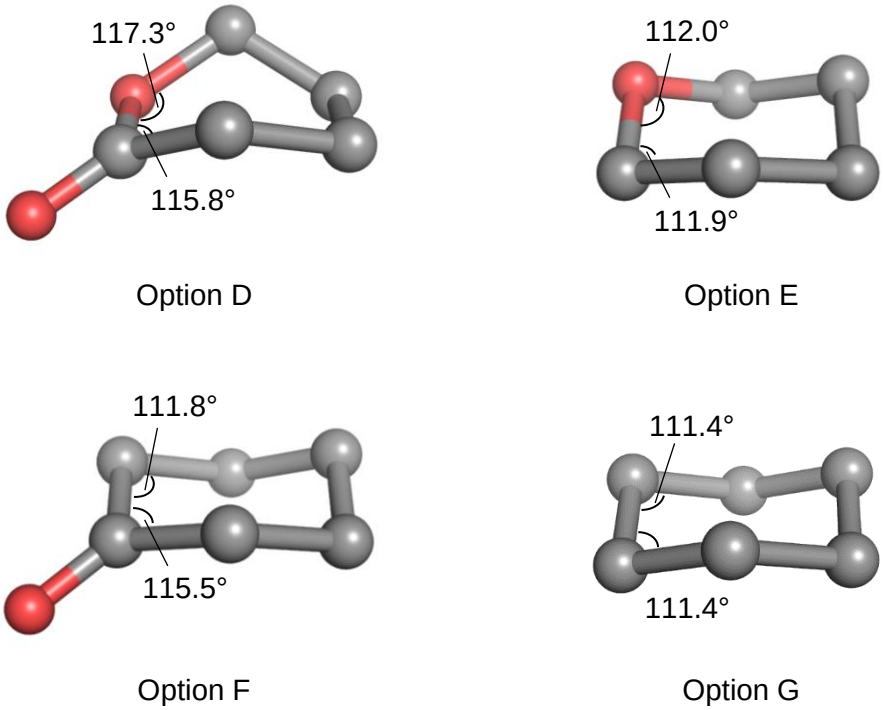

Figure 43: Conformations of 6-membered rings in options D-G, highlighting key bond angles

The next step in **P1** is the oxa-Michael addition of δ-lactone ***ent*-3** to γ-lactone ***ent*-4** (oM, Figure 42). The transition state calculations for this step were initially carried out by Dr Fernanda Duarte and the analysis was completed by myself. Upon computing the energies for the various orientations for both the *Re* and the *Si* face oxa-Michael additions, we noted that *Si* face addition was favoured by 3.2 kcal/mol (TS_{oM}). Examination of the two transition states showed that in both the *Re*- and *Si*-TS_{oM}, the δ-lactone configurations were identical, with the methyl groups in the pseudo-equatorial (pseudo-eq) position (Figure 44). The preference for the *Si*-TS_{oM} species arises from the favourable hydrogen bond interaction between the nucleophilic alkoxide and the hydroxyl of the γ-lactone, which is only observed in this orientation and is absent in the *Re*-TS_{oM} species.

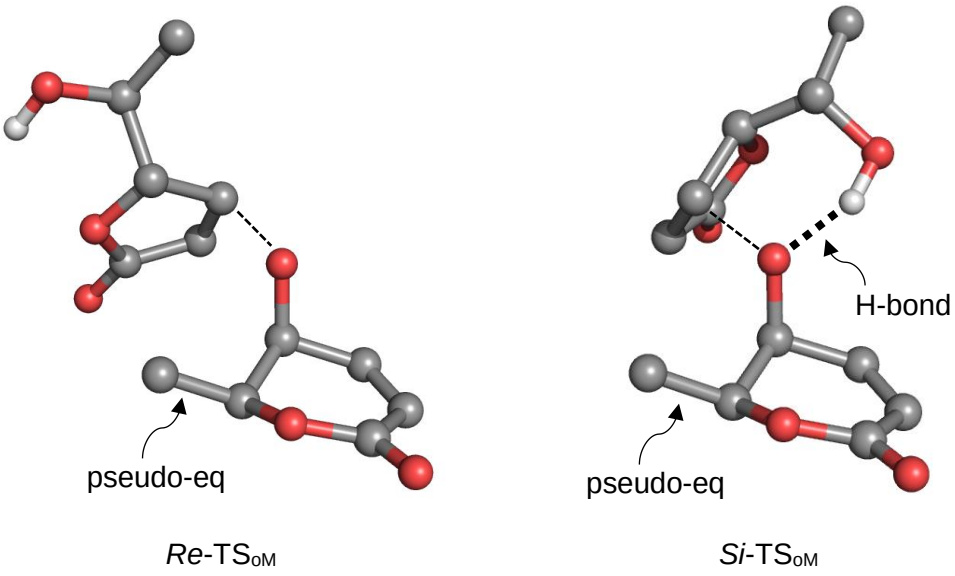

Figure 44: Transition state for the *Re* and the *Si* face oxa-Michael (oM) addition

The final step in **P1** is the intramolecular Michael addition (M, Figure 42), for which the required activation energies for the *Re* and the *Si* pathways are very similar. The most notable difference is the stability of the product, with the *Re* product being 3.3 kcal/mol more stable than the *Si* product. It is interesting to note that the former resulted in an open chain-like structure, whereas the latter was arranged in a more sterically congested bowl-like shape (Figure 45). We speculated that the stability of the product is therefore related to sterics.

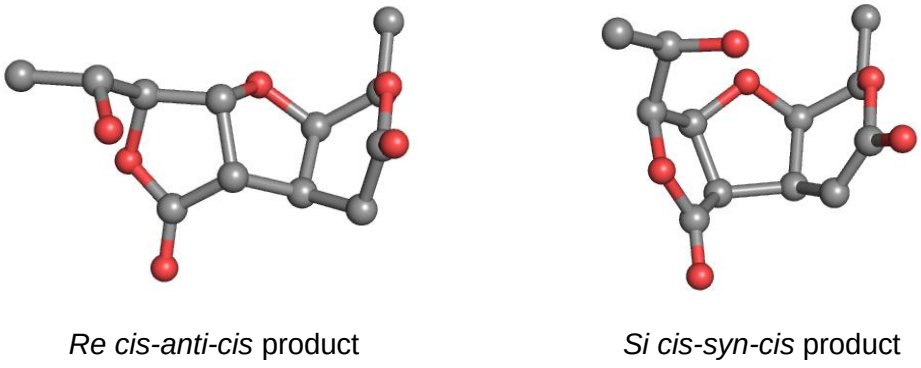

Figure 45: Final product for the *Re*- and *Si*-pathways

To confirm this hypothesis, we conducted several tests (Table 33). First, we investigated if the flexible side chain attached to the γ-lactone has an effect on the relative energy of the products. Removal of this side chain resulted in a ΔG of 3.7 kcal/mol in favour of the *Re* product, thus demonstrating that the side chain arrangement was not responsible for the difference in energy (option B). Next we removed the γ-lactone half of the molecule, which resulted in an energy

difference of only 1.5 kcal/mol in favour of the *Re* product (option C), indicating that the energy difference between the *Re* and *Si* product is indeed due to sterics.

Option	*Re*	*Si*	*ΔG* (kcal/mol)
A	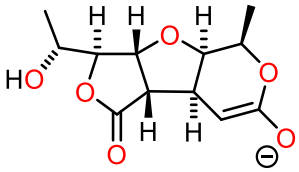	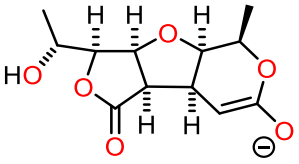	3.3
B	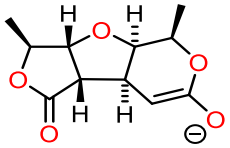	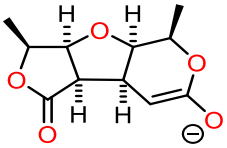	3.7
C	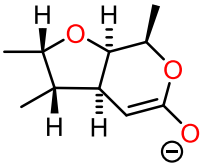	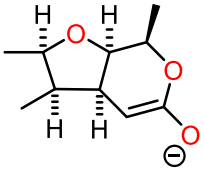	1.5

Table 33: Stability tests of angiopterlactone B (**2**) (option A) derivatives (positive values indicate that *Re* is favoured)

In conclusion, examination of the overall energy profiles for pathway 1 indicated that the rate-limiting step is the initial ring contraction (TS_{RC}). Similar energetics were obtained for both the *Re*- and *Si*-pathways, with the main differences being the transition state of the oxa-Michael addition (TS_{oM}) and the product stability. The thermodynamic product of this reaction profile would be the *Re* product, which is not the product we observed experimentally. Given the large initial activation barrier of 19.3 kcal/mol for the ring contraction (TS_{RC}), we moved to investigate pathways 2 and 3 to identify whether pathway 1 was a viable option.

Pathway 2 (P2)

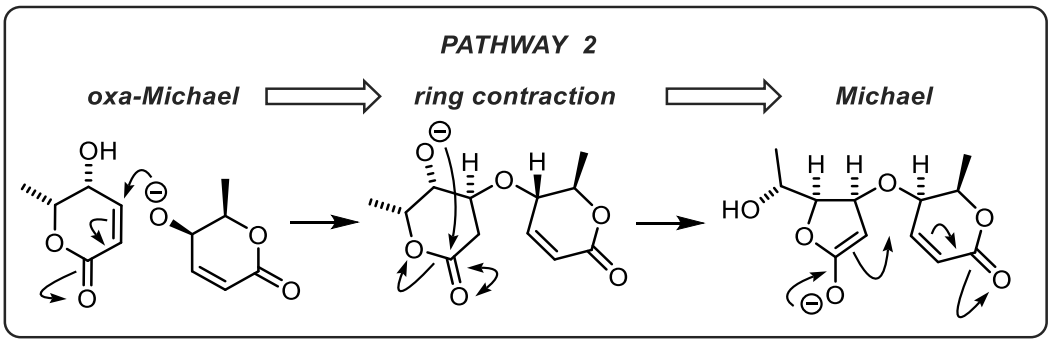

The energy profiles for pathway 2 (**P2**) are shown in Figure 47. **P2** is initiated by an oxa-Michael addition (oM) between two units of δ-lactone ***ent*-3**, which can occur from the *Re* or the *Si* face.

As seen in Figure 47, the activation energy for the *Re* and *Si* face oxa-Michael addition is nearly identical (TS_{oM}). However, the resulting *Si*-INT_{oM} species is 2.3 kcal/mol more stable than *Re*-INT_{oM}. Upon inspection of the structures, we noted that whereas in the *Si* species both methyl groups were in the pseudo-equatorial, the *Re* species had one methyl group in the pseudo-axial (pseudo-ax) position (Figure 46). This conformation allows a hydrogen bond interaction between the OH group of the lactone and the ether linkage between the rings. To draw a better comparison to the energetically favourable *Si* species, we computed the energy of the *Re* species with both methyl groups in the pseudo-equatorial position and found that this resulted in the loss of the stabilising hydrogen bond interaction and increased the energy by a further 2.0 kcal/mol.

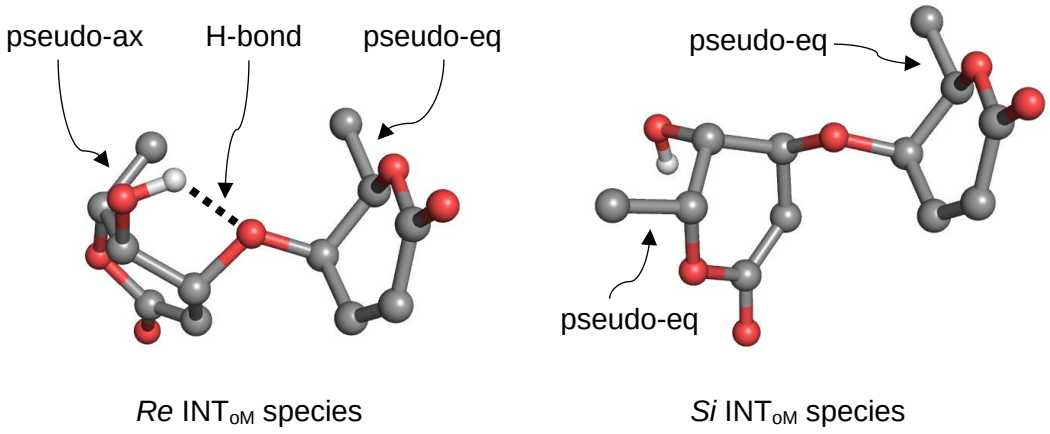

Figure 46: *Re* and *Si* INT_{oM} species

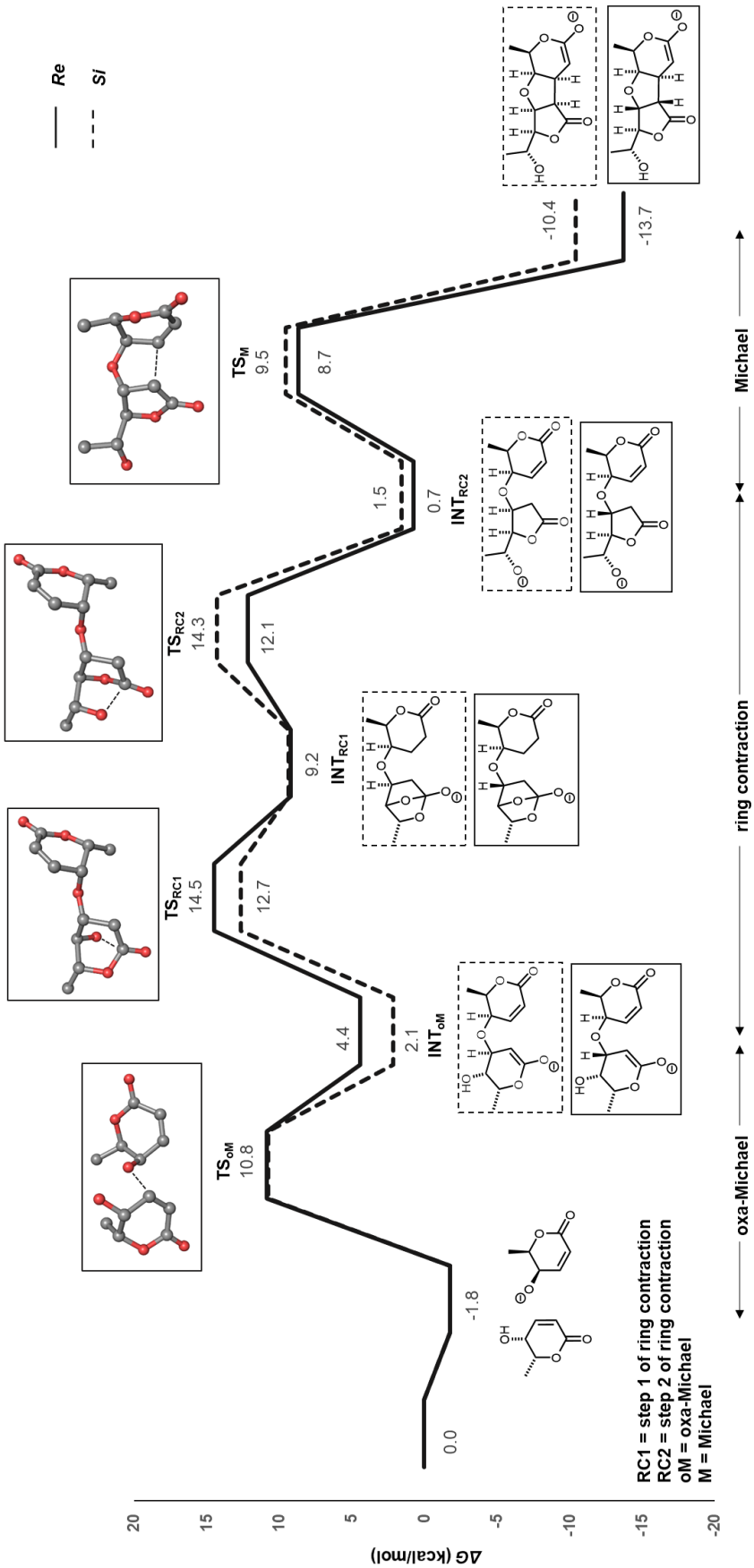

Figure 47: Energy profile for pathway 2 of the homo-coupling of δ-lactone ***ent*-3**

The next step in **P2** is the ring contraction, for which the highest *Re*- and *Si*-pathway transition states (TS_{RC}) are almost equal in energy. The final step is the Michael addition (M), which is identical to the one reported for pathway 1.

Overall, as a result of the similarities in the overall activation energies for the *Re* and *Si* pathways, we did not draw a conclusion with respect to which pathway would be kinetically favoured. However, if the reaction is under thermodynamic control, the product resulting from the *Re* pathway would be preferred, which is not the product we observed experimentally.

Pathway 3 (P3)

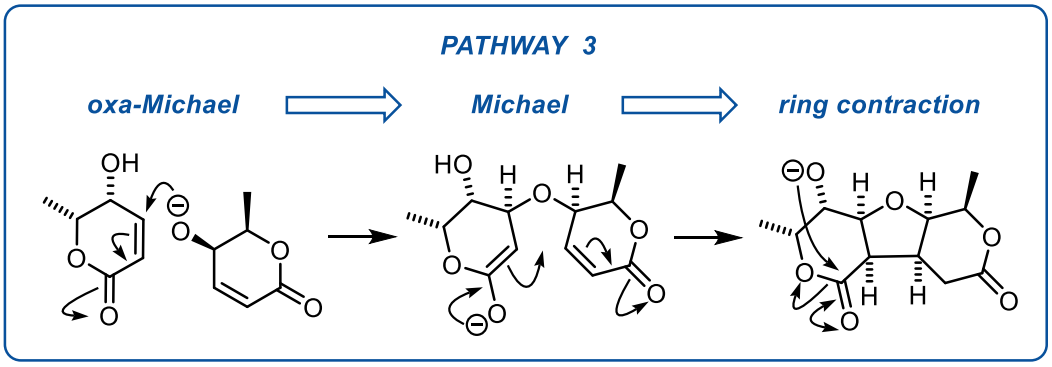

Similarly to pathway 2, pathway 3 (**P3**) began with the oxa-Michael addition (oM) between two units of δ-lactone ***ent*-3** (Figure 49). The next step in **P3** is the intramolecular Michael addition (M). The activation barriers for the Michael addition in the *Re* and *Si* pathways are similar to one another (TS_M), with the *Si* pathway being slightly preferred by 2.1 kcal/mol. The final step in **P3** is the ring contraction, for which we noted that the *Si* pathway is higher in energy than the *Re* pathway (TS_{RC}, $\Delta\Delta G^{\ddagger}$ = 6.6 kcal/mol). Similarly to our observations for **P1**, we noted that whereas the *Re*-TS_{RC} was arranged in a flat and more open structure, the *Si*-TS_{RC} was arranged in a bowl-like and more sterically congested structure (Figure 48).

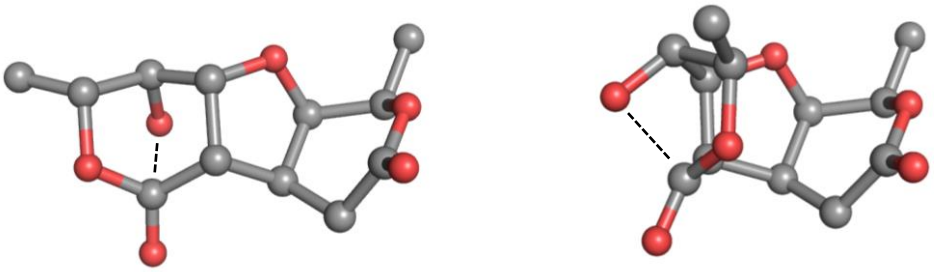

Re TS_{RC1} species *Si* TS_{RC1} species

Figure 48: TS_{RC1} for the *Re*- and the *Si*-pathway

In order to investigate the effect of these different arrangements on the activation energy, we examined simplified structures for TS_{RC}. For the first system we studied, the nucleophilic δ-lactone from the initial oxa-Michael addition was removed, which barely affected the energy difference between *Re*- and *Si*-TS_{RC} ($\Delta\Delta G^{\ddagger}$ = 6.1 kcal/mol in favour of the *Re*-TS_{RC}) (*option B*, Table 34). Inspection of the transition state species showed that as observed previously, the *Si* species represented a more closed bowl-like structure, whereas the *Re* species was flatter and less sterically congested. Upon further simplification of the molecule (*option C*, Table 34), $\Delta\Delta G^{\ddagger}$ between the *Re* and the *Si* species was reduced to 2.1 kcal/mol. This suggests that the high $\Delta G^{\ddagger}$ observed for the ring contraction in the *Si* pathway, is linked to the overall sterics of the molecule.

Option	***Re***	***Si***	***ΔΔG‡* (kcal/mol)**
A	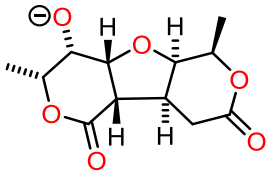	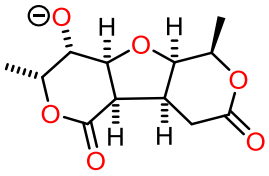	6.6
B	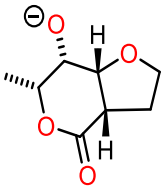	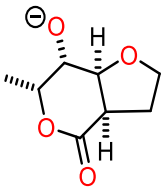	6.1
C	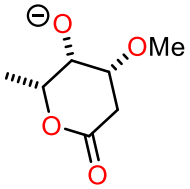	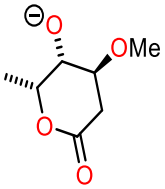	2.1

Table 34: Differences in activation energy for the ring contraction in simplified compounds (positive values indicate that *Re* is favoured

In summary, the *Si*-TS_M has a lower $\Delta G^{\ddagger}$ than the *Re*-TS_M. As this step is likely to be irreversible under the experimental conditions, **P3** would preferentially proceed to form the *Si* product. It is interesting to note that this is the experimentally observed product and thus if **P3** represents the correct pathway for the synthesis of angiopterlactone B (**2**), it suggests that the reaction is under kinetic control. The next step in our investigation was to directly compare the lowest energy profiles for pathways 1, 2 and 3 to examine which pathway was most likely for the synthesis of angiopterlactone B (**2**).

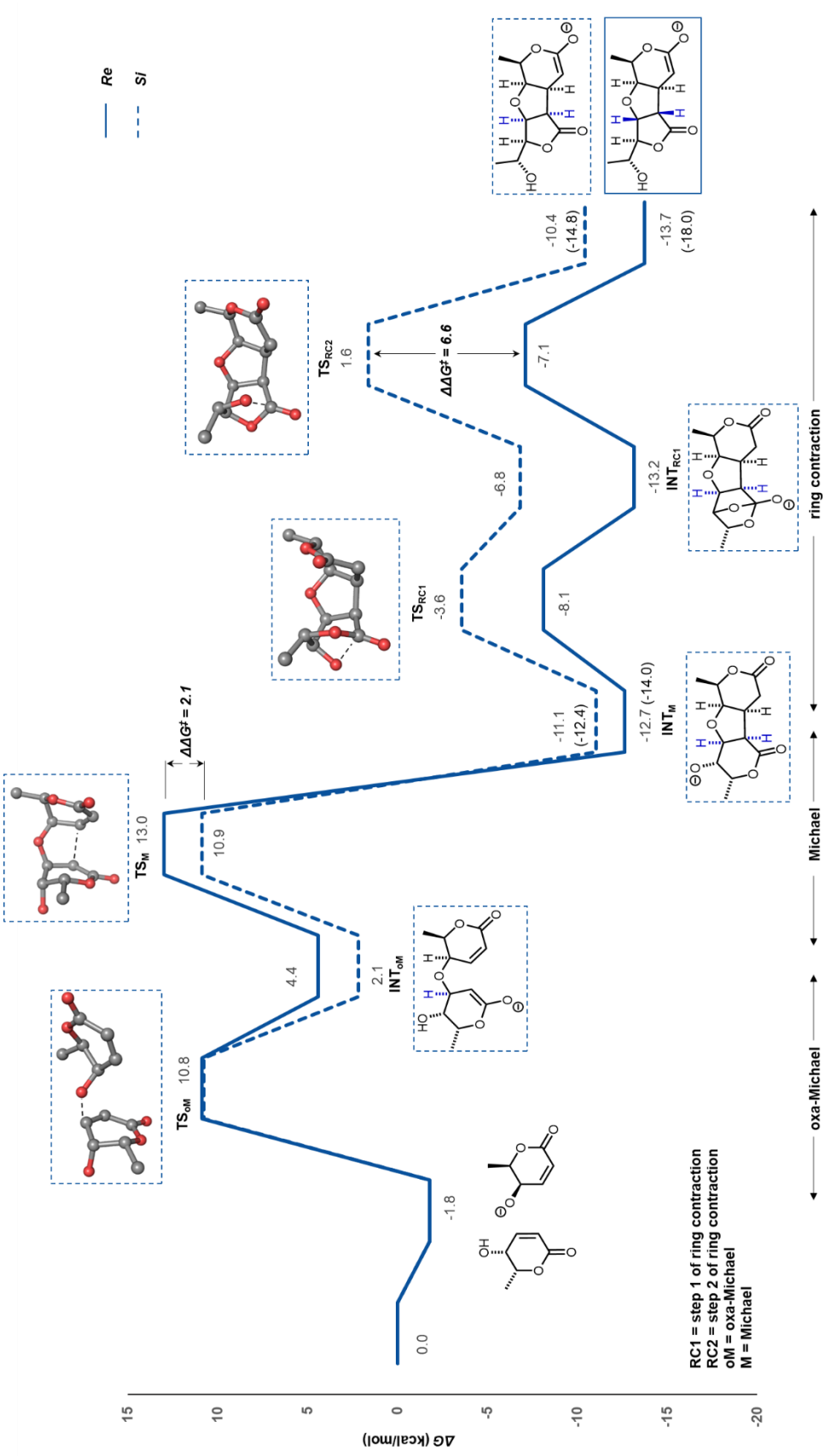

Figure 49: Energy profile for **P3** of the homo-coupling of δ-lactone ***ent*-3** (bracketed values are for protonated species)

Comparison of Pathways 1-3

In order to investigate which pathway was most likely for the synthesis of (+)-angiopterlactone B (**2**), we summarise their energy profiles in Figure 51. As the rate limiting step for **P1** is the initial ring contraction (TS_{RC}), which is identical for the *Re* and *Si* pathway, we have only shown the *Si* pathway as a representative example. The *Re* and *Si* pathways in **P2** had nearly identical activation energy barriers (TS_{RC}) and thus we have only included the *Re* pathway as a representative example. We previously concluded for **P3**, that the reaction preferentially proceeds *via* the *Si* pathway and thus only this pathway is included on the energy profile.

It is interesting to note that the activation energy for the ring contraction varies substantially between **P1** and **P2/3**. In **P1**, $\Delta G^{\ddagger}$ is more than 7 kcal/mol higher than in either **P2** or **P3** (Figure 50). One of the main differences between the ring contractions is that in **P1**, the δ-lactone contains an alkene, which is not present in either **P2** or **P3**. To determine the effect the alkene may have on the activation energy of the ring contraction (TS_{RC}), we carried out an analogous study in which we removed the alkene functionality in the δ-lactone. This resulted in an activation energy of 7.7 kcal/mol, which is 11.6 kcal/mol lower than that observed in **P1**.

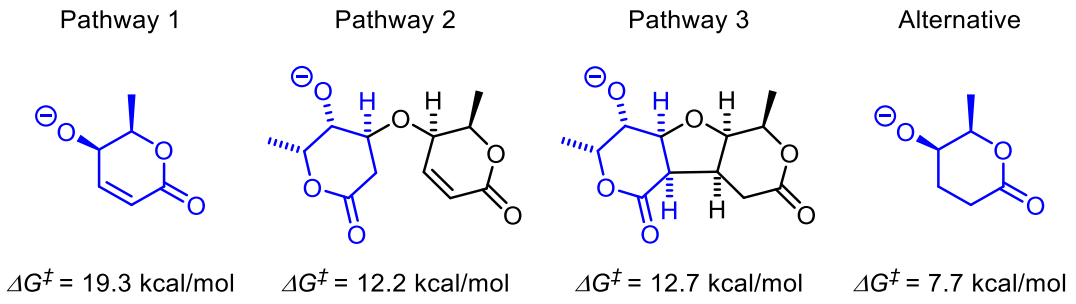

Figure 50: Summarised activation barriers for the ring contractions in pathways 1, 2 and 3, as well as the hydrogenated alternative

We previously noted that the rate-limiting step for **P1** corresponds to the ring contraction ($\Delta G^{\ddagger}$ = 19.3 kcal/mol), which is much higher in energy than that of **P3** ($\Delta G^{\ddagger}$ = 12.7 kcal/mol; $\Delta\Delta G^{\ddagger}$ = 6.6 kcal/mol). Based on this large energy difference, **P1** was excluded from further analysis. It is interesting to note that **P1** most closely resembled our initial biosynthetic speculations (Chapter 1, Section 1.1.2).

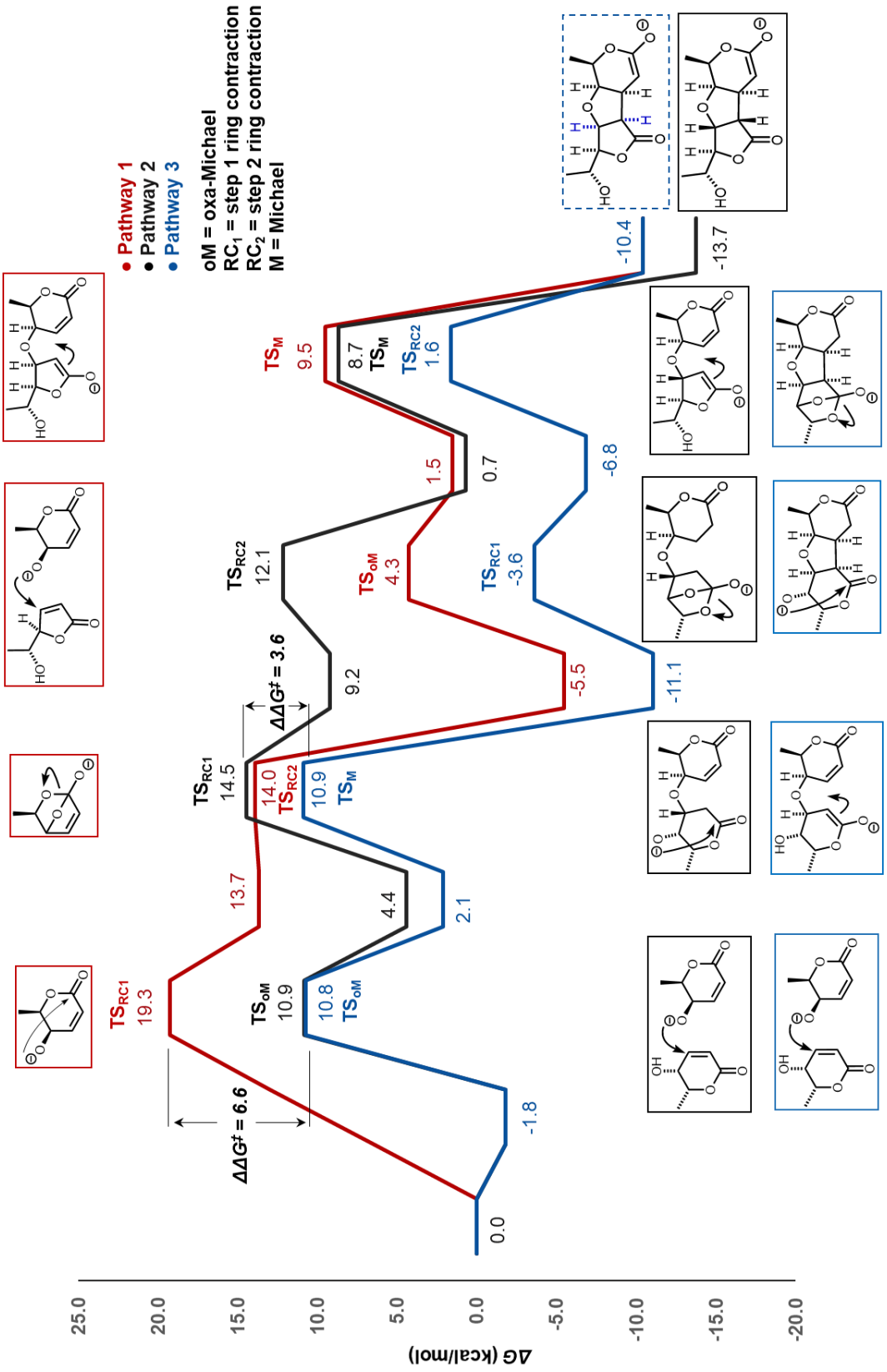

Figure 51: Energy profile featuring examples from pathways 1, 2 and 3

The highest energy barrier in **P3** is 3.6 kcal/mol lower than that in **P2** and therefore we disregard **P2** and propose **P3** to be the most energetically favourable reaction pathway. This pathway results in the *Si-cis-syn-cis*-product, which agrees with our experimentally observed outcome.

In summary we propose that **P3** represents the most likely pathway for the synthesis of angiopterlactone B (**2**). It is interesting to note that the *Si*-product is not thermodynamically favoured and that **P3** does not proceed *via* a γ,δ-dimer. This could offer an explanation as to why angiopterlactone A (**1**) was not observed during our synthetic investigations.

3.3.2 Investigating the mechanism for the synthesis of *dia*-angiopterlactone B

Our mechanistic investigations of δ-lactone ***ent*-3** to form (+)-angiopterlactone B (**2**) resulted in proposing **P3** as the most likely mechanism leading to its formation. Next we examined the mechanism for the homo-coupling of δ-lactone **5** to form *dia*-angiopterlactone B (**2.VI**) (the synthesis of dimer **2.VI** was completed by Dr Katherine Law (Lawrence group) (Scheme 30)). As the product observed corresponds to the opposite facial addition to that of the oxa-Michael addition to form (–)-angiopterlactone B (**2**), we were intrigued to investigate the mechanism for this reaction.

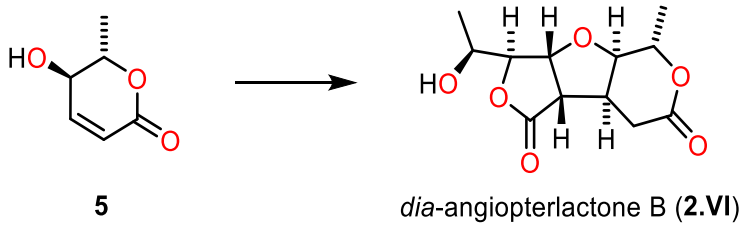

5 *dia*-angiopterlactone B (**2.VI**)

Scheme 30: Dimerisation reaction of δ-lactone **5** to form *dia*-angiopterlactone B (**2.VI**)

Pathway 1 (P1)

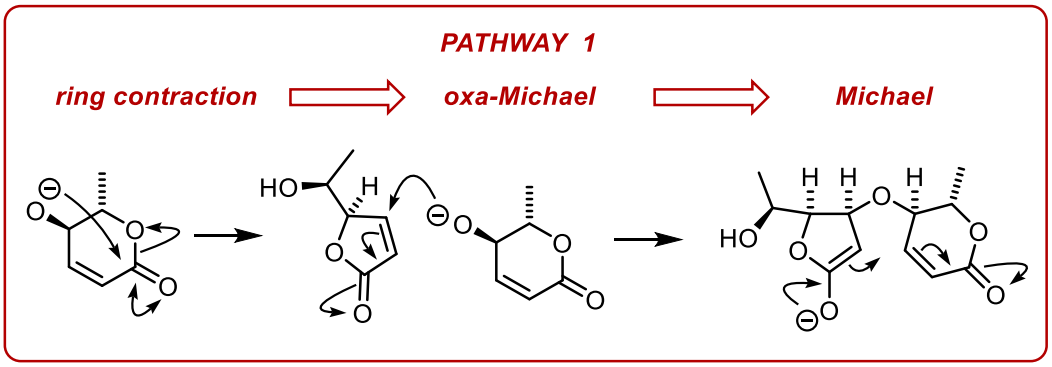

We began by investigating the ring contraction from δ-lactone **5** to the corresponding γ-lactone **6**. Similarly to our previous studies, the ring contraction involves a high energy transition state ($\Delta G^{\ddagger}$ of 18.6 kcal/mol). Due to this large activation energy barrier, we investigated **P2** and **P3** and then draw comparisons between the three pathways at the end of this section.

Pathway 2 (P2)

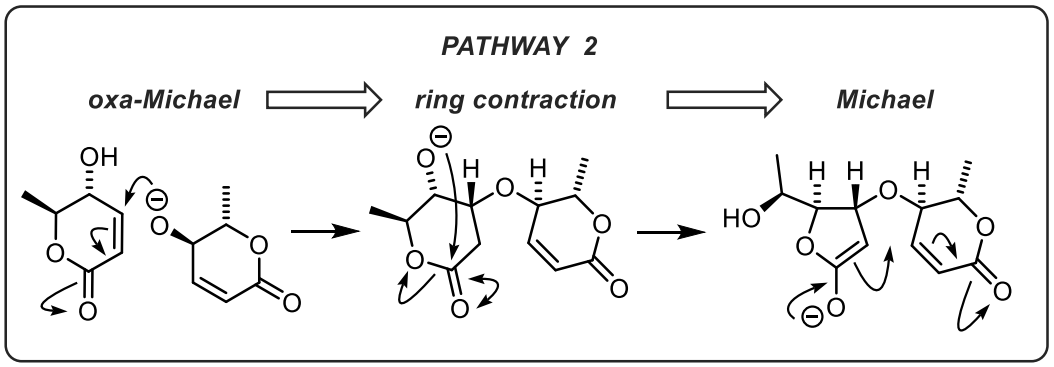

The energy profile for **P2** is presented in Figure 53. The first step is the oxa-Michael addition between two units of δ-lactone **5**, for which we found that addition from the *Re* face is favoured by 5.1 kcal/mol over addition from the *Si* face (TS_{oM}). Upon examination of the TS_{oM} species (Figure 52), it became evident that for the *Re* species each of the δ-lactones was arranged with the methyl groups in the pseudo-equatorial position and the hydroxyl group provided a stabilising hydrogen bond interaction. The *Si* species on the other hand lacked this stabilising hydrogen bond interaction and favoured one methyl group in the pseudo-axial position. This trend is repeated in the resulting INT_{oM} species (the δ,δ-dimer) and explains the differences in energy between the *Re* and *Si* species.

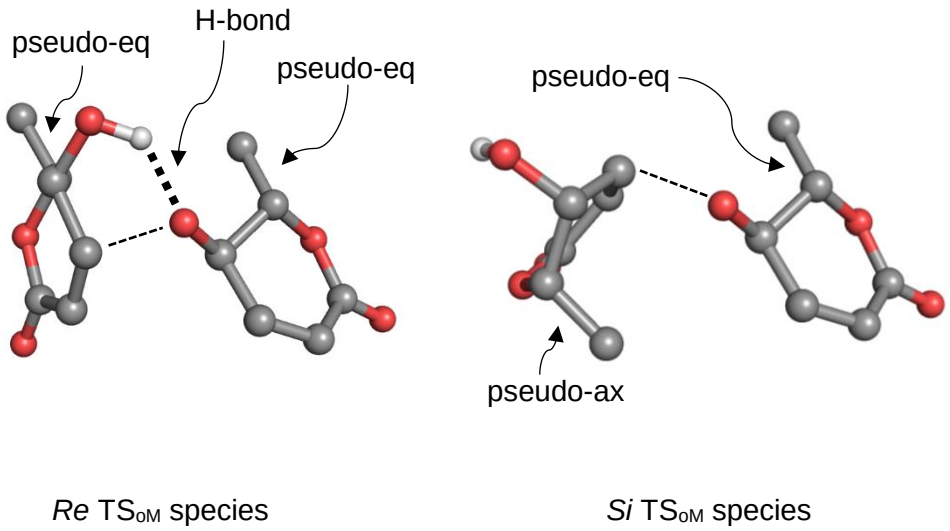

Figure 52: *Re* and *Si* transition state species for the oxa-Michael addition

The activation energy for the second step in **P2**, the ring contraction (RC), is similar between the *Re* and *Si* pathways. Finally, the Michael addition step (M) favours the *Re* pathway by 4.0 kcal/mol. Upon inspection of the optimised TS_M species, we observed (as we had previously) that the *Si* species was more sterically congested than the *Re* species.

The similarities in the overall energy values prevented us from concluding which pathway would be kinetically favoured, however the *Re* product is thermodynamically favoured. We continued our investigations by examining pathway 3.

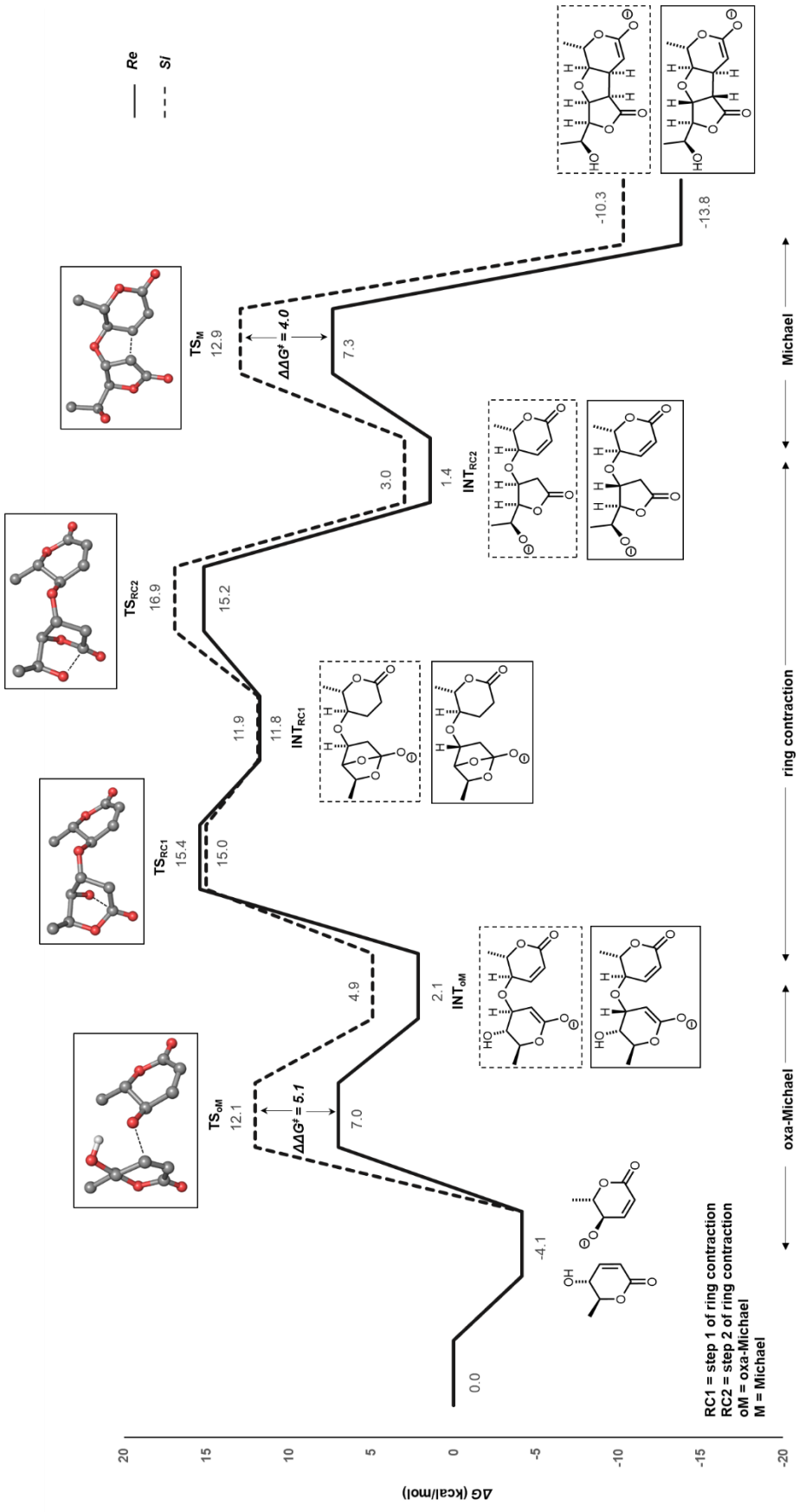

Figure 53: Pathway 2 energy profile for the homo-coupling of δ-lactone **5**

Pathway 3 (P3)

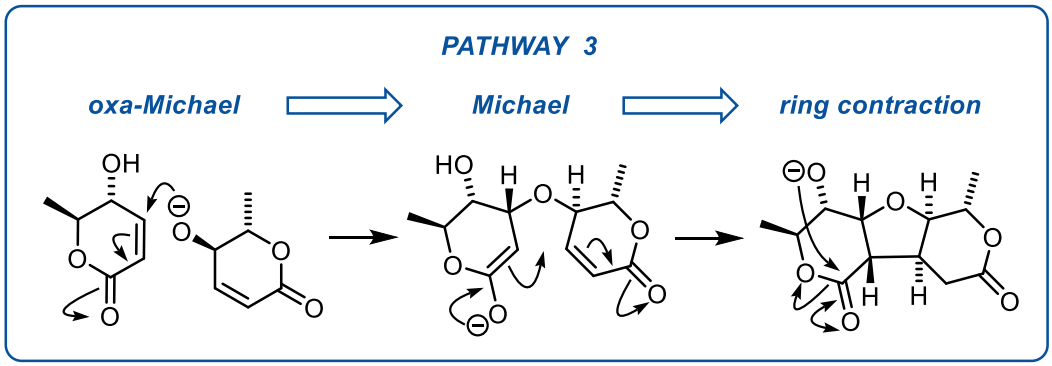

The first step of **P3** is equivalent to that of **P2** and involves the oxa-Michael addition between two units of δ-lactone **5**. The results showed that the addition from the *Re* face (TS_{oM}) was favoured by 5.1 kcal/mol (Figure 54). This trend is upheld throughout the Michael addition (M) and subsequent ring contraction (RC). Upon inspection of the intermediate and transition state species, we generally noted (as observed previously) that the *Re* species tended to be arranged in a flatter, open-chain like structure, with both methyl groups in the pseudo-equatorial positions. The *Si* species on the other hand were bowl-like, more sterically congested and were thus more stable when one methyl group was placed in the pseudo-axial position. This could explain why the *Si* species are typically higher in energy.

Overall **P3** favours the *Re* product both kinetically and thermodynamically. It is interesting to note that this is the product which was observed experimentally by Dr Katherine Law. Next we compared **P1**, **P2** and **P3**, in order to determine which one is most likely for the reaction of δ-lactone **5** to form *dia*-angiopterlactone B (**2.VI**).

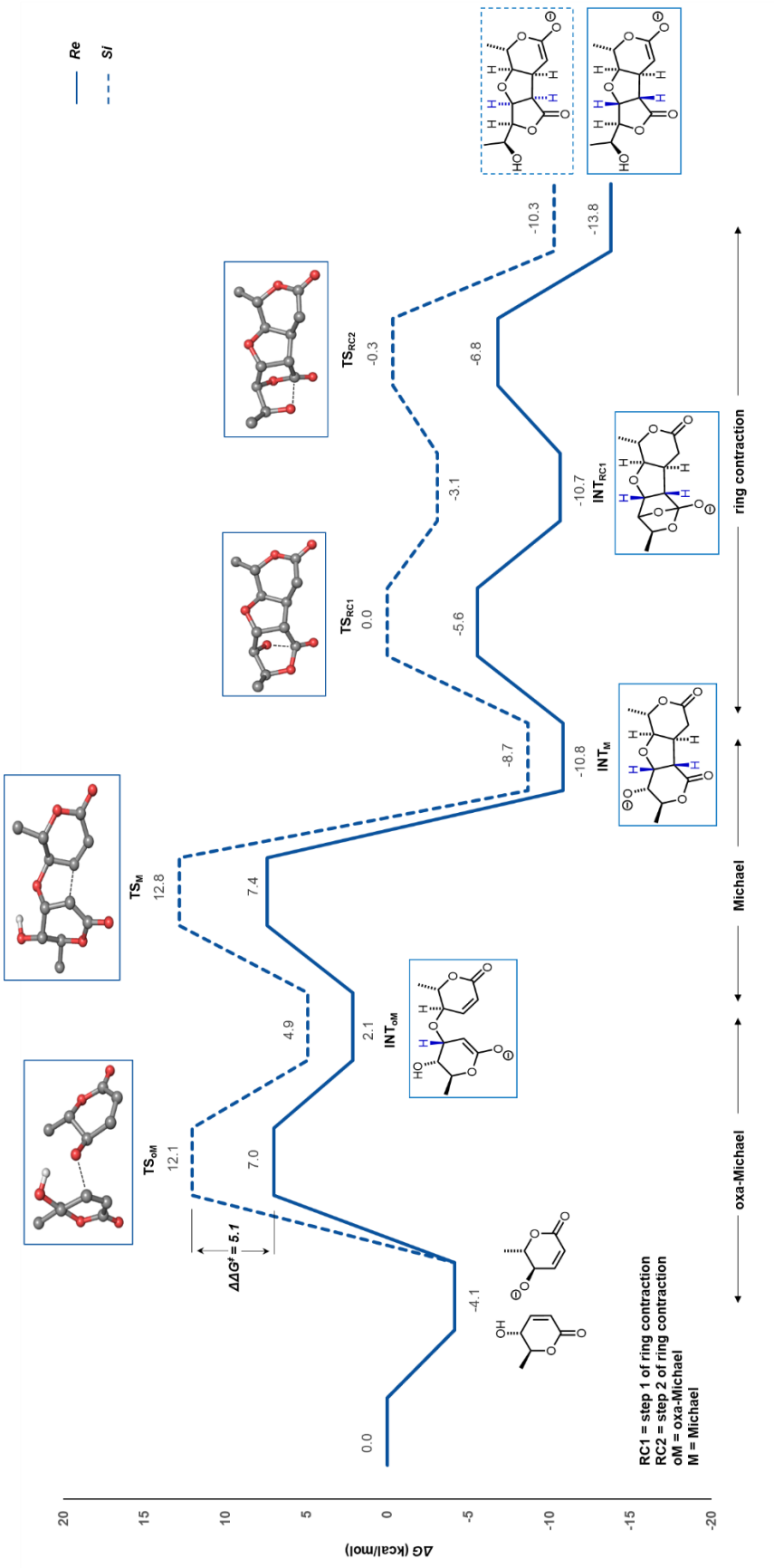

Figure 54: Energy profile for pathway 3 for the homo-coupling of δ-lactone **5**

Comparison of Pathways 1-3

A summary of the energy profiles for **P2** and the lowest energy profile for **P3** is shown in Figure 55. For **P1** the rate-limiting step is the ring contraction, which requires an activation energy of 18.6 kcal/mol. The highest energy barrier to overcome in **P3**, is 11.3 kcal/mol (TS_M) ($\Delta\Delta G^{\ddagger}$ = 7.1) and thus we disregarded **P1**.

The highest energy transition state for both the *Re* and *Si* pathways in **P2** is that of the ring contraction (TS_{RC}). There was a substantial difference in energy to overcome these transition states when compared to TS_M in **P3** ($\Delta\Delta G^{\ddagger}$ = 8.0 and 9.5 kcal/mol respectively) and thus **P2** could also be disregarded. We therefore propose that the dimerisation of δ-lactone **5** to *dia*-angiopterlactone B (**2.VI**) proceeds *via* pathway 3.

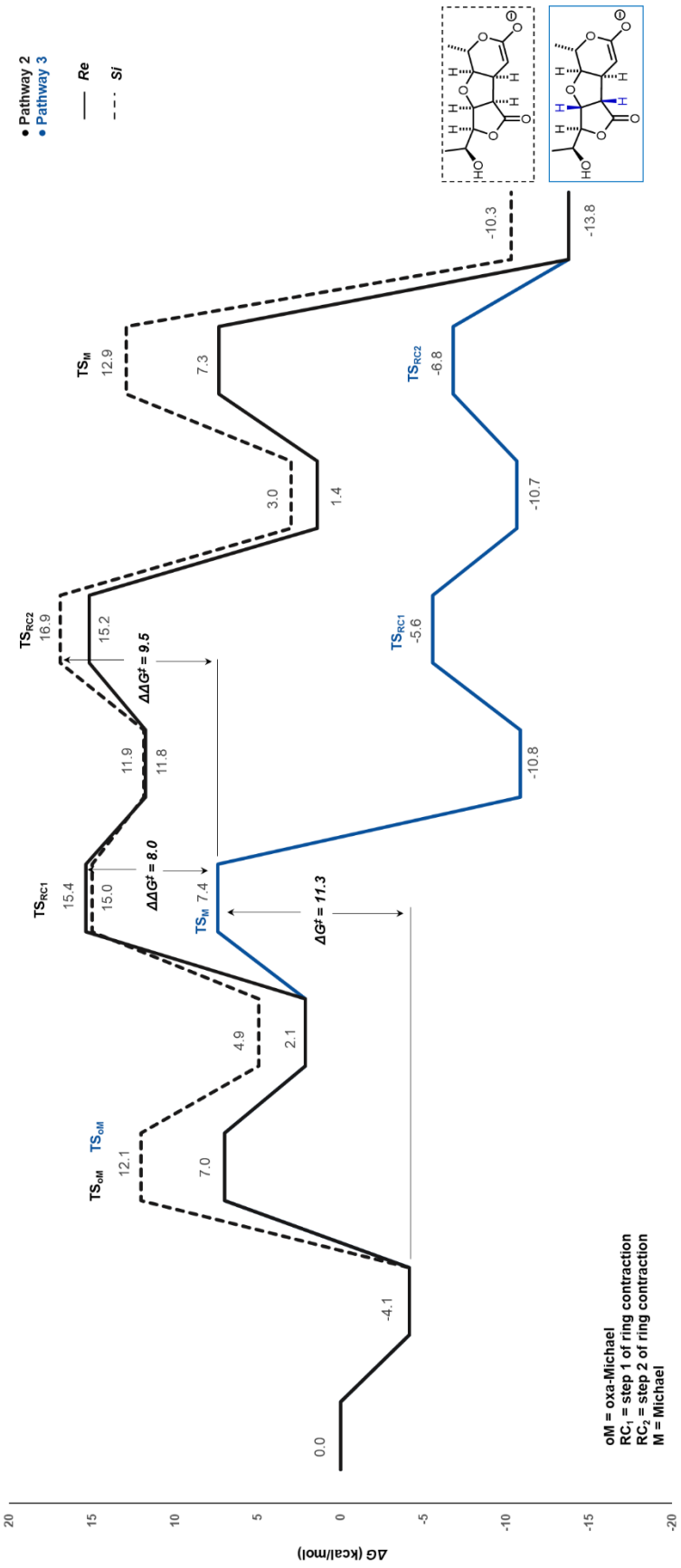

Figure 55: Energy profile summarising pathways 2 and 3 for the homo-coupling of δ-lactone **5**

3.3.3 Cross Dimerisations

Subsequent to our mechanistic investigations into the homo-coupling reactions of δ-lactone ***ent*-3** and δ-lactone **5**, we turned our attention to investigating their cross-coupling reactions. While no experimental data is available for these reactions, this study will serve as a guide to further synthetic efforts in the Lawrence group. Our interest in exploring their mechanism stems from our proposed structure for (–)-angiopterlactone A (**1.II**). The formation of this compound presumably results from a cross dimerisation of δ-lactone ***ent*-3** and an (*R*,*S*)-δ- or γ-lactone, where the former acts as the nucleophile and the latter as the electrophile (Scheme 27, Page 117). Thus we began our investigations by examining the three pathways for such a cross-coupling.

Pathway 1 (P1)

As discussed in Section 3.3.2, the ring contraction of **P1** has a high initial activation energy barrier ($\Delta G^{\ddagger}$ = 18.6 kcal/mol). This will be compared to pathways 2 and 3 at the end of this section.

Pathway 2 (P2)

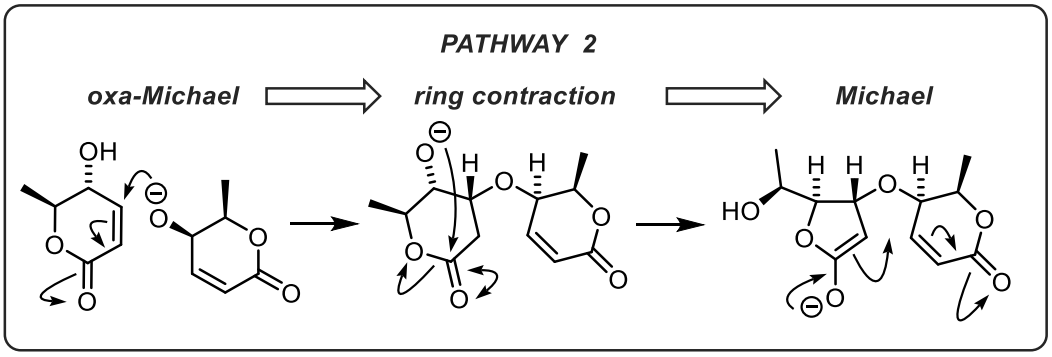

The energy profile for **P2** is summarised in Figure 58. The first step is the oxa-Michael addition of δ-lactone ***ent*-3** to δ-lactone **5**. It is interesting to note that similarly to the oxa-Michael addition between two units of δ-lactone **5**, the *Re* addition is preferred ($\Delta\Delta G^{\ddagger}$ = 6.0 kcal/mol). Upon inspection of the oxa-Michael transition state species (TS_{oM}) we noted that the *Re* species had a favourable hydrogen bond interaction between the nucleophile and the hydroxyl group

of the electrophile (Figure 56). The *Si* transition state species on the other hand lacked such a H-bonding interaction and furthermore the methyl group of the electrophile was in the pseudo-axial position. Attempts to place both methyl groups in the pseudo-equatorial position, increased the energy by +0.5 kcal/mol.

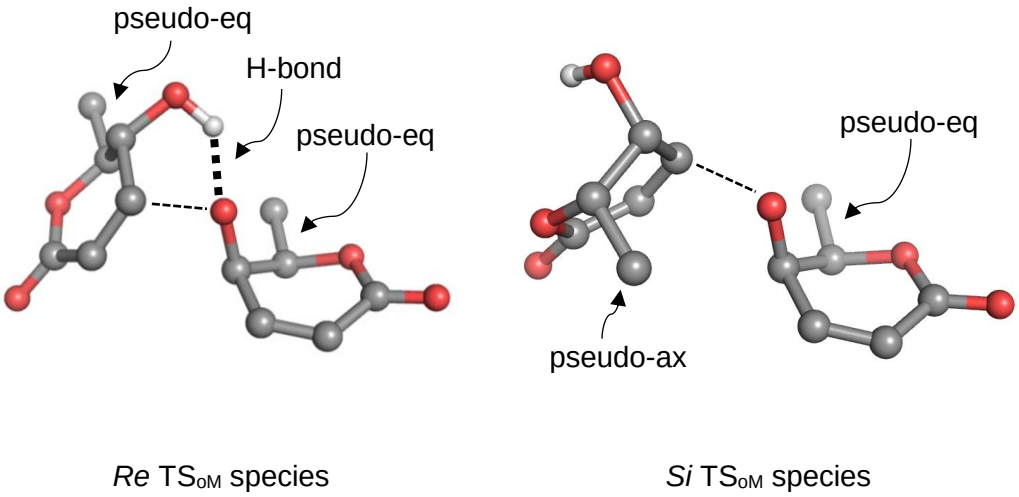

Figure 56: *Re* and *Si* transition state species for the oxa-Michael addition

The ring contraction (RC) and the final Michael addition (M) in **P2** have similar activation barriers for both the *Re* and *Si* pathways. Inspection of the transition state species (TS_M) showed that similarly to our previous investigations, the *Re* species had an open-chained and uncongested structure (Figure 57). Although the *Si*-TS_M is stabilised by a H-bond, it is destabilised by its sterically congested bowl-like structure. In the product species, this stabilising hydrogen bond is weaker than in *Si*-TS_M and thus the *Re* product is more stable.

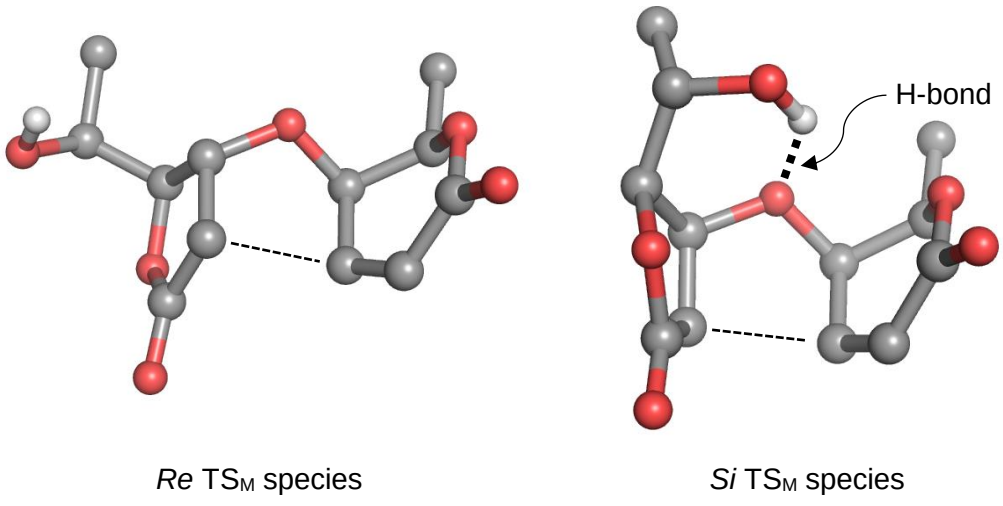

Figure 57: *Re* and *Si* transition state species for the Michael addition

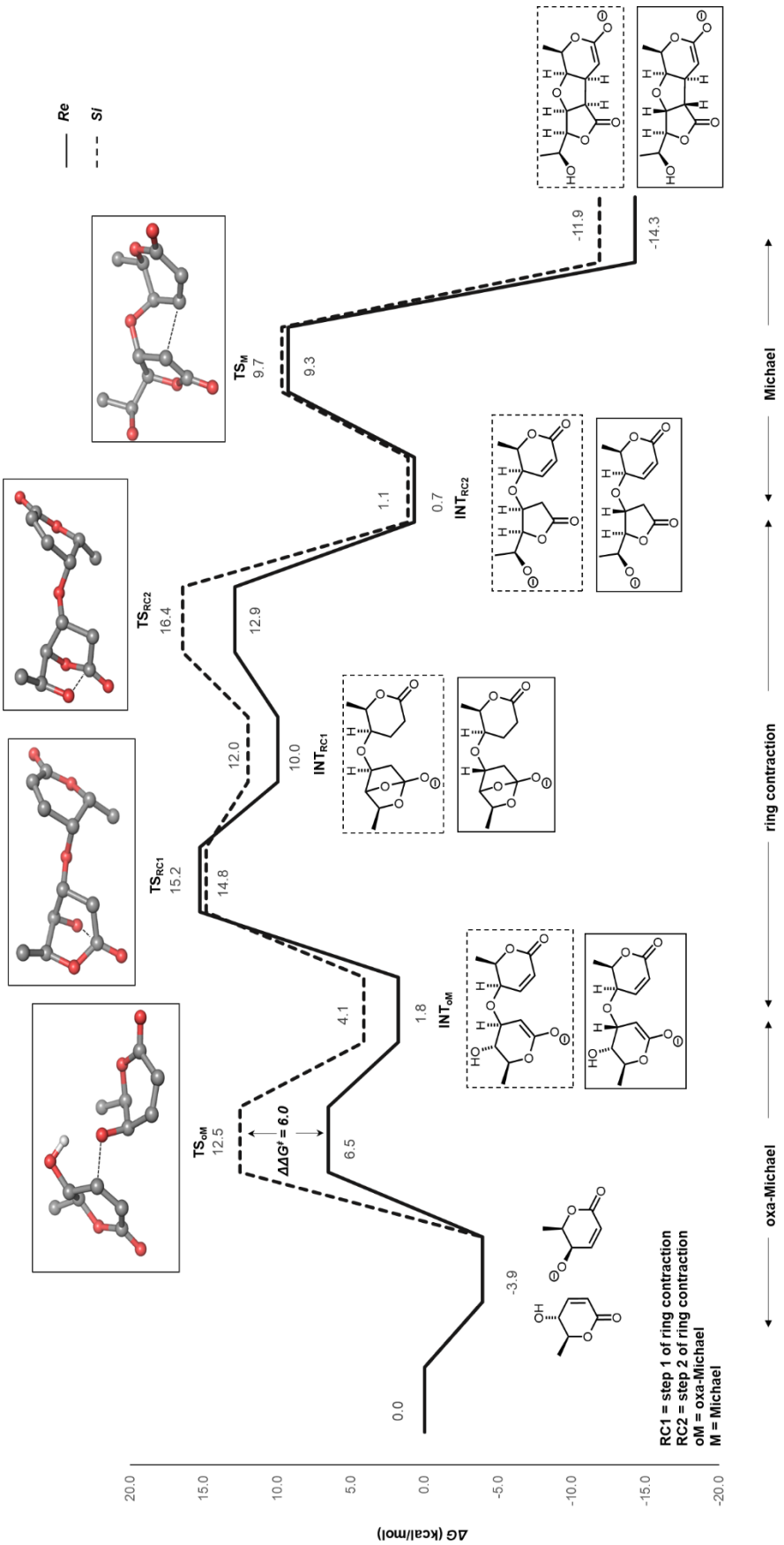

Figure 58: Energy profile for pathway 2 for the cross coupling of lactones ***ent*-3** and **5**

Pathway 3 (P3)

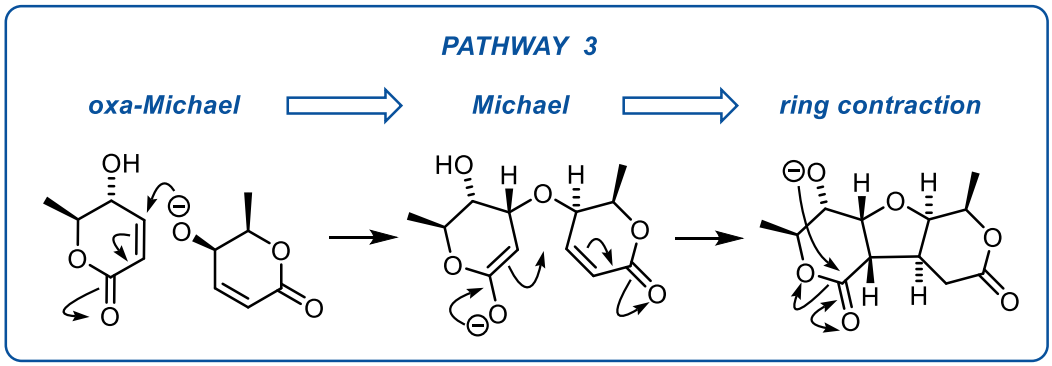

The first step of **P3** is identical to the one discussed in **P2** (see Figure 60 for full energy profile of **P3**). The subsequent INT_{oM} *Re* and *Si* species show a clear energy difference between them. Inspection of the structures reflected that the *Re* intermediate has both methyl groups in the pseudo-equatorial position and a stabilising H-bond interaction. The *Si* species on the other hand lacks this hydrogen bond interaction and one of its methyl groups is in the pseudo-axial position. Attempts to re-create the lower energy structure of *Re*-INT_{oM} in *Si*-INT_{oM}, resulted in an energy increase of 1.4 kcal/mol (Figure 59).

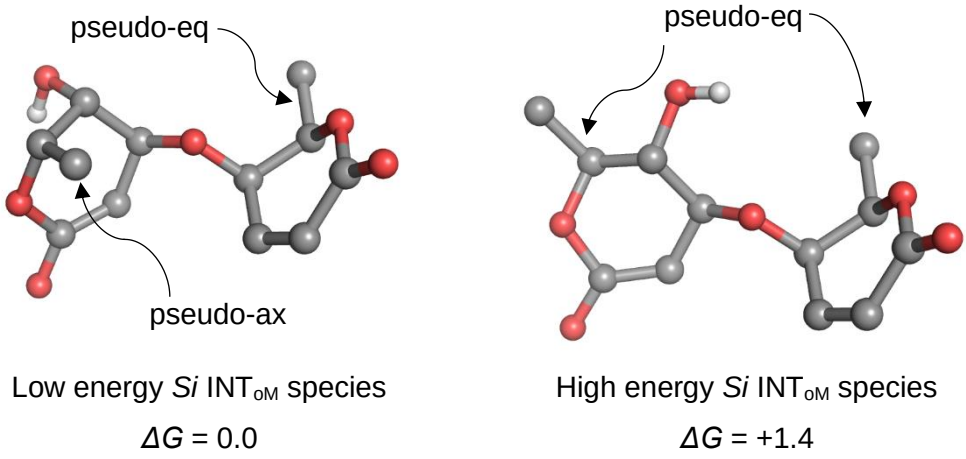

Figure 59: *Si* pathway intermediate species post oxa-Michael addition

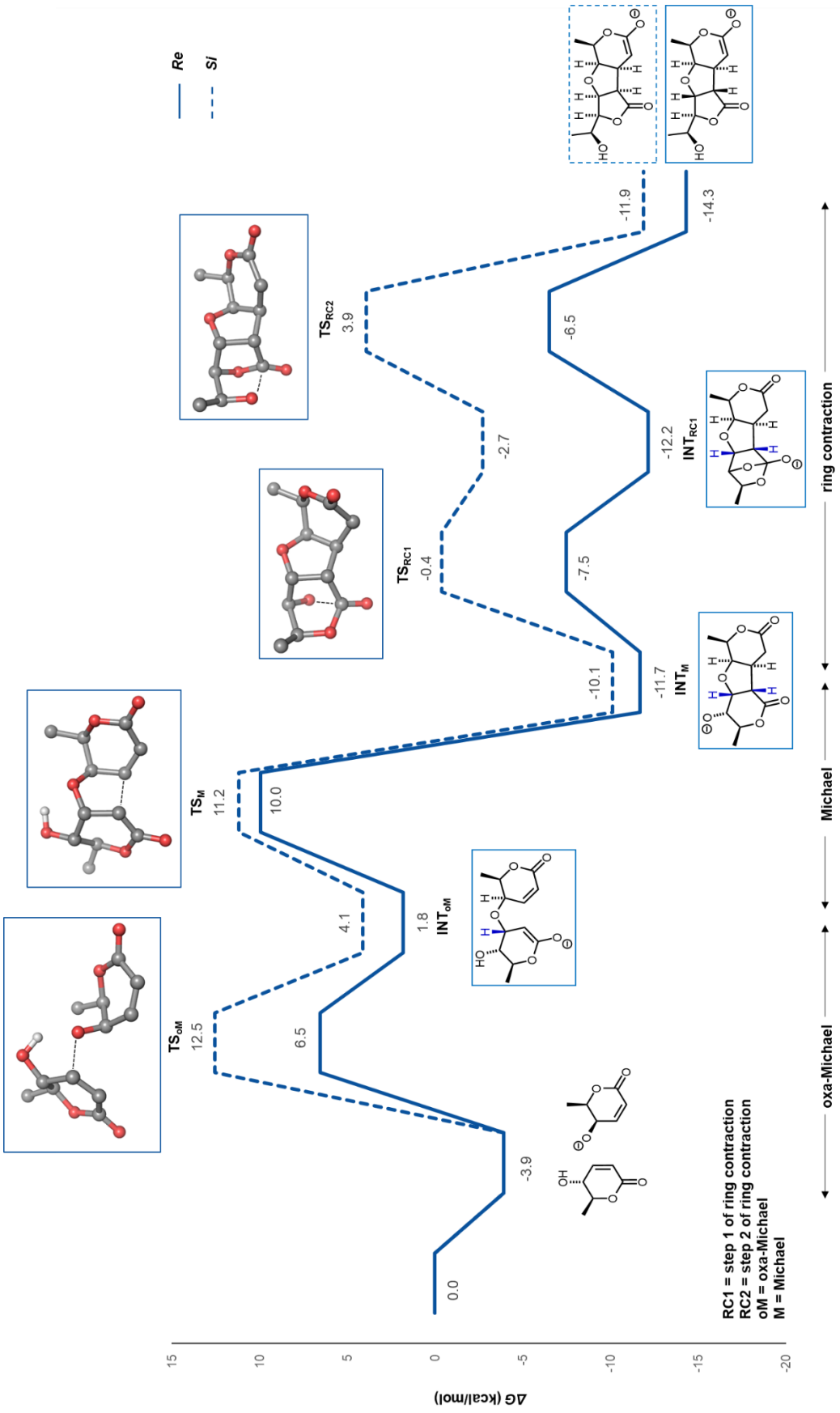

Figure 60: Energy profile for Pathway 3 for the cross-coupling of lactones ***ent*-3** and **5**

The final step in **P3** is the ring contraction (RC), in which the *Re*- is preferred over the *Si*-pathway. Similarly to previous observations, we noted that whereas the *Re* INT_M and TS_{RC} species were arranged in a flat, open structure, the *Si* INT_M and TS_{RC} are arranged in a bowl-like and more sterically congested structure.

Overall, the *Re* product is both kinetically and thermodynamically favoured. The final step of our mechanistic investigations of this cross-coupling, was to consider which of pathways 1, 2 or 3 was most likely.

Pathway 1 vs 2 vs 3

The energy profiles for pathways 2 and 3 are summarised in Figure 61. The rate-limiting step of **P1** is the ring contraction ($\Delta G^{\ddagger}$ = 18.6 kcal/mol), which has a much larger activation energy barrier than that in *Re*-**P3** (TS_M, $\Delta G^{\ddagger}$ = 13.9 kcal/mol). Therefore, as we have done previously, **P1** was disregarded from further analysis. Comparison of the highest energy transition state species for *Re*-**P2** (TS_{RC1}) and *Re*-**P3** (TS_M) shows that **P3** was favoured by 5.2 kcal/mol.

In summary, **P3** provides the lowest energy pathway for the cross-coupling of δ-lactone ***ent*-3** with δ-lactone **5**. It is interesting to note that this pathway does not proceed *via* a γ,δ-dimer. Given the results of this mechanistic investigations, we have re-directed our synthetic efforts in the laboratory, to utilise an alternative method to synthesise our proposed structure for (–)-angiopterlactone A (**1.II**).

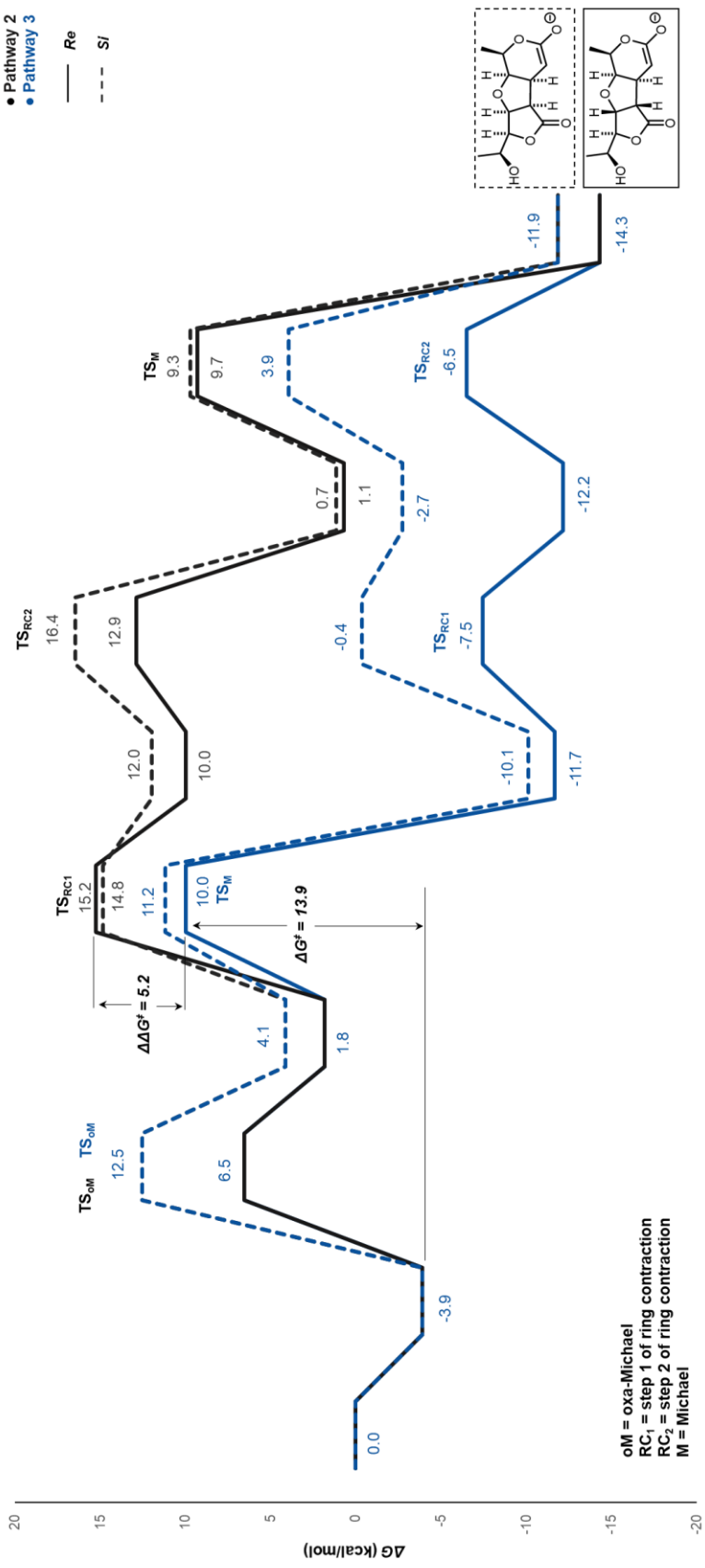

Figure 61: Energy profile for pathways 2 and 3 for the cross-coupling of lactones ***ent*-3** and **5**

*Alternative cross coupling: δ-lactone **5** as the nucleophile*

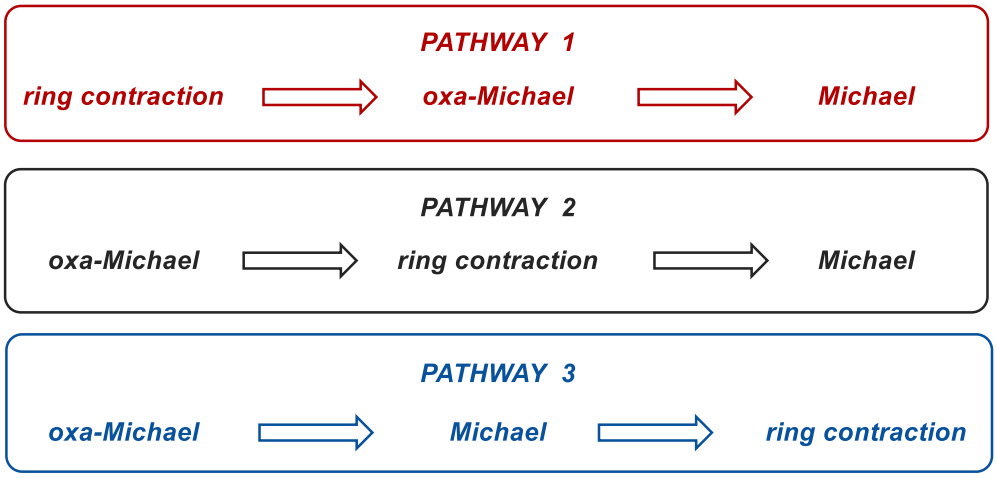

The results of both homo-couplings as well as the cross-coupling of δ-lactone ***ent*-3** with δ-lactone **5**, indicated that the lowest energy pathway does not proceed *via* a γ,δ-dimer intermediate. This was an interesting outcome, particularly in relation to our initial biosynthetic proposal (Chapter 1, Section 1.1.2). We were thus eager to explore whether the cross-coupling of δ-lactone **5** with δ-lactone ***ent*-3** would proceed *via* a γ,δ-dimer.

Pathways 1, 2 and 3 were studied and similarly to our previous investigations, comparison of the highest activation barriers of each pathway led to the exclusion of **P1**. The energy profiles for pathways 2 and 3 are summarised in Figure 63.

The first step of **P2** and **P3** is the oxa-Michael addition of δ-lactone **5** to δ-lactone ***ent*-3**, for which the *Re*-TS_{oM} was preferred over the *Si*-TS_{oM} species by 4.1 kcal/mol. Upon inspection of the transition state structures, we noted that the main difference between them was that the *Re* species had a stabilising hydrogen bond interaction (Figure 62).

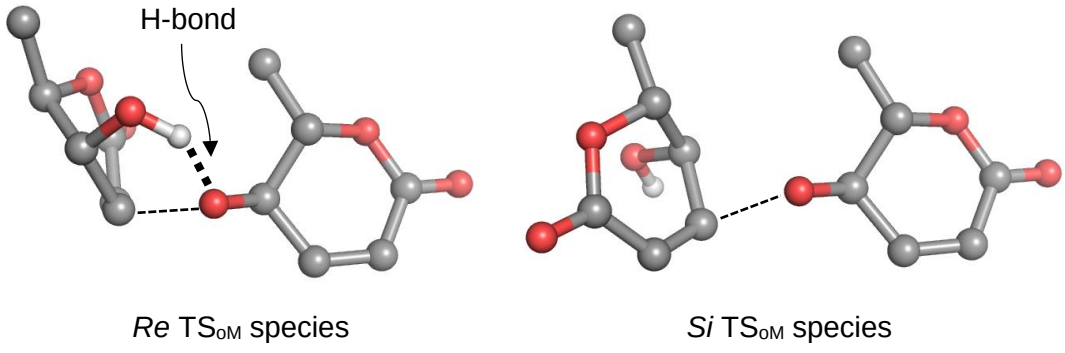

Figure 62: *Re* and *Si* transition state species for the oxa-Michael addition

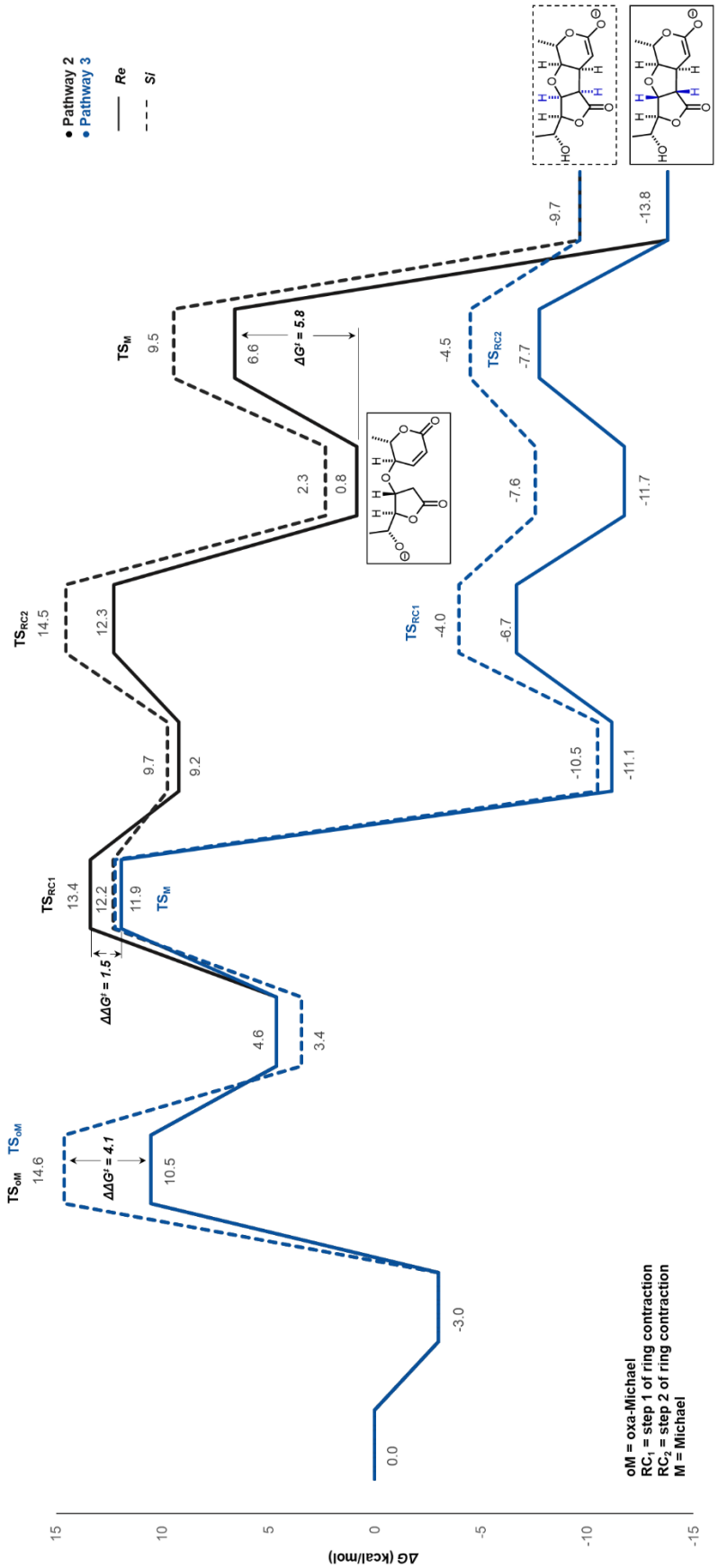

Figure 63: Pathway 2 and 3 for the alternative cross coupling of δ-lactone **5** with ***ent*-3**

Throughout the energy profile there is a consistent trend that the activation barriers for the *Re* pathway are lower than those of the *Si* pathway. We therefore proceeded to exclude the *Si* pathways from further analysis and instead drew comparisons between the *Re* pathways of **P2** and **P3**. Whereas the initial oxa-Michael addition is identical in required energy (TS_{oM}), the subsequent Michael addition favours **P3** by 1.5 kcal/mol (TS_M). As this is a small difference in energy, it is possible that pathways 2 and 3 are competing with one another.

Our main interest in computing the pathways for this cross-dimerisation of lactone **5** with ***ent*-3**, was to investigate whether or not it would allow us to access a γ,δ-dimer (*i.e.*, a diastereoisomer of angiopterlactone A (**1**)). If the reaction proceeds solely *via* **P3**, then this is not possible, as angiopterlactone A (**1**) is not an intermediate of this pathway. However, even if the reaction were to partially proceed *via* **P2**, in which a γ,δ-dimer is an intermediate (intermediate prior to TS_M), it is unlikely that this reaction would result in the isolation of this compound. This is due to the low energy barrier of 5.8 kcal/mol for TS_M, with a subsequent gain in energy of 14.6 kcal/mol to proceed to the final product. Given the high energy barrier this pathway has to overcome in the first (TS_{oM}) and second step (TS_{RC}), it is likely that the γ,δ-dimer would funnel straight through to the final product, angiopterlactone B (**2**). Overall the cross-coupling of lactone **5** with ***ent*-3** is unlikely to allow us to gain access to a γ,δ-dimer under the reaction conditions.

3.4 Conclusion

In this Chapter we have investigated the underlying mechanism leading to the formation of angiopterlactone B (**2**). The reaction mechanism is suggested to consist of an intermolecular oxa-Michael addition between two units of δ-lactone **3**, followed by an intramolecular Michael addition to form δ,δ-tricyclic dimer **26**, before a final ring contraction provides (–)-angiopterlactone B (**2**) (Scheme 31).

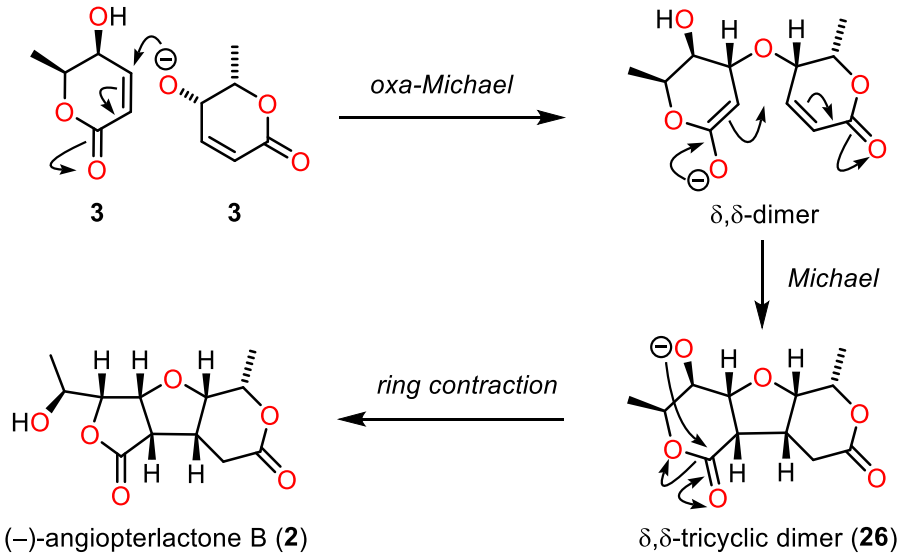

Scheme 31: Proposed mechanism for our synthesis of (–)-angiopterlactone B (**2**)

We have also investigated the underlying reaction mechanism for the formation of *dia*-angiopterlactone B (**2.VI**) (synthesis completed by Dr Katherine Law (Lawrence Group), Scheme 32). We suggest that this reaction proceeds *via* the same elementary steps as in the formation of angiopterlactone B (**2**). Interestingly, however, the oxa-Michael addition now proceeds from the opposite face, which is a result of a favourable hydrogen-bond interaction.

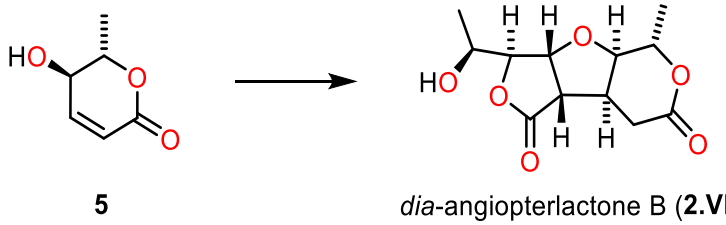

Scheme 32: Synthesis of *dia*-angiopterlactone B (**2.VI**) (Dr Katherine Law, unpublished work)

Finally, a mechanistic investigation of the possible cross-coupling reactions of lactones ***ent*-3** and **5** was carried out, to reveal whether any of them would give rise to a γ,δ-dimer (connectivity of angiopterlactone A (**1**)). As none of the mechanistic pathways are likely to allow us to gain access to such structures, synthetic efforts must be re-directed in order to access our proposed structure of (–)-angiopterlactone A (**1.II**) (see Chapter 4, Future Work).

Chapter 4: Final Remarks

4.1 Biosynthetic Speculations

Upon isolation of angiopterlactones A and B (**1**, **2**), Zou and co-workers hypothesised that these two natural products are biosynthetically related (Scheme 33).[2] Our initial biosynthetic speculations resulted in proposing that (–)-angiopterlactone A (**1**) is formed *via* an oxa-Michael addition between δ-lactone **3** and the corresponding ring contracted γ-lactone **4** (Scheme 33). We further speculated that the precursor to lactone **3** could be lactone **7**, which bears resemblance to the known natural products osmundalin (**8**) and angiopteroside (**9**). The results obtained both experimentally and computationally, suggest that these initial biosynthetic speculations may be (partially) incorrect and therefore need to be revised.

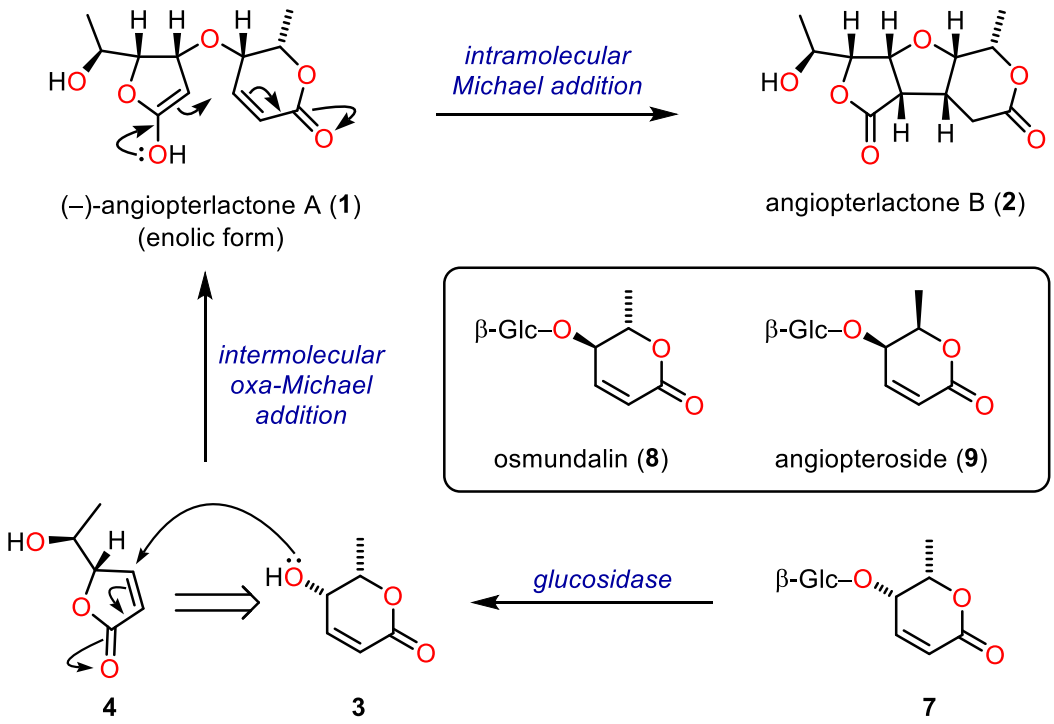

Scheme 33: Our initial biosynthetic speculations (final Michael addition proposed by Zou and co-workers)[2]

During our dimerisation studies on δ-lactone **3** to synthesise (–)-angiopterlactone B (**2**) (Chapter 1), we never observed the proposed precursor (–)-angiopterlactone A (**1**). This observation combined with our examination of available NMR data, led us to hypothesise that the structural assignment of (–)-angiopterlactone A (**1**) may be incorrect. The results of our

computational NMR prediction studies (detailed in Chapter 2) suggest that (–)-angiopterlactone A (**1**) may be a diastereoisomer of the structure depicted in Scheme 33. Computational mechanistic investigations (outlined in Chapter 3) indicated that the formation of (–)-angiopterlactone A (**1**) is unlikely to be a result of spontaneous reactivity between any combination of δ-lactones **3** and ***ent*-5**. This led us to re-examine our biosynthetic speculations and propose alternative pathways, which are outlined in Scheme 34.

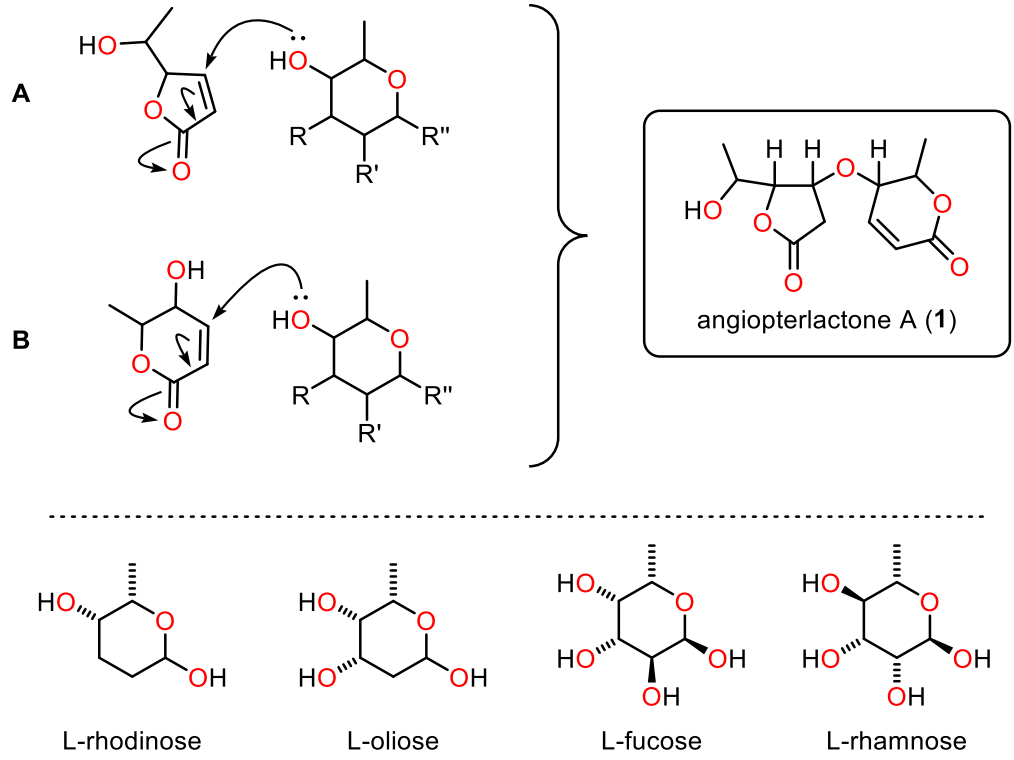

Scheme 34: Further biosynthetic speculations for angiopterlactone A (**1**) and possible biosynthetic precursors

One possibility is that the biosynthesis of angiopterlactone A (**1**) involves a sugar derivative, which lacks the α,β-unsaturated moiety (examples of such sugar derivatives are depicted in the lower half of Scheme 34). An oxa-Michael addition with a γ-lactone (option A) could then form angiopterlactone A (**1**). Alternatively, an oxa-Michael addition with a δ-lactone, followed by a ring contraction, could form angiopterlactone A (**1**) (option B). It is also possible, however, that the biosynthesis of angiopterlactone A (**1**) is governed entirely by enzymes, allowing direct and selective access to the natural product *via* alternative routes.

In summary, even if there is no conclusive answer with respect to the biosynthetic origins of angiopterlactone A (**1**), our experimental and computational studies suggest that the structure originally proposed is incorrect and that it is unlikely that we can synthetically access this natural product on route to (–)-angiopterlactone B (**2**).

4.2 Conclusions

The total synthesis of (–)-angiopterlactone B (**2**) was successfully achieved in four steps (Scheme 35). The highlight of the synthesis is the final dimerisation reaction, in which three new bonds, three new rings and three new stereogenic centres are formed in a single step, with complete control of the relative stereochemistry. With (–)-angiopterlactone B (**2**) in hand, we proposed that the stereochemistry of the natural material needed revising. Throughout our screening of dimerisation conditions, we never observed the related natural product (–)-angiopterlactone A (**1**) (Scheme 35). This led us to investigate the structure originally suggested by Zou and co-workers.[2]

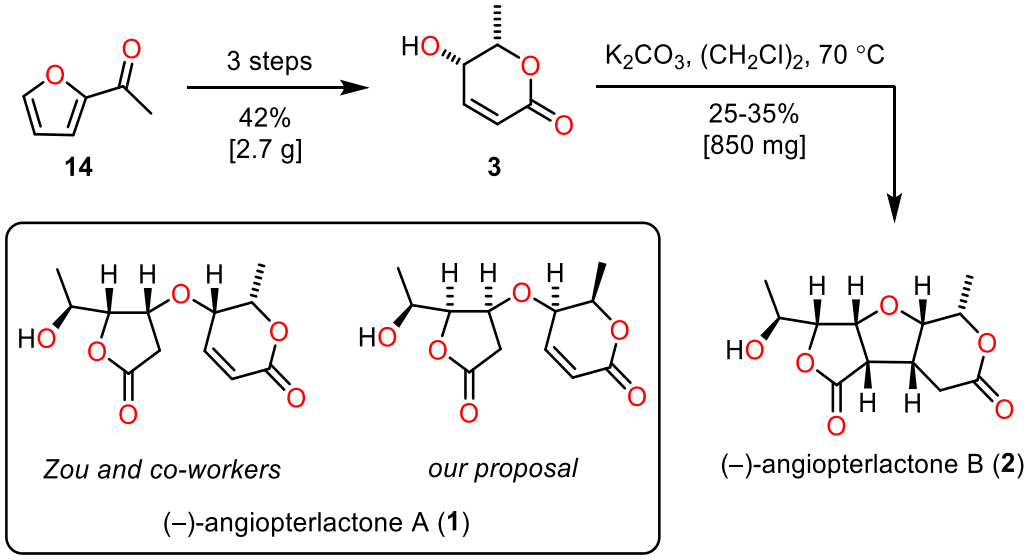

Scheme 35: Structures of (−)-angiopterlactone A (**1**) (proposed by Zou and co-workers[2] and by us) and (−)-angiopterlactone B (**2**)

Upon analysis of the available NMR data for (–)-angiopterlactone A (**1**), we proposed that the natural material may be a diastereoisomer of the originally reported structure. By utilising biosynthetic speculations, we reduced the number of possible structures from sixteen to eight. We investigated these eight diastereoisomers by conducting computational NMR prediction studies, which led us to propose a revised structure for (–)-angiopterlactone A (**1**) (Scheme 35).

The remarkable selectivity we observed in the dimerisation reaction towards (–)-angiopterlactone B (**2**), inspired us to complete computational mechanistic investigations with which we could probe its (bio)synthesis. This led us to the conclusion that (–)-angiopterlactone B (**2**) is formed *via* a domino oxa-Michael/Michael/ring contraction process (Scheme 36). We then studied the synthesis of the related compound *dia*-angiopterlactone B (**2.VI**) from δ-lactone **5** and concluded that it is formed following the same synthetic route. It is interesting

to note that these syntheses do not proceed *via* the corresponding diastereoisomers of angiopterlactone A (**1**).

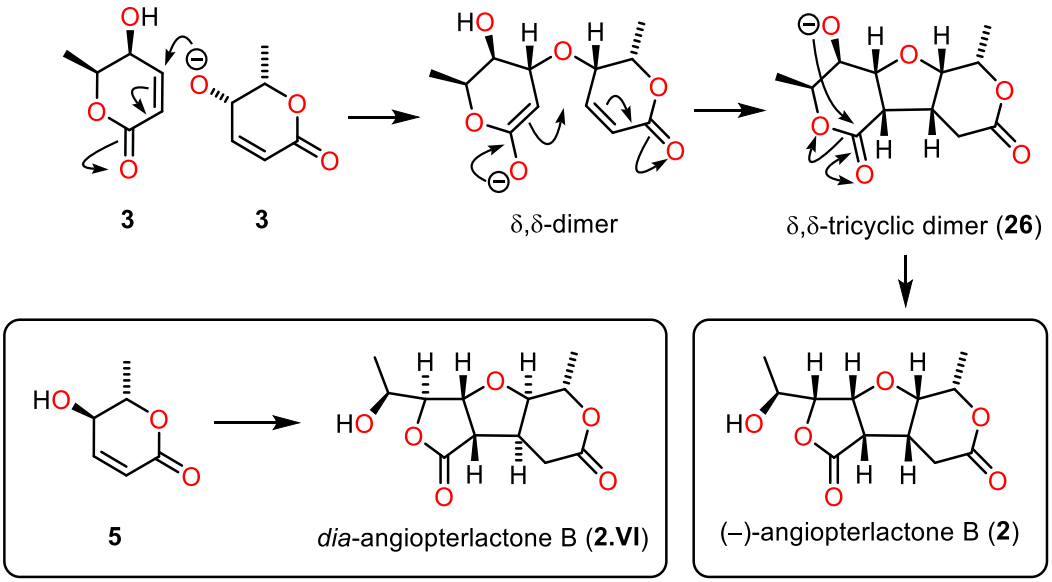

Scheme 36: Proposed mechanism for the formation of (–)-angiopterlactone B (**2**) and *dia*-angiopterlactone B (**2.VI**)

In an effort to further probe why we had not observed the related natural product (–)-angiopterlactone A (**1**), we completed computational mechanistic studies for the possible cross-couplings between lactones ***ent*-3** and **5**. Similarly to the homo-dimerisations of lactones ***ent*-3** and **5**, these showed that it is unlikely that (–)-angiopterlactone A (**1**) can be accessed *via* this route. As a result of these studies, synthetic efforts in the Lawrence group have been re-directed.

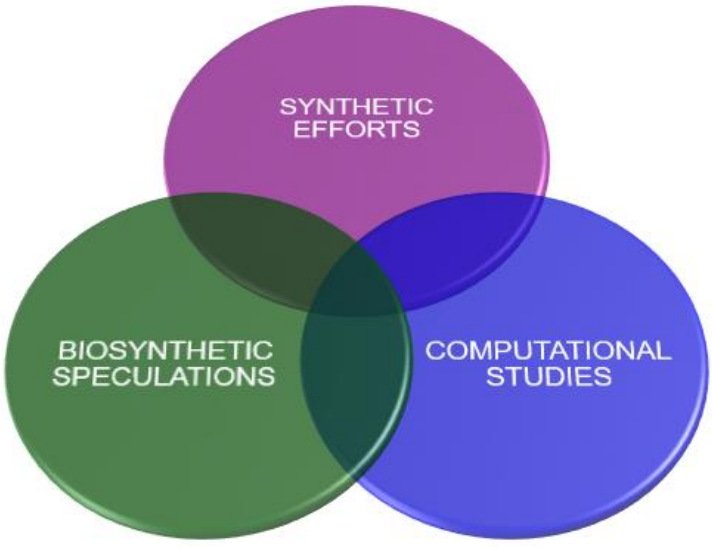

Figure 64: Combining synthetic efforts, biosynthetic speculations and computational studies to work towards answering complex questions

In conclusion, the interplay between synthetic efforts, biosynthetic speculations and computational studies, allowed us to propose a revised structure for the natural product (–)-angiopterlactone A (**1.II**). Furthermore this multi-disciplinary approach assisted us in our understanding of the underlying reaction mechanism in the (bio)synthesis of (–)-angiopterlactone B (**2**). The combination of these techniques has facilitated working towards answering some of the more complex, underlying questions surrounding the (bio)synthesis of the angiopterlactones (**1**, **2**).

4.3 Future Work

Following our successful synthesis of (–)-angiopterlactone B (**2**) and our computational NMR and mechanistic studies, there are various aspects of the (bio)syntheses of the angiopterlactones (**1**, **2**) which could still be explored.

In order to further examine the (bio)synthesis of (–)-angiopterlactone B (**2**) and rule out a dimerisation between δ-lactone **3** and γ-lactone **4**, isotopic labelling studies could be completed. These could involve synthesising a ^{13}C-labelled derivative of the γ-lactone **4** and reacting it with unlabelled δ-lactone **3** (Scheme 37). The absence of isotopic labelling in the product would suggest that (–)-angiopterlactone B (**2**) is formed by reacting two units of δ-lactone **3**, as proposed during our computational mechanistic investigations (Chapter 3).

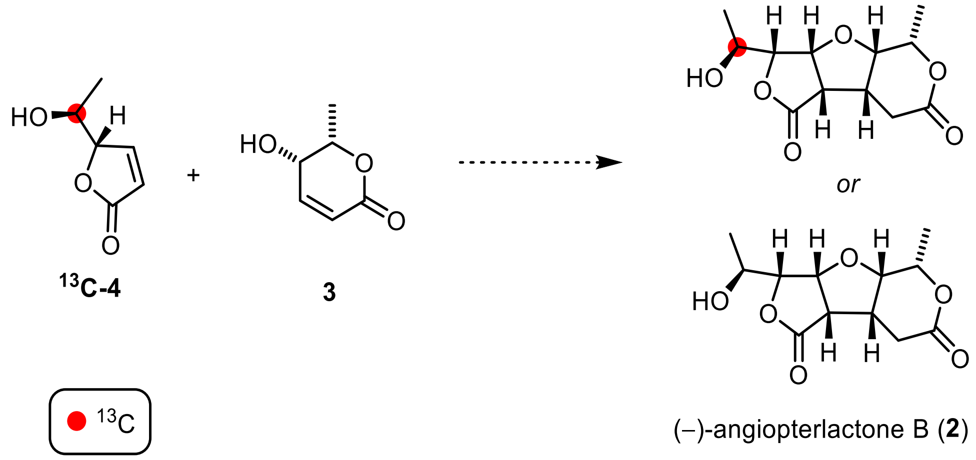

Scheme 37: Isotopic labelling studies of the (bio)synthesis of (–)-angiopterlactone B (**2**)

Following our computational mechanistic investigations of cross-couplings between δ-lactones ***ent*-3** and **5**, we concluded that these would be unlikely to proceed *via* angiopterlactone A (**1.II**). In order to validate this computational result, synthetic test reactions could be performed and closely monitored by NMR spectroscopy (Scheme 38). Dr Katherine Law (Lawrence group) is currently investigating such cross-dimerisations.

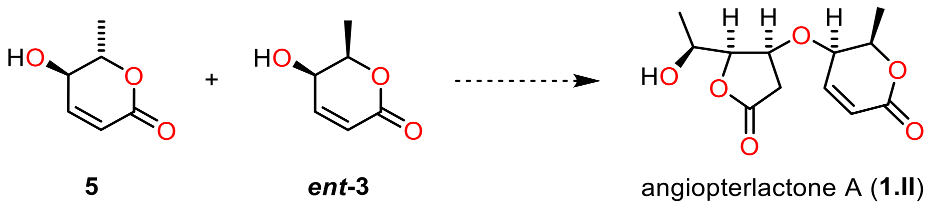

Scheme 38: Cross-coupling of lactones **5** and ***ent*-3** to investigate whether this would result in angiopterlactone A (**1.II**) (currently being studied by Dr Katherine Law, Lawrence group)

If the results from these synthetic studies indicate that angiopterlactone A (**1.II**) cannot be targeted by such a cross-coupling, alternative strategies to access this natural product could be investigated. These could include masking the alkene in the nucleophilic δ-lactone in the oxa-Michael addition (as suggested in our biosynthetic speculations above), to prevent the subsequent Michael addition from occurring (Scheme 39). Upon completing the oxa-Michael addition, the alkene could be revealed and provide our proposed structure of (–)-angiopterlactone A (**1.II**).

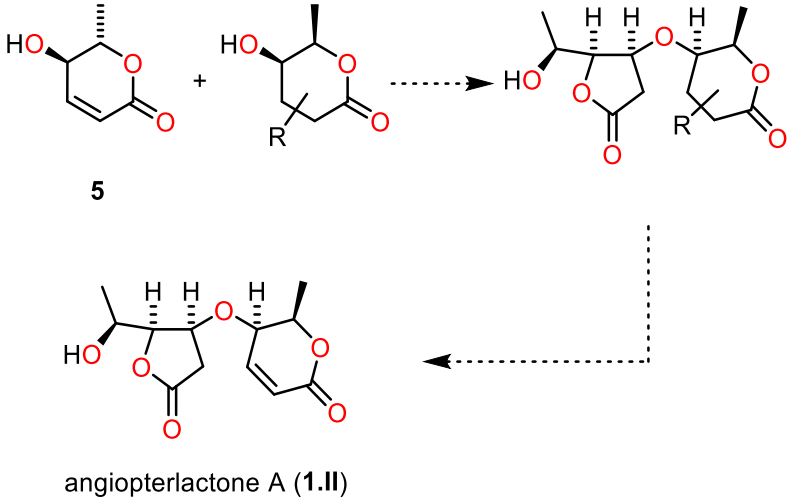

Scheme 39: Alternative synthetic strategy to access our proposed structure of angiopterlactone A (**1.II**)

References

(1) Thomson, M. I.; Nichol, G. S.; Lawrence, A. L. Total Synthesis of (−)-Angiopterlactone B. *Org. Lett.* **2017**, *19* (9), 2199–2201.

(2) Yu, Y.-M.; Yang, J.-S.; Peng, C.-Z.; Caer, V.; Cong, P.-Z.; Zou, Z.-M.; Lu, Y.; Yang, S.-Y.; Gu, Y.-C. Lactones from Angiopteris Caudatiformis. *J. Nat. Prod.* **2009**, *72* (5), 921–924.

(3) Taveepanich, S.; Kamthong, N.; Sawasdipuksa, N.; Roengsumran, S. Inhibitory Activities of Angiopteroside for HIV-1 Reverse Transcriptase and Lung Cancer Cell-Line. *J. Sci. Res. Chula. Univ.* **2005**, *30* (2), 187–192.

(4) Buchanan, M. S.; Hashimoto, T.; Takaoka, S.; Asakawa, Y. (+)-Osmundalactone, γ-Lactones and Spiromentins from the Fungus Paxillus Atrotomentosus. *Phytochemistry* **1995**, *40* (4), 1251–1257.

(5) Ono, M.; Zhao, X. Y.; Shida, Y.; Akita, H. δ-Lactone Formation from δ-Hydroxy-Trans-A,β-Unsaturated Carboxylic Acids Accompanied by Trans–cis Isomerization: Synthesis of (−)-Tetra-O-Acetylosmundalin. *Tetrahedron* **2007**, *63* (41), 10140–10148.

(6) Hollenbeak, K. H.; Kuehne, M. E. The Isolation and Structure Determination of the Fern Glycoside Osmundalin and the Synthesis of Its Aglycone Osmundalactone. *Tetrahedron* **1974**, *30* (15), 2307–2316.

(7) Carda, M.; Rodríguez, S.; González, F.; Castillo, E.; Villanueva, A.; Marco, J. A. Stereoselective Synthesis of the Naturally Occurring Lactones (−)-Osmundalactone and (−)-Muricatacine Using Ring-Closing Metathesis. *European J. Org. Chem.* **2002**, *2002* (20), 3491–3491.

(8) Zhang, G.; Shi, L.; Liu, Q.; Wang, J.; Li, L.; Liu, X. A Divergent Strategy for Constructing a Sugar Library Containing 2,6-Dideoxy Sugars and Uncommon Sugars with 4-Substitution. *Tetrahedron* **2007**, *63* (39), 9705–9711.

(9) Rosenbrook, W.; Carney, R. E. A New Metabolite from an Unidentified Aspergillus Species. *Tetrahedron Lett.* **1970**, *11* (22), 1867–1870.

(10) Hseu, T. H. Structure of Angiopteroside (4-O-β-D-Glucopyranosyl-L-Threo-2-Hexen-5-Olide) Monohydrate, a Fern Glycoside from Angiopteris Lygodiifolla Ros. *Acta Crystallogr. Sect. B Struct. Crystallogr. Cryst. Chem.* **1981**, *37* (11), 2095–2098.

(11) Nising, C. F.; Bräse, S. The Oxa-Michael Reaction: From Recent Developments to Applications in Natural Product Synthesis. *Chem. Soc. Rev.* **2008**, *37* (6), 1218–1228.

(12) Nising, C. F.; Bräse, S. Recent Developments in the Field of Oxa-Michael Reactions. *Chem. Soc. Rev.* **2012**, *41* (3), 988–999.

(13) *Domino Reactions*; Tietze, L. F., Ed.; Wiley-VCH Verlag GmbH & Co. KGaA: Weinheim, Germany, 2014.

(14) Greatrex, B. W.; Kimber, M. C.; Taylor, D. K.; Tiekink, E. R. T. A Novel Synthesis of Functionalized Tetrahydrofurans by an Oxa-Michael/Michael Cyclization of γ-Hydroxyenones. *J. Org. Chem.* **2003**, *68*, 4239–4246.

(15) Carreño, M. C.; Ribagorda, M. Stereoselective Trimerization of [(S)R]-[(P-Tolylsulfinyl)methyl]-P-Quinols and P-Quinamines. *Org. Lett.* **2003**, *5* (14), 2425–2428.

(16) Zhao, K.; Cheng, G.-J.; Yang, H.; Shang, H.; Zhang, X.; Wu, Y.-D.; Tang, Y. Total Synthesis of Incarvilleatone and Incarviditone: Insight into Their Biosynthetic Pathways and Structure Determination. *Org. Lett.* **2012**, *14* (18), 4878–4881.

(17) Brown, P. D.; Willis, A. C.; Sherburn, M. S.; Lawrence, A. L. Total Synthesis of Incarviditone and Incarvilleatone. *Org. Lett.* **2012**, *14* (17), 4537–4539.

(18) Wu, J.-S.; Zhang, X.; Zhang, Y.-L.; Xie, J.-W. Synthesis and Antifungal Activities of Novel Polyheterocyclic Spirooxindole Derivatives. *Org. Biomol. Chem.* **2015**, *13* (17), 4967–4975.

(19) Chang, E. L.; Bolte, B.; Lan, P.; Willis, A. C.; Banwell, M. G. Chemoenzymatic Total Syntheses of the Enantiomers of the Protoilludanes 8-Deoxydihydrotsugicoline and Radudiol. *J. Org. Chem.* **2016**, *81* (5), 2078–2086.

(20) Rykers, E. Towards the Biomimetic Synthesis of Angiopterlactones. *Res. Proj. ANU* **2013**.

(21) Wang, H.-Y.; Yang, K.; Bennett, S. R.; Guo, S.; Tang, W. Iridium-Catalyzed Dynamic Kinetic Isomerization: Expedient Synthesis of Carbohydrates from Achmatowicz Rearrangement Products. *Angew. Chem. Int. Ed.* **2015**, *54* (30), 8756–8759.

(22) Kurti, L.; Czako, B. *Strategic Applications of Named Reactions in Organic Synthesis Background and Detailed Mechanisms.*; Elsevier Science, 2005.

(23) Holson, E. B.; Roush, W. R. Diastereoselective Synthesis of the C(17)−C(28) Fragment (The C−D Spiroketal Unit) of Spongistatin 1 (Altohyrtin A) via a Kinetically Controlled Iodo-Spiroketalization Reaction. *Org. Lett.* **2002**, *4* (21), 3719–3722.

(24) Ball, M.; Gaunt, M. J.; Hook, D. F.; Jessiman, A. S.; Kawahara, S.; Orsini, P.; Scolaro, A.; Talbot, A. C.; Tanner, H. R.; Yamanoi, S.; et al. Total Synthesis of Spongistatin 1: A Synthetic Strategy Exploiting Its Latent Pseudo-Symmetry. *Angew. Chem. Int. Ed.* **2005**, *44* (34), 5433–5438.

(25) Hashiguchi, S.; Fujii, A.; Takehara, J.; Ikariya, T.; Noyori, R. Asymmetric Transfer Hydrogenation of Aromatic Ketones Catalyzed by Chiral Ruthenium(II) Complexes. *J. Am. Chem. Soc.* **1995**, *117* (28), 7562–7563.

(26) Wu, X.; Li, X.; Zanotti-Gerosa, A.; Pettman, A.; Liu, J.; Mills, A. J.; Xiao, J. Rh III- and Ir III-Catalyzed Asymmetric Transfer Hydrogenation of Ketones in Water. *Chemistry* **2008**, *14* (7), 2209–2222.

(27) Croatt, M. P.; Carreira, E. M. Probing the Role of the Mycosamine C2'-OH on the Activity of Amphotericin B. *Org. Lett.* **2011**, *13* (6), 1390–1393.

(28) Paterson, I.; Haslett, G. W. Synthesis of the C1-C11 Western Fragment of Madeirolide A. *Org. Lett.* **2013**, *15* (6), 1338–1341.

(29) Haack, K.-J.; Hashiguchi, S.; Fujii, A.; Ikariya, T.; Noyori, R. The Catalyst Precursor, Catalyst, and Intermediate in the RuII-Promoted Asymmetric Hydrogen Transfer between Alcohols and Ketones. *Angew. Chem. Int. Ed.* **1997**, *36* (3), 285–288.

(30) Deska, J.; Thiel, D.; Gianolio, E. The Achmatowicz Rearrangement – Oxidative Ring Expansion of Furfuryl Alcohols. *Synthesis (Stuttg).* **2015**, *47* (22), 3435–3450.

(31) Tsubuki, M.; Keino, K.; Honda, T. Stereoselective Synthesis of Plant-Growth-Regulating Steroids: Brassinolide, Castasterone, and Their 24,25-Substituted Analogues. *J. Chem. Soc. Perkin Trans. 1* **1992**, No. 20, 2643–2649.

(32) Achmatowicz, O.; Bukowski, P.; Szechner, B.; Zwierzchowska, Z.; Zamojski, A. Synthesis of Methyl 2,3-Dideoxy-DL-Alk-2-Enopyranosides from Furan Compounds. *Tetrahedron* **1971**, *27* (10), 1973–1996.

(33) Smallwood, I. M. *Handbook of Organic Solvent Properties*; Arnold, 1996.

(34) Flack, H. D.; Bernardinelli, G. Reporting and Evaluating Absolute-Structure and Absolute-Configuration Determinations. *J. Appl. Crystallogr.* **2000**, *33* (4), 1143–1148.

(35) Chen, Y.; Tao, Y.; Lian, X.; Wang, L.; Zhao, Y.; Jiang, J.; Zhang, Y. Chemical Constituents of Angiopteris Esculenta Including Two New Natural Lactones. *Food Chem.* **2010**, *122* (4), 1173–1175.

(36) Kotammagari, T. K.; Gonnade, R. G.; Bhattacharya, A. K. Biomimetic Total Synthesis of Angiopterlactone B and Other Potential Natural Products. *Org. Lett.* **2017**, *19* (13), 3564–3567.

(37) Flack, H. D.; Bernardinelli, G. The Use of X-Ray Crystallography to Determine Absolute Configuration. *Chirality* **2008**, *20* (5), 681–690.

(38) Hoye, T. R.; Jeffrey, C. S.; Shao, F. Mosher Ester Analysis for the Determination of Absolute Configuration of Stereogenic (Chiral) Carbinol Carbons. *Nat. Protoc.* **2007**, *2* (10), 2451–2458.

(39) Mathieson, A. M.; Taylor, J. C. The Structure of the Bromodilactone from Jacobine and the Conformation of the Lactone Group. *Tetrahedron Lett.* **1961**, *2* (17), 590–592.

(40) McConnell, J. F.; Mathieson, A. M.; Schoenborn, B. P. Conformation of Iridomyrmecin and Isoiridomyrmecin. *Tetrahedron Lett.* **1962**, *3* (10), 445–448.

(41) Wolf, H. δ-Lactone Cotton - Effekt Und Konformation Des δ-Lactonringes. *Tetrahedron Lett.* **1966**, *7* (42), 5151–5156.

(42) Beecham, A. F. Optical Activity and Lactone Ring Configurations. *Tetrahedron Lett.* **1968**, *9* (32), 3591–3594.

(43) Winkler, J. D.; Rouse, M. B.; Greaney, M. F.; Harrison, S. J.; Jeon, Y. T. The First Total Synthesis of (±)-Ingenol. *J. Am. Chem. Soc.* **2002**, *124*, 9726–9728.

(44) Marshall, J. A.; Eidam, P.; Eidam, H. S. Synthesis of 4-Triisopropylsilyl-3-Butyn-2-Ol by Asymmetric Transfer Hydrogenation. *Org. Synth.* **2007**, *84*, 120–128.

(45) Herrmann, A. T.; Martinez, S. R.; Zakarian, A. A Concise Asymmetric Total Synthesis of (+)-Brevisamide. *Org. Lett.* **2011**, *13* (14), 3636–3639.

(46) Armarego, W. L. F.; Chai, C. L. L. *Purification of Laboratory Chemicals*; Elsevier, 2009.

(47) Ley, S. V.; Armstrong, A.; Al., E. Total Synthesis of the Anthelmintic Macrolide Avermectin B1a. *J. Chem. Soc., Perkin Trans. 1* **1991**, *15* (4), 667–692.

(48) Murayama, T.; Sugiyama, T.; Yamashita, K. Syntheses of Natural (−)-Osmundalactone and Its Epimer. *Agric. Biol. Chem.* **1986**, *50* (9), 2347–2351.

(49) Von der Ohe, F.; Brückner, R. Stereoselective Synthesis of Freelingyne and Related γ-Alkylidenebutenolides via Vinylogous Mukaiyama Aldol Additions. *New J. Chem.* **2000**, *24* (9), 659–669.

(50) Perry, N. B.; Benn, M. H.; Foster, L. M.; Routledge, A.; Weavers, R. T. The Glycosidic Precursor of (Z)-5-Ethylidene-2(5H)-Furanone in Halocarpus Biformis Juvenile Foliage. *Phytochemistry* **1996**, *42* (2), 453–459.

(51) Atkins, P.; Friedman, R. *Molecular Quantum Mechanics*, Fourth Edi.; Oxford University Press, 2005.

(52) Grant, G. H.; Richards, G. *Computational Chemistry*; Oxford University Press, 2005.

(53) Harvey, J. *Computational Chemistry*; Oxford University Press, 2018.

(54) Cramer, C. J. *Essentials of Computational Chemistry - Theories and Models*, Second Edi.; Wiley, 2008.

(55) Hohenberg, P.; Kohn, W. Inhomogeneous Electron Gas. *Phys. Rev.* **1964**, *136* (3B), B864–B871.

(56) Jensen, F. *Introduction to Computational Chemistry*, Third Edi.; John Wiley & Sons, Ltd., 2017.

(57) Kohn, W.; Sham, L. J. Self-Consistent Equations Including Exchange and Correlation Effects. *Phys. Rev.* **1965**, *140* (4A), A1133–A1138.

(58) Sérgio Filipe Sousa; Pedro Alexandrino Fernandes, A.; Ramos*, M. J. General Performance of Density Functionals. *J. Phys. Chem. A* **2007**, *111* (42), 10439–10452.

(59) Peng, Q.; Duarte, F.; Paton, R. S. Computing Organic Stereoselectivity – from Concepts to Quantitative Calculations and Predictions. *Chem. Soc. Rev.* **2016**, *45* (22), 6093–6107.

(60) Lodewyk, M. W.; Siebert, M. R.; Tantillo, D. J. Computational Prediction of 1H and 13C Chemical Shifts: A Useful Tool for Natural Product, Mechanistic, and Synthetic Organic Chemistry. *Chem. Rev.* **2012**, *112* (3), 1839–1862.

(61) Jackson, K. E.; Paton, R. S. *Applied Theoretical Organic Chemistry. Chapter 6*; Tantillo, D. J., Ed.; World Scientific (Europe), 2018.

(62) Nicolaou, K. C.; Snyder, S. A. Chasing Molecules That Were Never There: Misassigned Natural Products and the Role of Chemical Synthesis in Modern Structure Elucidation. *Angew. Chem. Int. Ed.* **2005**, *44* (7), 1012–1044.

(63) Facelli, J. C. Calculations of Chemical Shieldings: Theory and Applications. *Concepts Magn. Reson.* **2004**, *20A* (1), 42–69.

(64) Paul R. Rablen; Shoshannah A. Pearlman, A.; Finkbiner, J. A Comparison of Density Functional Methods for the Estimation of Proton Chemical Shifts with Chemical Accuracy. *J. Phys. Chem. A* **1999**, *103*, 7357–7363.

(65) Pierens, G. K. 1H and 13C NMR Scaling Factors for the Calculation of Chemical Shifts in Commonly Used Solvents Using Density Functional Theory. *J. Comput. Chem.* **2014**, *35* (18), 1388–1394.

(66) Karplus, M. Vicinal Proton Coupling in Nuclear Magnetic Resonance. *J. Am. Chem. Soc.* **1963**, *85* (18), 2870–2871.

(67) Dickson, C. L.; Blundell, C. D.; Butts, C. P.; Felton, A.; Jeffreys, A.; Takacs, Z. Accurate Measurement of Long Range Proton–carbon Scalar Coupling Constants. *Analyst* **2017**, *142* (4), 621–633.

(68) Bally, T.; Rablen, P. R. Quantum-Chemical Simulation of 1H NMR Spectra. 2. Comparison of DFT-Based Procedures for Computing Proton-Proton Coupling Constants in Organic Molecules. *J. Org. Chem.* **2011**, *76* (12), 4818–4830.

(69) Kupka, T.; Nieradka, M.; Stachów, M.; Pluta, T.; Nowak, P.; Kjær, H.; Kongsted, J.; Kaminsky, J. Basis Set Convergence of Indirect Spin–Spin Coupling Constants in the Kohn–Sham Limit for Several Small Molecules. *J. Phys. Chem. A* **2012**, *116* (14), 3728–3738.

(70) Fabián, J. S.; García de la Vega, J. M.; San Fabián, E. Improvements in DFT Calculations of Spin–Spin Coupling Constants. *J. Chem. Theory Comput.* **2014**, *10* (11), 4938–4949.

(71) Iron, M. A. Evaluation of the Factors Impacting the Accuracy of 13C NMR Chemical Shift Predictions Using Density Functional Theory—The Advantage of Long-Range Corrected Functionals. *J. Chem. Theory Comput.* **2017**, *13* (11), 5798–5819.

(72) Jensen, F. Method Calibration or Data Fitting? *J. Chem. Theory Comput.* **2018**, *14* (9), 4651–4661.

(73) Tantillo, D. CHEMical SHIft REpository with Coupling Constants Added Too http://cheshirenmr.info/index.htm.

(74) Smith, S. G.; Goodman, J. M. Assigning the Stereochemistry of Pairs of Diastereoisomers Using GIAO NMR Shift Calculation. *J. Org. Chem.* **2009**, *74* (12), 4597–4607.

(75) Willoughby, P. H.; Jansma, M. J.; Hoye, T. R. A Guide to Small-Molecule Structure Assignment through Computation of (1H and 13C) NMR Chemical Shifts. *Nat. Protoc.* **2014**, *9* (3), 643–660.

(76) Bagno, A.; Saielli, G. Addressing the Stereochemistry of Complex Organic Molecules by Density Functional Theory - NMR. *Comput. Mol. Sci.* **2014**, *5*, 228–240.

(77) Smith, S. G.; Goodman, J. M. Assigning Stereochemistry to Single Diastereoisomers by GIAO NMR Calculation: The DP4 Probability. *J. Am. Chem. Soc.* **2010**, *132* (37), 12946–12959.

(78) Grimblat, N.; Zanardi, M. M.; Sarotti, A. M. Beyond DP4: An Improved Probability for the Stereochemical Assignment of Isomeric Compounds Using Quantum Chemical Calculations of NMR Shifts. *J. Org. Chem.* **2015**, *80* (24), 12526–12534.

(79) Grimblat, N.; Sarotti, A. M. Computational Chemistry to the Rescue: Modern Toolboxes for the Assignment of Complex Molecules by GIAO NMR Calculations. *Chem. - A Eur. J.* **2016**, *22* (35), 12246–12261.

(80) Guella, G.; Dini, F.; Pietra, F. Metabolites with a Novel C30 Backbone from Marine Ciliates. *Angew. Chem. Int. Ed.* **1999**, *38* (8), 1134–1136.

(81) Nicolaou, K. C.; Ortiz, A.; Zhang, H.; Dagneau, P.; Lanver, A.; Jennings, M. P.;

Arseniyadis, S.; Faraoni, R.; Lizos, D. E. Total Synthesis and Structural Revision of Vannusals A and B: Synthesis of the Originally Assigned Structure of Vannusal B. *J. Am. Chem. Soc.* **2010**, *132* (20), 7138–7152.

(82) Nicolaou, K. C.; Ortiz, A.; Zhang, H.; Guella, G. Total Synthesis and Structural Revision of Vannusals A and B: Synthesis of the True Structures of Vannusals A and B. *J. Am. Chem. Soc.* **2010**, *132* (20), 7153–7176.

(83) Saielli, G.; Nicolaou, K. C.; Ortiz, A.; Zhang, H.; Bagno, A. Addressing the Stereochemistry of Complex Organic Molecules by Density Functional Theory-NMR: Vannusal B in Retrospective. *J. Am. Chem. Soc.* **2011**, *133* (15), 6072–6077.

(84) Evidente, A.; Abou-Donia, A. H.; Darwish, F. A.; Amer, M. E.; Kassem, F. F.; Hammoda, H. A. M.; Motta, A. Nobilisitine A and B, Two Masanane-Type Alkaloids from Clivia Nobilis. *Phytochemistry* **1999**, *51* (8), 1151–1155.

(85) Schwartz, B. D.; Jones, M. T.; Banwell, M. G.; Cade, I. A. Synthesis of the Enantiomer of the Structure Assigned to the Natural Product Nobilisitine A. *Org. Lett.* **2010**, *12* (22), 5210–5213.

(86) Lodewyk, M. W.; Tantillo, D. J. Prediction of the Structure of Nobilisitine A Using Computed NMR Chemical Shifts. *J. Nat. Prod.* **2011**, *74* (5), 1339–1343.

(87) Schwartz, B. D.; White, L. V.; Banwell, M. G.; Willis, A. C. Structure of the Lycorinine Alkaloid Nobilisitine A. *J. Org. Chem.* **2011**, *76* (20), 8560–8563.

(88) Schmiedel, V. M.; Hong, Y. J.; Lentz, D.; Tantillo, D. J.; Christmann, M. Synthesis and Structure Revision of Dichrocephones A and B. *Angew. Chem. Int. Ed.* **2018**, *57* (9), 2419–2422.

(89) Tian, X.; Li, L.; Hu, Y.; Zhang, H.; Liu, Y.; Chen, H.; Ding, G.; Zou, Z. Dichrocephones A and B, Two Cytotoxic Sesquiterpenoids with the Unique [3.3.3] Propellane Nucleus Skeleton from Dichrocephala Benthamii. *RSC Adv.* **2013**, *3*, 7880–7883.

(90) Numata, A.; Hokimoto, K.; Takemura, T.; Katsuno, T.; Yamamoto, K. Plant Constituents Biologically Active to Insects. V. Antifeedants for the Larvae of the Yellow Butterfly, Eurema Hecabe Mandarina, in Osmunda Japonica. *Chem. Pharm. Bull. (Tokyo).* **1984**, *32* (7), 2815–2820.

(91) Wu, J.; Lorenzo, P.; Zhong, S.; Ali, M.; Butts, C. P.; Myers, E. L.; Aggarwal, V. K. Synergy of Synthesis, Computation and NMR Reveals Correct Baulamycin Structures. *Nature* **2017**, *547* (7664), 436–440.

(92) Frisch, M. J.; Trucks, G. W.; Schlegel, H. B.; Scuseria, G. E.; Robb, M. A.; Cheeseman, J. R.; Scalmani, G.; Barone, V.; Mennucci, B.; Petersson, G. A.; et al. Gaussian 09. Gaussian, Inc.: Wallingford CT 2013.

(93) Becke, A. D. Density-functional Thermochemistry. III. The Role of Exact Exchange. *J. Chem. Phys.* **1993**, *98* (7), 5648–5652.

(94) Stephens, P. J.; Devlin, F. J.; Chabalowski, C. F.; Frisch, M. J. Ab Initio Calculation of Vibrational Absorption and Circular Dichroism Spectra Using Density Functional Force Fields. *J. Phys. Chem.* **1994**, *98* (45), 11623–11627.

(95) Adamo, C.; Barone, V. Exchange Functionals with Improved Long-Range Behavior and Adiabatic Connection Methods without Adjustable Parameters: The mPW and mPW1PW Models. *J. Chem. Phys.* **1998**, *108* (2), 664–675.

(96) Perdew, J. P.; Burke, K.; Wang, Y. Generalized Gradient Approximation for the Exchange-Correlation Hole of a Many-Electron System. *Phys. Rev. B* **1996**, *54* (23), 16533–16539.

(97) Zhao, Y.; Truhlar, D. G. The M06 Suite of Density Functionals for Main Group Thermochemistry, Thermochemical Kinetics, Noncovalent Interactions, Excited States, and Transition Elements: Two New Functionals and Systematic Testing of Four M06-Class Functionals and 12 Other Functionals. *Theor. Chem. Acc.* **2008**, *120* (1–3), 215–241.

(98) Chai, J.-D.; Head-Gordon, M. Systematic Optimization of Long-Range Corrected Hybrid Density Functionals. *J. Chem. Phys.* **2008**, *128* (8), 84106.

(99) Marenich, A. V.; Cramer, C. J.; Truhlar, D. G. Universal Solvation Model Based on Solute Electron Density and on a Continuum Model of the Solvent Defined by the Bulk Dielectric Constant and Atomic Surface Tensions. *J. Phys. Chem. B* **2009**, *113* (18), 6378–6396.

(100) Rappe, A. K.; Casewit, C. J.; Colwell, K. S.; Goddard, W. A.; Skiff, W. M. UFF, a Full Periodic Table Force Field for Molecular Mechanics and Molecular Dynamics Simulations. *J. Am. Chem. Soc.* **1992**, *114* (25), 10024–10035.

(101) Bondi, A. Van Der Waals Volumes and Radii. *J. Phys. Chem.* **1964**, *68* (3), 441–451.

(102) Paton, R. S.; Funes-Ardoiz, I. GoodVibes. 2016.

(103) Grimme, S. Supramolecular Binding Thermodynamics by Dispersion-Corrected Density Functional Theory. *Chem. - A Eur. J.* **2012**, *18* (32), 9955–9964.

(104) Ponder, J. W.; Rackers, J. A.; Laury, M. L.; Lu, C.; Wang, Z.; Lagardere, L.; Piquemal, J.-P.; Ren, P. TINKER 8: A Modular Software Package for Molecular Design and Simulation. Saint Louis, MO 2017.

(105) Jain, R.; Bally, T.; Rablen, P. R. Calculating Accurate Proton Chemical Shifts of Organic Molecules with Density Functional Methods and Modest Basis Sets. *J. Org. Chem.* **2009**, *74* (11), 4017–4023.

(106) Bock, K.; Lundt, I.; Pedersen, C. The Base Catalyzed Rearrangement of Some 6-Bromo-2,6-Dideoxyaldono-1,4-Lactones. Preparation of L-Digitoxose. *Acta Chem. Scand.* **1984**, *B38*, 555–561.

(107) Bock, K.; Lundt, I.; Pedersen, C.; Refn, S. Reaction of Aldonic Acids with Hydrogen Bromide. VII. Preparation of Some 2,6-Dideoxyhexoses. *Acta Chem. Scand.* **1986**, *B40* (9), 740–744.

(108) Zanardi, M. M.; Biglione, F. A.; Sortino, M. A.; Sarotti, A. M. General Quantum-Based NMR Method for the Assignment of Absolute Configuration by Single or Double Derivatization: Scope and Limitations. *J. Org. Chem.* **2018**, *83* (19), 11839–11849.

(109) Glendening, E. D.; Reed, A. E.; Carpenter, J. E.; Weinhold, F. NBO. 1998.

(110) Schrödinger. The PyMOL Molecular Graphics System.

(111) Hratchian, H. P.; Schlegel, H. B. Accurate Reaction Paths Using a Hessian Based Predictor–corrector Integrator. *J. Chem. Phys.* **2004**, *120* (21), 9918–9924.

(112) Klicić, J. J.; Friesner, R. A.; Liu, S.-Y.; Guida, W. C. Accurate Prediction of Acidity

Constants in Aqueous Solution via Density Functional Theory and Self-Consistent Reaction Field Methods. *J. Phys Chem.* **2002**, *106*, 1327–1335.

(113) Levy, D. E.; Fügedi, P. *The Organic Chemistry of Sugars*; Taylor & Francis, 2006.

(114) Stedjan, M. K.; Augspurger, J. D. Ring Strain Energy in Ether- and Lactone-Containing Spiro Compounds. *J. Phys. Org. Chem.* **2015**, *28* (4), 298–303.

(115) Clayden, J.; Greeves, N.; Warren, S.; Wothers, P. *Organic Chemistry*; Oxford University Press, 2001.

(116) Ho, J. Are Thermodynamic Cycles Necessary for Continuum Solvent Calculation of pKas and Reduction Potentials? *Phys. Chem. Chem. Phys.* **2015**, *17* (4), 2859–2868.

(117) Kelly, C. P.; Cramer, C. J.; Truhlar, D. G. Single-Ion Solvation Free Energies and the Normal Hydrogen Electrode Potential in Methanol, Acetonitrile, and Dimethyl Sulfoxide. *J. Phys. Chem. B* **2007**, *111*, 408–422.

Appendices for Chapter 1

1.1 NMR Spectra for Chapter 1

1.1.1 ^{1}H NMR Spectrum of Compound **15**

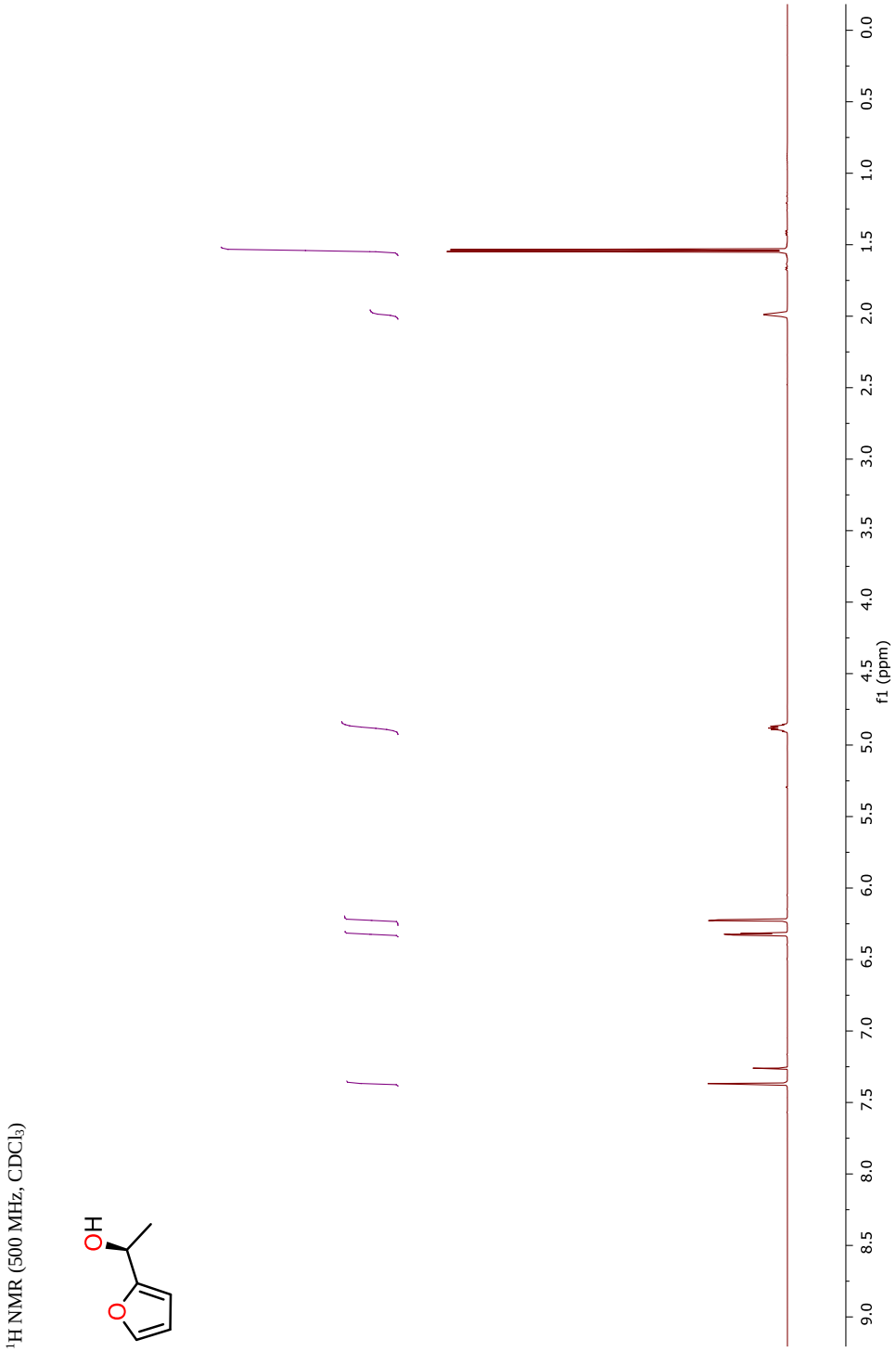

1.1.2 ^{13}C NMR Spectrum of Compound **15**

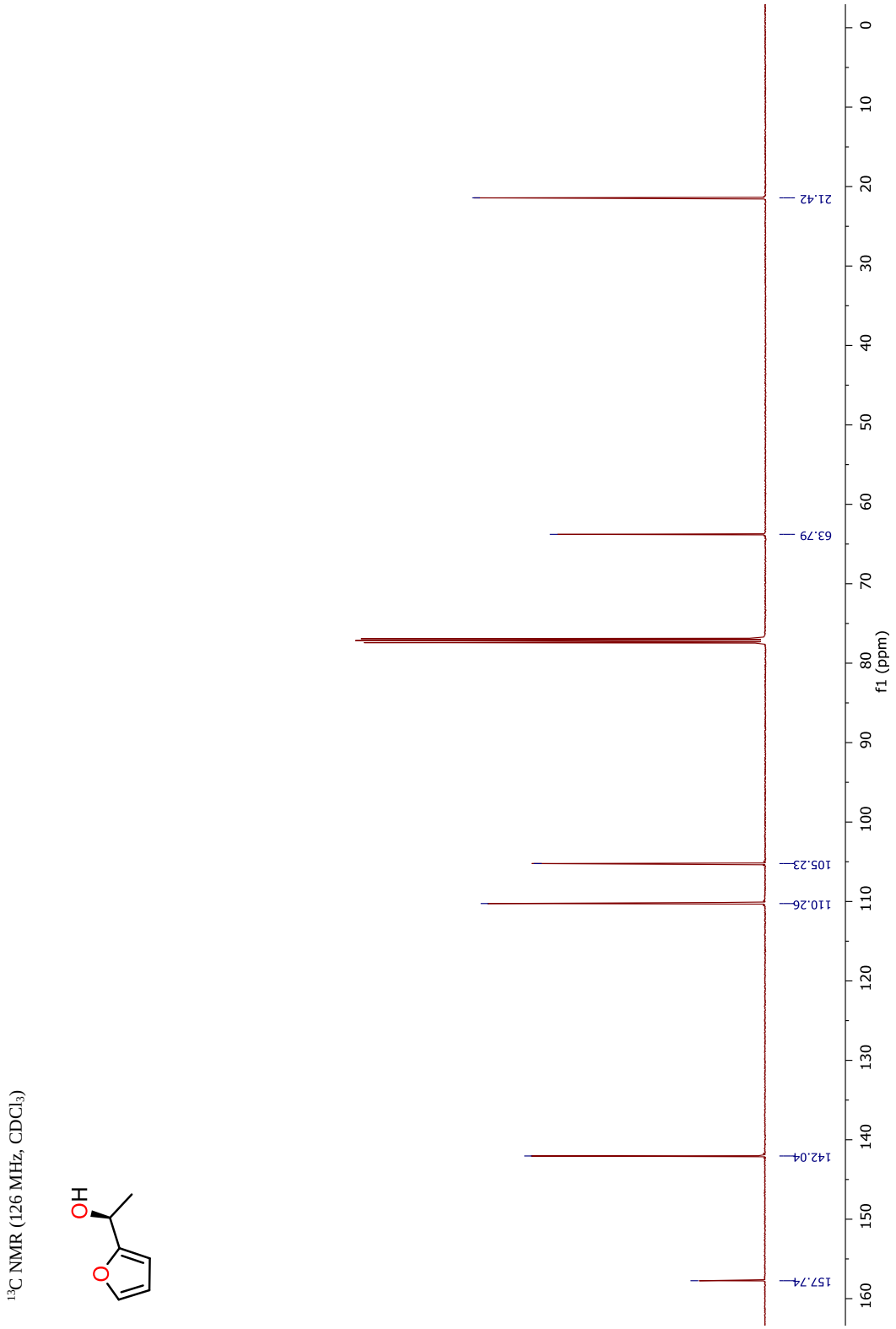

1.1.3 ^{1}H NMR Spectrum of Compound **16**

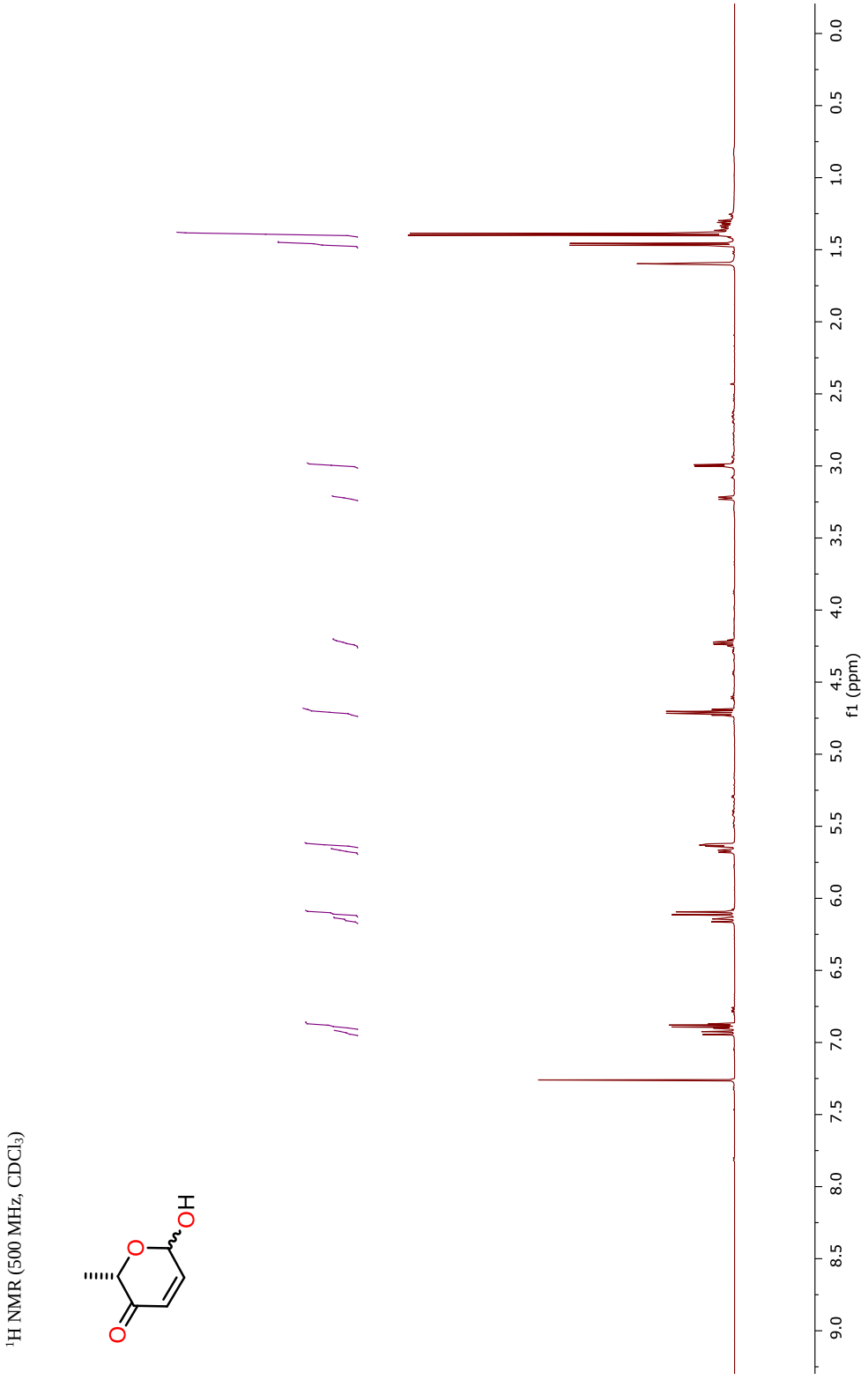

1.1.4 ^{13}C NMR Spectrum of Compound **16**

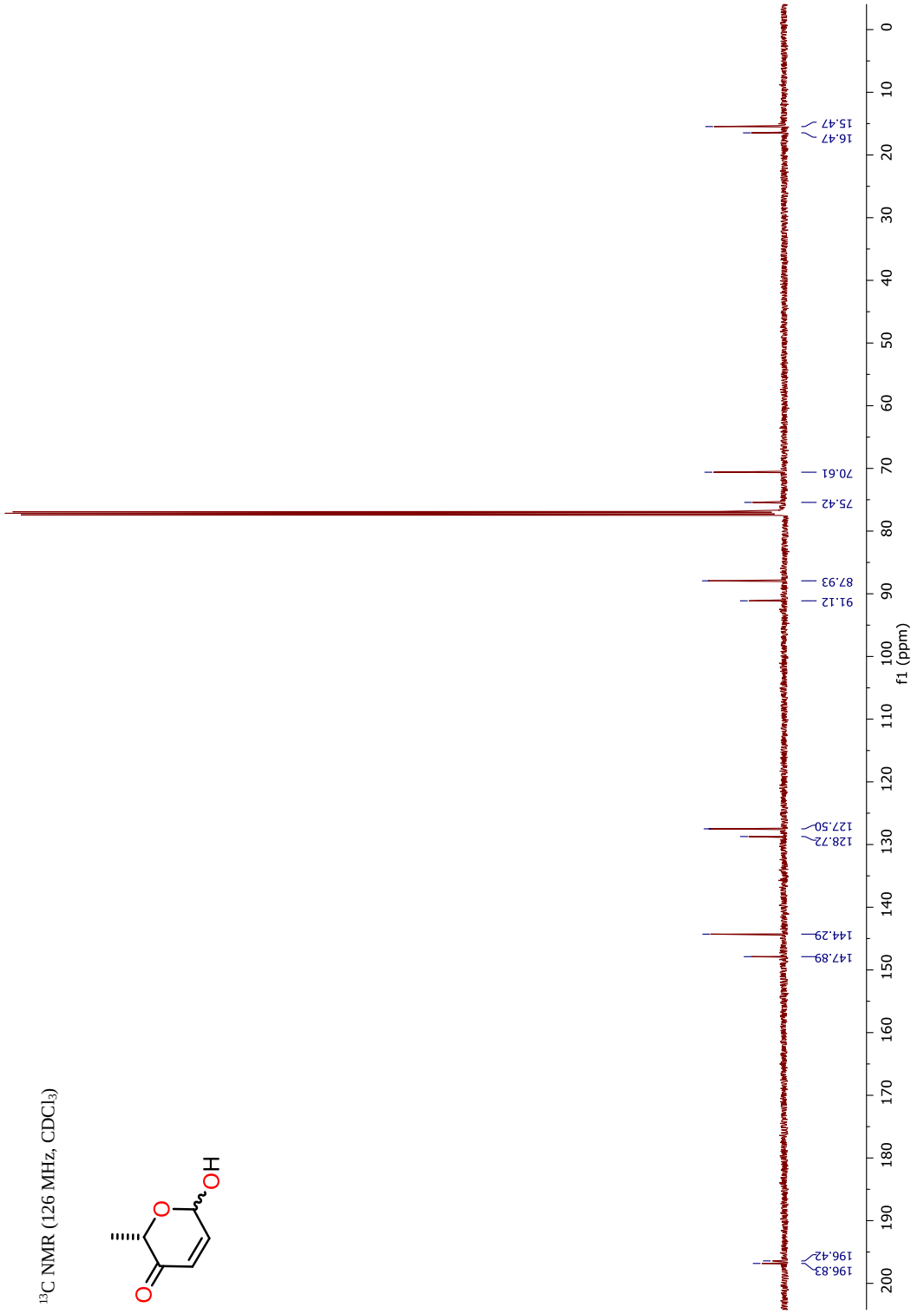

1.1.5 ^{1}H NMR Spectrum of Compound **3**

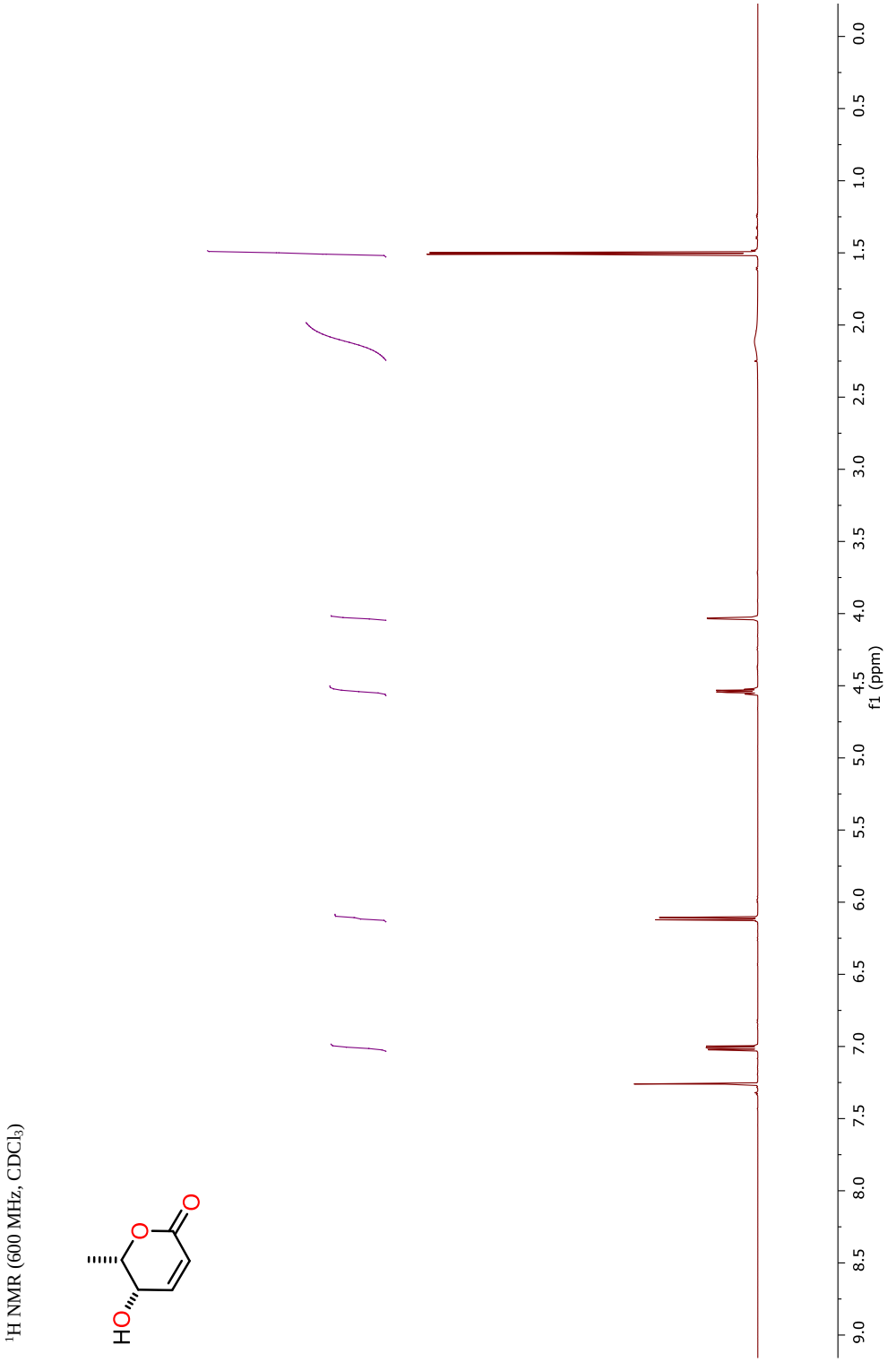

1.1.6 ^{13}C NMR Spectrum of Compound **3**

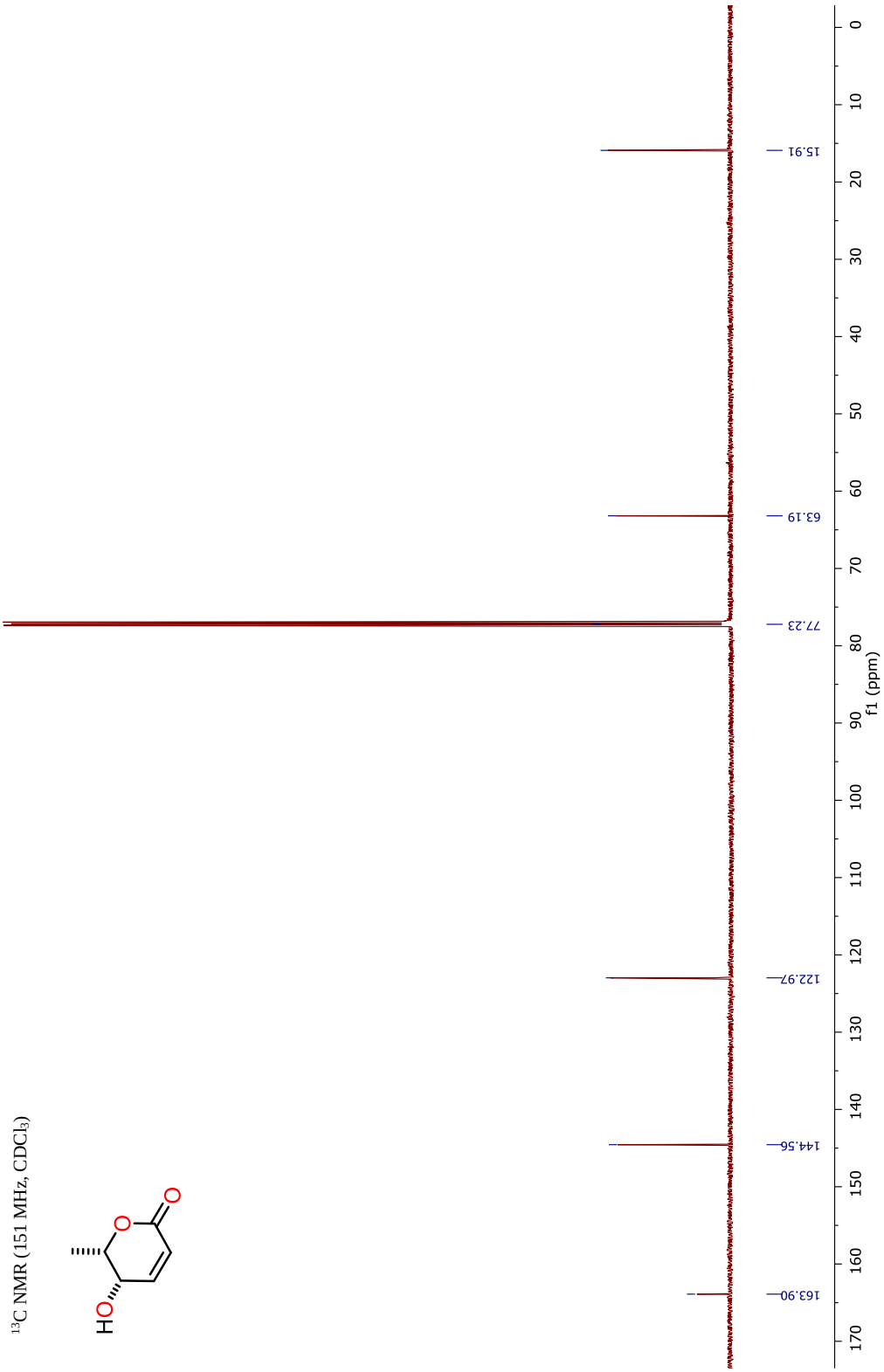

1.1.7 ^{1}H NMR Spectrum of the Crude Dimerisation Product

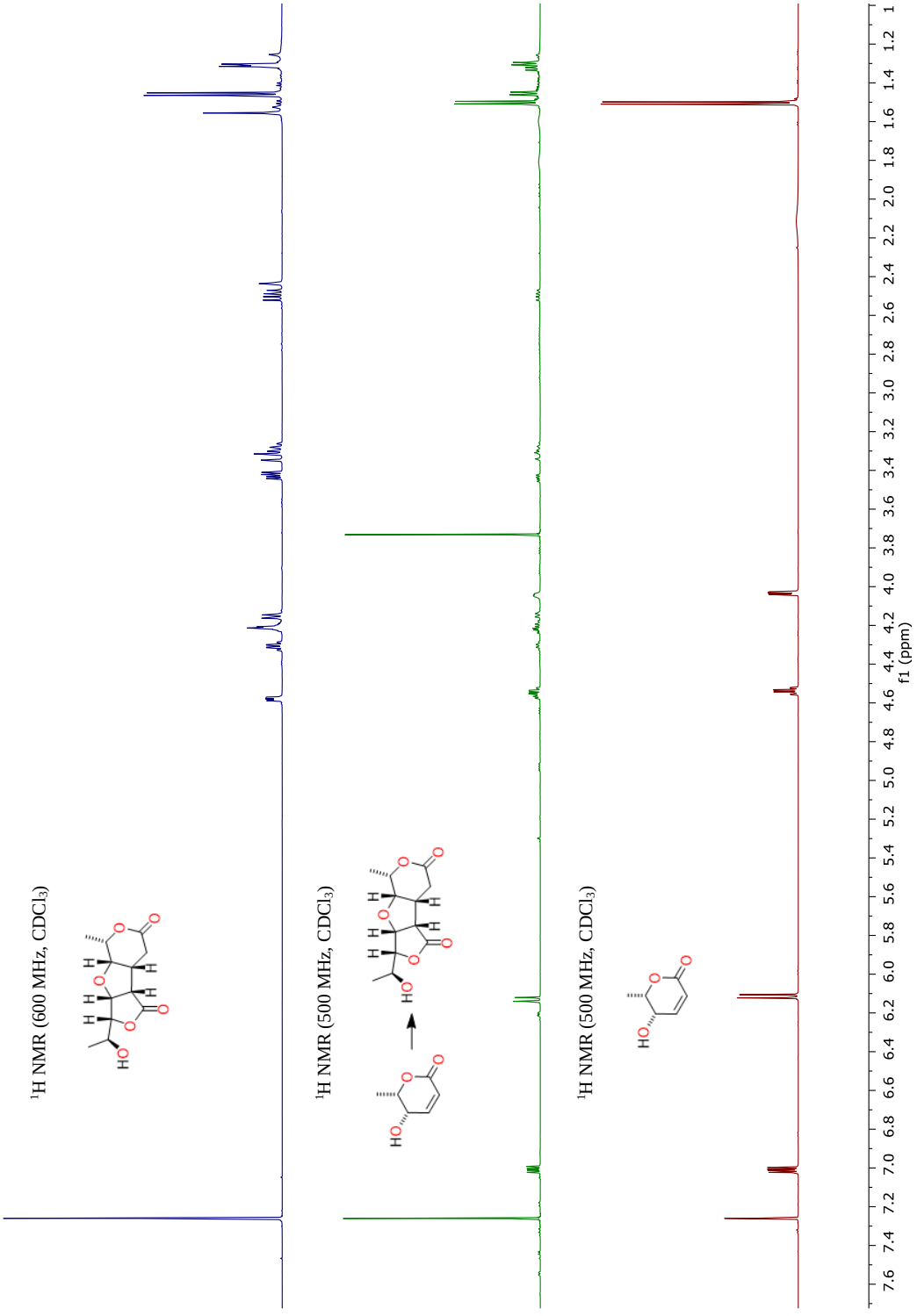

1.1.8 ^{1}H NMR Spectrum of (–)-Angiopterlactone B (**2**) in $CDCl_3$

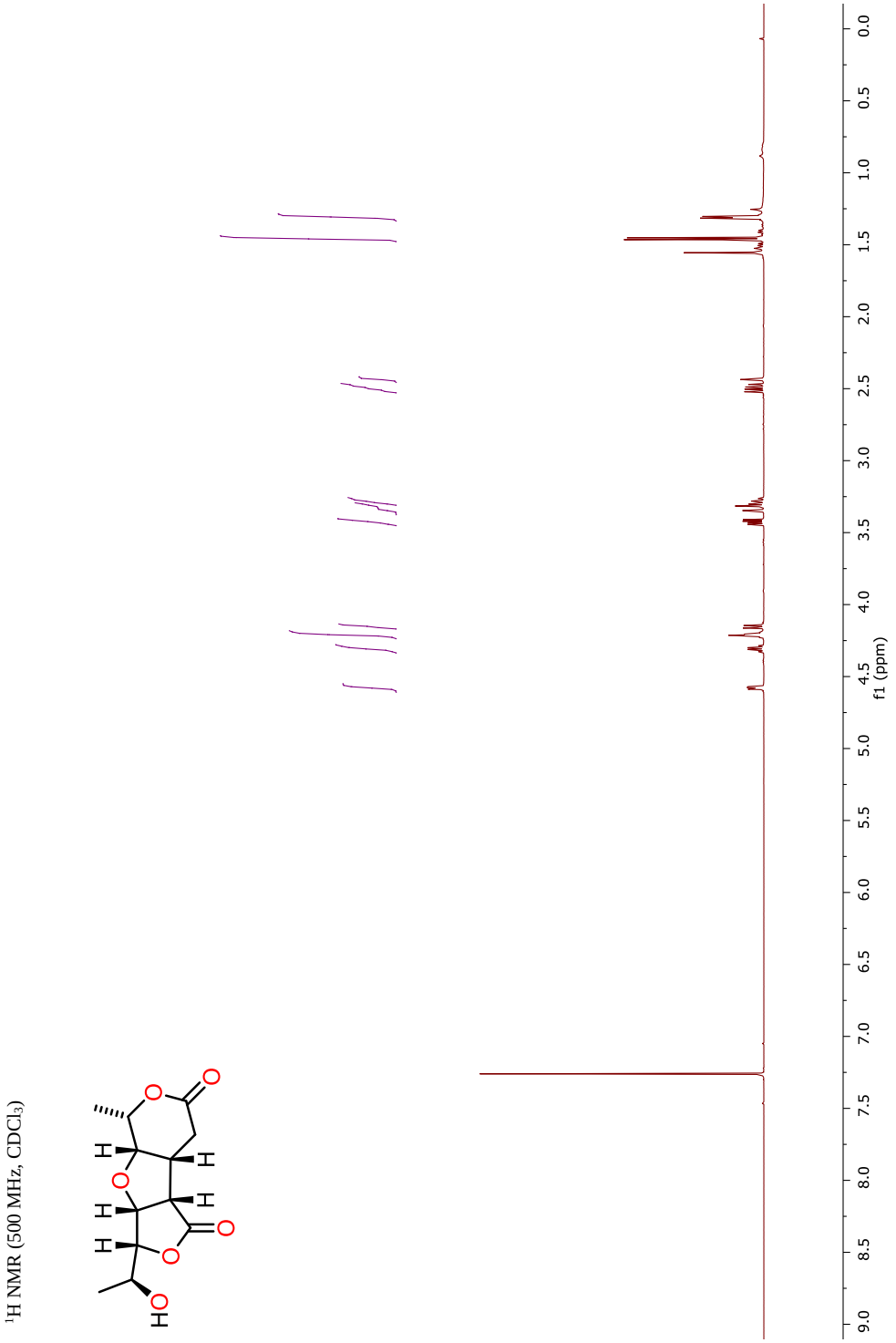

1.1.9 ^{13}C NMR Spectrum of (–)-Angiopterlactone B (**2**) in $CDCl_3$

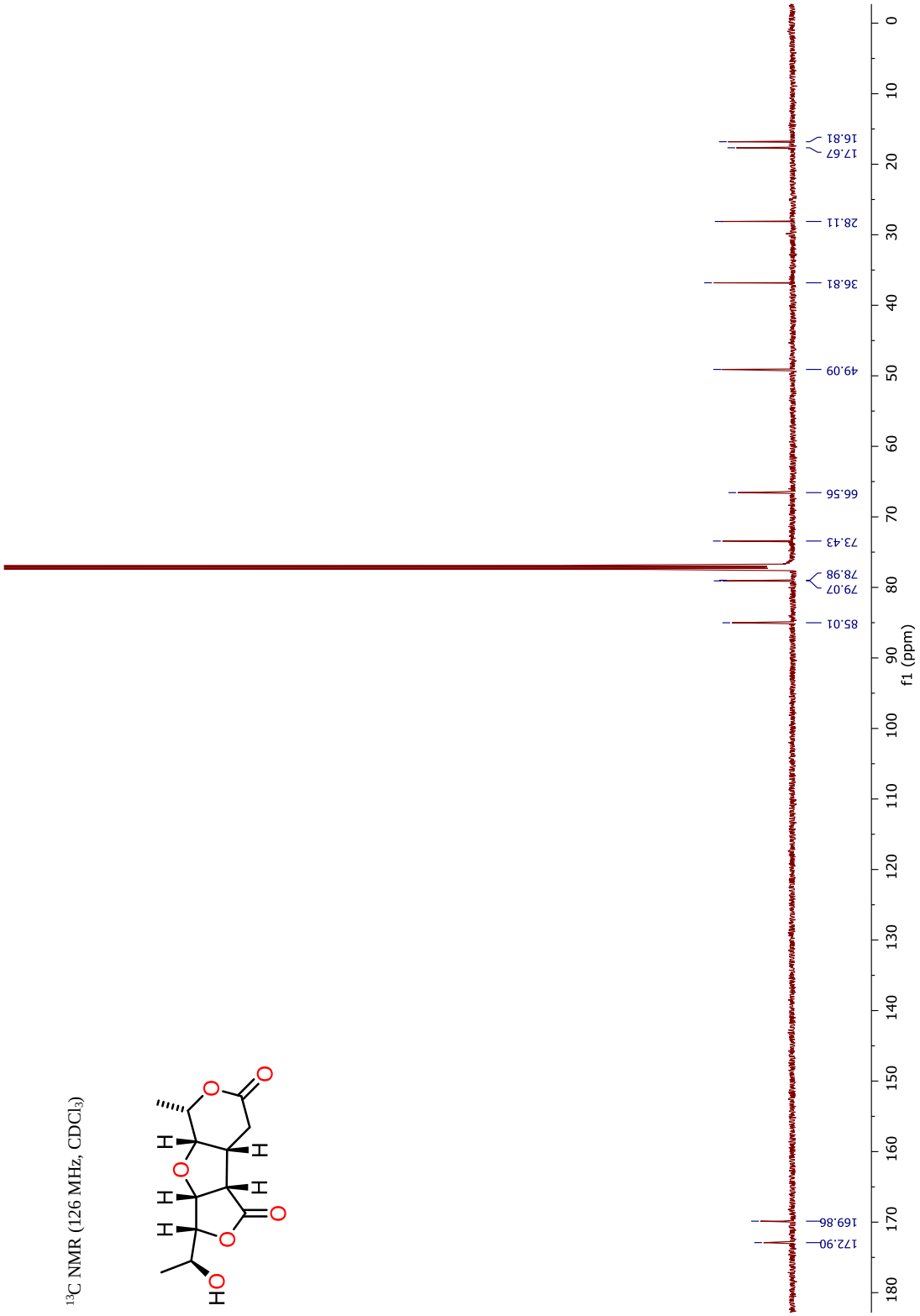

1.1.10 ^{1}H-^{1}H COSY Spectrum of Compound **2** in $CDCl_3$

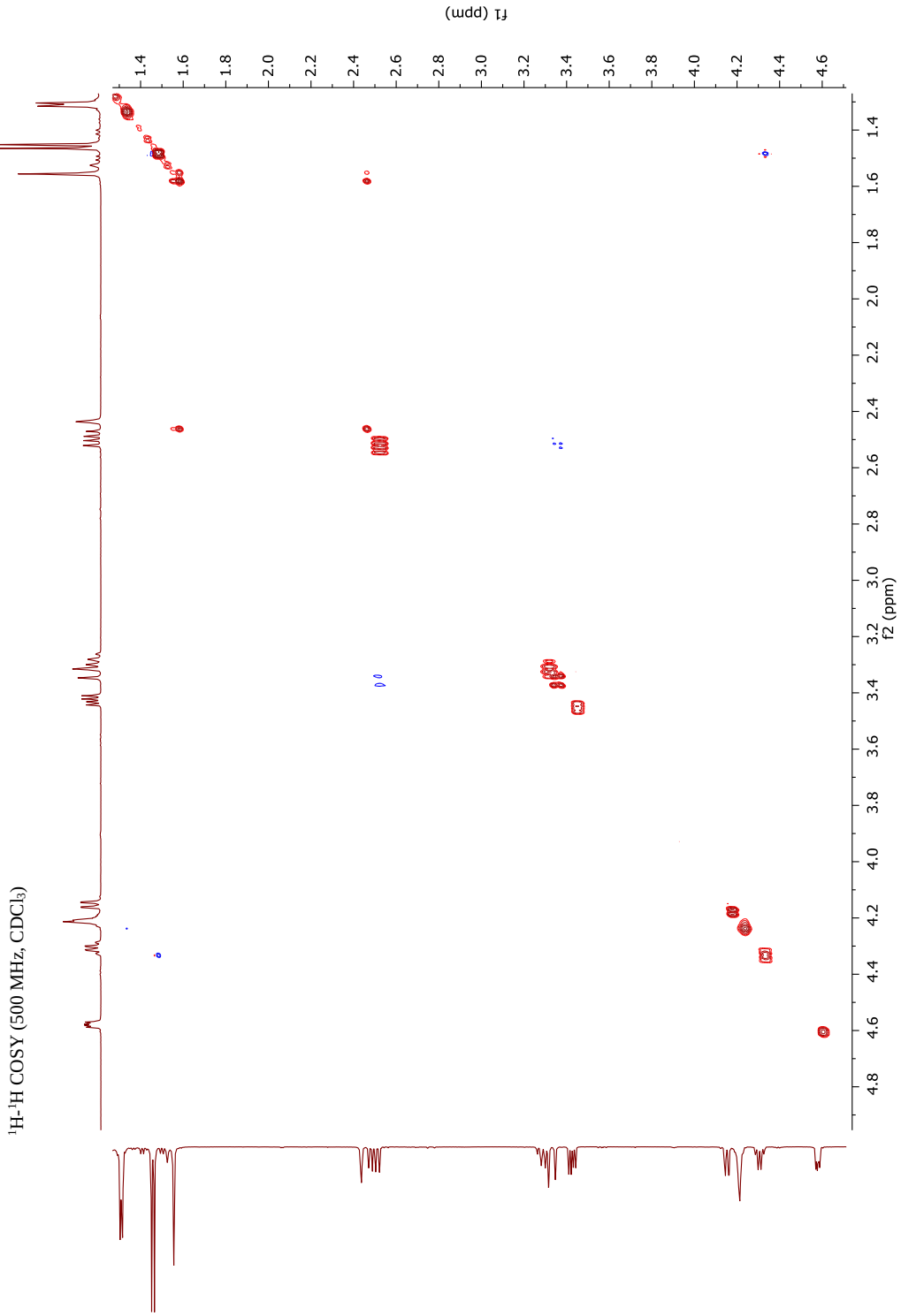

1.1.11 ^{1}H-^{13}C HSQC Spectrum of Compound **2** in $CDCl_3$

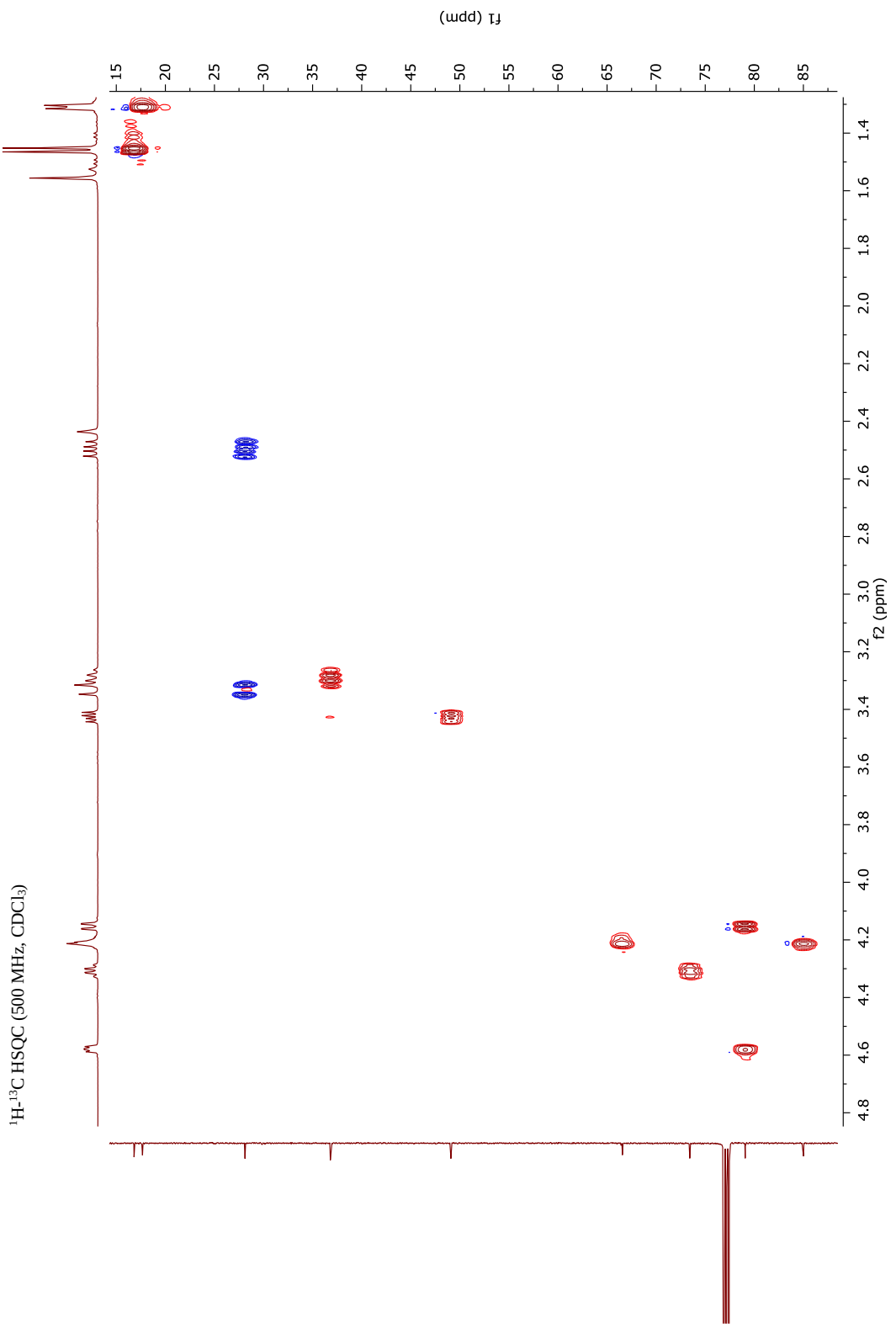

1.1.12 ^{1}H-^{13}C HMBC Spectrum of Compound **2** in $CDCl_3$

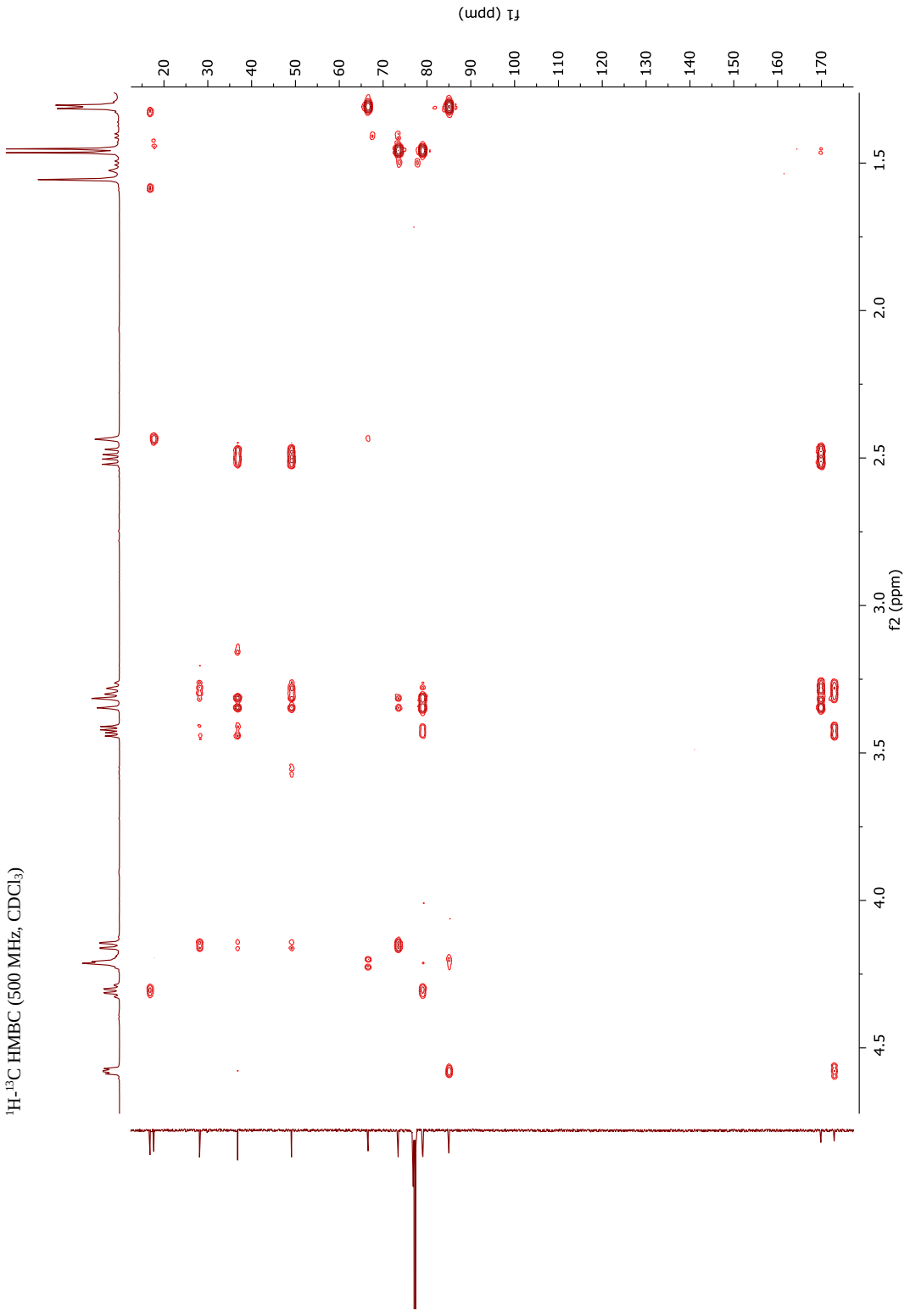

1.1.13 NOESY Spectrum of Compound **2** in $CDCl_3$

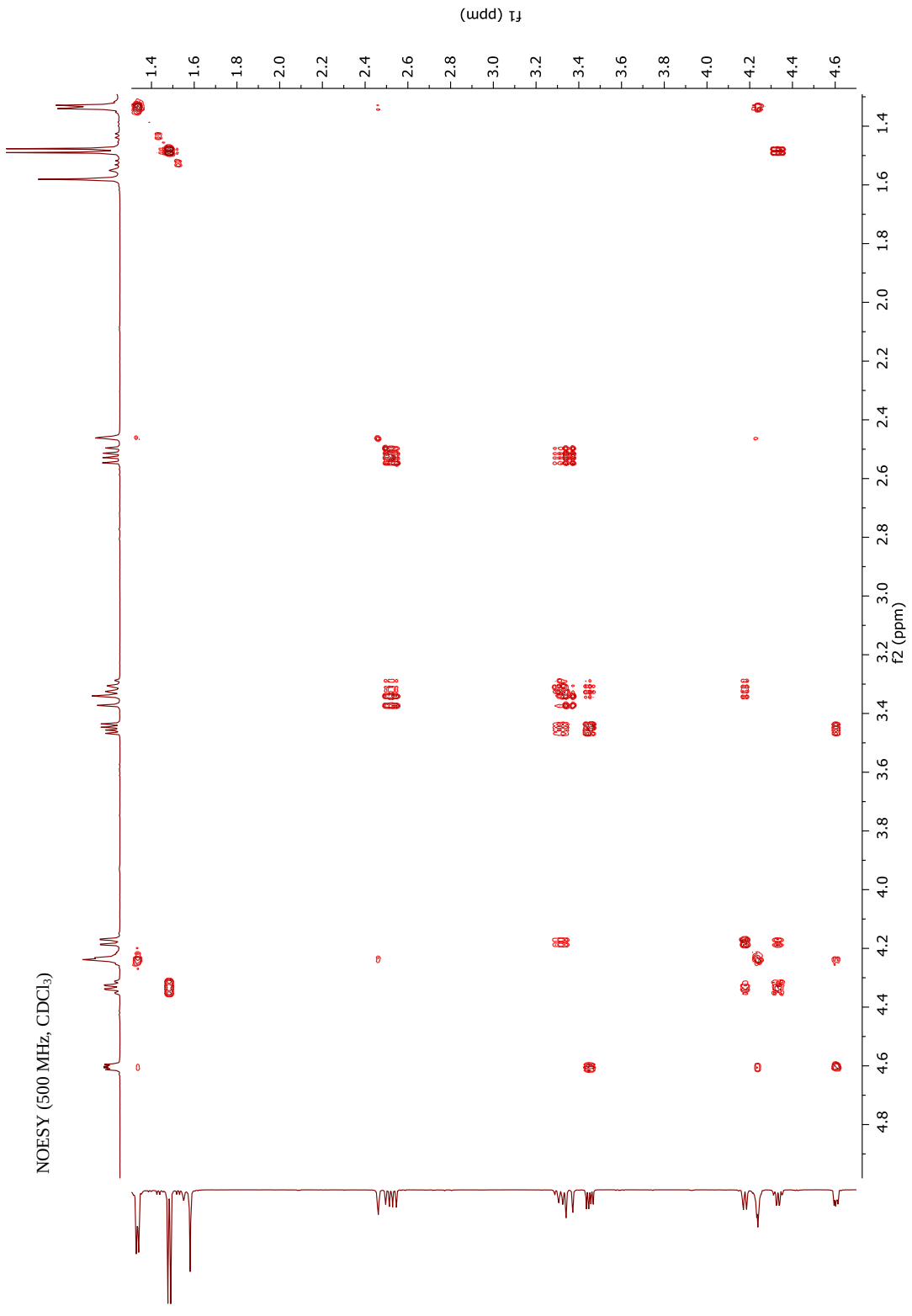

1.1.14 ^{1}H NMR Spectrum of Compound **2** in CD_3OD

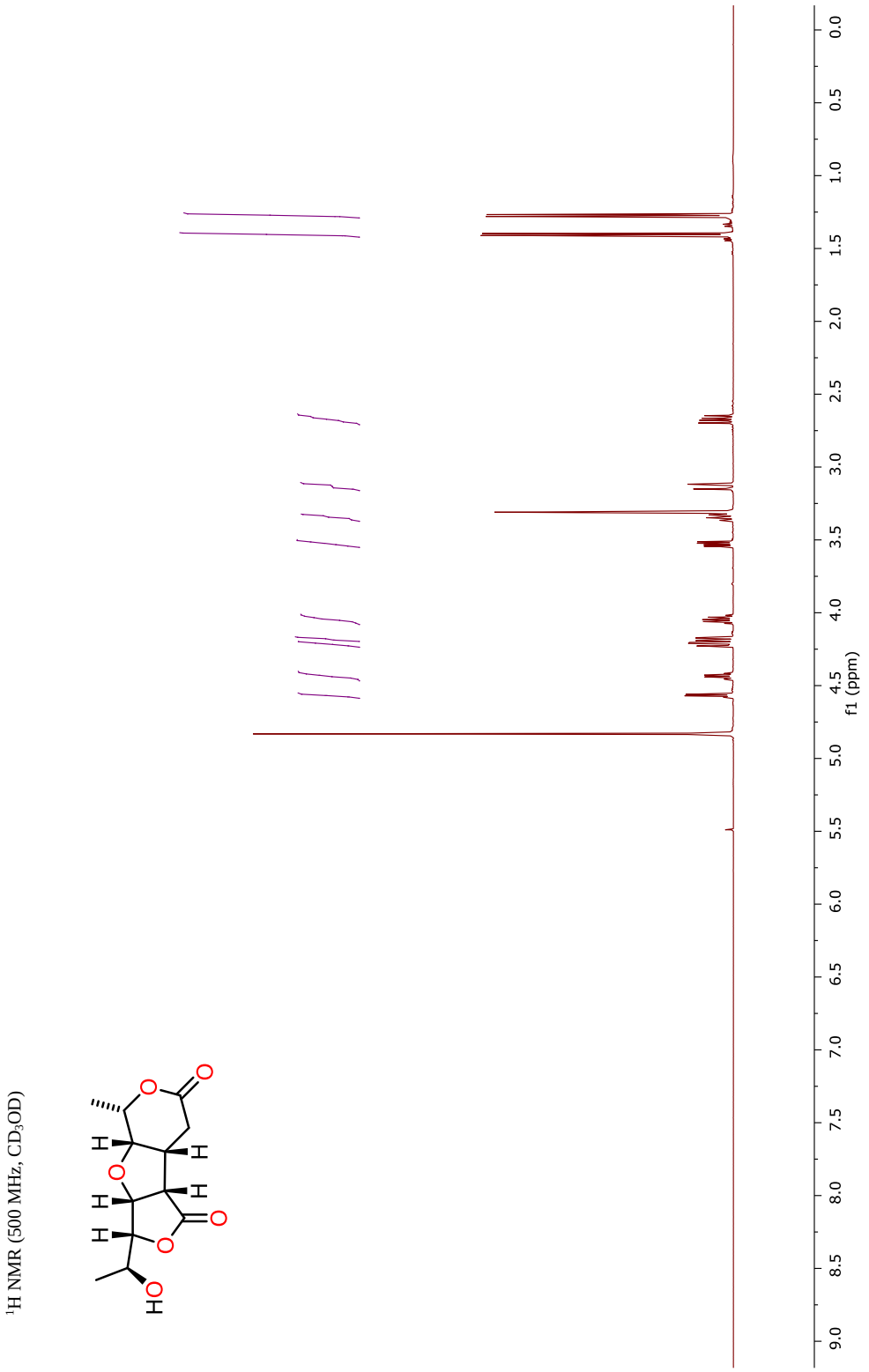

1.1.15 ^{13}C NMR Spectrum of Compound **2** in CD_3OD

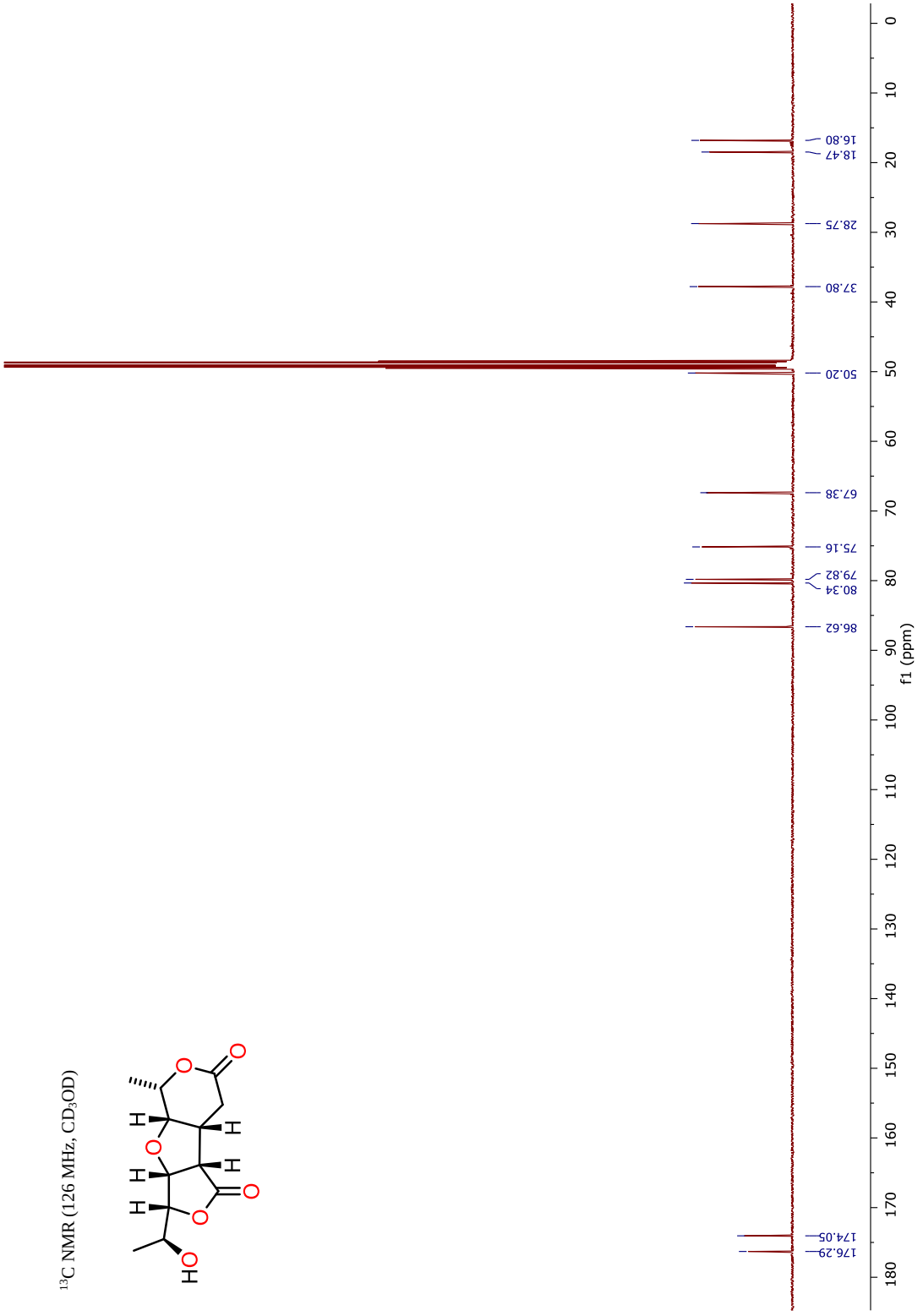

1.1.16 ^{1}H-^{1}H COSY Spectrum of Compound **2** in CD_3OD

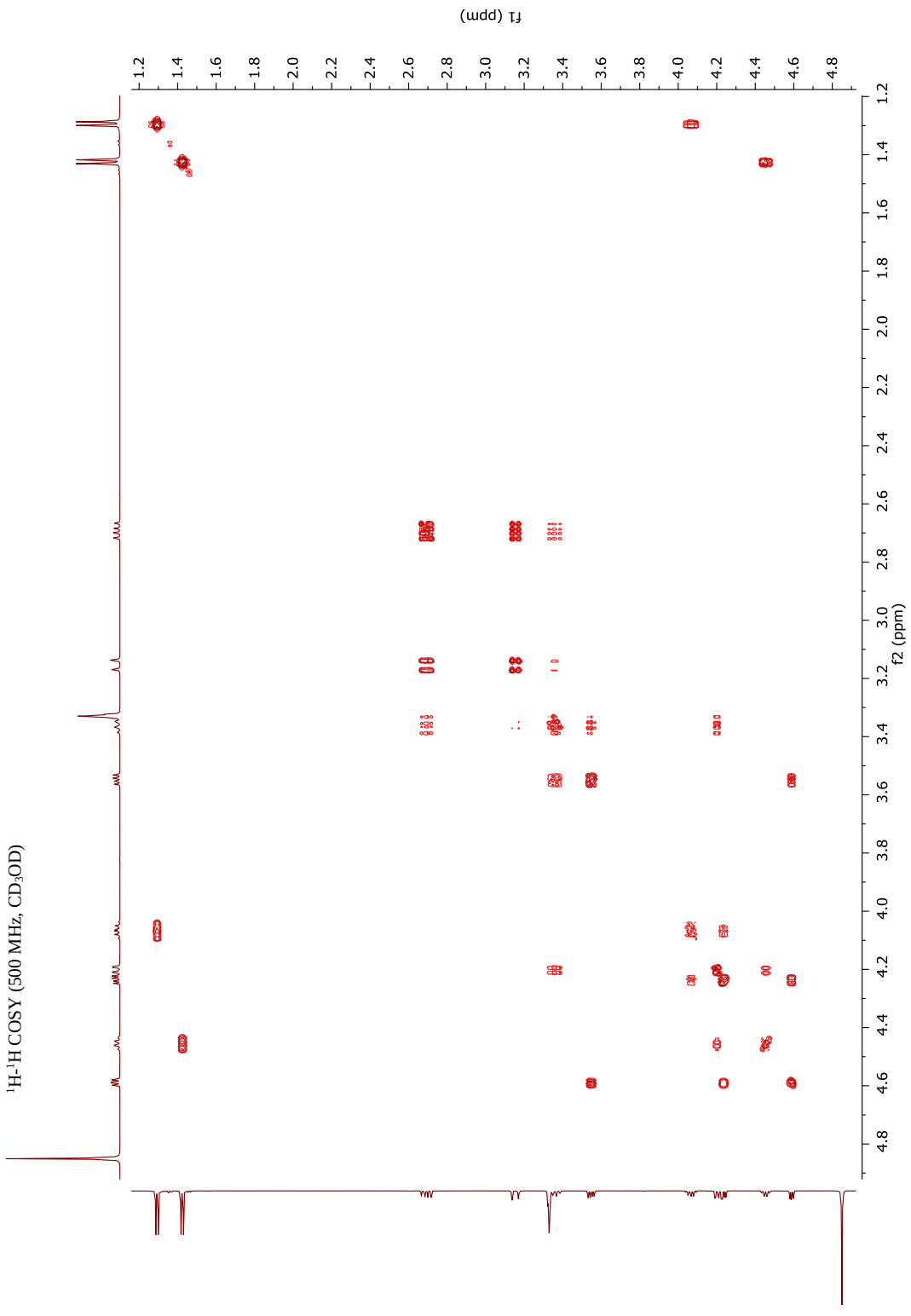

1.1.17 ^{1}H-^{13}C HSQC Spectrum of Compound **2** in CD_3OD

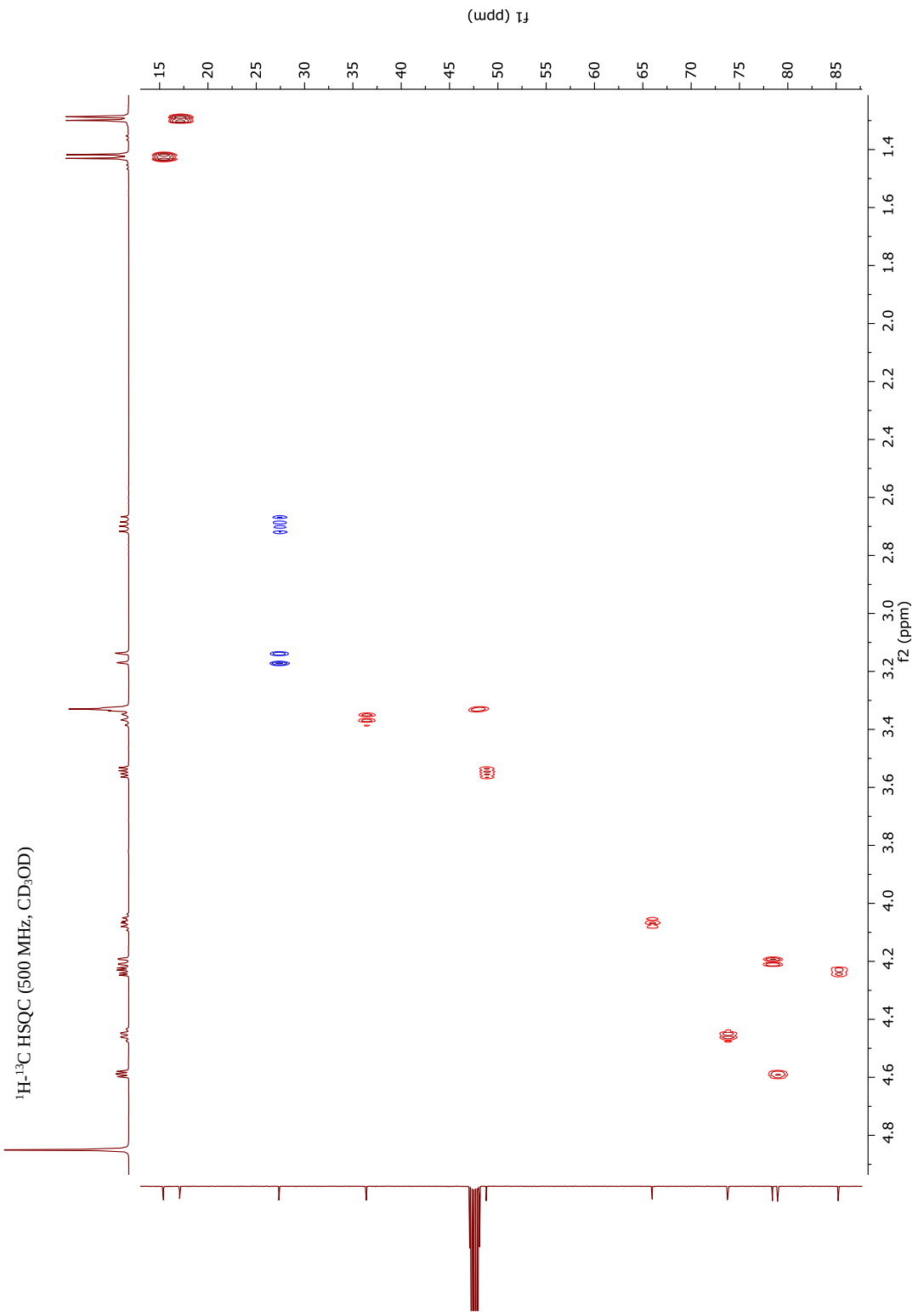

1.1.18 ^{1}H-^{13}C HMBC Spectrum of Compound **2** in CD_3OD

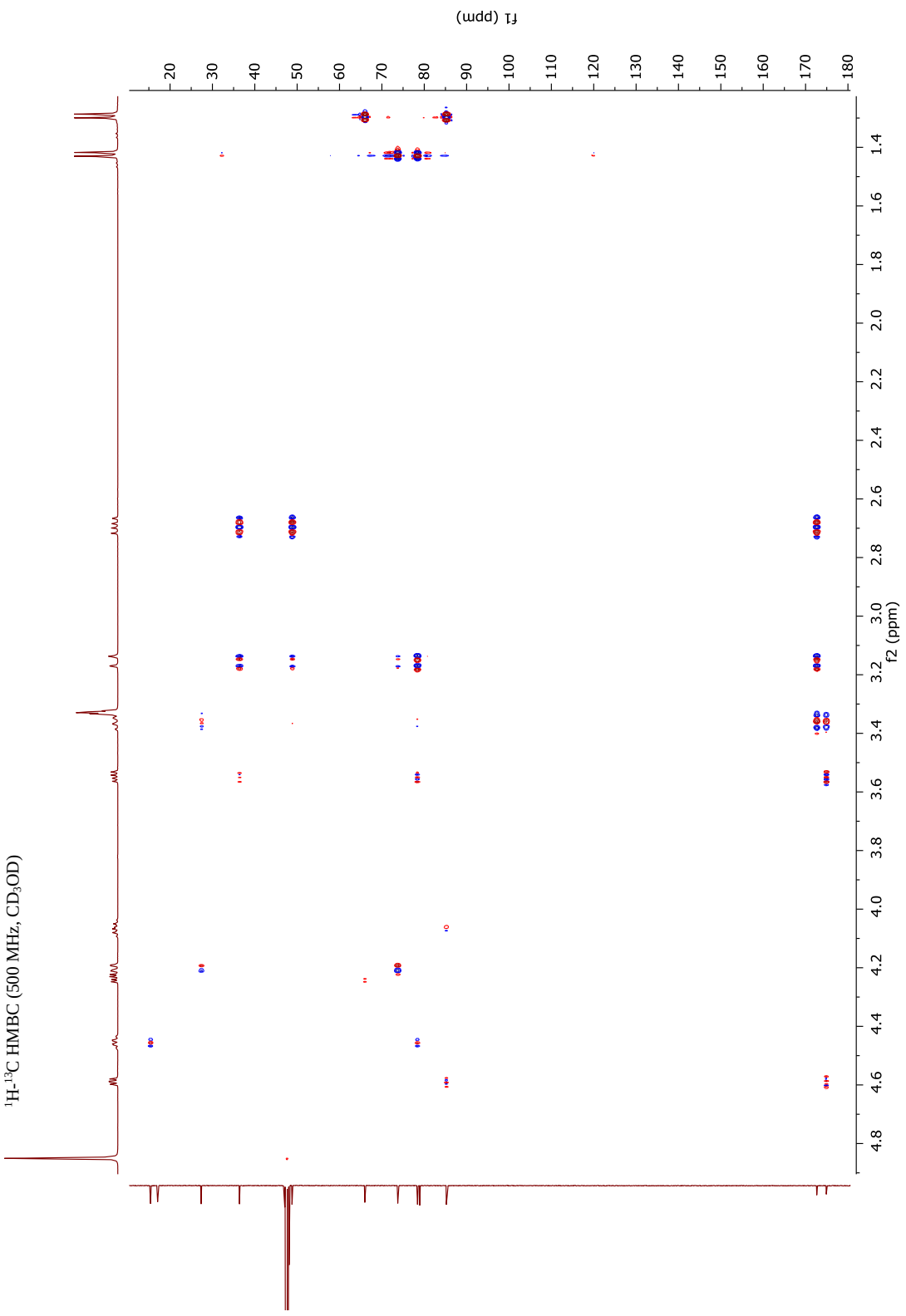

1.1.19 NOESY Spectrum of Compound **2** in CD_3OD

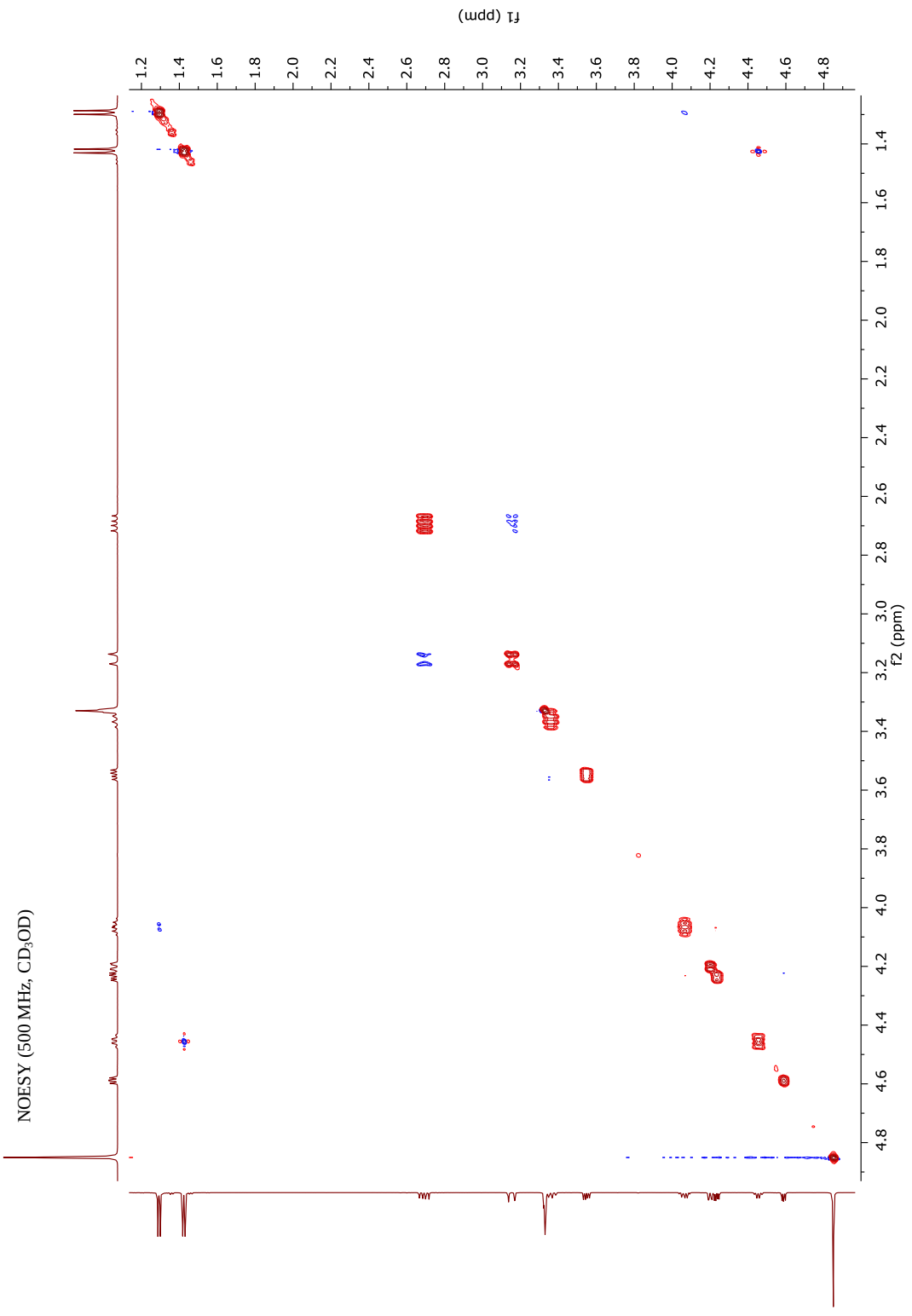

1.1.20 ^{1}H NMR Spectrum of Compound **4** in $CDCl_3$

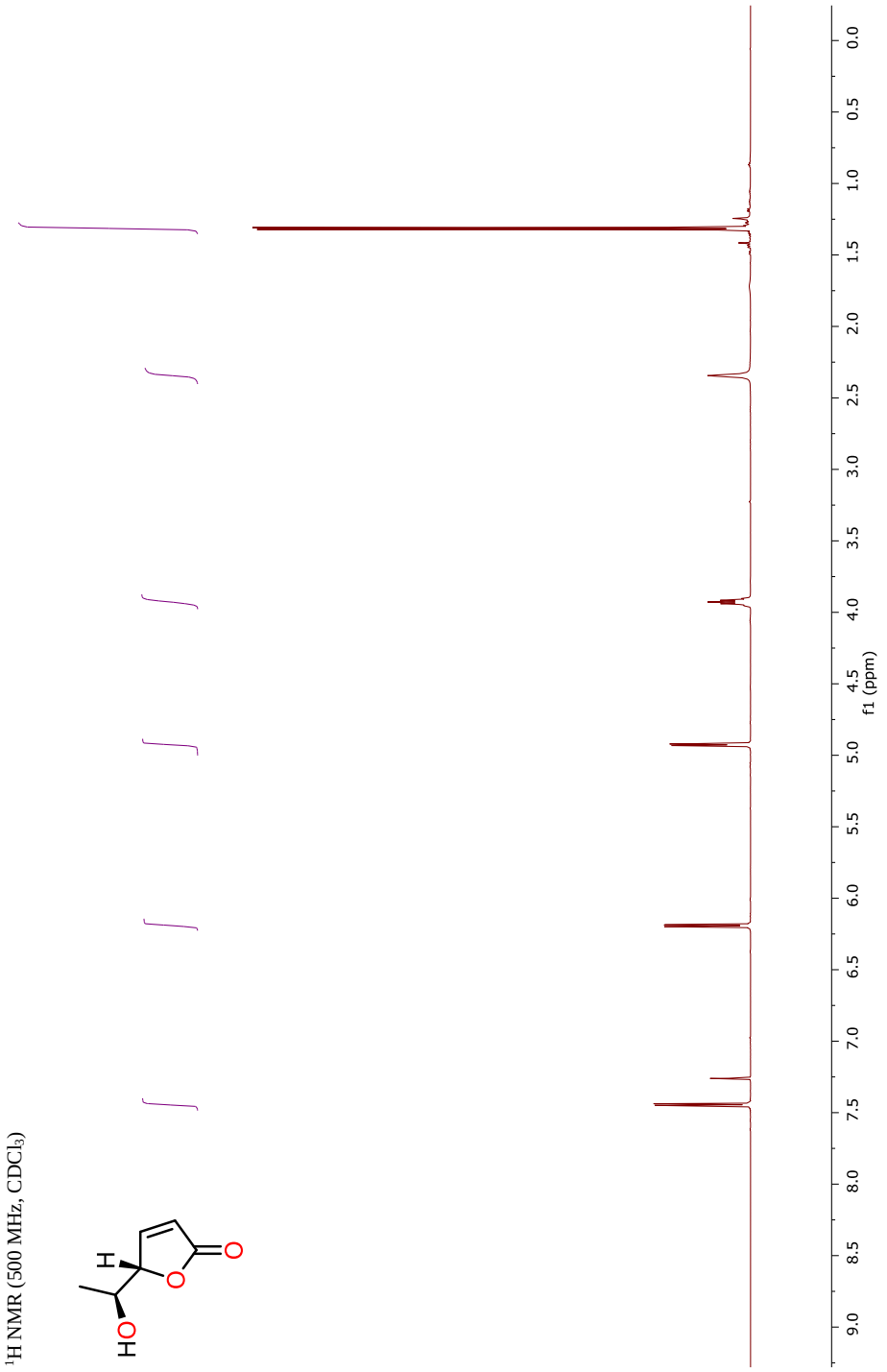

1.1.21 ^{13}C NMR Spectrum of Compound **4** in $CDCl_3$

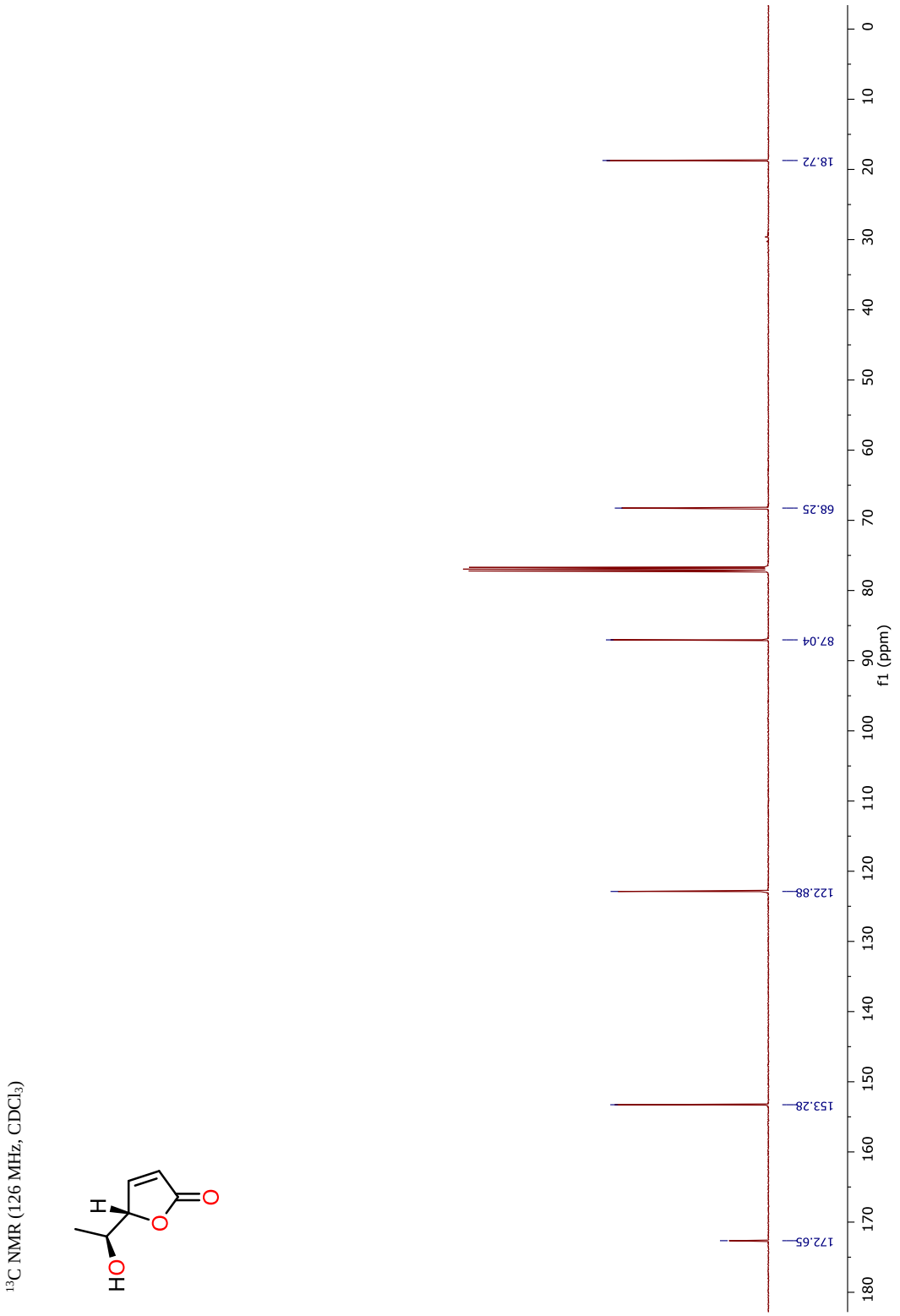

1.1.22 ^{1}H NMR Spectrum of Compound **4** in CD_3OD

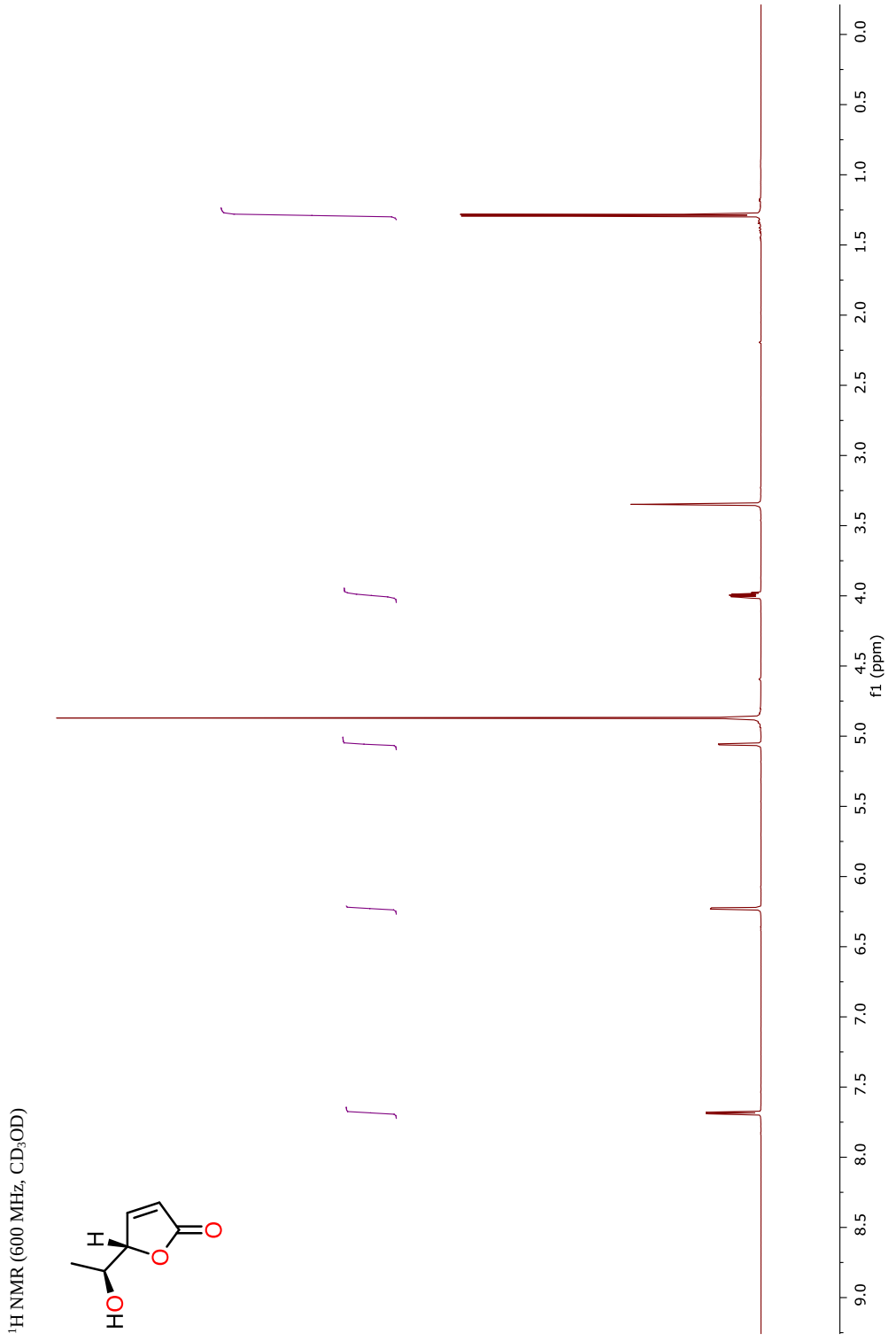

1.1.23 ^{13}C NMR Spectrum of Compound **4** in CD_3OD

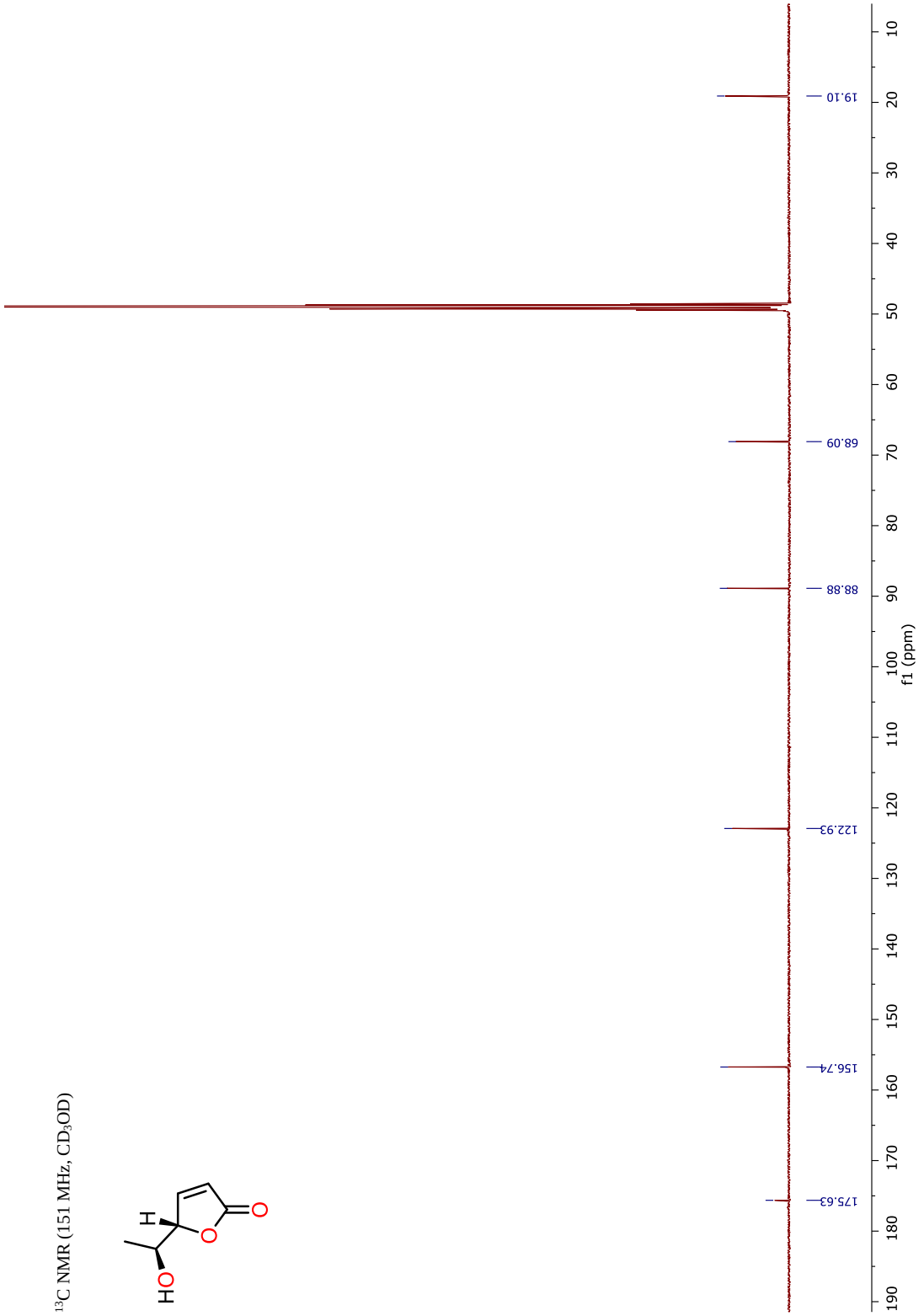

1.1.24 ^{1}H NMR Spectrum of Compound **25**

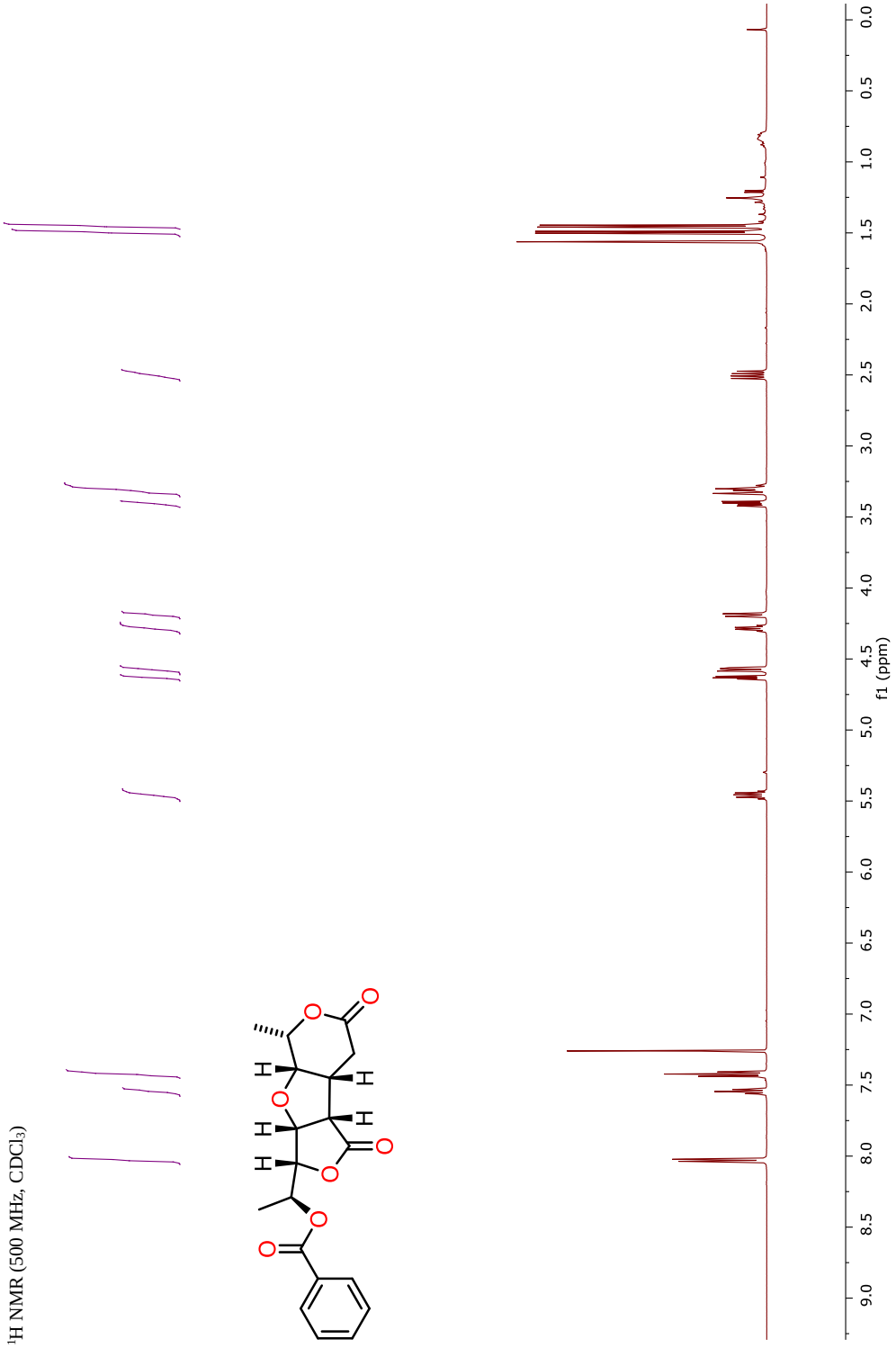

1.1.25 ^{13}C NMR Spectrum of Compound **25**

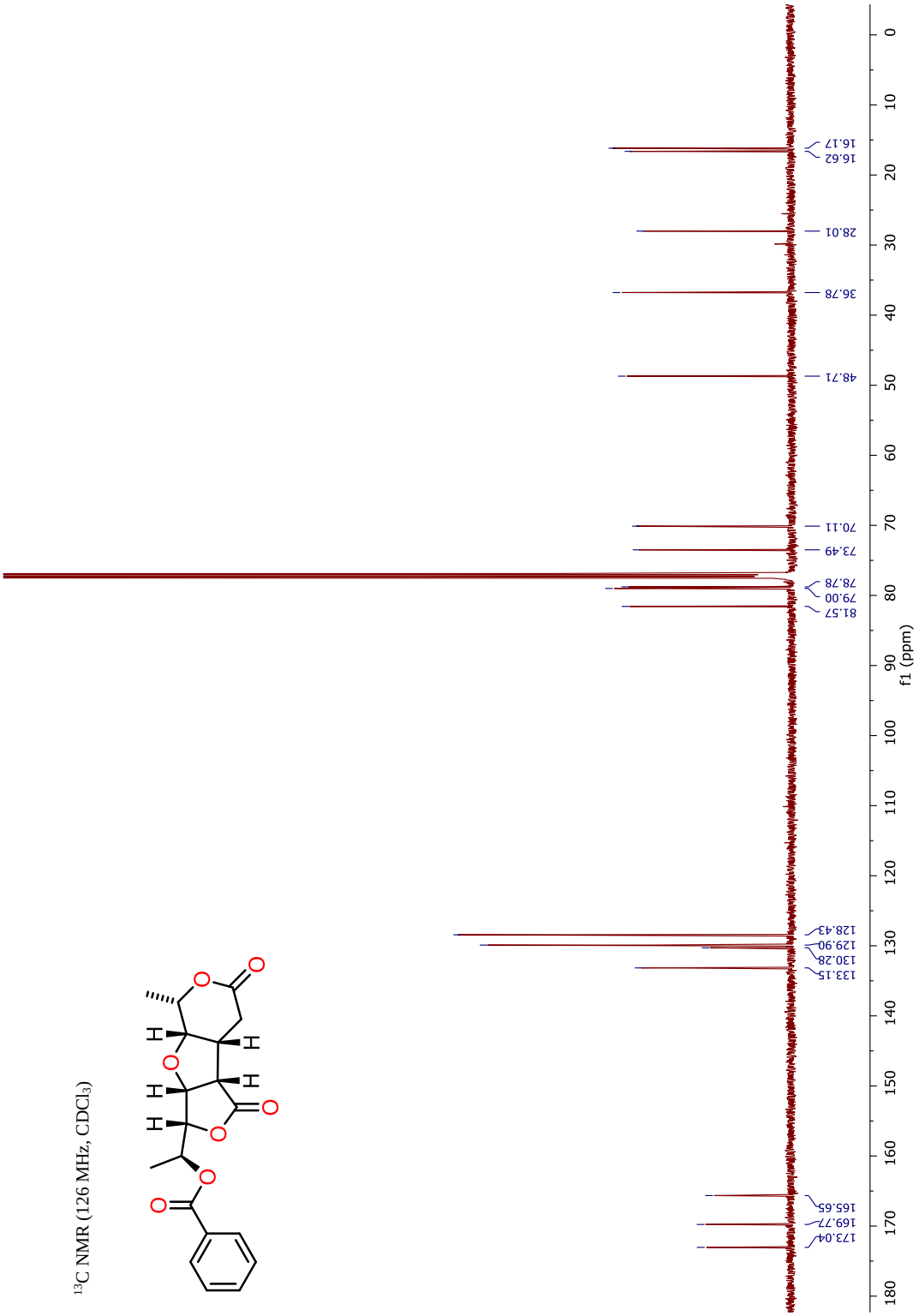

1.1.26 ^{1}H-^{1}H COSY Spectrum of Compound **25** in $CDCl_3$

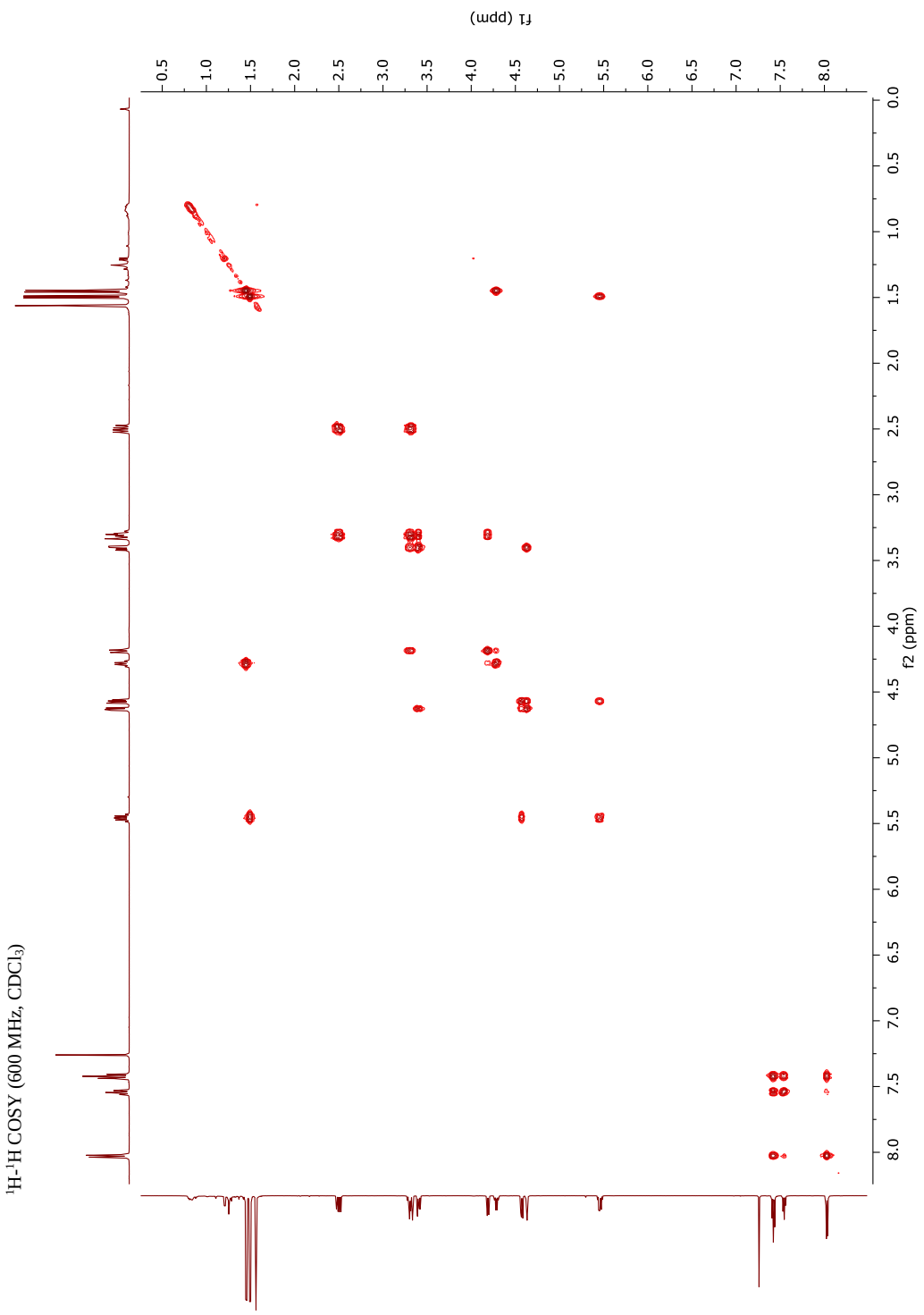

1.1.27 ^{1}H-^{13}C HSQC Spectrum of Compound **25** in $CDCl_3$

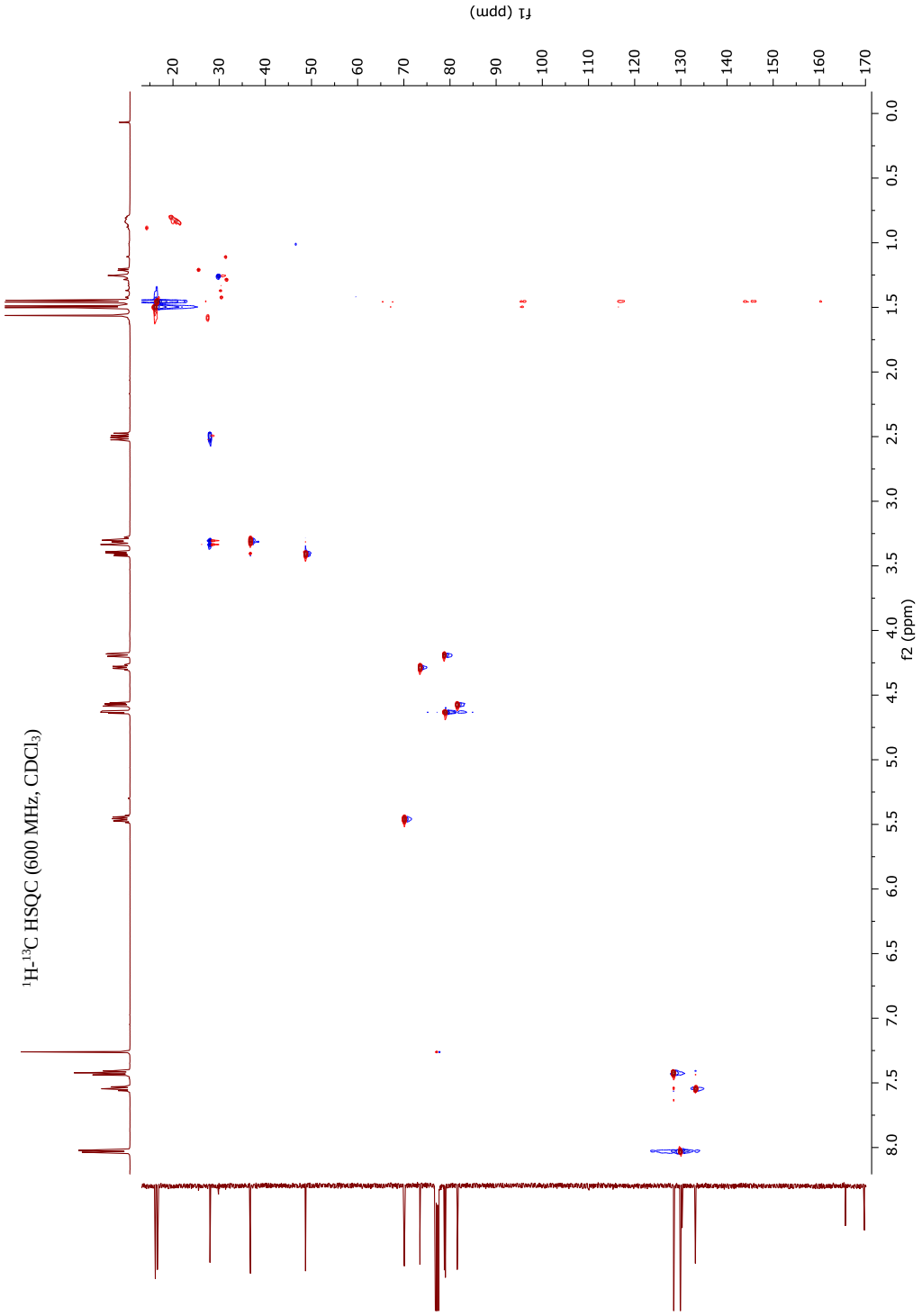

1.1.28 ^{1}H-^{13}C HMBC Spectrum of Compound **25** in $CDCl_3$

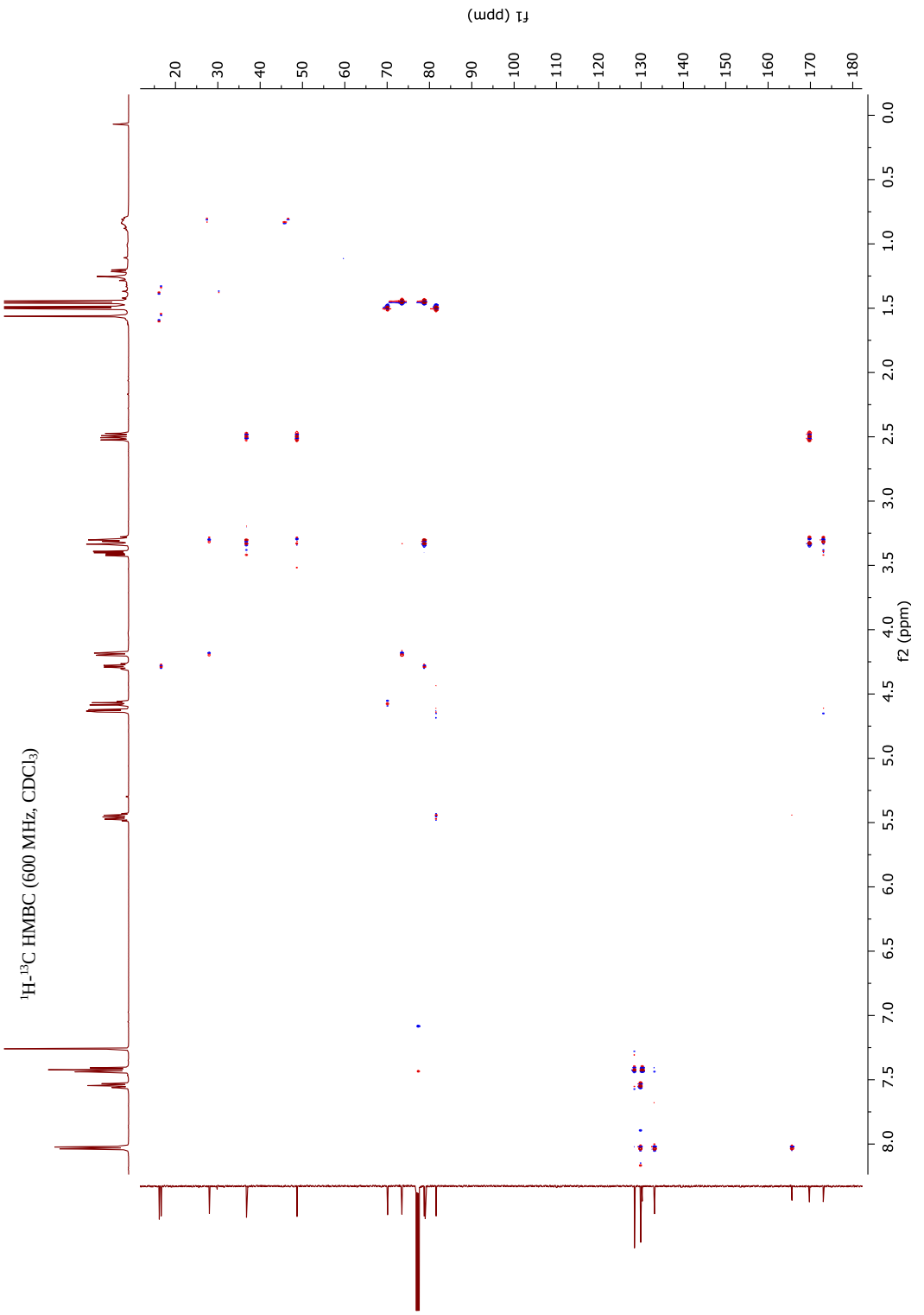

1.1.29 NOESY Spectrum of Compound **25** in $CDCl_3$

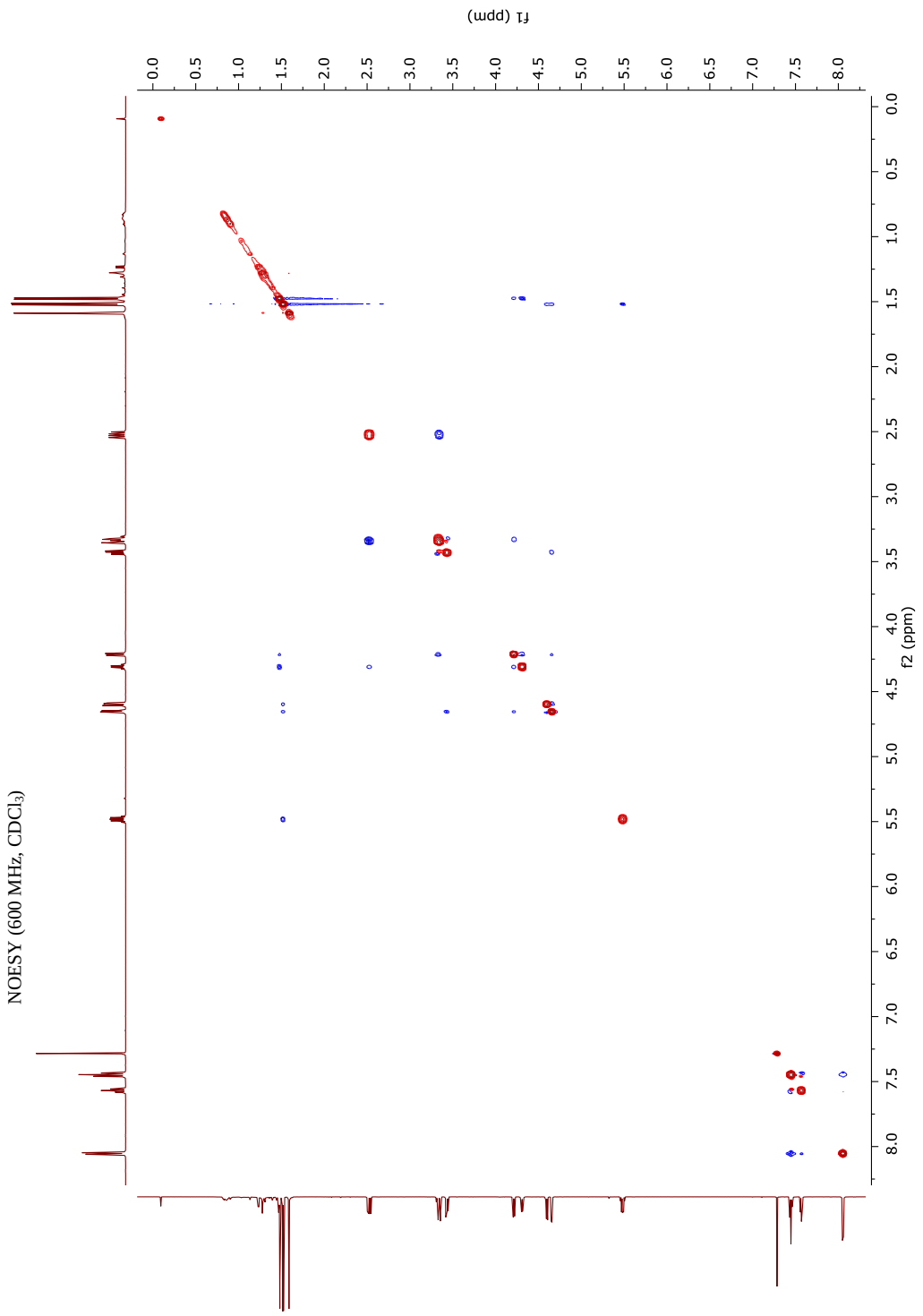

1.2 HPLC Data for Chapter 1

1.2.1 HPLC Data for Compound **15**

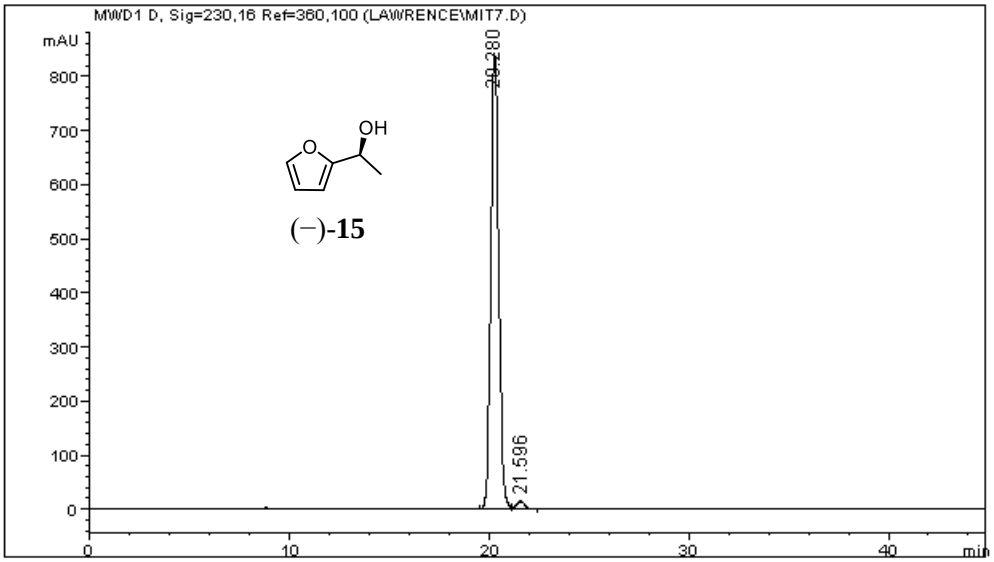

(−)-**15**

Peak #	RetTime [min]	Type	Width [min]	Area [mAU*s]	Height [mAU]	Area %
1	20.280	BV	0.4336	2.34817e4	841.36511	98.1648
2	21.596	VB	0.4521	439.00284	14.62994	1.8352

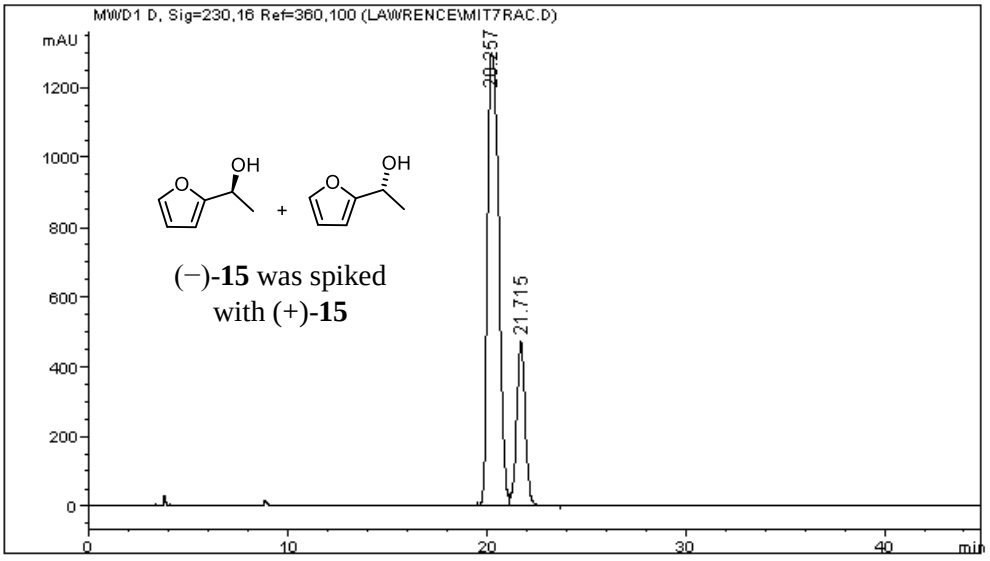

(−)-**15** was spiked with (+)-**15**

Peak #	RetTime [min]	Type	Width [min]	Area [mAU*s]	Height [mAU]	Area %
1	20.257	BV	0.6504	5.14429e4	1298.03650	78.3373
2	21.715	VB	0.4608	1.42256e4	473.11588	21.6627

1.2.2 HPLC Data for Compound **3**

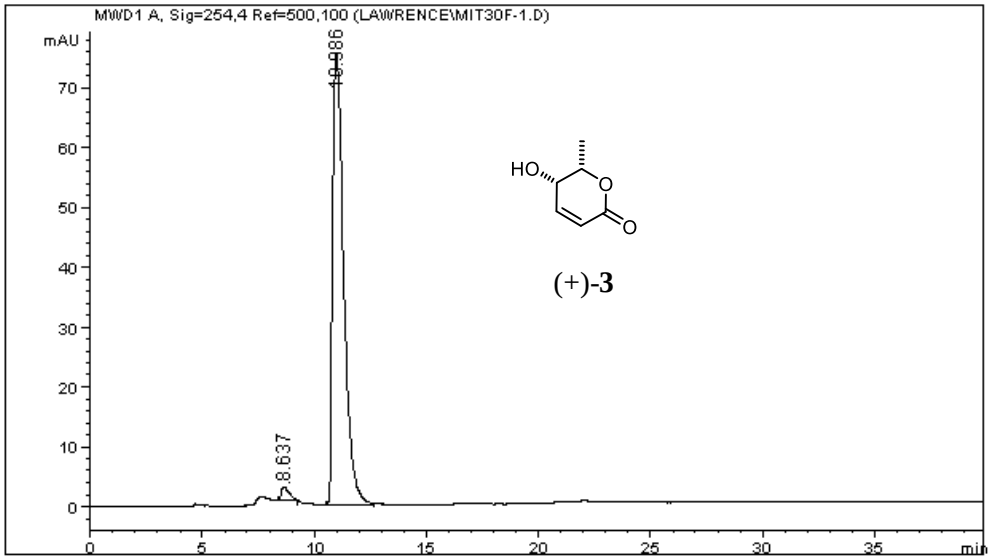

(+)-**3**

Peak #	RetTime [min]	Type	Width [min]	Area [mAU*s]	Height [mAU]	Area %
1	8.637	MM	0.4378	59.63604	2.27009	2.2629
2	10.986	PB	0.5268	2575.73755	75.35605	97.7371

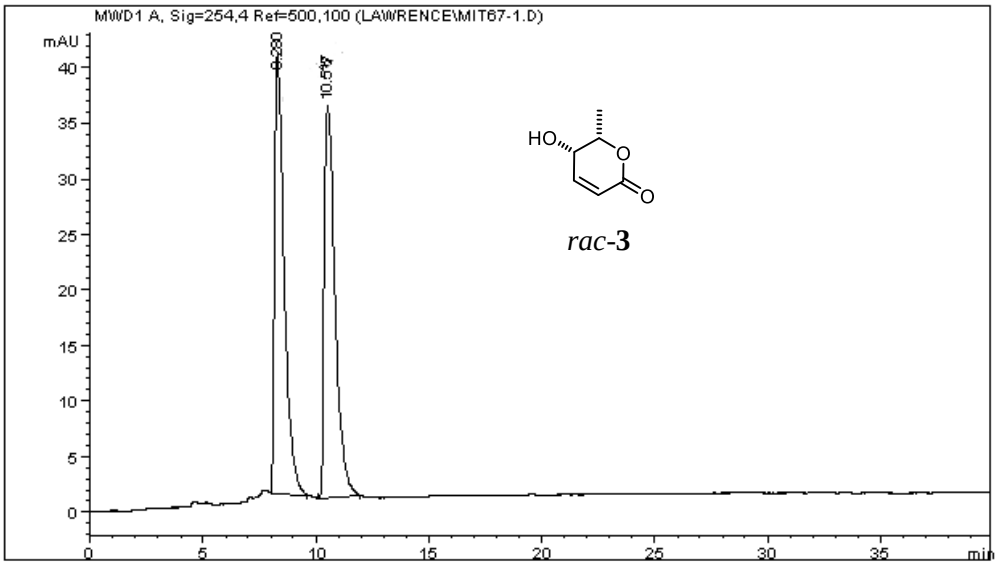

rac-**3**

Peak #	RetTime [min]	Type	Width [min]	Area [mAU*s]	Height [mAU]	Area %
1	8.280	MM	0.4873	1155.23853	39.51545	49.4240
2	10.517	PB	0.5198	1182.16675	35.20548	50.5760

Appendices for Chapter 2

2.1 Further Information for Methods M1-M4

Approach	Geometry Optimisation		NMR Calculation	
	Method	**Solvent (model)**	**Method**	**Solvent (model)**
M1[75]	M06-2X 6-31+G(d,p)	**Yes (PCM)**	B3LYP 6-11+G(2d,p)	**Yes (PCM)**
M2A[73]	M06-2X 6-31+G(d,p)	**No**	mPW1PW91 6-311+G(2d,p)	**Yes (SMD)**
M2B[73]	M06-2X 6-311+G(2d,p)	**No**	mPW1PW91 6-311+G(2d,p)	**Yes (SMD)**
M3[65]	B3LYP 6-31+G(d,p)	**No**	mPW1PW91 6-311+G(2d,p)	**Yes (PCM)**
M4[91]	mPW1PW91 6-311G(d,p)	**Yes (PCM)**	mPW1PW91 6-311G(d,p)	**Yes (PCM)**

Table 35: Summary of conditions used for each of the approaches

An overview of the slope and intercept factors for each of the methodologies (M1-M3), as well as their performance, is listed in Table 36.

Method	**Solvent**	**^{1}H Scaling Factors and Performance**			**^{13}C Scaling Factors and Performance**		
		Slope	**Intercept**	**R^2**	**Slope**	**Intercept**	**R^2**
M1	$CHCl_3$	-1.0767	31.9477	-	-1.0522	181.2412	-
M2A	$CHCl_3$	-1.0938	31.8723	0.9975	-1.0446	186.7246	0.9989
M2B	$CHCl_3$	-1.0951	31.9773	0.9975	-1.0379	187.2065	0.9990
M3	$CHCl_3$	-1.0719	31.8733	0.9983	-1.0420	186.3567	0.9990
M3	DMSO	-1.0580	31.7217	0.9985	-1.0496	186.2534	0.9989

Table 36: Summary of the reported scaling factors and the performance of each method[73,75]

2.2 Computed TMS Scaling Values

Method	Geometry Optimisation	Solvent	Shielding tensor values	
			^{1}H	^{13}C
M1	Solvent	$CHCl_3$	31.8717	183.6718
	Gas	$CHCl_3$	31.8780	183.7506
M2A	Solvent	$CHCl_3$	31.6968	187.936
	Gas	$CHCl_3$	31.7280	188.1028
M3	Gas	DMSO	31.6974	187.1118
M4	Solvent	DMSO	31.9121	189.4251
Sarotti Method	Gas	$CHCl_3$	31.5506	196.4797

Table 37: ^{1}H and ^{13}C shielding tensor values for TMS computed at varying levels of theory

2.3 Energies for all Conformers for each Section

Energies for all the compounds computed utilising methods M1-M4, are listed in the relevant sections below. All energies are provided in Hartrees (a.u.). Input and output files for each section have been archived with the University of Edinburgh.

2.3.1 Conformational Search: Manual *vs* TINKER

Structure	**Solvent**	**Creation of Conformer**	**Conformer #**	E_{low}	E_{high}
γ-lactone ***4***	$CHCl_3$	Manual	1	-459.1479	-459.1562
			2	-459.1428	-459.1536
			3	-459.1444	-459.1538
		TINKER	1	-459.1479	-459.1562
			2	-459.1451	-459.1537
			3	-459.1463	-459.1555
			4	-459.1479	-459.1562
			5	-459.1432	-459.1535
			6	-459.1434	-459.1531
			7	-459.1407	-459.1526
			8	-459.1428	-459.1536
	DMSO	Manual	1	-459.1479	-459.1598
			2	-459.1428	-459.1584
			3	-459.1444	-459.1577
		TINKER	1	-459.1479	-459.1598
			2	-459.1451	-459.1573
			3	-459.1463	-459.1593
			4	-459.1479	-459.1598
			5	-459.1432	-459.1580
			6	-459.1434	-459.1571
			7	-459.1407	-459.1578
			8	-459.1428	-459.1584
δ-lactone ***3***	$CHCl_3$	Manual	1	-459.1383	-459.1473
			2	-459.1371	-459.1454
		TINKER	1	-459.1383	-459.1473
			2	-459.1383	-459.1469
			3	-459.1414	-459.1491
	DMSO	Manual	1	-459.1383	-459.1520
			2	-459.1371	-459.1494
		TINKER	1	-459.1383	-459.1520
			2	-459.1383	-459.1514
			3	-459.1414	-459.1528

Table 38: Manual *vs* TINKER creation of conformers, Method M3, chloroform / DMSO

2.3.2 Effect of Basis Set Size

Method M2A:

Structure	**Conformer #**	E_{low}	G_{low}	E_{high}	G_{high}
γ-lactone ***4***	1	-458.9511	-458.8466	-459.1629	-459.0584
	2	-458.9492	-458.8451	-459.1605	-459.0563
	3	-458.9502	-458.8457	-459.1625	-459.0579
	4	-458.9511	-458.8466	-459.1629	-459.0584
	5	-458.9470	-458.8434	-459.1603	-459.0567
	6	-458.9474	-458.8437	-459.1600	-459.0563
	7	-458.9437	-458.8399	-459.1597	-459.0559
	8	-458.9467	-458.8425	-459.1605	-459.0563
γ-lactone ***6***	1	-458.9497	-458.8458	-459.1615	-459.0576
	2	-458.9458	-458.8418	-459.1598	-459.0557
	3	-458.9507	-458.8460	-459.1625	-459.0578
	4	-458.9488	-458.8450	-459.1615	-459.0578
	5	-458.9502	-458.8455	-459.1617	-459.0570
δ-lactone ***3***	1	-458.9418	-458.8366	-459.1542	-459.0490
	2	-458.9418	-458.8373	-459.1535	-459.0490
	3	-458.9451	-458.8398	-459.1559	-459.0505
δ-lactone ***5***	1	-458.9436	-458.8392	-459.1545	-459.0501
	2	-458.9441	-458.8392	-459.1552	-459.0503
	3	-458.9440	-458.8394	-459.1551	-459.0505
	4	-458.9403	-458.8358	-459.1526	-459.0480
	5	-458.9436	-458.8383	-459.1544	-459.0490
	6	-458.9399	-458.8350	-459.1525	-459.0475

Table 39: Method M2A, chloroform

Method M2B:

Structure	**Conformer #**	E_{low}	G_{low}	E_{high}	G_{high}
γ-lactone ***4***	1	-459.0797	-458.9754	-459.1630	-459.0587
	2	-459.0780	-458.9740	-459.1606	-459.0567
	3	-459.0791	-458.9748	-459.1626	-459.0583
	4	-459.0797	-458.9754	-459.1630	-459.0587
	5	-459.0791	-458.9748	-459.1626	-459.0583
	6	-459.0765	-458.9727	-459.1602	-459.0564
	7	-459.0731	-458.9694	-459.1598	-459.0561
	8	-459.0759	-458.9719	-459.1605	-459.0565
γ-lactone ***6***	1	-459.0784	-458.9746	-459.1616	-459.0578
	2	-459.0750	-458.9712	-459.1599	-459.0560
	3	-459.0794	-458.9749	-459.1626	-459.0582
	4	-459.0778	-458.9741	-459.1616	-459.0580
	5	-459.0790	-458.9746	-459.1618	-459.0574
δ-lactone ***3***	1	-459.0705	-458.9654	-459.1543	-459.0492
	2	-459.0738	-458.9686	-459.1560	-459.0509
	3	-459.0738	-458.9686	-459.1560	-459.0509
δ-lactone ***5***	1	-459.0719	-458.9678	-459.1546	-459.0505
	2	-459.0727	-458.9680	-459.1553	-459.0506
	3	-459.0725	-458.9680	-459.1552	-459.0507
	4	-459.0690	-458.9647	-459.1526	-459.0483
	5	-459.0723	-458.9671	-459.1546	-459.0494
	6	-459.0686	-458.9637	-459.1526	-459.0478

Table 40: Method M2B, chloroform

2.3.3 Solvent Effects on Geometry Optimisation

Method M2A:

See Table 39 for geometry optimisations in the gas phase for γ-lactone **4** and δ-lactone **3**.

Structure	**Conformer #**	E_{low}	G_{low}	E_{high}	G_{high}
*γ-lactone **4***	1	-458.9669	-458.8630	-459.1632	-459.0593
	2	-458.9654	-458.8614	-459.1608	-459.0569
	3	-458.9669	-458.8625	-459.1628	-459.0584
	4	-458.9635	-458.8600	-459.1600	-459.0565
	5	-458.9649	-458.8614	-459.1607	-459.0572
	6	-458.9645	-458.8605	-459.1604	-459.0564
	7	-458.9631	-458.8592	-459.1600	-459.0561
	8	-458.9648	-458.8607	-459.1608	-459.0567
*δ-lactone **3***	1	-458.9599	-458.8547	-459.1545	-459.0493
	2	-458.9594	-458.8548	-459.1540	-459.0493
	3	-458.9614	-458.8561	-459.1562	-459.0509

Table 41: Method M2A; utilising solvent in the geometry optimisation; chloroform

Method M1:

Structure	**Conformer #**	E_{low}	G_{low}	E_{high}	G_{high}
*γ-lactone **4***	1	-458.9606	-458.8563	-459.2808	-459.1765
	2	-458.9589	-458.8550	-459.2780	-459.1740
	3	-458.9602	-458.8558	-459.2800	-459.1755
	4	-458.9569	-458.8532	-459.2777	-459.1740
	5	-458.9582	-458.8545	-459.2779	-459.1742
	6	-458.9578	-458.8537	-459.2777	-459.1736
	7	-458.9564	-458.8527	-459.2777	-459.1740
	8	-458.9582	-458.8541	-459.2779	-459.1738
*δ-lactone **3***	1	-458.9533	-458.8479	-459.2729	-459.1675
	2	-458.9530	-458.8483	-459.2723	-459.1676
	3	-458.9548	-458.8496	-459.2746	-459.1694
*γ-lactone **4** (gas)*	1	-458.9511	-458.8466	-459.2804	-459.1759
	2	-458.9492	-458.8451	-459.2776	-459.1734
	3	-458.9502	-458.8457	-459.2796	-459.1750
	4	-458.9511	-458.8466	-459.2804	-459.1759
	5	-458.9470	-458.8434	-459.2774	-459.1738
	6	-458.9474	-458.8437	-459.2772	-459.1735
	7	-458.9437	-458.8399	-459.2773	-459.1736
	8	-458.9467	-458.8425	-459.2775	-459.1733
*δ-lactone **3** (gas)*	1	-458.9418	-458.8366	-459.2724	-459.1672
	2	-458.9418	-458.8373	-459.2717	-459.1672
	3	-458.9451	-458.8398	-459.2740	-459.1686

Table 42: Method M1; utilising solvent in the geometry optimisation, unless stated otherwise; chloroform

2.3.4 Method M1 *vs* M2 *vs* M3

Method M2A

See Table 39 for the γ-lactone **4** and δ-lactone **3**, as well as their respective diastereoisomers **6** and **5**.

Structure	**Conformer #**	E_{low}	G_{low}	E_{high}	G_{high}
(+)-Angiopterlactone B ***2*** *(Compound I)*	1	-917.9485	-917.7061	-918.3517	-918.1093
	2	-917.9406	-917.6999	-918.3456	-918.1048
	3	-917.9492	-917.7074	-918.3560	-918.1142
	4	-917.9474	-917.7062	-918.3515	-918.1103
	5	-917.9485	-917.7068	-918.3477	-918.1061
	6	-917.9436	-917.7027	-918.3500	-918.1091
	7	-917.9514	-917.7105	-918.3580	-918.1172
	8	-917.9453	-917.7039	-918.3487	-918.1072
	9	-917.9441	-917.7039	-918.3552	-918.1149
	10	-917.9406	-917.7006	-918.3460	-918.1059
	11	-917.9403	-917.7009	-918.3501	-918.1108
	12	-917.9466	-917.7064	-918.3530	-918.1128
	13	-917.9458	-917.7054	-918.3496	-918.1092
	14	-917.9500	-917.7079	-918.3526	-918.1105
	15	-917.9502	-917.7087	-918.3536	-918.1122
	16	-917.9444	-917.7035	-918.3508	-918.1098

Table 43: Method M2A; chloroform

Method M3: Chloroform

Structure	**Conformer #**	E_{low}	G_{low}	E_{high}	G_{high}
γ-lactone ***4***	1	-459.1479	-459.0452	-459.1562	-459.0536
	2	-459.1451	-459.0430	-459.1537	-459.0516
	3	-459.1463	-459.0438	-459.1555	-459.0530
	4	-459.1479	-459.0452	-459.1562	-459.0536
	5	-459.1432	-459.0415	-459.1535	-459.0517
	6	-459.1434	-459.0414	-459.1531	-459.0511
	7	-459.1407	-459.0389	-459.1526	-459.0508
	8	-459.1428	-459.0407	-459.1536	-459.0516
δ-lactone ***3***	1	-459.1383	-459.0352	-459.1473	-459.0442
	2	-459.1383	-459.0358	-459.1469	-459.0444
	3	-459.1414	-459.0382	-459.1491	-459.0458
(+)-Angiopterlactone B ***2*** *(Compound I)*	1	-918.3151	-918.0772	-918.3412	-918.1033
	2	-918.3075	-918.0712	-918.3347	-918.0985
	3	-918.3168	-918.0797	-918.3458	-918.1086
	4	-918.3146	-918.0778	-918.3415	-918.1046
	5	-918.3120	-918.0751	-918.3374	-918.1005
	6	-918.3119	-918.0751	-918.3384	-918.1016
	7	-918.3196	-918.0831	-918.3469	-918.1104
	8	-918.3118	-918.0751	-918.3378	-918.1011
	9	-918.3128	-918.0767	-918.3435	-918.1075
	10	-918.3086	-918.0729	-918.3350	-918.0993
	11	-918.3092	-918.0739	-918.3383	-918.1030
	12	-918.3153	-918.0794	-918.3414	-918.1054
	13	-918.3130	-918.0767	-918.3404	-918.1041
	14	-918.3157	-918.0781	-918.3426	-918.1050
	15	-918.3172	-918.0804	-918.3424	-918.1056
	16	-918.3114	-918.0751	-918.3396	-918.1034

Table 44: Method M3; chloroform

Method M3: DMSO

Structure	**Conformer #**	E_{low}	G_{low}	E_{high}	G_{high}
γ-lactone ***4***	1	-459.1479	-459.0452	-459.1598	-459.0572
	2	-459.1451	-459.0430	-459.1573	-459.0552
	3	-459.1463	-459.0438	-459.1593	-459.0568
	4	-459.1479	-459.0452	-459.1598	-459.0572
	5	-459.1432	-459.0415	-459.1580	-459.0562
	6	-459.1434	-459.0414	-459.1571	-459.0551
	7	-459.1407	-459.0389	-459.1578	-459.0559
	8	-459.1428	-459.0407	-459.1584	-459.0563
δ-lactone ***3***	1	-459.1383	-459.0352	-459.1520	-459.0489
	2	-459.1383	-459.0358	-459.1514	-459.0489
	3	-459.1414	-459.0382	-459.1528	-459.0496
(+)-Angiopterlactone B ***2*** *(Compound I)*	1	-918.3151	-918.0772	-918.3481	-918.1102
	2	-918.3075	-918.0712	-918.3418	-918.1056
	3	-918.3168	-918.0797	-918.3548	-918.1177
	4	-918.3146	-918.0778	-918.3489	-918.1121
	5	-918.3120	-918.0751	-918.3443	-918.1074
	6	-918.3119	-918.0751	-918.3454	-918.1086
	7	-918.3196	-918.0831	-918.3545	-918.1181
	8	-918.3118	-918.0751	-918.3444	-918.1077
	9	-918.3128	-918.0767	-918.3529	-918.1169
	10	-918.3086	-918.0729	-918.3419	-918.1062
	11	-918.3092	-918.0739	-918.3464	-918.1111
	12	-918.3153	-918.0794	-918.3481	-918.1122
	13	-918.3130	-918.0767	-918.3482	-918.1119
	14	-918.3157	-918.0781	-918.3500	-918.1124
	15	-918.3172	-918.0804	-918.3486	-918.1117
	16	-918.3114	-918.0751	-918.3471	-918.1109

Table 45: Method M3; DMSO

2.3.5 Method M3 (DMSO) – Investigation Into Energies

See Table 45 for γ-lactone **4**, δ-lactone **3** and (+)-angiopterlactone B (**2**) (Compound I).

Structure	**Conformer #**	E_{low}	G_{low}	E_{high}	G_{high}
*γ-lactone **6***	1	-459.1464	-459.0444	-459.1581	-459.0561
	2	-459.1421	-459.0401	-459.1574	-459.0555
	3	-459.1468	-459.0442	-459.1595	-459.0569
	4	-459.1457	-459.0437	-459.1584	-459.0564
	5	-459.1459	-459.0434	-459.1587	-459.0562
*δ-lactone **5***	1	-459.1399	-459.0375	-459.1518	-459.0494
	2	-459.1406	-459.0377	-459.1522	-459.0493
	3	-459.1404	-459.0377	-459.1520	-459.0494
	4	-459.1368	-459.0341	-459.1504	-459.0476
	5	-459.1398	-459.0364	-459.1513	-459.0479
	6	-459.1362	-459.0334	-459.1505	-459.0476
*Angiopterlactone B **2** (Compound II)*	1	-918.3140	-918.0775	-918.3468	-918.1104
	2	-918.3151	-918.0790	-918.3467	-918.1106
	3	-918.3173	-918.0800	-918.3482	-918.1109
	4	-918.3116	-918.0761	-918.3460	-918.1106
	5	-918.3122	-918.0752	-918.3444	-918.1074
	6	-918.3156	-918.0783	-918.3543	-918.1170
	7	-918.3140	-918.0761	-918.3476	-918.1097
	8	-918.3166	-918.0802	-918.3490	-918.1126
	9	-918.3172	-918.0815	-918.3524	-918.1167
	10	-918.3140	-918.0761	-918.3476	-918.1097
	11	-918.3135	-918.0767	-918.3483	-918.1115
	12	-918.3201	-918.0832	-918.3544	-918.1174
	13	-918.3105	-918.0742	-918.3444	-918.1081
	14	-918.3105	-918.0742	-918.3444	-918.1081
	15	-918.3161	-918.0801	-918.3527	-918.1166
*Angiopterlactone B **2** (Compound III)*	1	-918.3203	-918.0844	-918.3532	-918.1172
	2	-918.3214	-918.0858	-918.3530	-918.1174
	3	-918.3236	-918.0871	-918.3546	-918.1180
	4	-918.3174	-918.0817	-918.3506	-918.1149
	5	-918.3191	-918.0829	-918.3510	-918.1148
*Angiopterlactone B **2** (Compound IV)*	1	-918.3213	-918.0846	-918.3549	-918.1182
	2	-918.3182	-918.0812	-918.3487	-918.1117
	3	-918.3187	-918.0819	-918.3500	-918.1132
	4	-918.3104	-918.0735	-918.3430	-918.1060
	5	-918.3235	-918.0871	-918.3549	-918.1185
	6	-918.3171	-918.0814	-918.3486	-918.1128
	7	-918.3141	-918.0769	-918.3518	-918.1146
	8	-918.3100	-918.0740	-918.3498	-918.1137
	9	-918.3131	-918.0754	-918.3470	-918.1093
	10	-918.3177	-918.0818	-918.3534	-918.1176
	11	-918.3168	-918.0800	-918.3515	-918.1147
	12	-918.3103	-918.0740	-918.3452	-918.1088
	13	-918.3235	-918.0871	-918.3549	-918.1185
*Angiopterlactone B **2** (Compound V)*	1	-918.3262	-918.0904	-918.3580	-918.1222
	2	-918.3262	-918.0904	-918.3580	-918.1221
	3	-918.3258	-918.0903	-918.3578	-918.1223
	4	-918.3258	-918.0903	-918.3578	-918.1223
	5	-918.3245	-918.0887	-918.3573	-918.1215
	6	-918.3227	-918.0871	-918.3548	-918.1192
	7	-918.3223	-918.0858	-918.3537	-918.1172
	8	-918.3226	-918.0875	-918.3543	-918.1192
	9	-918.3245	-918.0887	-918.3573	-918.1215
	10	-918.3162	-918.0811	-918.3514	-918.1163
	11	-918.3223	-918.0858	-918.3537	-918.1172

	12	-918.3161	-918.0809	-918.3511	-918.1158
	13	-918.3161	-918.0809	-918.3511	-918.1158
	14	-918.3162	-918.0811	-918.3514	-918.1163
Angiopterlactone B ***2*** *(Compound VI)*	1	-918.3239	-918.0884	-918.3567	-918.1213
	2	-918.3240	-918.0886	-918.3563	-918.1210
	3	-918.3240	-918.0886	-918.3563	-918.1210
	4	-918.3194	-918.0843	-918.3521	-918.1170
	5	-918.3208	-918.0850	-918.3527	-918.1168
	6	-918.3205	-918.0846	-918.3530	-918.1171
Angiopterlactone B ***2*** *(Compound VII)*	1	-918.3172	-918.0811	-918.3499	-918.1138
	2	-918.3128	-918.0773	-918.3451	-918.1096
	3	-918.3172	-918.0812	-918.3494	-918.1134
	4	-918.3172	-918.0812	-918.3494	-918.1134
	5	-918.3247	-918.0892	-918.3568	-918.1212
	6	-918.3244	-918.0887	-918.3571	-918.1215
	7	-918.3247	-918.0892	-918.3568	-918.1212
	8	-918.3244	-918.0887	-918.3571	-918.1215
	9	-918.3197	-918.0845	-918.3530	-918.1179
Angiopterlactone B ***2*** *(Compound VIII)*	1	-918.3195	-918.0829	-918.3512	-918.1146
	2	-918.3169	-918.0810	-918.3480	-918.1121
	3	-918.3191	-918.0829	-918.3510	-918.1148
	4	-918.3191	-918.0829	-918.3510	-918.1148
	5	-918.3266	-918.0907	-918.3583	-918.1224
	6	-918.3266	-918.0907	-918.3583	-918.1224
	7	-918.3267	-918.0906	-918.3583	-918.1222
	8	-918.3267	-918.0906	-918.3583	-918.1222
	9	-918.3262	-918.0901	-918.3578	-918.1216
	10	-918.3231	-918.0874	-918.3558	-918.1201
	11	-918.3201	-918.0849	-918.3552	-918.1201
	12	-918.3161	-918.0800	-918.3480	-918.1119
	13	-918.3201	-918.0849	-918.3552	-918.1201
	14	-918.3202	-918.0848	-918.3555	-918.1201
	15	-918.3106	-918.0753	-918.3461	-918.1108
	16	-918.3175	-918.0826	-918.3538	-918.1189

Table 46: Method M3; DMSO

2.3.6 An alternative approach: method M4

Note that when utilising method M4 for the eight viable (–)-angiopterlactone A (**1**) structures, conformers within the 10 kcal/mol energy window set by TINKER were pre-optimised utilising SMD (DCE), wB97XD/6-311+G(d,p)//wB97XD/6-31G(d). For structures I-IV, the G_{high} energy value was then utilised to exclude any conformers outwith 5 kcal/mol (21 kJ/mol) of the lowest energy conformer. All conformers within 5 kcal/mol of the lowest energy conformer were then subjected to the final geometry optimisation and NMR calculation.

Structure	**Conformer #**	E_{low}	G_{low}	E_{high}	G_{high}
γ-lactone ***4***	1	-459.1348	-459.0313	-459.1348	-459.0313
	2	-459.1340	-459.0307	-459.1340	-459.0307
	3	-459.1362	-459.0326	-459.1362	-459.0326
	4	-459.1359	-459.0322	-459.1359	-459.0322
	5	-459.1344	-459.0311	-459.1344	-459.0311
	6	-459.1333	-459.0302	-459.1333	-459.0302
	7	-459.1338	-459.0303	-459.1338	-459.0303
	8	-459.1337	-459.0303	-459.1337	-459.0303
γ-lactone ***6***	1	-459.1348	-459.0317	-459.1348	-459.0317
	2	-459.1338	-459.0303	-459.1338	-459.0303
	3	-459.1356	-459.0318	-459.1356	-459.0318
	4	-459.1354	-459.0317	-459.1354	-459.0317
	5	-459.1355	-459.0318	-459.1355	-459.0318
δ-lactone ***3***	1	-459.1283	-459.0238	-459.1283	-459.0238
	2	-459.1279	-459.0238	-459.1279	-459.0238
	3	-459.1296	-459.0250	-459.1296	-459.0250
	4	-459.1259	-459.0218	-459.1259	-459.0218
	5	-459.1263	-459.0218	-459.1263	-459.0218
	6	-459.1266	-459.0222	-459.1266	-459.0222
δ-lactone ***5***	1	-459.1284	-459.0248	-459.1284	-459.0248
	2	-459.1292	-459.0249	-459.1292	-459.0249
	3	-459.1286	-459.0248	-459.1286	-459.0248
	4	-459.1265	-459.0223	-459.1265	-459.0223
	5	-459.1277	-459.0231	-459.1277	-459.0231
	6	-459.1263	-459.0220	-459.1263	-459.0220
(+)-Angiopterlactone B ***2*** *(Compound I)*	1	-918.3082	-918.0673	-918.3082	-918.0673
	2	-918.3005	-918.0615	-918.3005	-918.0615
	3	-918.3141	-918.0738	-918.3141	-918.0738
	4	-918.3085	-918.0689	-918.3085	-918.0689
	5	-918.3141	-918.0738	-918.3141	-918.0738
	6	-918.3044	-918.0653	-918.3044	-918.0653
	7	-918.3127	-918.0734	-918.3127	-918.0734
	8	-918.3031	-918.0633	-918.3031	-918.0633
	9	-918.3107	-918.0713	-918.3107	-918.0713
	10	-918.2994	-918.0612	-918.2994	-918.0612
	11	-918.3033	-918.0651	-918.3033	-918.0651
	12	-918.3053	-918.0672	-918.3053	-918.0672
	13	-918.3067	-918.0680	-918.3067	-918.0680
	14	-918.3100	-918.0695	-918.3100	-918.0695
	15	-918.3068	-918.0674	-918.3068	-918.0674
	16	-918.3050	-918.0657	-918.3050	-918.0657
Angiopterlactone B ***2***	1	-918.3055	-918.0662	-918.3055	-918.0662
	2	-918.3050	-918.0663	-918.3050	-918.0663

(Compound II)	3	-918.3070	-918.0674	-918.3070	-918.0674
	4	-918.3035	-918.0653	-918.3035	-918.0653
	5	-918.3040	-918.0641	-918.3040	-918.0641
	6	-918.3136	-918.0734	-918.3136	-918.0734
	7	-918.3078	-918.0670	-918.3078	-918.0670
	8	-918.3069	-918.0681	-918.3069	-918.0681
	9	-918.3107	-918.0719	-918.3107	-918.0719
	10	-918.3078	-918.0670	-918.3078	-918.0670
	11	-918.3081	-918.0684	-918.3081	-918.0684
	12	-918.3135	-918.0736	-918.3135	-918.0736
	13	-918.3029	-918.0640	-918.3029	-918.0640
	14	-918.3029	-918.0640	-918.3029	-918.0640
	15	-918.3111	-918.0717	-918.3111	-918.0717
Angiopterlactone B ***2*** *(Compound III)*	1	-918.3111	-918.0722	-918.3111	-918.0722
	2	-918.3106	-918.0723	-918.3106	-918.0723
	3	-918.3127	-918.0739	-918.3127	-918.0739
	4	-918.3081	-918.0697	-918.3081	-918.0697
	5	-918.3087	-918.0701	-918.3087	-918.0701
Angiopterlactone B ***2*** *(Compound IV)*	1	-918.3129	-918.0735	-918.3129	-918.0735
	2	-918.3053	-918.0672	-918.3053	-918.0672
	3	-918.3088	-918.0693	-918.3088	-918.0693
	4	-918.3027	-918.0645	-918.3027	-918.0645
	5	-918.3123	-918.0736	-918.3123	-918.0736
	6	-918.3066	-918.0682	-918.3066	-918.0682
	7	-918.3105	-918.0707	-918.3105	-918.0707
	8	-918.3076	-918.0683	-918.3076	-918.0683
	9	-918.3069	-918.0666	-918.3069	-918.0666
	10	-918.3106	-918.0720	-918.3106	-918.0720
	11	-918.3095	-918.0704	-918.3095	-918.0704
	12	-918.3039	-918.0649	-918.3039	-918.0649
	13	-918.3103	-918.0717	-918.3103	-918.0717
Angiopterlactone B ***2*** *(Compound V)*	1	-918.3163	-918.0778	-918.3163	-918.0778
	2	-918.3163	-918.0778	-918.3163	-918.0778
	3	-918.3162	-918.0782	-918.3162	-918.0782
	4	-918.3162	-918.0782	-918.3162	-918.0782
	5	-918.3145	-918.0762	-918.3145	-918.0762
	6	-918.3135	-918.0752	-918.3135	-918.0752
	7	-918.3113	-918.0731	-918.3113	-918.0731
	8	-918.3134	-918.0756	-918.3134	-918.0756
	9	-918.3115	-918.0737	-918.3115	-918.0737
	10	-918.3085	-918.0707	-918.3085	-918.0707
	11	-918.3117	-918.0739	-918.3117	-918.0739
	12	-918.3092	-918.0712	-918.3092	-918.0712
	13	-918.3088	-918.0704	-918.3088	-918.0704
	14	-918.3088	-918.0711	-918.3088	-918.0711
Angiopterlactone B ***2*** *(Compound VI)*	1	-918.3147	-918.0765	-918.3147	-918.0765
	2	-918.3142	-918.0763	-918.3142	-918.0763
	3	-918.3142	-918.0763	-918.3142	-918.0763
	4	-918.3130	-918.0757	-918.3130	-918.0757
	5	-918.3113	-918.0740	-918.3113	-918.0740
	6	-918.3118	-918.0737	-918.3118	-918.0737
Angiopterlactone B ***2*** *(Compound VII)*	1	-918.3081	-918.0692	-918.3081	-918.0692
	2	-918.3032	-918.0652	-918.3032	-918.0652
	3	-918.3076	-918.0691	-918.3076	-918.0691
	4	-918.3076	-918.0691	-918.3076	-918.0691
	5	-918.3152	-918.0769	-918.3152	-918.0769
	6	-918.3157	-918.0773	-918.3157	-918.0773
	7	-918.3152	-918.0769	-918.3152	-918.0769
	8	-918.3157	-918.0773	-918.3157	-918.0773
	9	-918.3142	-918.0767	-918.3142	-918.0767
Angiopterlactone B ***2*** *(Compound VIII)*	1	-918.3097	-918.0707	-918.3097	-918.0707
	2	-918.3064	-918.0682	-918.3064	-918.0682
	3	-918.3096	-918.0713	-918.3096	-918.0713

	4	-918.3096	-918.0713	-918.3096	-918.0713
	5	-918.3172	-918.0788	-918.3172	-918.0788
	6	-918.3172	-918.0788	-918.3172	-918.0788
	7	-918.3173	-918.0785	-918.3173	-918.0785
	8	-918.3173	-918.0785	-918.3173	-918.0785
	9	-918.3156	-918.0772	-918.3156	-918.0772
	10	-918.3129	-918.0747	-918.3129	-918.0747
	11	-918.3132	-918.0744	-918.3132	-918.0744
	12	-918.3056	-918.0672	-918.3056	-918.0672
	13	-918.3106	-918.0724	-918.3106	-918.0724
	14	-918.3129	-918.0746	-918.3129	-918.0746
	15	-918.3032	-918.0649	-918.3032	-918.0649
	16	-918.3104	-918.0723	-918.3104	-918.0723
	1	-918.2738	-918.0398	-918.2738	-918.0398
	2	-918.2706	-918.0362	-918.2706	-918.0362
	3	-918.2761	-918.0414	-918.2761	-918.0414
	4	-918.2753	-918.0407	-918.2753	-918.0407
	5	-918.2762	-918.0425	-918.2762	-918.0425
	6	-918.2795	-918.0450	-918.2795	-918.0450
	7	-918.2808	-918.0456	-918.2808	-918.0456
	8	-918.2776	-918.0432	-918.2776	-918.0432
	9	-918.2756	-918.0412	-918.2756	-918.0412
	10	-918.2758	-918.0417	-918.2758	-918.0417
	11	-918.2788	-918.0447	-918.2788	-918.0447
	12	-918.2741	-918.0400	-918.2741	-918.0400
	13	-918.2783	-918.0436	-918.2783	-918.0436
	14	-918.2765	-918.0422	-918.2765	-918.0422
	15	-918.2755	-918.0408	-918.2755	-918.0408
	16	-918.2812	-918.0459	-918.2812	-918.0459
Angiopterlactone A	17	-918.2787	-918.0442	-918.2787	-918.0442
1	18	-918.2761	-918.0414	-918.2761	-918.0414
(Compound I)	19	-918.2730	-918.0381	-918.2730	-918.0381
	20	-918.2784	-918.0436	-918.2784	-918.0436
	21	-918.2765	-918.0422	-918.2765	-918.0422
	22	-918.2763	-918.0418	-918.2763	-918.0418
	23	-918.2737	-918.0377	-918.2737	-918.0377
	24	-918.2728	-918.0380	-918.2728	-918.0380
	25	-918.2737	-918.0392	-918.2737	-918.0392
	26	-918.2736	-918.0393	-918.2736	-918.0393
	27	-918.2781	-918.0424	-918.2781	-918.0424
	28	-918.2747	-918.0394	-918.2747	-918.0394
	29	-918.2775	-918.0433	-918.2775	-918.0433
	30	-918.2770	-918.0411	-918.2770	-918.0411
	31	-918.2767	-918.0423	-918.2767	-918.0423
	32	-918.2734	-918.0392	-918.2734	-918.0392
	33	-918.2716	-918.0366	-918.2716	-918.0366
	34	-918.2732	-918.0384	-918.2732	-918.0384
	35	-918.2734	-918.0389	-918.2734	-918.0389
	1	-918.2726	-918.0392	-918.2726	-918.0392
	2	-918.2751	-918.0410	-918.2751	-918.0410
	3	-918.2718	-918.0371	-918.2718	-918.0371
	4	-918.2740	-918.0397	-918.2740	-918.0397
	5	-918.2731	-918.0397	-918.2731	-918.0397
	6	-918.2788	-918.0434	-918.2788	-918.0434
Angiopterlactone A	7	-918.2750	-918.0404	-918.2750	-918.0404
1	8	-918.2729	-918.0395	-918.2729	-918.0395
(Compound II)	9	-918.2722	-918.0384	-918.2722	-918.0384
	10	-918.2778	-918.0435	-918.2778	-918.0435
	11	-918.2763	-918.0412	-918.2763	-918.0412
	12	-918.2779	-918.0438	-918.2779	-918.0438
	13	-918.2763	-918.0410	-918.2763	-918.0410
	14	-918.2742	-918.0402	-918.2742	-918.0402
	15	-918.2745	-918.0403	-918.2745	-918.0403

	16	-918.2738	-918.0395	-918.2738	-918.0395
	17	-918.2725	-918.0393	-918.2725	-918.0393
	18	-918.2781	-918.0437	-918.2781	-918.0437
	19	-918.2740	-918.0401	-918.2740	-918.0401
	20	-918.2751	-918.0411	-918.2751	-918.0411
	21	-918.2747	-918.0405	-918.2747	-918.0405
	22	-918.2734	-918.0390	-918.2734	-918.0390
	23	-918.2776	-918.0431	-918.2776	-918.0431
	24	-918.2754	-918.0400	-918.2754	-918.0400
	25	-918.2722	-918.0383	-918.2722	-918.0383
	26	-918.2757	-918.0413	-918.2757	-918.0413
	27	-918.2729	-918.0381	-918.2729	-918.0381
	28	-918.2756	-918.0407	-918.2756	-918.0407
	29	-918.2718	-918.0378	-918.2718	-918.0378
	30	-918.2805	-918.0451	-918.2805	-918.0451
	31	-918.2721	-918.0380	-918.2721	-918.0380
	32	-918.2745	-918.0400	-918.2745	-918.0400
	33	-918.2772	-918.0420	-918.2772	-918.0420
	34	-918.2796	-918.0451	-918.2796	-918.0451
	35	-918.2791	-918.0452	-918.2791	-918.0452
	36	-918.2789	-918.0440	-918.2789	-918.0440
	37	-918.2806	-918.0451	-918.2806	-918.0451
	38	-918.2740	-918.0385	-918.2740	-918.0385
	39	-918.2754	-918.0409	-918.2754	-918.0409
	40	-918.2723	-918.0379	-918.2723	-918.0379
	41	-918.2758	-918.0411	-918.2758	-918.0411
	42	-918.2756	-918.0409	-918.2756	-918.0409
	43	-918.2745	-918.0407	-918.2745	-918.0407
	44	-918.2741	-918.0400	-918.2741	-918.0400
	45	-918.2763	-918.0417	-918.2763	-918.0417
	46	-918.2765	-918.0410	-918.2765	-918.0410
	47	-918.2766	-918.0422	-918.2766	-918.0422
	48	-918.2765	-918.0410	-918.2765	-918.0410
	49	-918.2726	-918.0378	-918.2726	-918.0378
Angiopterlactone A ***1*** *(Compound III)*	1	-918.2748	-918.0416	-918.2748	-918.0416
	2	-918.2748	-918.0409	-918.2748	-918.0409
	3	-918.2761	-918.0417	-918.2761	-918.0417
	4	-918.2753	-918.0408	-918.2753	-918.0408
	5	-918.2755	-918.0409	-918.2755	-918.0409
	6	-918.2742	-918.0405	-918.2742	-918.0405
	7	-918.2741	-918.0398	-918.2741	-918.0398
	8	-918.2723	-918.0382	-918.2723	-918.0382
	9	-918.2765	-918.0425	-918.2765	-918.0425
	10	-918.2740	-918.0394	-918.2740	-918.0394
	11	-918.2743	-918.0404	-918.2743	-918.0404
	12	-918.2760	-918.0423	-918.2760	-918.0423
	13	-918.2784	-918.0436	-918.2784	-918.0436
	14	-918.2766	-918.0424	-918.2766	-918.0424
	15	-918.2732	-918.0393	-918.2732	-918.0393
	16	-918.2761	-918.0419	-918.2761	-918.0419
	17	-918.2747	-918.0407	-918.2747	-918.0407
	18	-918.2792	-918.0444	-918.2792	-918.0444
	19	-918.2783	-918.0448	-918.2783	-918.0448
	20	-918.2814	-918.0467	-918.2814	-918.0467
	21	-918.2733	-918.0394	-918.2733	-918.0394
	22	-918.2752	-918.0409	-918.2752	-918.0409
	23	-918.2751	-918.0407	-918.2751	-918.0407
	24	-918.2738	-918.0401	-918.2738	-918.0401
	25	-918.2752	-918.0405	-918.2752	-918.0405
	26	-918.2804	-918.0450	-918.2804	-918.0450
	27	-918.2795	-918.0450	-918.2795	-918.0450
	28	-918.2746	-918.0405	-918.2746	-918.0405
	29	-918.2798	-918.0461	-918.2798	-918.0461

	30	-918.2737	-918.0399	-918.2737	-918.0399
	31	-918.2724	-918.0387	-918.2724	-918.0387
	32	-918.2775	-918.0421	-918.2775	-918.0421
	33	-918.2775	-918.0421	-918.2775	-918.0421
	34	-918.2753	-918.0404	-918.2753	-918.0404
	35	-918.2786	-918.0434	-918.2786	-918.0434
	36	-918.2743	-918.0407	-918.2743	-918.0407
	37	-918.2777	-918.0429	-918.2777	-918.0429
	38	-918.2749	-918.0412	-918.2749	-918.0412
	39	-918.2784	-918.0437	-918.2784	-918.0437
	40	-918.2728	-918.0378	-918.2728	-918.0378
	41	-918.2743	-918.0407	-918.2743	-918.0407
	42	-918.2734	-918.0390	-918.2734	-918.0390
	43	-918.2729	-918.0388	-918.2729	-918.0388
	44	-918.2742	-918.0403	-918.2742	-918.0403
Angiopterlactone A ***1*** *(Compound IV)*	1	-918.2759	-918.0421	-918.2759	-918.0421
	2	-918.2715	-918.0368	-918.2715	-918.0368
	3	-918.2787	-918.0450	-918.2787	-918.0450
	4	-918.2749	-918.0410	-918.2749	-918.0410
	5	-918.2727	-918.0382	-918.2727	-918.0382
	6	-918.2809	-918.0459	-918.2809	-918.0459
	7	-918.2714	-918.0370	-918.2714	-918.0370
	8	-918.2799	-918.0453	-918.2799	-918.0453
	9	-918.2755	-918.0414	-918.2755	-918.0414
	10	-918.2768	-918.0416	-918.2768	-918.0416
	11	-918.2714	-918.0370	-918.2714	-918.0370
	12	-918.2759	-918.0405	-918.2759	-918.0405
	13	-918.2804	-918.0457	-918.2804	-918.0457
	14	-918.2771	-918.0418	-918.2771	-918.0418
	15	-918.2796	-918.0446	-918.2796	-918.0446
	16	-918.2800	-918.0450	-918.2800	-918.0450
	17	-918.2747	-918.0403	-918.2747	-918.0403
	18	-918.2768	-918.0416	-918.2768	-918.0416
	19	-918.2779	-918.0431	-918.2779	-918.0431
	20	-918.2738	-918.0390	-918.2738	-918.0390
	21	-918.2775	-918.0425	-918.2775	-918.0425
	22	-918.2751	-918.0393	-918.2751	-918.0393
	23	-918.2777	-918.0436	-918.2777	-918.0436
	24	-918.2808	-918.0461	-918.2808	-918.0461
	25	-918.2758	-918.0419	-918.2758	-918.0419
	26	-918.2763	-918.0410	-918.2763	-918.0410
	27	-918.2781	-918.0446	-918.2781	-918.0446
	28	-918.2763	-918.0418	-918.2763	-918.0418
	29	-918.2761	-918.0415	-918.2761	-918.0415
	30	-918.2771	-918.0434	-918.2771	-918.0434
	31	-918.2759	-918.0421	-918.2759	-918.0421
	32	-918.2771	-918.0434	-918.2771	-918.0434
	33	-918.2782	-918.0441	-918.2782	-918.0441
	34	-918.2756	-918.0411	-918.2756	-918.0411
	35	-918.2762	-918.0416	-918.2762	-918.0416
	36	-918.2784	-918.0429	-918.2784	-918.0429
	37	-918.2738	-918.0390	-918.2738	-918.0390
	38	-918.2797	-918.0446	-918.2797	-918.0446
	39	-918.2763	-918.0410	-918.2763	-918.0410
	40	-918.2785	-918.0435	-918.2785	-918.0435
	41	-918.2786	-918.0443	-918.2786	-918.0443
	42	-918.2775	-918.0425	-918.2775	-918.0425
	43	-918.2744	-918.0392	-918.2744	-918.0392
	44	-918.2765	-918.0421	-918.2765	-918.0421
	45	-918.2774	-918.0430	-918.2774	-918.0430
	46	-918.2785	-918.0434	-918.2785	-918.0434
	47	-918.2797	-918.0449	-918.2797	-918.0449
	48	-918.2784	-918.0429	-918.2784	-918.0429

	49	-918.2752	-918.0405	-918.2752	-918.0405
	50	-918.2759	-918.0419	-918.2759	-918.0419
	51	-918.2773	-918.0431	-918.2773	-918.0431
	52	-918.2761	-918.0415	-918.2761	-918.0415
	53	-918.2754	-918.0414	-918.2754	-918.0414
	54	-918.2773	-918.0417	-918.2773	-918.0417
	55	-918.2777	-918.0441	-918.2777	-918.0441
Angiopterlactone A ***1*** *(Compound V)*	1	-918.2795	-918.0459	-918.2795	-918.0459
	2	-918.2805	-918.0466	-918.2805	-918.0466
	3	-918.2743	-918.0403	-918.2743	-918.0403
	4	-918.2785	-918.0448	-918.2785	-918.0448
	5	-918.2736	-918.0393	-918.2736	-918.0393
	6	-918.2790	-918.0449	-918.2790	-918.0449
	7	-918.2773	-918.0432	-918.2773	-918.0432
	8	-918.2710	-918.0366	-918.2710	-918.0366
Angiopterlactone A ***1*** *(Compound VI)*	1	-918.2797	-918.0461	-918.2797	-918.0461
	2	-918.2749	-918.0404	-918.2749	-918.0404
	3	-918.2752	-918.0412	-918.2752	-918.0412
	4	-918.2810	-918.0475	-918.2810	-918.0475
	5	-918.2775	-918.0436	-918.2775	-918.0436
	6	-918.2791	-918.0455	-918.2791	-918.0455
	7	-918.2745	-918.0402	-918.2745	-918.0402
	8	-918.2741	-918.0399	-918.2741	-918.0399
	9	-918.2792	-918.0458	-918.2792	-918.0458
Angiopterlactone A ***1*** *(Compound VII)*	1	-918.2782	-918.0446	-918.2782	-918.0446
	2	-918.2787	-918.0452	-918.2787	-918.0452
	3	-918.2735	-918.0395	-918.2735	-918.0395
	4	-918.2796	-918.0458	-918.2796	-918.0458
	5	-918.2790	-918.0450	-918.2790	-918.0450
	6	-918.2760	-918.0415	-918.2760	-918.0415
	7	-918.2807	-918.0466	-918.2807	-918.0466
	8	-918.2738	-918.0400	-918.2738	-918.0400
	9	-918.2756	-918.0411	-918.2756	-918.0411
	10	-918.2776	-918.0436	-918.2776	-918.0436
	11	-918.2780	-918.0439	-918.2780	-918.0439
Angiopterlactone A ***1*** *(Compound VIII)*	1	-918.2794	-918.0450	-918.2794	-918.0450
	2	-918.2800	-918.0460	-918.2800	-918.0460
	3	-918.2787	-918.0446	-918.2787	-918.0446
	4	-918.2725	-918.0381	-918.2725	-918.0381
	5	-918.2751	-918.0408	-918.2751	-918.0408
	6	-918.2779	-918.0438	-918.2779	-918.0438
	7	-918.2782	-918.0442	-918.2782	-918.0442
	8	-918.2723	-918.0381	-918.2723	-918.0381
	9	-918.2729	-918.0393	-918.2729	-918.0393

Table 47: Method M4; DMSO

	I	II	III	IV	V	VI	VII	VIII
^{1}H *MAE*	0.18	0.17	0.22	0.24	0.24	0.25	0.27	0.23
Difference wrt ***I***	0.00	-0.01	0.04	0.07	0.07	0.07	0.09	0.05
^{13}C *MAE*	1.1	1.1	1.0	1.1	1.6	1.3	1.4	1.8
Difference wrt ***I***	0.0	0.0	-0.1	0.1	0.5	0.3	0.3	0.8
$J_{H\text{-}H}$ *MAE*	1.4	0.8	1.4	1.8	4.0	3.2	2.2	3.0
Difference wrt ***I***	0.0	-0.6	0.0	0.4	2.6	1.8	0.7	1.5

Table 48: Method M4; DMSO; angiopterlactone B (**2**); MAE values including all data points (wrt = with respect to)

	I	II	III	IV	V	VI	VII	VIII
^{1}H *MAE*	0.08	0.09	0.11	0.12	0.22	0.22	0.22	0.22
Difference wrt ***I***	0.00	0.00	0.03	0.04	0.14	0.13	0.14	0.14
^{13}C *MAE*	1.1	0.8	1.1	1.4	2.6	2.4	3.1	3.2
Difference wrt ***I***	0.0	-0.3	0.0	0.3	1.4	1.2	1.9	2.1
$J_{H\text{-}H}$ *MAE*	0.6	0.6	1.5	1.4	3.6	3.7	2.4	2.3
Difference wrt ***I***	0.0	-0.1	0.8	0.8	2.9	3.0	1.8	1.7

Table 49: Method M4; DMSO; angiopterlactone B (**2**); MAE values excluding certain data points, as discussed in main text (wrt = with respect to)

2.3.7 Final method choice: Method M3 (DMSO)

See Table 45 for γ-lactone **4**, δ-lactone **3** and (+)-angiopterlactone B (**2**) (compound I). For all relevant diastereoisomers of these compounds, see Table 46.

Structure	**Conformer #**	E_{low}	G_{low}	E_{high}	G_{high}
Angiopterlactone A ***1*** *(Compound I)*	1	-918.2915	-918.0598	-918.3163	-918.0846
	2	-918.2860	-918.0536	-918.3104	-918.0780
	3	-918.2885	-918.0563	-918.3129	-918.0807
	4	-918.2902	-918.0590	-918.3150	-918.0838
	5	-918.2869	-918.0552	-918.3116	-918.0800
	6	-918.2839	-918.0515	-918.3091	-918.0767
	7	-918.2825	-918.0508	-918.3113	-918.0797
	8	-918.2871	-918.0550	-918.3106	-918.0785
	9	-918.2833	-918.0520	-918.3112	-918.0798
	10	-918.2881	-918.0553	-918.3142	-918.0814
	11	-918.2898	-918.0580	-918.3136	-918.0817
	12	-918.2927	-918.0607	-918.3180	-918.0860
	13	-918.2913	-918.0587	-918.3165	-918.0840
	14	-918.2845	-918.0523	-918.3077	-918.0756
	15	-918.2939	-918.0625	-918.3193	-918.0879
	16	-918.2882	-918.0568	-918.3153	-918.0840
	17	-918.2871	-918.0550	-918.3106	-918.0785
	18	-918.2934	-918.0612	-918.3215	-918.0893
	19	-918.2959	-918.0634	-918.3228	-918.0902
	20	-918.2926	-918.0602	-918.3193	-918.0869

	21	-918.2924	-918.0602	-918.3170	-918.0849
	22	-918.2870	-918.0547	-918.3124	-918.0801
	23	-918.2915	-918.0604	-918.3176	-918.0865
	24	-918.2903	-918.0583	-918.3141	-918.0821
	25	-918.2954	-918.0633	-918.3226	-918.0906
	26	-918.2874	-918.0567	-918.3176	-918.0869
	27	-918.2933	-918.0612	-918.3198	-918.0877
	28	-918.2923	-918.0613	-918.3175	-918.0865
	29	-918.2919	-918.0597	-918.3172	-918.0850
	30	-918.2941	-918.0620	-918.3239	-918.0918
	31	-918.2949	-918.0630	-918.3209	-918.0890
	32	-918.2927	-918.0607	-918.3180	-918.0860
	33	-918.2876	-918.0557	-918.3131	-918.0812
	34	-918.2910	-918.0585	-918.3162	-918.0837
	35	-918.2956	-918.0634	-918.3219	-918.0897
	36	-918.2937	-918.0619	-918.3182	-918.0865
	37	-918.2934	-918.0613	-918.3190	-918.0869
	38	-918.2897	-918.0573	-918.3148	-918.0824
	39	-918.2901	-918.0571	-918.3153	-918.0823
	40	-918.2907	-918.0586	-918.3147	-918.0826
	41	-918.2918	-918.0594	-918.3159	-918.0835
	42	-918.2832	-918.0515	-918.3100	-918.0783
	43	-918.2907	-918.0587	-918.3148	-918.0829
	44	-918.2932	-918.0602	-918.3189	-918.0860
	45	-918.2908	-918.0589	-918.3145	-918.0826
	46	-918.2900	-918.0574	-918.3167	-918.0842
	47	-918.2953	-918.0635	-918.3206	-918.0888
	48	-918.2877	-918.0554	-918.3116	-918.0793
	49	-918.2924	-918.0595	-918.3177	-918.0848
	50	-918.2876	-918.0555	-918.3144	-918.0823
	51	-918.2885	-918.0571	-918.3208	-918.0894
	52	-918.2890	-918.0574	-918.3146	-918.0830
	53	-918.2934	-918.0613	-918.3190	-918.0869
	54	-918.2865	-918.0543	-918.3146	-918.0825
	55	-918.2914	-918.0588	-918.3159	-918.0833
	56	-918.2872	-918.0558	-918.3170	-918.0856
Angiopterlactone A ***1*** *(Compound II)*	1	-918.2900	-918.0587	-918.3147	-918.0835
	2	-918.2914	-918.0593	-918.3173	-918.0852
	3	-918.2860	-918.0535	-918.3108	-918.0783
	4	-918.2890	-918.0566	-918.3132	-918.0808
	5	-918.2913	-918.0595	-918.3165	-918.0847
	6	-918.2897	-918.0587	-918.3148	-918.0839
	7	-918.2860	-918.0545	-918.3109	-918.0794
	8	-918.2918	-918.0591	-918.3218	-918.0891
	9	-918.2919	-918.0602	-918.3159	-918.0842
	10	-918.2897	-918.0584	-918.3158	-918.0844
	11	-918.2876	-918.0565	-918.3153	-918.0842
	12	-918.2942	-918.0625	-918.3193	-918.0876
	13	-918.2891	-918.0572	-918.3125	-918.0806
	14	-918.2855	-918.0539	-918.3110	-918.0794
	15	-918.2868	-918.0544	-918.3104	-918.0780
	16	-918.2910	-918.0588	-918.3175	-918.0853
	17	-918.2957	-918.0643	-918.3195	-918.0882
	18	-918.2929	-918.0606	-918.3177	-918.0854
	19	-918.2899	-918.0586	-918.3170	-918.0858
	20	-918.2920	-918.0604	-918.3156	-918.0840
	21	-918.2907	-918.0588	-918.3154	-918.0836
	22	-918.2882	-918.0572	-918.3155	-918.0845
	23	-918.2868	-918.0545	-918.3104	-918.0780
	24	-918.2882	-918.0555	-918.3122	-918.0795
	25	-918.2866	-918.0548	-918.3099	-918.0782
	26	-918.2955	-918.0637	-918.3196	-918.0878
	27	-918.2906	-918.0589	-918.3161	-918.0844

	28	-918.2952	-918.0635	-918.3198	-918.0881
	29	-918.2897	-918.0584	-918.3186	-918.0873
	30	-918.2916	-918.0600	-918.3174	-918.0857
	31	-918.2908	-918.0585	-918.3162	-918.0839
	32	-918.2946	-918.0626	-918.3197	-918.0877
	33	-918.2885	-918.0569	-918.3137	-918.0821
	34	-918.2859	-918.0546	-918.3099	-918.0786
	35	-918.2907	-918.0582	-918.3166	-918.0841
	36	-918.2894	-918.0578	-918.3143	-918.0827
	37	-918.2916	-918.0598	-918.3189	-918.0871
	38	-918.2881	-918.0566	-918.3166	-918.0851
	39	-918.2909	-918.0588	-918.3182	-918.0862
	40	-918.2872	-918.0557	-918.3150	-918.0835
	41	-918.2960	-918.0638	-918.3218	-918.0896
	42	-918.2894	-918.0578	-918.3143	-918.0827
	43	-918.2919	-918.0598	-918.3180	-918.0859
	44	-918.2936	-918.0609	-918.3203	-918.0877
	45	-918.2967	-918.0645	-918.3220	-918.0898
	46	-918.2962	-918.0646	-918.3210	-918.0894
	47	-918.2934	-918.0616	-918.3202	-918.0883
	48	-918.2970	-918.0644	-918.3222	-918.0896
	49	-918.2922	-918.0595	-918.3160	-918.0833
	50	-918.2929	-918.0612	-918.3169	-918.0852
	51	-918.2886	-918.0560	-918.3145	-918.0819
	52	-918.2934	-918.0610	-918.3179	-918.0854
	53	-918.2926	-918.0609	-918.3169	-918.0852
	54	-918.2900	-918.0585	-918.3182	-918.0867
	55	-918.2895	-918.0571	-918.3141	-918.0816
	56	-918.2886	-918.0560	-918.3145	-918.0819
	57	-918.2895	-918.0585	-918.3159	-918.0849
	58	-918.2935	-918.0623	-918.3195	-918.0882
	59	-918.2912	-918.0585	-918.3171	-918.0843
	60	-918.2889	-918.0571	-918.3144	-918.0826
	61	-918.2928	-918.0609	-918.3198	-918.0879
	62	-918.2912	-918.0585	-918.3171	-918.0843
	63	-918.2895	-918.0571	-918.3141	-918.0816
	1	-918.2930	-918.0621	-918.3171	-918.0862
	2	-918.2923	-918.0609	-918.3181	-918.0867
	3	-918.2943	-918.0626	-918.3190	-918.0873
	4	-918.2928	-918.0618	-918.3175	-918.0865
	5	-918.2922	-918.0600	-918.3188	-918.0867
	6	-918.2912	-918.0593	-918.3170	-918.0850
	7	-918.2914	-918.0590	-918.3162	-918.0838
	8	-918.2874	-918.0562	-918.3162	-918.0850
	9	-918.2945	-918.0632	-918.3196	-918.0883
	10	-918.2912	-918.0593	-918.3175	-918.0856
	11	-918.2906	-918.0596	-918.3177	-918.0867
	12	-918.2929	-918.0620	-918.3193	-918.0884
Angiopterlactone A ***1*** *(Compound III)*	13	-918.2943	-918.0621	-918.3199	-918.0877
	14	-918.2929	-918.0611	-918.3200	-918.0882
	15	-918.2886	-918.0570	-918.3164	-918.0847
	16	-918.2916	-918.0601	-918.3198	-918.0883
	17	-918.2906	-918.0588	-918.3135	-918.0816
	18	-918.2883	-918.0554	-918.3117	-918.0789
	19	-918.2911	-918.0596	-918.3174	-918.0859
	20	-918.2899	-918.0575	-918.3142	-918.0818
	21	-918.2951	-918.0631	-918.3217	-918.0897
	22	-918.2952	-918.0643	-918.3204	-918.0895
	23	-918.2880	-918.0558	-918.3145	-918.0823
	24	-918.2984	-918.0661	-918.3224	-918.0901
	25	-918.2887	-918.0579	-918.3170	-918.0861
	26	-918.2909	-918.0596	-918.3183	-918.0870
	27	-918.2925	-918.0611	-918.3170	-918.0856

	28	-918.2905	-918.0595	-918.3174	-918.0864
	29	-918.2924	-918.0601	-918.3183	-918.0860
	30	-918.2929	-918.0606	-918.3231	-918.0907
	31	-918.2969	-918.0651	-918.3216	-918.0897
	32	-918.2891	-918.0585	-918.3180	-918.0875
	33	-918.2983	-918.0669	-918.3219	-918.0905
	34	-918.2888	-918.0575	-918.3177	-918.0864
	35	-918.2904	-918.0586	-918.3190	-918.0872
	36	-918.2947	-918.0616	-918.3191	-918.0861
	37	-918.2947	-918.0616	-918.3191	-918.0860
	38	-918.2947	-918.0628	-918.3205	-918.0887
	39	-918.2883	-918.0566	-918.3125	-918.0808
	40	-918.2899	-918.0575	-918.3142	-918.0818
	41	-918.2932	-918.0610	-918.3201	-918.0878
	42	-918.2890	-918.0576	-918.3156	-918.0842
	43	-918.2921	-918.0608	-918.3177	-918.0863
	44	-918.2908	-918.0579	-918.3146	-918.0817
	45	-918.2925	-918.0600	-918.3192	-918.0867
	46	-918.2924	-918.0607	-918.3173	-918.0856
	47	-918.2947	-918.0628	-918.3205	-918.0887
	48	-918.2902	-918.0587	-918.3165	-918.0850
	49	-918.2908	-918.0584	-918.3153	-918.0829
	50	-918.2874	-918.0563	-918.3122	-918.0811
	51	-918.2921	-918.0608	-918.3177	-918.0863
	52	-918.2911	-918.0594	-918.3159	-918.0842
	53	-918.2891	-918.0580	-918.3166	-918.0855
	54	-918.2902	-918.0587	-918.3165	-918.0850
	55	-918.2902	-918.0582	-918.3161	-918.0841
	1	-918.2944	-918.0630	-918.3188	-918.0873
	2	-918.2911	-918.0593	-918.3144	-918.0827
	3	-918.2899	-918.0573	-918.3145	-918.0819
	4	-918.2861	-918.0542	-918.3129	-918.0810
	5	-918.2979	-918.0665	-918.3222	-918.0908
	6	-918.2922	-918.0606	-918.3178	-918.0862
	7	-918.2905	-918.0581	-918.3149	-918.0826
	8	-918.2943	-918.0620	-918.3241	-918.0918
	9	-918.2851	-918.0537	-918.3131	-918.0817
	10	-918.2897	-918.0577	-918.3147	-918.0827
	11	-918.2968	-918.0648	-918.3234	-918.0914
	12	-918.2926	-918.0608	-918.3187	-918.0869
	13	-918.2914	-918.0585	-918.3163	-918.0834
	14	-918.2850	-918.0529	-918.3132	-918.0811
	15	-918.2897	-918.0577	-918.3147	-918.0827
Angiopterlactone A	16	-918.2920	-918.0593	-918.3181	-918.0854
1	17	-918.2905	-918.0581	-918.3149	-918.0826
(Compound IV)	18	-918.2966	-918.0646	-918.3222	-918.0902
	19	-918.2939	-918.0616	-918.3188	-918.0865
	20	-918.2921	-918.0604	-918.3222	-918.0904
	21	-918.2952	-918.0629	-918.3222	-918.0899
	22	-918.2844	-918.0529	-918.3134	-918.0818
	23	-918.2935	-918.0611	-918.3177	-918.0853
	24	-918.2922	-918.0595	-918.3192	-918.0865
	25	-918.2905	-918.0591	-918.3217	-918.0903
	26	-918.2921	-918.0595	-918.3159	-918.0833
	27	-918.2851	-918.0538	-918.3131	-918.0817
	28	-918.2934	-918.0609	-918.3183	-918.0858
	29	-918.2917	-918.0585	-918.3165	-918.0832
	30	-918.2947	-918.0628	-918.3204	-918.0885
	31	-918.2961	-918.0643	-918.3237	-918.0919
	32	-918.2927	-918.0617	-918.3190	-918.0880
	33	-918.2934	-918.0612	-918.3177	-918.0855

	34	-918.2954	-918.0645	-918.3203	-918.0894
	35	-918.2918	-918.0598	-918.3187	-918.0868
	36	-918.2926	-918.0610	-918.3180	-918.0864
	37	-918.2935	-918.0624	-918.3200	-918.0888
	38	-918.2924	-918.0612	-918.3179	-918.0866
	39	-918.2926	-918.0612	-918.3190	-918.0876
	40	-918.2946	-918.0629	-918.3220	-918.0903
	41	-918.2918	-918.0601	-918.3172	-918.0855
	42	-918.2935	-918.0611	-918.3177	-918.0853
	43	-918.2940	-918.0609	-918.3195	-918.0865
	44	-918.2921	-918.0595	-918.3159	-918.0833
	45	-918.2961	-918.0643	-918.3237	-918.0919
	46	-918.2934	-918.0612	-918.3177	-918.0855
	47	-918.2928	-918.0606	-918.3208	-918.0886
	48	-918.2966	-918.0649	-918.3208	-918.0891
	49	-918.2920	-918.0605	-918.3165	-918.0849
	50	-918.2894	-918.0574	-918.3165	-918.0846
	51	-918.2892	-918.0575	-918.3165	-918.0848
	52	-918.2937	-918.0618	-918.3182	-918.0863
	53	-918.2949	-918.0631	-918.3197	-918.0880
	54	-918.2942	-918.0619	-918.3199	-918.0877
	55	-918.2947	-918.0626	-918.3216	-918.0894
	56	-918.2940	-918.0609	-918.3196	-918.0865
	57	-918.2935	-918.0611	-918.3177	-918.0853
	58	-918.2904	-918.0595	-918.3187	-918.0878
	59	-918.2949	-918.0631	-918.3198	-918.0880
	60	-918.2869	-918.0550	-918.3116	-918.0797
	61	-918.2926	-918.0610	-918.3180	-918.0864
	62	-918.2935	-918.0619	-918.3172	-918.0856
	63	-918.2935	-918.0618	-918.3197	-918.0879
	64	-918.2962	-918.0646	-918.3213	-918.0897
Angiopterlactone A ***1*** *(Compound V)*	1	-918.2985	-918.0672	-918.3233	-918.0920
	2	-918.2992	-918.0679	-918.3245	-918.0931
	3	-918.2933	-918.0614	-918.3175	-918.0856
	4	-918.2964	-918.0646	-918.3228	-918.0910
	5	-918.2923	-918.0601	-918.3170	-918.0848
	6	-918.2963	-918.0645	-918.3235	-918.0916
	7	-918.2943	-918.0625	-918.3214	-918.0896
	8	-918.2858	-918.0547	-918.3142	-918.0831
Angiopterlactone A ***1*** *(Compound VI)*	1	-918.2989	-918.0674	-918.3231	-918.0916
	2	-918.2940	-918.0621	-918.3178	-918.0860
	3	-918.2935	-918.0620	-918.3177	-918.0862
	4	-918.3004	-918.0693	-918.3246	-918.0935
	5	-918.2948	-918.0630	-918.3211	-918.0893
	6	-918.2979	-918.0666	-918.3231	-918.0917
	7	-918.2921	-918.0604	-918.3170	-918.0853
	8	-918.2925	-918.0605	-918.3170	-918.0851
	9	-918.2965	-918.0651	-918.3232	-918.0918
Angiopterlactone A ***1*** *(Compound VII)*	1	-918.2966	-918.0651	-918.3214	-918.0898
	2	-918.2974	-918.0660	-918.3220	-918.0906
	3	-918.2920	-918.0605	-918.3164	-918.0848
	4	-918.2966	-918.0650	-918.3233	-918.0918
	5	-918.2962	-918.0650	-918.3224	-918.0912
	6	-918.2935	-918.0617	-918.3182	-918.0864
	7	-918.2992	-918.0677	-918.3242	-918.0927
	8	-918.2913	-918.0597	-918.3160	-918.0845
	9	-918.2939	-918.0619	-918.3183	-918.0862
	10	-918.2963	-918.0642	-918.3202	-918.0881
	11	-918.2957	-918.0640	-918.3203	-918.0887
Angiopterlactone A ***1***	1	-918.2965	-918.0646	-918.3235	-918.0916
	2	-918.2976	-918.0663	-918.3240	-918.0927

(Compound VIII)	3	-918.2956	-918.0640	-918.3226	-918.0910
	4	-918.2872	-918.0559	-918.3155	-918.0841
	5	-918.2937	-918.0613	-918.3182	-918.0858
	6	-918.2960	-918.0641	-918.3215	-918.0897
	7	-918.2963	-918.0647	-918.3219	-918.0903
	8	-918.2911	-918.0595	-918.3161	-918.0845
	9	-918.2911	-918.0595	-918.3161	-918.0845

Table 50: Method M3; DMSO

	I	**II**	**III**	**IV**	**V**	**VI**	**VII**	**VIII**
^{1}H MAE	0.12	0.12	0.18	0.18	0.18	0.26	0.23	0.15
*Difference wrt **I***	0.00	0.00	0.06	0.05	0.05	0.13	0.11	0.02
^{13}C MAE	1.3	1.4	2.2	2.2	3.1	2.7	3.1	3.4
*Difference wrt **I***	0.0	0.1	0.9	0.9	1.8	1.3	1.8	2.1
$J_{H\text{-}H}$ MAE	0.9	0.8	2.4	2.5	4.1	3.6	1.8	2.3
*Difference wrt **I***	0.0	-0.1	1.5	1.7	3.2	2.7	1.0	1.4

Table 51: Method M3; DMSO; angiopterlactone B (**2**); MAE values including all data points (wrt = with respect to)

	I	**II**	**III**	**IV**	**V**	**VI**	**VII**	**VIII**
^{1}H MAE	0.09	0.10	0.19	0.18	0.17	0.27	0.24	0.13
*Difference wrt **I***	0.00	0.00	0.10	0.09	0.07	0.17	0.14	0.03
^{13}C MAE	0.9	1.0	2.0	2.1	2.7	2.3	2.7	2.9
*Difference wrt **I***	0.0	0.1	1.1	1.1	1.8	1.4	1.8	2.0
$J_{H\text{-}H}$ MAE	0.5	0.6	1.7	1.7	3.5	3.6	2.5	2.4
*Difference wrt **I***	0.0	0.1	1.2	1.2	3.0	3.1	2.0	1.9

Table 52: Method M3; DMSO; angiopterlactone B (**2**); MAE values excluding certain data points, as discussed in main text (wrt = with respect to)

2.4 Slope and Intercept Values for Linear Regression Analyses

Slope and intercept values for the TMS referenced ^{1}H and ^{13}C chemical shifts, for methods M3 and M4.

Compound		^{1}H chemical shift data		^{13}C chemical shift data	
		Slope	**Intercept**	**Slope**	**Intercept**
γ-lactone	**4**	1.0110	0.0696	1.0467	1.7479
	6	1.0303	0.0513	1.0543	0.7937
δ-lactone	**3**	1.0660	-0.0379	1.0512	1.3651
	5	1.0233	0.1107	1.0339	4.9700
Angiopterlactone B ***(2)***	I	1.0423	0.0199	1.0455	2.1237
	II	1.0441	0.0337	1.0423	2.4012
	III	1.0117	0.0505	1.0454	3.0563
	IV	1.0234	0.0014	1.0497	2.7318
	V	1.0271	-0.0164	1.0439	4.4608
	VI	1.0137	-0.0155	1.0394	4.3894
	VII	1.0094	0.0258	1.0459	4.2049
	VIII	1.0273	0.0218	1.0486	4.3878
Angiopterlactone A ***(1)***	I	1.0148	0.1220	1.0508	1.1814
	II	1.0116	0.1488	1.0519	0.8284
	III	1.0084	0.1358	1.0444	1.6129
	IV	1.0031	0.1495	1.0458	1.9378
	V	1.0156	-0.0252	1.0585	0.6747
	VI	1.0229	0.0583	1.0598	0.5046
	VII	1.0563	-0.0555	1.0689	-0.7388
	VIII	1.0565	-0.1640	1.0680	-0.8138

Table 53: Method M3, using all chemical shifts that could be confidently assigned

Compound		^{1}H chemical shift data		^{13}C chemical shift data	
		Slope	**Intercept**	**Slope**	**Intercept**
γ-lactone	**4**	0.9933	0.0999	-	-
	6	1.0204	-0.0020	-	-
δ-lactone	**3**	0.9967	0.1097	-	-
	5	0.9554	0.2318	-	-
Angiopterlactone B ***(2)***	I	0.9364	0.2063	0.9625	4.3242
	II	0.9220	0.2526	0.9675	3.9466
	III	0.8540	0.3152	0.9537	5.6315
	IV	0.8757	0.2390	0.9556	5.7555
	V	0.9014	0.1987	0.9332	10.4099
	VI	0.8656	0.2427	0.9435	9.2430
	VII	0.8949	0.2405	0.9374	10.1175
	VIII	0.9335	0.1840	0.9281	11.1060
Angiopterlactone A ***(1)***	I	0.9747	0.1399	-	-
	II	0.9538	0.2096	-	-
	III	0.9749	0.1201	-	-
	IV	0.9758	0.1255	-	-
	V	0.9556	0.1246	-	-
	VI	0.9577	0.1552	-	-
	VII	0.9899	0.0696	-	-
	VIII	0.9902	0.0195	-	-

Table 54: Method M4, excluding largely deviating chemical shifts

Appendices for Chapter 3

All input and output files have been archived with the University of Edinburgh.

3.1 Energy values

All energies (*E*) and Gibbs Free energies (*G*) are provided in Hartrees (a.u.) at 343 K. Only the energies of the lowest energy conformer are provided. The energies and imaginary frequencies for all transition states (TS) are listed below (cm^{-1}). Transition states are labelled as follows: $RC_{1/2}$ are the first and second step of the ring contraction, *oM* is the oxa-Michael addition and *M* is the Michael addition. Furthermore, energy values for all ground state (GS) species are provided. These dimeric species are defined by the nomenclature used within Chapter 3 (Figure 65).

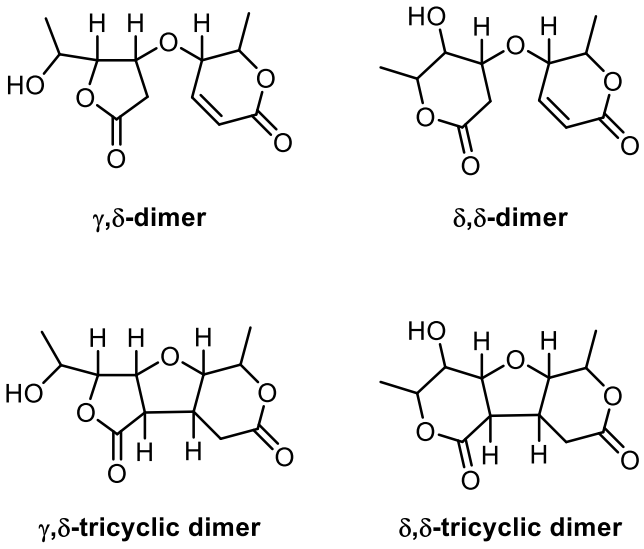

Figure 65: Nomenclature utilised to describe the dimeric ground state species

CO_3^{2-} and HCO_3^{1-}

	Species	***E***	***G***	**Imaginary Frequency**
CO_3^{2-}	GS	-264.004662	-264.020189	
HCO_3^{1-}	GS	-264.547187	-264.551086	

Table 55: Energies of CO_3^{2-} and HCO_3^{1-}

*Homo-coupling of **ent-3***

Pathway 1 - Re	***Species***	***E***	***G***	**Imaginary Frequency**
*Lactone **ent-3***	GS	-458.598816	-458.514077	
RC_1	TS	-458.568036	-458.483337	-285.77
RC intermediate	GS	-458.577393	-458.492242	
RC_2	TS	-458.577016	-458.491844	-194.19
Encounter complex	GS	-917.748085	-917.539703	
oM	TS	-917.728998	-917.518948	-172.81
γ,δ-dimer	GS	-917.741526	-917.529806	
M	TS	-917.729734	-917.517116	-299.86
γ,δ-tricyclic dimer	GS	-917.769585	-917.552848	

Table 56: Energies for the *Re*-pathway (P1) of the homo-coupling of ***ent-3***

Pathway 1 - Si	***Species***	***E***	***G***	**Imaginary Frequency**
oM	TS	-917.734906	-917.524120	-297.53
γ,δ-dimer	GS	-917.740281	-917.528517	
M	TS	-917.729953	-917.515762	-344.44
γ,δ-tricyclic dimer	GS	-917.765910	-917.547584	

Table 57: Energies for the *Si*-pathway (P1) of the homo-coupling of ***ent-3***

Ring Contraction M06-2X	***Species***	***E***	***G***	**Imaginary Frequency**
Reactant State	GS	-458.565317	-458.480739	
RC_1	TS	-458.537719	-458.452897	-272.82
RC intermediate	GS	-458.548675	-458.462852	
RC_2	TS	-458.547511	-458.462167	-198.34
Product State	GS	-458.564284	-458.480633	

Table 58: Ring contraction in P1 utilising the M06-2X functional

Ring-fused	*Cis/trans*	*E*	*G*
Option A	*cis*	-313.289084	-313.119484
	trans	-313.274656	-313.106684
Option B	*cis*	-352.607254	-352.410104
	trans	-352.597905	-352.402148

Table 59: Testing the stability of *cis*- and *trans*- fused ring systems

Lactone Stability Tests	*5/6-membered ring*	*E*	*G*
Option A	5	-459.121758	-459.024656
	6	-459.115478	-459.016887
Option B	5	-460.357227	-460.236739
	6	-460.350223	-460.228657
Option C	5	-344.583766	-344.516128
	6	-344.576253	-344.506593
Option D	5	-345.817870	-345.726615
	6	-345.808432	-345.715610
Option E	5	-271.768991	-271.658496
	6	-271.770294	-271.657421
Option F	5	-309.890650	-309.777669
	6	-309.894459	-309.779103
Option G	5	-235.869315	-235.736216
	6	-235.877548	-235.739484
Option G (Twist-boat)	6	-235.867635	-235.731828

Table 60: Testing the stability of various 5- and 6-membered rings

Product Stability Tests	*Re / Si*	*E*	*G*
Option B	*Re*	-803.230063	-803.044497
	Si	-803.225201	-803.038497
Option C	*Re*	-615.864411	-615.670438
	Si	-615.861770	-615.668076

Table 61: Testing the stability of the *Re* and *Si* products from P1

RC - hydrogenated	*Species*	*E*	*G*	**Imaginary Frequency**
Reactant State	GS	-459.828288	-459.721221	
RC_1	TS	-459.817601	-459.708976	-251.30
RC intermediate	GS	-459.825648	-459.715980	
RC_2	TS	-459.820105	-459.711363	-216.71
Product State	GS	-459.829814	-459.723127	

Table 62: Computing the ring contraction for the hydrogenated δ-lactone

RC – simplified structure		*Re/Si*	*E*	*G*	**Imaginary Frequency**
Option B	Reactant State	*Re*	-612.456055	-612.310949	
		Si	-612.460504	-612.315261	
	RC_1	*Re*	-612.451098	-612.305156	-251.48
		Si	-612.450251	-612.304003	-228.44
	RC intermediate	*Re*	-612.460235	-612.313022	
		Si	-612.455434	-612.308134	
	RC_2	*Re*	-612.454031	-612.308221	-222.58
		Si	-612.445654	-612.299714	-221.87
	Product State	*Re*	-612.461371	-612.316873	
		Si	-612.450407	-612.305565	
Option C	Reactant State	*Re*	-574.348898	-574.211768	
		Si	-574.351588	-574.215597	
	RC_1	*Re*	-574.335710	-574.198715	-250.79
		Si	-574.338407	-574.201080	-234.63
	RC intermediate	*Re*	-574.344557	-574.206771	
		Si	-574.344469	-574.206494	
	RC_2	*Re*	-574.339437	-574.202328	-210.70
		Si	-574.336505	-574.199279	-230.55
	Product State	*Re*	-574.349257	-574.213762	
		Si	-574.342112	-574.205647	

Table 63: Testing the ring contraction in simplified structures

Pathway 2 - Re	*Species*	*E*	*G*	**Imaginary Frequency**
Encounter complex	GS	-917.741601	-917.533829	
oM	TS	-917.725746	-917.513668	-256.14
δ,δ-dimer	GS	-917.737223	-917.523941	
RC_1	TS	-917.721602	-917.507927	-240.24
RC intermediate	GS	-917.730433	-917.516291	
RC_2	TS	-917.724985	-917.511605	-220.34

Table 64: Energies for the *Re*-pathway (P2) of the homo-coupling of ***ent-3***

Pathway 2 - Si	*Species*	*E*	*G*	**Imaginary Frequency**
oM	TS	-917.723006	-917.513813	-129.59
δ,δ-dimer	GS	-917.739312	-917.527540	
RC_1	TS	-917.724537	-917.510795	-233.90
RC intermediate	GS	-917.730279	-917.516084	
RC_2	TS	-917.721756	-917.508212	-225.24

Table 65: Energies for the *Si* pathway (P2) of the homo-coupling of ***ent-3***

Pathway 3 - Re	*Species*	*E*	*G*	**Imaginary Frequency**
M	TS	-917.725518	-917.510300	-278.31
δ,δ-tricyclic dimer	GS	-917.768868	-917.551132	
RC_1	TS	-917.762430	-917.543938	-236.38
RC intermediate	GS	-917.770943	-917.551934	
RC_2	TS	-917.760045	-917.542328	-207.25

Table 66: Energies for the *Re* pathway (P3) of the homo-coupling of ***ent-3***

Pathway 3 - Si	*Species*	*E*	*G*	**Imaginary Frequency**
M	TS	-917.727386	-917.513629	-266.37
δ,δ-tricyclic dimer	GS	-917.766782	-917.548574	
RC_1	TS	-917.756509	-917.536673	-195.65
RC intermediate	GS	-917.761788	-917.541839	
RC_2	TS	-917.746473	-917.528370	-214.49

Table 67: Energies for the *Si* pathway (P3) of the homo-coupling of ***ent-3***

Testing axial vs equatorial		*Ax/eq*	*E*	*G*
*Lactone **ent-3***	Protonated	ax	-459.111861	-459.013868
	Protonated	eq	-459.115478	-459.016887
	Deprotonated	ax	-458.596662	-458.512225
	Deprotonated	eq	-458.598816	-458.514077
*Lactone **5***	Protonated	ax	-459.11287	-459.014848
	Protonated	eq	-459.113881	-459.016554
	Deprotonated	ax	-458.597313	-458.512619
	Deprotonated	eq	-458.599114	-458.515214

Table 68: Testing the energies of protonated/deprotonated ***ent-3*** and **5** with the methyl group in the axial or equatorial position

*Homo-coupling of **5***

Pathway 1	***Species***	***E***	***G***	**Imaginary Frequency**
*Lactone **5***	GS	-458.599114	-458.515214	
RC_1	TS	-458.567587	-458.482903	-283.75
RC intermediate	GS	-458.577156	-458.491902	
RC_2	TS	-458.576915	-458.491656	-196.01

Table 69: Energies for P1 in the homo-coupling of **5**

Pathway 2 - Re	***Species***	***E***	***G***	**Imaginary Frequency**
Encounter complex	GS	-917.745789	-917.538372	
oM	TS	-917.732040	-917.520631	-303.80
δ,δ-dimer	GS	-917.740022	-917.528372	
RC_1	TS	-917.721397	-917.507263	-241.86
RC intermediate	GS	-917.727898	-917.513002	
RC_2	TS	-917.722053	-917.507601	-202.84
γ,δ-dimer	GS	-917.740106	-917.529513	
M	TS	-917.733027	-917.520069	-304.49
γ,δ-tricyclic dimer	GS	-917.769906	-917.553732	

Table 70: Energies for the *Re* pathway (P2) in the homo-coupling of **5**

Pathway 2 - Si	*Species*	*E*	*G*	**Imaginary Frequency**
oM	TS	-917.721587	-917.512555	-142.74
δ,δ-dimer	GS	-917.735821	-917.523927	
RC_1	TS	-917.720776	-917.507853	-210.40
RC intermediate	GS	-917.726127	-917.512832	
RC_2	TS	-917.718662	-917.504814	-212.59
γ,δ-dimer	GS	-917.740014	-917.527041	
M	TS	-917.725465	-917.511163	-290.71
γ,δ-tricyclic dimer	GS	-917.765473	-917.548180	

Table 71: Energies for the *Si* pathway (P2) in the homo-coupling of **5**

Pathway 3 - Re	*Species*	*E*	*G*	**Imaginary Frequency**
M	TS	-917.733879	-917.519941	-328.61
δ,δ-tricyclic dimer	GS	-917.765241	-917.549035	
RC_1	TS	-917.759599	-917.540655	-227.66
RC intermediate	GS	-917.768061	-917.548758	
RC_2	TS	-917.760914	-917.542627	-188.10

Table 72: Energies for the *Re* pathway (P3) in the homo-coupling of **5**

Pathway 3 - Si	*Species*	*E*	*G*	**Imaginary Frequency**
M	TS	-917.725456	-917.511320	-284.98
δ,δ-tricyclic dimer	GS	-917.761893	-917.545613	
RC_1	TS	-917.751238	-917.531757	-222.23
RC intermediate	GS	-917.756242	-917.536705	
RC_2	TS	-917.752242	-917.532318	-166.23

Table 73: Energies for the *Si* pathway (P3) in the homo-coupling of **5**

*Cross-coupling of **ent-3** with **5***

Pathway 2 - Re	***Species***	***E***	***G***	**Imaginary Frequency**
Encounter complex	GS	-917.743763	-917.536877	
oM	TS	-917.731761	-917.520207	-280.31
δ,δ-dimer	GS	-917.740279	-917.527757	
RC_1	TS	-917.720121	-917.506340	-244.83
RC intermediate	GS	-917.728910	-917.514761	
RC_2	TS	-917.724018	-917.510118	-180.55
γ,δ-dimer	GS	-917.740749	-917.529529	
M	TS	-917.728483	-917.515857	-365.49
γ,δ-tricyclic dimer	GS	-917.768915	-917.553426	

Table 74: Energies for the *Re* pathway (P2) in the cross-coupling of ***ent*-3** with **5**

Pathway 2 - Si	***Species***	***E***	***G***	**Imaginary Frequency**
oM	TS	-917.721348	-917.510645	-155.44
δ,δ-dimer	GS	-917.736088	-917.524079	
RC_1	TS	-917.720743	-917.507033	-234.51
RC intermediate	GS	-917.726150	-917.511556	
RC_2	TS	-917.718353	-917.504433	-208.70
γ,δ-dimer	GS	-917.740596	-917.528836	
M	TS	-917.730207	-917.515181	-339.93
γ,δ-tricyclic dimer	GS	-917.767620	-917.549538	

Table 75: Energies for the *Si* pathway (P2) in the cross-coupling of ***ent*-3** with **5**

Pathway 3 - Re	***Species***	***E***	***G***	**Imaginary Frequency**
M	TS	-917.729664	-917.514756	-310.15
δ,δ-tricyclic dimer	GS	-917.767356	-917.549257	
RC_1	TS	-917.760876	-917.542532	-224.78
RC intermediate	GS	-917.769436	-917.550011	
RC_2	TS	-917.758983	-917.541002	-183.11

Table 76: Energies for the *Re* pathway (P3) in the cross-coupling of ***ent*-3** with **5**

Pathway 3 - Si	*Species*	*E*	*G*	**Imaginary Frequency**
M	TS	-917.727406	-917.512813	-276.98
δ,δ-tricyclic dimer	GS	-917.763515	-917.546772	
RC_1	TS	-917.750580	-917.531245	-224.02
RC intermediate	GS	-917.755492	-917.534986	
RC_2	TS	-917.742791	-917.524394	-205.00

Table 77: Energies for the *Si* pathway (P3) in the cross-coupling of ***ent*-3** with **5**

*Cross-coupling of **5** with **ent-3***

Pathway 2 - Re	*Species*	*E*	*G*	**Imaginary Frequency**
Encounter complex	GS	-917.743617	-917.536883	
oM	TS	-917.727872	-917.515318	-294.42
δ,δ-dimer	GS	-917.736956	-917.524714	
RC_1	TS	-917.724463	-917.510783	-220.86
RC intermediate	GS	-917.731599	-917.517398	
RC_2	TS	-917.726186	-917.512539	-211.73
γ,δ-dimer	GS	-917.741849	-917.530758	
M	TS	-917.734230	-917.521594	-347.62
γ,δ-tricyclic dimer	GS	-917.769832	-917.554046	

Table 78: Energies for the *Re* pathway (P2) in the cross-coupling of **5** with ***ent*-3**

Pathway 2 - Si	*Species*	*E*	*G*	**Imaginary Frequency**
oM	TS	-917.717402	-917.508812	-204.82
δ,δ-dimer	GS	-917.737402	-917.526605	
RC_1	TS	-917.725816	-917.512489	-223.22
RC intermediate	GS	-917.730796	-917.516567	
RC_2	TS	-917.722949	-917.508944	-219.11
γ,δ-dimer	GS	-917.740086	-917.528417	
M	TS	-917.731038	-917.517013	-304.21
γ,δ-tricyclic dimer	GS	-917.764150	-917.547492	

Table 79: Energies for the *Si* pathway (P2) in the cross-coupling of **5** with ***ent*-3**

Pathway 3 - Re	*Species*	*E*	*G*	**Imaginary Frequency**
M	TS	-917.727221	-917.513104	-285.21
δ,δ-tricyclic dimer	GS	-917.766919	-917.549850	
RC₁	TS	-917.760903	-917.542742	-224.28
RC intermediate	GS	-917.769656	-917.550815	
RC₂	TS	-917.762091	-917.544425	-202.18

Table 80: Energies for the *Re* pathway (P3) in the cross-coupling of **5** with ***ent*-3**

Pathway 3 - Si	*Species*	*E*	*G*	**Imaginary Frequency**
M	TS	-917.726055	-917.512638	-292.24
δ,δ-tricyclic dimer	GS	-917.766863	-917.548797	
RC₁	TS	-917.757389	-917.538412	-248.14
RC intermediate	GS	-917.764707	-917.544133	
RC₂	TS	-917.758521	-917.539282	-202.09

Table 81: Energies for the *Si* pathway (P3) in the cross-coupling of **5** with ***ent*-3**

3.2 pK_a Studies

The pK_a studies were completed by following the approach reported by Ho[116], in which solution phase dissociation free energies are calculated following: $\Delta G^* = G(A^-) - G(HA) + G^*(H^+)$. In this equation, $G(A^-)$ and $G(HA)$ are computed directly within the SMD solvation model on the solution-phase optimised geometry and the value for the proton free energy ($G^*(H^+)$) is used from the literature and corrected at a standard state of 1 mol/L. Values have been reported for various solvents, such as water, dimethylsulfoxide (DMSO) and methanol. As a result of the lack in literature data in dichloroethane (DCE), the reported value for methanol (-263.5 kcal/mol) was utilised.[117] As the aim was to compare the relative pK_a values of the different species rather than obtain an absolute pK_a, we considered that this approximation should not affect our conclusions. Nonetheless, pK_a calculations were also completed in DMSO to gain a comparative analysis. Energies were calculated at 343 K.

3.3 NBO Analysis

This section contains the second-order perturbation analysis from which the relevant hydrogen-bond contributions (in kcal/mol) are obtained. LP refers to the lone pair, σ^* to the antibonding orbital.

Coupling	***Pathway***	***TS/INT***	***Step***	***Donor***	***Acceptor***	***H-bond contribution (kcal/mol)***
*Homo (**ent-3**)*	1	TS-*Si*	oM	LP(1)O3	σ^*(1)O6-H33	6.3
				LP(2)O3	σ^*(1)O6-H33	25.3
*Homo (**ent-3**)*	2	INT-*Re*	δ,δ-dimer	LP(1)O7	σ^*(1)O21-H31	3.0
*Homo (**5**)*	2	TS-*Re*	oM	LP(1)O7	σ^*(1)O21-H31	4.2
				LP(2)O7	σ^*(1)O21-H31	13.9
*Cross (**ent-3** with **5**)*	2	TS-*Re*	oM	LP(1)O7	σ^*(1)O21-H31	5.1
				LP(2)O7	σ^*(1)O21-H31	11.4
*Cross (**ent-3** with **5**)*	2	TS-*Si*	M	LP(1)O7	σ^*(1)O22-H33	2.7
				LP(2)O7	σ^*(1)O22-H33	5.3
*Cross (**ent-3** with **5**)*	2	*Si*	Product	LP(1)O5	σ^*(1)O8-H33	4.1
*Cross (**ent-3** with **5**)*	3	INT-*Re*	δ,δ-dimer	LP(1)O7	σ^*(1)O21-H31	3.2 (nbodel: 3.1)
*Cross (**5** with **ent-3**)*	2	TS-*Re*	oM	LP(1)O7	σ^*(1)O21-H31	4.5
				LP(2)O7	σ^*(1)O21-H31	25.0

Table 82: H-bond contributions for key intermediate and transition state species

Useful Figures for Chapter 2

Figure A: Our eight investigated structures of (+)-angiopterlactone A (**1**). Structure originally proposed by isolation chemists is compound I. *Si* face oxa-Michael addition denoted by blue, *Re* by red

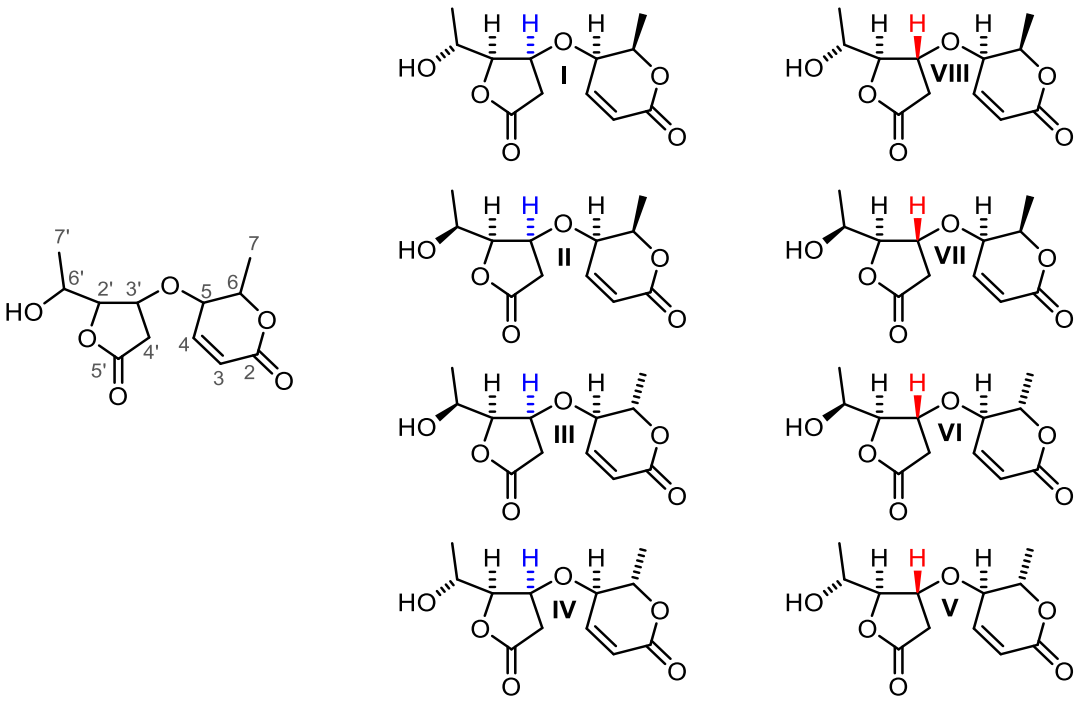

Figure B: Our eight investigated structures of (+)-angiopterlactone B (**2**). *Si* face oxa-Michael addition denoted by blue, *Re* by red)